INTEGRATING NEUROIMAGING AND BEHAVIORAL DATA USING THE MULTIDIMENSIONAL GENERALIZED GRADED UNFOLDING MODEL

A Dissertation
Presented to
The Academic Faculty

by

Matthew E. Barrett

In Partial Fulfillment
of the Requirements for the Degree
Doctor of Philosophy in the
School of Psychology

Georgia Institute of Technology
May, 2021

Integrating Neuroimaging and Behavioral Data Using The Multidimensional Generalized Graded Unfolding Model For The Response Process

Approved By:

Dr. James Roberts, Advisor
School of Psychology
Georgia Institute of Technology

Dr. Daniel Spieler
School of Psychology
Georgia Institute of Technology

Dr. Eric Schumacher
School of Psychology
Georgia Institute of Technology

Dr. Jessica Turner
Department of Psychology
Georgia State University

Dr. Susan Embretson
School of Psychology
Georgia Institute of Technology

Date Approved: April 16th, 2021

TABLE OF CONTENTS

LIST OF FIGURES

LIST OF TABLES

LIST OF EQUATIONS

SUMMARY

A study investigating the relationship between two distinct data structures resulting from the same stimulus was examined. Participants made attractiveness judgments to computer generated models in two phases. Phase 1 of the study was conducted in the laboratory (behavioral) while phase 2 was conducted in the fMRI scanner (neuroimaging). Data from the behavioral component was composed of attractiveness ratings for computer generated models, whereas the neuroimaging component was composed of signal change in five pre-specified ROIs when responding to the identical stimulus. It was hypothesized that both of these outcomes were a function of the distance between a subject's ideal point and the stimulus location in a latent multidimensional preference space. The attractiveness ratings were modeled with the multidimensional generalized graded unfolding model (MGGUM), which is an item response theory model for proximity-based data presumed to underlie the general preference ratings. The signal change data was simultaneously modeled as a function of the estimated distance between a subject and stimulus derived from the MGGUM. Estimation of models for both types of data was conducted simultaneously using a system of two simultaneous equations with parameters that are updated using a Markov chain Monte Carlo procedure. Information about signal change and its relationship to person-stimulus distances (i.e., idealness) in the multidimensional latent space was utilized to update estimates of the individual's location in that space and this, in turn, lead to updated predictions of signal change in each ROI. This project was predicated on the notion that both behavioral and neural signal data are a function of the proximity between

a given individual and stimulus, and was the first study to integrate models for neural signal into an item response theory framework.

CHAPTER 1. INTRODUCTION

1.1 Background (Item Response Theory)

1.1.1 Unfolding Item Response Theory (IRT) Models

Item response theory (IRT) models are utilized to determine the probability that a person uses a particular response category (e.g., an available response option) when responding to a stimulus or item. The process of fitting an IRT model to data yields parameter estimates relevant to the item (most commonly: its "location" and "discrimination") and to the person (often referred to as "trait", "ability" or "location"). The interaction between the characteristics of the item and the traits of the person determines the probability of endorsement.

Traditional IRT models are most commonly applied in educational contexts (Lord, 1980), using either binary or graded responses (Yen & Fitzpatrick, 2006), and are cumulative in nature. The cumulative nature of common IRT models such as the Rasch model (Rasch, 1960), the two 2PLM and 3PLM (Birnbaum, 1968), the partial credit and generalized partial credit models (Masters, 1982; Muraki, 1992) and the graded response models (Samejima, 1969) implies a dominance response process in that the ability of an individual is monotonically related to the probability of obtaining a higher item score. All other things being equal, a dominance-based process requires that greater ability levels (i.e., person locations on the latent continuum) lead to higher expected response values. There are a variety of models that provide a dominance based characterization about the process underlying an individual's response to any given item. These models

also provide varying degrees of information about the items themselves. However, all cumulative models will have item and test characteristic curves that increase monotonically with the latent trait. Although most commonly applied in educational contexts, these models work well for any data which result from a dominance-based, or "more is better" response process.

Cumulative IRT models do not suffice for all psychological measurement, however. Consider the area of preferences as an example. There are types of preferences for which a cumulative or dominance-based response process might fit well, such as a preference for money or happiness, but there exist other types of preferences where these models would not fit the data. For example, when considering how individuals prefer to take milk or sugar in their coffee, there exists a point in which the preference for the coffee will start to decrease when too little or too much milk or sugar is added. Furthermore, this point differs among individuals, as people tend to take their coffee in a variety of different ways. This point on the latent continuum associated with maximum preference can be referred to as an "ideal point." It is analogous to the notion of latent ability in the context of the cumulative IRT models use in achievement testing. With respect to the coffee scenario, we might presume that an individual coffee drinker would have a point in a two-dimensional space that represents his or her ideal level of milk and sugar. Too much milk and the coffee becomes too creamy, too little and it becomes too bitter. In both cases, the individual would prefer the coffee less than their ideal. A similar reaction would be obtained if the amount of sugar was varied relative to the ideal point. This situation, whether "too much or too little" constitutes a departure from an ideal preference point in the latent space, and as such, would presumably lead to less

preference for the cup of coffee. The process that leads to this type of data is often referred to as an ideal point response process, or alternatively, a proximity-based response process.

Thurstone (1928) was the first researcher to derive measures from responses that presumably followed an ideal point process. He did this in the context of attitude measurement, which in his method, was a 2-stage processes. In the first stage, Thurstone obtained ratings from individuals who indicated how unfavorable or favorable each item was with respect to the attitude object under study. These ratings were used to produce scale values for each item, and these scale values were essentially locations of stimuli on a latent continuum. In the second step, Thurstone had subjects indicate how much they disagreed or agreed with each item. His subsequent estimate of attitude was based on the idea that individuals would endorse items which were close to their own positions on the latent attitude continuum. Indeed, each individual's attitude estimate was simply the median of scale values associated with the items the individual had endorsed. In essence, this way of scoring tests assumed that disagree-agree responses were a result of an ideal point process. Instead of utilizing total score models, scores were developed for individuals and items together which jointly reflected their position on a continuum and were consistent with a proximity relation. This contrasts with other methods developed around the same time which calculated total scores for people that presumably increase in magnitude with the trait (Likert, 1932). Thurstone's work on developing a measurement procedure for the ideal point process would be built upon throughout the years (Coombs, 1950; Bennett & Hayes, 1960) and later incorporated into the IRT paradigm (Andrich,

1988; Andrich & Luo, 1993; Andrich, 1996; Roberts & Laughlin, 1996; Roberts, Donoghue, & Laughlin, 2000).

Responses to items (or, more generally, to stimuli) may follow from a dominance or ideal point response process. These are two different theoretical processes which lead to data with different characteristics. Data which follow from a dominance response process are best modeled with some sort of cumulative IRT model. In a cumulative model, the expected value of a response to a stimulus increases (or remains stable) as the signed distance between the locations of an individual and a stimulus on the latent continuum increases. Figure 1 illustrates this response process below.

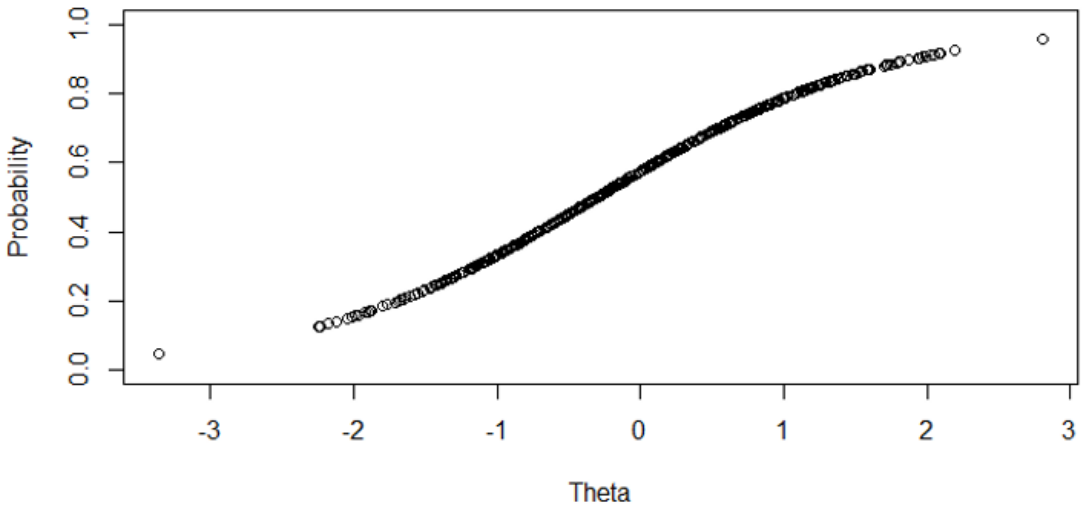

Figure 1

Probability of endorsing a binary item under a model for a cumulative response process as a function of "trait" theta.

In contrast, data from an ideal point response process are not theoretically consistent with a cumulative model. Such data are best described with some form of unfolding model. An unfolding model suggests that the expected value of a response to a stimulus will be maximum when the individual and stimulus locations on the latent continuum are

identical, and expected responses will decrease as these locations become more discrepant in any direction. Figure 2 illustrates this process below. Note that the probability of endorsement does not increase monotonically with the latent trait, but instead peaks when the location of the item matches that of the person.

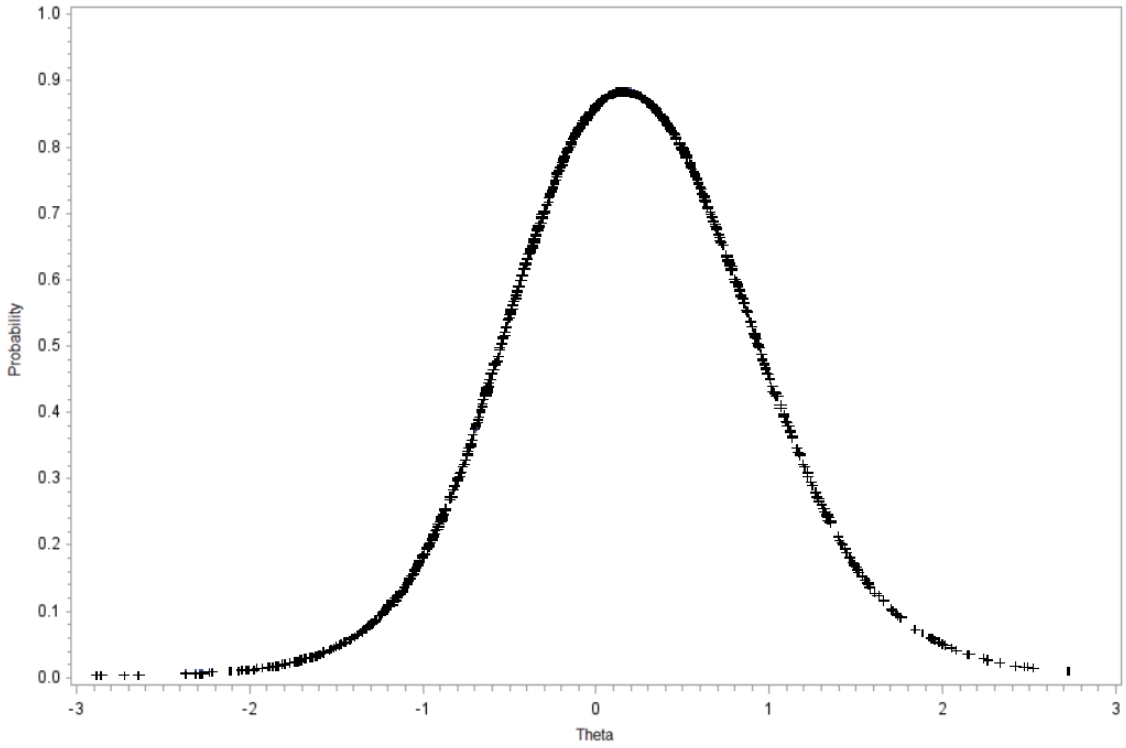

Figure 2

Probability of endorsing a binary item under a model for an ideal-point response process as a function of "trait" theta.

These unidimensional depictions of two different response processes can be generalized to a multidimensional framework in a straightforward way by extending the model parameters to contain information about each dimension of interest (Reckase, 2009; Roberts & Shim, 2010).

1.2 Multidimensional Generalized Graded Unfolding Model (MGGUM)

The multidimensional generalized graded unfolding model (MGGUM; Roberts & Shim, 2010) is an unfolding IRT model suitable for data that result from an ideal point response process. The MGGUM is a multidimensional variant of the generalized graded unfolding model (Roberts & Laughlin, 1996; Roberts et al., 2000). The functional form of the MGGUM can be written as:

$$P\left[Z_i = z|\underline{\theta}_j\right] =$$

$$\frac{\exp\left[\left(z\sqrt{\sum_{d=1}^{D}\alpha_{id}^2(\theta_{jd}-\delta_{id})^2}\right)+\sum_{k=0}^{z}\psi_{ik}\right]+\exp\left[\left((M-z)\sqrt{\sum_{d=1}^{D}\alpha_{id}^2(\theta_{jd}-\delta_{id})^2}\right)+\sum_{k=0}^{z}\psi_{ik}\right]}{\sum_{w=0}^{C}\left(\exp\left[\left(w\sqrt{\sum_{d=1}^{D}\alpha_{id}^2(\theta_{jd}-\delta_{id})^2}\right)+\sum_{k=0}^{w}\psi_{ik}\right]+\exp\left[\left((M-w)\sqrt{\sum_{d=1}^{D}\alpha_{id}^2(\theta_{jd}-\delta_{id})^2}\right)+\sum_{k=0}^{w}\psi_{ik}\right]\right)} \quad (1)$$

where:

Z_i = Observed response to the i^{th} item,
z = 0, 1, 2, … , C; with z = 0 indicating the lowest level of preference on the rating scale, and z= C indicating the highest level of preference,
D = the total number of latent dimensions,
C = the number of observed response categories minus 1,
M = 2C + 1 = the number of subjective response category thresholds,
θ_{jd} = the location of the j^{th}individual on the d^{th} dimension,
δ_{id} = the location of the i^{th} item on the d^{th} dimension,
α_{id} = the discrimination parameter of the i^{th} item on the d^{th} dimension,
τ_{ik} = the k^{th} subjective response category threshold for the i^{th} item which is a component of
$\psi_{ik} = \sum_{d=1}^{D}\alpha_{id}\ \tau_{ik}$, is the weighted subjective response category threshold for the i^{th} item.

Note that the parameters τ_{ik} and ψ_{ik} are constrained to be symmetric about the location of an item and do not vary across dimensions. The MGGUM is a divide-by-total model (Thissen & Steinberg, 1986), and thus, the denominator is the sum of all possible numerators (i.e., the sum of numerators across all possible response categories). This

rescales the numerators so that they sum to one across all possible responses as would any probability function. The MGGUM can be used for either binary or graded preference ratings. In its exploratory form shown in (1), it assumes that all stimuli can be legitimately represented on all *D* dimensions (i.e., no discrimination parameters are equal to zero for any dimension[1]).

Consider again the preference for coffee; an individual may dislike the amount of milk and sugar in the coffee for two reasons; there might be either too much or too little for their taste. The MGGUM presumes that there are two reasons an individual might use any response on a rating scale (Roberts & Laughlin, 1996; Roberts et al., 2000). In the literature, these reasons are referred to as "subjective response categories." Consider a person who dislikes the amount of milk in a cup of coffee. This reaction can occur because the coffee has too much milk (i.e., the individual's ideal amount of milk is less than that contained in the coffee) or too little milk (the individual's ideal amount of milk is greater than that contained in the coffee). Unless the respondent tells us why they dislike the coffee, we will not know which of these subjective responses is operating. With a typical preference scale, we will only know how much they dislike or like the coffee, not the reason why they feel that way. Similarly, these two reasons for disliking a cup of coffee also exist with regard to the amount of sugar in it. Indeed, these two reasons exist for any response on the rating scale, and for every dimension which subjects attend to when examining the coffee. It is illustrated in (1) how each of the two reasons for a response is explicitly parameterized in the MGGUM. Both the numerator and

[1] One could easily envision a confirmatory version of the MGGUM in which some discrimination parameters were set to zero based on theory or item content. However, the exploratory version of the model will be the focus of this report.

denominator have exponential functions on the left ("too much" of the attribute) and right ("too little of the attribute) that contribute to the probability of a given observed response. These two functions parameterize the probability of the corresponding subjective responses that might be operating, and they are simply summed in the numerator (and, consequently, the denominator) of (1) in order to obtain the probability of the associated observed response. (This is rational because the two subjective responses are mutually exclusive and exhaustive.) The MGGUM, and its unidimensional counterpart (GGUM), have seen wide applications in psychology, ranging from the measurement of attitudes (Roberts & Laughlin, 1996); stages of change (Noel, 1999); emotion (Roberts & Sparks, 2015); physical attraction (Roberts, Barrett, & King, 2016); and personality traits (Stark, Chernyshenko, & Drasgow, 2005; Carter et al., 2014). There have also been many variants of these models proposed in the literature (Cui, 2008; Wang & Liu, 2011).

1.2.1 Estimation of MGGUM Parameters

1.2.1.1 Markov chain Monte Carlo estimation. Roberts and Shim (2010) performed the first parameter estimation study of the MGGUM. In their study, they used Markov chain Monte Carlo (MCMC; Patz & Junker, 1999) methods to estimate model parameters. MCMC is a Bayesian technique which iterates through sampling values of a parameter, conditioned on the current estimates of other parameters in the model. A popular sampling process that is often employed with IRT models is called Metropolis-Hastings within Gibbs (MHwG; Patz & Junker, 1999). In the MHwG algorithm, a set of possible parameter estimates for the model in question is drawn from a corresponding set of proposal distributions. The higher the posterior likelihood of the current parameter set relative to that for the previous set, the more likely it is to be retained. Otherwise, the

parameter set from the previous iteration is kept. Eventually, repetition of this sampling/retention process leads to a stationary joint posterior distribution of all model parameters. The number of iterations required to achieve a stationary distribution varies from one application to the next, but once this "burn-in" has been completed, subsequent draws can be taken as though they are being sampled directly from the joint posterior distribution of all model parameters. If one completes *N* more iterations beyond the burn-in, then each parameter will have *N* sampled values. The distributional characteristics of each parameters' sampled values may be explored or point estimates such as the mean of these values can be calculated. Parameter estimates based on the mean of sampled values are known as expected a posterior (EAP) estimates.

In Bayesian estimation procedures, prior distributions are specified for each parameter and serve as an additional source of information for parameter values during the estimation process. To the extent that the stimuli and persons are not located in extreme regions of the multidimensional space, the estimation process relies less on the prior distribution of the parameter and more on the data to determine parameter values (Roberts & Thompson, 2011). Similarly, during the sampling process, the data may at times be less informative about the correct value of a parameter, and the procedure begins to rely more heavily on information from the prior distribution in those cases.

MCMC estimation of highly parameterized models such as the MGGUM can take quite a bit of time due to the number of parameters and iterations required to estimate them with accuracy. The long computation times for parameter estimation in the MGGUM are a function of the number of parameters being estimated. This computation time can be drastically reduced if item parameters are known beforehand. For example, in

some instances where item banks exist, where item estimates have been derived from other samples, or where other information has been used to estimate item parameters (e.g., multidimensional scaling; Williams, July, 2016), information about items is readily available and can be treated as fixed parameters in the model (Williams, July, 2016). In the case of the MGGUM, if item parameters are known, then MCMC can be used to estimate the multidimensional location for each subject in a much more efficient manner. Indeed, the responses from a single subject could be used to develop the location estimate for that individual.

1.2.1.2 Marginal maximum a posteriori estimation of item parameters. Marginal maximum a posteriori (MMAP) estimation is another strategy for calibrating item parameters in the MGGUM. In MMAP, the likelihood function is augmented with prior distributions for all parameters. The θ_j values are subsequently integrated out of this Bayesian likelihood function, and the resulting "marginal" Bayesian likelihood is maximized to solve for item parameter estimates. Removing θ_j from the likelihood in this way yields estimates of item parameters that are statistically consistent. The integration is generally performed using numeric quadrature. An expectation-maximization algorithm (EM; Dempster et al., 1977) is employed to first estimate the number of people using different response categories at each preselected point on the latent continuum. These points are denoted as quadrature points, and are used to approximate integrals for the marginal Bayesian likelihood across θ_j, which in turn, are maximized with respect to item parameters.

A separate estimation process, such as EAP, is applied to obtain person parameter estimates treating the item parameter values from MMAP as fixed quantities. Thompson (2014) showed that EAP estimates of person locations can be obtained with MMAP item parameters as a computationally efficient alternative to fully Bayesian MCMC methods which estimate the item and person parameters simultaneously.

1.2.1.3 Metropolis-Hastings Robbins-Monro estimation of item parameters. Estimating model parameters for higher dimensional models is a difficult computational task which may require a lot of computer time regardless of which estimation method is used. It can be especially cumbersome for the MMAP procedure because computational time for simple rectangular quadrature increases exponentially as the number of dimensions increases. Metropolis-Hastings Robbins-Monro (MHRM) estimation is a stochastic integration method in which θ_j values are drawn from an approximated posterior distribution using a Metropolis-Hastings (MH) algorithm along with provisional item parameter estimates and the item responses. With these values in hand, maximum likelihood estimates of item parameters are derived under the assumption that the θ_j values are estimated with error. This is accomplished using the Robbins-Monro (RM) approach to maximization. The RM procedure is a multidimensional variant of the Newton-Raphson algorithm suitable for finding the root of a function that contains noise.

King (2017) developed a modified version of the MH-RM procedure that improved upon the limitations of the root finding RM update by avoiding the need to solve for the inverse of the Hessian matrix. The modification led to improvements in both computational speed and accuracy of parameter estimates. Moreover, when the

dimensionality of the MGGUM model was increased to three, the modified MH-RM algorithm was relatively faster than a competing MMAP approach to item parameter estimation. Once item parameter estimates were obtained with the MH-RM method, King used an EAP procedure to calculate estimates of θ_j.

1.2.1.4 Advantages of EAP estimates of person parameters. In all three methods of estimating MGGUM parameters performed to date, EAP estimates of person parameters have been derived. This state of affairs is due as much to practicality as it is to statistics. With respect to the former, it has long been known that the posterior likelihood of person locations in the univariate GGUM often lacks a single-peak (Roberts & Laughlin, 1996). Therefore, any procedure designed to find the maximum of that posterior likelihood runs some risk of identifying a local, rather than global, maximum. In contrast the EAP procedure does not attempt to find the maximum, but rather, the mean of the posterior distribution for an individual's location on the latent continuum. Thus, it avoids the multimodal behavior of the likelihood altogether. The statistical benefits of the EAP technique are that it exists for any response pattern and, if the prior distribution for the parameter(s) is correct, then the estimate will have the lowest root mean squared error (Bock & Mislevy, 1982) in the population. For these reasons, the EAP estimate of person locations has been preferred among GGUM and MGGUM researchers.

When using the MCMC approach to parameter estimation in the MGGUM, obtaining an EAP estimation of an individual's location in the latent space is obtained simply by averaging the values drawn for the location in the iterations following the burn-in. In contrast, with both the MMAP and MH-RM approaches, the item parameter

estimates are treated a known and fixed following convergence of the algorithm. These values are used along with the item responses, and prior distribution to derive the EAP estimate. In particular, numerical quadrature (i.e., numerical integration) is used to develop the mean of the posterior distribution for each person location coordinate as follows:

$$\hat{\theta}_{jd} \approx \frac{\sum_{q_d=1}^{Q_d} \dots \sum_{q_2=1}^{Q_2} \sum_{q_1=1}^{Q} A_{qd}\, L(\boldsymbol{X}_j | A_{q1}, A_{q2}, \dots, A_{qd}) \mathrm{W}(A_{q1}) \mathrm{W}(A_{q2}) \dots \mathrm{W}(A_{qd})}{\sum_{q_d=1}^{Q_d} \dots \sum_{q_2=1}^{Q_2} \sum_{q_1=1}^{Q_1} L(\boldsymbol{X}_j | A_{q1}, A_{q2}, \dots, A_{qd}) \mathrm{W}(A_{q1}) \mathrm{W}(A_{q2}) \dots \mathrm{W}(A_{qd})} \quad (2)$$

Where A_{qd} is a quadrature point on dimension *D*, W(A_{qd}) is the density of the prior distribution at point A_{qd}, and the conditional likelihood of the response vector for person j is given by $L(\boldsymbol{X}_j | A_{q1}, A_{q2}, \dots, A_{qd})$**.** The approximation of the integrals via quadrature in (2) can be done rapidly (Muraki & Carlson, 1995).

1.2.2 Collateral Sources of Information for Parameter Estimation

Inclusion of external data into IRT models is a topic of interest for psychometricians who attempt to relate the response process to covariates or data other than the item responses themselves. Research on this topic has spanned different applications ranging from the analysis of a testing environment (Wang & Hanson, 2005; Cho & Bottge, 2015; Li, Jiao, & Macready, 2016); differential item functioning (DIF; Tay, Huang, & Vermunt, 2016; Liu, Magnus, & Thissen, 2016); modeling response times in conjunction with responses (Fox, Entink, van der Linden, 2007); and computer based testing (Widiatmo & Wright, 2015) to name a few. Current applications which incorporate external information into IRT models generally have one of three forms:

conditioning on the external information during estimation of item parameters, conditioning on such information during estimation of the person parameters, or conditioning on it when estimating both types of parameters. In any application, the goal is to better model some functional relationship between the item and person by way of the covariate.

One method of incorporating covariates into the IRT framework is conditioning on it when estimating item parameters. This can be accomplished by reparametrizing commonly used IRT models to incorporate the external variable, which alters the value of one or more item parameters. Mislevy and Sheehan (1988) provided several examples of incorporating covariates into an IRT model within the context of marginal maximum likelihood. They distinguished between cases where sampling of persons and items was independent of the covariate and those in which they were dependent. In the former case, the covariate could be ignored, but more information about item parameters could be obtained by including the covariate in the model. In the later cases, failure to include the covariate in the model could lead to biased parameter estimates. Other popular examples of using collateral information when estimating item parameters include DIF models which provide different estimates of item parameters on the basis of covariates. One of the more recent DIF models proposed by Tay, Huang, and Vermunt, (2016) examines DIF as a function of one or more covariates that is/are introduced into a parametric IRT model such as a 2-PLM. Similarly, another interesting IRT model for DIF has been proposed recently by Liu, Magnus, & Thissen, (2016). This model, like many before it, directly incorporates a categorical covariate to produce different estimates of item parameters between reference and focal groups. It is unique in that it only assumes

response probabilities are a semiparametric function of the latent trait and covariate rather than some parametric form.

Other models have incorporated collateral information into an IRT model to estimate person parameters and/or properties of alternative person distributions. A fairly recent example is provided by the work of Li, Jiao, & Macready, (2016). These authors developed a latent mixture IRT model within the Rasch framework that utilizes collateral information to estimate latent ability in both respects. First, collateral information, typically in the form of a continuous variable(s), is used to predict the latent trait for a given person in each possible latent class using a linear regression equation. These latent trait equations are used within a mixture of *g* alternative Rasch models. Second, collateral categorical information about the respondent is used to predict the probability of membership in each of the *g* latent classes. Research by Usami (2011) provides an interesting example using collateral information to estimate latent traits in the GGUM. The model makes use of two different sets of collateral variables. The first is a set of continuous random variables that are used to specify *P* orthogonal latent factors in the traditional exploratory factor analysis sense. The second set of *Q* collateral variables is simply treated as observed covariates (measured without error). The latent trait for each respondent in the GGUM is predicted by a linear combination of the respondent's *P* is latent factor scores, the respondent's *Q* observed covariates and a random error component. All parameters required for prediction of the latent trait along with all GGUM item parameters are estimated simultaneously using a Markov chain Monte Carlo method.

Other models in the literature incorporate collateral data into IRT models that are used to estimate both person and items parameters. For example, Wang and Hanson (2005) used item response time as a predictor in a 3-parameter logistic IRT model (3-PLM). In addition to the traditional parameters estimated in the 3-PLM, they also estimated a "slowness" parameter for each person and for each item. All other things being equal, the probability of a correct response in their model decreases as either of these slowness parameters increases. An alternative means to incorporate response time into an IRT model was proposed by Fox, Entink, van der Linden, (2007). These authors simultaneously calibrated two models - one for item responses and another for item response times - using a hierarchical Bayesian (MCMC) technique. Each of the models contained person and item parameters, albeit for different latent continua. In the Fox et al. (2007) method, item responses were explained using a 3-PLM whereas, item response times were simultaneously modeled using a lognormal distribution. The 3-PLM contained the traditional person ability and item slope/difficulty/pseudo-guessing parameters. The lognormal distribution for response times was parameterized with a different set of person and item parameters that reflected a latent speediness continuum. The two continua were brought together by assuming that person parameters from each model followed a multivariate normal distribution with an estimated centroid and variance-covariance matrix. These covariances provided information about the linear relationship between individual ability and speed. Similarly, the item parameters from the 3-PLM and the lognormal distribution were also presumed to follow a multivariate normal distribution, and the corresponding variance-covariance matrix provided more information relating the two continua.

All of these approaches to incorporating collateral information into IRT models share a common thread: modeling sound theoretical relationships between the collateral data source and its relationship with the latent trait and items characteristics. The study proposed here seeks to incorporate information about neural activity into the estimation of person parameters in the MGGUM on the basis that the response process for preference items has a predictable neural correlate that is a function of parameters in the MGGUM. This information will be incorporated into the estimation of the latent trait by establishing a second corresponding model for the functional relationship between the neural correlate and the metric distance between the locations of a person and item/stimulus that the unfolding response process is predicated on. This system of simultaneous equations will be solved in the EAP estimation procedure in tandem for determining values of θ_{jd} utilizing additional information outside of the MGGUM. This author is not aware of any attempts to incorporate information from neural activity into the estimation of IRT parameters to this date. The study proposed here stands to be the first of its kind to expand assessment utilizing physiological information from the brain.

In some respects, the method proposed for this dissertation is similar to that from Fox et al. (2007) in that item responses will be predicted with an IRT model whereas neural activity will be explained simultaneously using a different (regression) model. However, the proposed application presumes that both types of data are a function of the same latent variables; namely, θ_{jd} and δ_{id} as opposed to person and item parameters from two distinct continua. Moreover, the dependence of item responses and neural activity on the same latent parameters will allow for more general structural relationships that better explain the correlation between these observed variables.

1.3 Background (Analysis of Functional Magnetic Imaging Data)

Functional magnetic resonance imaging (fMRI) data comes in the form of a time series across successive images (referred to as "volumes" for the purpose of statistical analyses), which are collected throughout a scanning session. This type of data is special in that it not only spans across time but is also distributed spatially in nature. The time series is recorded in a "voxel" or a 3-dimensional section of the brain typically on the order of $1mm^3$ to $3mm^3$in size depending on the power of the scanner being used. Thus, the time-series is recorded for each voxel within each volume. The volumes are constructed through encoding rapidly collected slices (echo time, or TE is roughly 30 milliseconds for most studies), corrected for timing, to construct the final image. Functional scanning sessions typically first have a 4-5 minute structural scan which builds a three dimensional structure of white and grey matter in the brain. This serves as the basis for overlaying the functional time-series collected during the rest of the session, where the focus is instead on modeling the blood oxygenation level dependent (BOLD) hemodynamic response in the brain. The hemodynamic response is a result of neurons and other cells firing in the brain, and blood rushing to the area to restore energy to the cells. This blood flow forms the basis for the functional signal recorded in the time-series of fMRI data, and correlates with neural activation observed in fMRI studies (Logothetis, 2003).

There are a number of steps involved in preparing fMRI data for analysis. These preprocessing steps may vary from study to study depending on the specific goals, but in large part consist of several quality assurance steps. The first is slice acquisition time correction, which accounts for the difference in time between each slice of each volume

measured, and corrects it to assemble the full volume. This usually involves specifying the method in which the scanner collects the slices (ascending, descending, or interleaved) so that preprocessing software such as AFNI (Cox, 1996; https://afni.nimh.nih.gov/) or SPM (Friston, 2003; http://www.fil.ion.ucl.ac.uk/spm/) will apply temporal interpolation to the functional signal to determine the value of the time series. Once the timing is accounted for, the functional time-series is coregistered with the structural scan to ensure a proper spatial interpolation of the signal. During this process corrections for head motion in the scanner can be applied, as head motion is measured in the scanner six different ways. Coefficients for movements on the x, y, and z planar dimensions are calculated alongside roll, pitch, and yaw of the head for each image during this process and are appended to the design matrix to account for these movements. These coefficients assist in correction during preprocessing, but also provide an input into statistical models of the time series to reduce noise in the data related to movement. If a subject's head movement is too extreme (even as small as < 3 mm), the data may have to be discarded entirely, as even small movements cause spatial displacement of the BOLD signal (Spisak, 2014). During preprocessing, the researcher may choose to implement a smoothing technique which averages signals spatially across neighboring voxels called spatial filtering. There are numerous benefits for doing this in terms of signal detection and reduction of false positives (Poldrack & Farah, 2015), but localization of the signal is sacrificed and it may in some cases increase the autocorrelation present in the data (Zarahn, Aguirre, & D'Esposito, 1997). Furthermore, the amplitude of the signal in any of the regions in which spatial smoothing is applied may be dampened. If the primary measure of interest involves signal amplitude or

localization, heavy spatial smoothing is not recommended (Poldrack & Farah, 2015). Temporal filtering may also be applied in instances where the researcher knows the specific frequency of a signal they are looking to detect, to further increase the signal-to-noise ratio by filtering out nuance signal (Zarahn, Aguirre, & D'Esposito, 1997; Woolrich et al., 2001).

Once the data are preprocessed, the most common analysis technique of the fMRI time-series involves utilizing a massively univariate technique called statistical parametric mapping (SPM; Friston et al, 1994a, 1994b). SPM employs a general linear model (GLM) which can be written in matrix form as:

$$\begin{aligned} \mathbf{Y} &= \mathbf{X} \cdot \boldsymbol{\eta} + \mathbf{D} \cdot \boldsymbol{\gamma} + \mathbf{e} \\ &= \mathbf{G} \cdot \boldsymbol{\beta} + \mathbf{e} \end{aligned} \tag{3}$$

Where **X** is a NxK design matrix containing the modeled hemodynamic response for K events (e.g., presentations of stimuli) across N time points, and **D** is a NxJ matrix which parameterizes J other regressors desired in the model, most commonly motion correction parameters for head movement, or in the case of the current study, information about stimulus properties for covariation (see also: Bezdek, 2015). **Y** is a Nx1 vector of time series across N images (time) regressed onto this model producing a Kx1 vector $\boldsymbol{\eta}$ and Jx1 vector $\boldsymbol{\gamma}$ which contain regression weights that relate the experimental and nuisance events to the neural signal. Together $\boldsymbol{\eta}$ & $\boldsymbol{\gamma}$ form the basis for the voxel-wise analysis relationships with neural signal $\boldsymbol{\beta}$ and design matrix of events **G**, this is typically referred to as a first-level model or the "level-1" GLM.

The error term **e** in (3) for the first level model can be thought of as "noise" as in any the standard linear regression sense, however the nature of fMRI signal as a dependent measure, and the unique spatial correlation invoked by statistical parametric mapping cause a departure from traditional error term calculations. The spatial autocorrelation leads to the assumption that the error approximates a random field and follows a multivariate Gaussian distribution (Brett et. al., 2003). A "random field" addresses the spatial distribution of the signal across voxels. If the observed signal were random, then it would approximate a smooth surface, however if the signal was non-random, it would appear across voxels as a function of events (e.g., if a particular brain region was associated with a task). Therefore, the error term is a function not only of the signal, but also of the spatial resolution of the data, and is calculated using resels, which are a product of the spatial smoothness and non-random clustering of the signal detection in random field theory (Brett et. al., 2003). To the extent that the signal is non-random in a spatial sense, and the hemodynamic response is well modeled by the event, the residuals in the model will be low.

Parameters in the first level GLM are estimated using restricted maximum likelihood (Friston et al, 1994a, 1994b). Analysis of a time-series from a single voxel involves applying this GLM to assess differences between time points such as before and after viewing a stimulus or comparing levels of activation between sets of stimuli (Chen & Glover, 2015; Bezdek et al., 2015); assessing functional connectivity of brain regions (Shinkareva et al., 2008; Godwin et al., 2017); building profiles of whole-brain activation to different types of stimuli (Shinkareva et al., 2008); among a variety of other creative techniques.

In most all pursuits of data analysis in neuroimaging, the GLM is applied to every single voxel separately, and as such produces a large number of significance tests for model parameters. These tests are basic regression parameter tests of significance relating the effects in the model to the neural signal within each voxel. The null hypothesis for each test is that each of the observed beta's in the model are zero, which would indicate poor fit of the hemodynamic response to the timing of the event, and indication that no signal was present in the voxel at that time point.

The large number of univariate t-tests being conducted by applying the GLM to many voxels in this manner pose a unique type-I error rate problem that is a persistent issue in fMRI analysis (Hayasaka & Nichols, 2003; Bennet et al., 2009; Vul et al., 2009; Poldrack & Mumford, 2009; Poldrack & Farah, 2015). A number of different methods have been proposed to deal with the problem of multiple correction including imposing strict significance thresholds (Hayasaka & Nichols, 2003); Bonferonni corrections (Chen & Glover, 2015); cluster-based thresholding involving analysis of groups of voxels instead of single voxels (Woo, Krishnan, & Wager, 2014); and dimension reduction techniques such as independent components analysis (McKeown & Sejnowski, 1998; McKeown et al., 1998).

One of the more commonly used techniques involves establishing a region of interest (ROI) for analysis rather than analyzing the whole brain. This drastically reduces the number of voxels being tested by restricting the application of the GLM to a subset of voxels within the ROI (Geissler et al., 2007; Chen & Glover, 2015). ROI's for research can be established a number of different ways. There are established databases of ROI's such as the Harvard-Oxford Cortical and Subcortical Brain Atlas (Desikan et al., 2006),

and researchers may identify areas for experimental use from this database (Spisak, 2014). If the researcher has a hypothesis about which brain region or regions are associated with the brain process of interest, they can localize the analysis to just those areas. The regions can be generated from test subject data by observing voxels that exceed a threshold and applying that map to other subjects (Zarahn, Aguirre, & D'Esposito, 1997). ROI's may also be defined experimentally a number of different ways, so long as the researcher provides supporting evidence for the definition (such as showing that the region has a relationship with task) and is satisfied with observing a specific region of the brain rather than conducting a whole brain analysis. In practice, a "mask" is defined by the ROI coordinates and associated volume of voxels whose definition is assumed to be orthogonal to the task they are analyzed in. Any statistical analysis, including multiple comparisons, are filtered through this mask. The statistical model is not applied in voxels outside of the mask. Bonferroni corrections, cluster-based thresholding, or other techniques may then be applied within the mask to further correct for type I error rates.

1.3.1 Analysis of fMRI data with covariates

Including covariates in analyses of fMRI data can be done in several ways. There are two points in the analysis that a researcher may consider to enter a covariate into the model, at level one or level two. As described above, a level one model analyzes the time series within any given individual across voxels. A level two model runs ANOVA's across individuals to test for patterns of differences either within or across tasks. In a level two model, covariates typically take the form of person characteristics (e.g., gender or other person level attributes).

Covariates in a level one model can take several forms. The most common type of covariate entered into the design matrix is a temporal derivative of the signal designed to account for some of the variance related to the autocorrelation (Woolrich et al., 2001). Other types of nuance regressors may be entered into the model as well, such as detrended or orthogonalized motion parameters (Johnstone et al., 2006); a quantification of global signal to factor out (Spisak et al., 2014); among many others.

In addition to nuance regressors, the researcher may choose to account for stimulus features in the design matrix (Bezdek et al., 2015). By introducing stimulus features into the model, systematic variance associated with stimulus presentation that is unrelated to functional signal can be factored out of the time series. For example, Bezdek et al. (2015) accounted for ancillary visual properties of movies they showed in the scanner to isolate signal in cortical regions near the visual cortex that were relevant to attentional focus. No matter the nature of the covariate in the level one design matrix, nuance or not, the goal is to increase the ability to detect a signal of interest relevant to the task.

1.3.2 Signal-to-noise & Contrast-to-noise

Signal-to-noise (SNR) ratio in fMRI references the degree to which the signal of the BOLD response can be modeled relative to the noise in the data. The time series within each voxel in fMRI is modeled as a small fluctuation relative to the noise, and as such it is important for researchers to account for as much of the noise as possible. This is done in large part by correctly modeling the task data and nuance regressors in the level one model as described in (3). Contrast-to-noise (CNR) is a similar metric to SNR, but calculated slightly differently. SNR metric is calculated as the average signal amplitude

in a voxel divided by the variance of the residual across images[2], which is estimated as a function of the spatial sensitivity of the signal in random field theory from (3). In contrast, CNR is calculated based on the amplitude of the signal divided by the variance of the residual for a single image. Due to this, SNR is more of a global metric of quality while the CNR can change across the volumes. Both metrics give a measure of the quality of the fMRI data, but SNR metrics can fail to model the quality in small fluctuations in signal that are related to the task due to it being based on the average signal rather than the amplitude at any given point (Welvaert & Rosseel, 2013). In general, SNR & CNR indices give the researcher a measure of data quality, and have implications for clinical detection (Geissler et al., 2007) in addition to being a metric of general data quality in fMRI data analysis.

1.4 Integration of Data Modalities Using an Ideal-point Response Process Hypothesis

It stands to reason that there is a relationship between neuroimaging and behavioral data collected on the same task. The study proposed here seeks to investigate the extent to which these two data structures share information by virtue of their relationship to the proximity between a person and a stimulus in a multidimensional latent space. Moreover, to the extent to which this occurs, then simultaneously modeling both types of data can improve the prediction made for each. A set of simultaneous equations for the neuroimaging and behavioral data provides the basis for the following hypotheses:

[2] This is also sometimes referred to as the coefficient of variation.

H1: The distance between the locations of an individual and a stimulus in the latent space can be used to improve measures of contrast to noise in regions of interest for fMRI data analysis on the same task.

H2: Information about signal change in regions of interest can be used to improve EAP estimates of latent trait measures in the MGGUM by use of simultaneous equations for the behavioral response and the neurological response to a stimulus when both are modeled as a function of the latent trait.

If preference responses, as modeled by the MGGUM, systematically differ based on an ideal point response process, then the different neural signals that construct these preferences should also be dependent on proximity as well (i.e., dependent on $\theta_{sd} - \delta_{id}$). This person-item distance in latent multidimensional space is hypothesized to correlated with the neural activity, and consequently enable simultaneous modeling of these sets of data as a function of $(\theta_{sd} - \delta_{id})$. In short, inclusion of fMRI data may lead to better MGGUM person parameter estimates relative to preference responses alone, and will also yield a predictive model for that very fMRI data that is included. Furthermore, as person parameters improve, it will be possible to iteratively recalculate and improve the CNR associated with that fMRI data.

CHAPTER 2. METHOD

2.1 Behavioral Portion (Phase 1)

2.1.1 Experimental Design

A total of 81 different stimuli were included in the initial phase of the study. Each stimulus is a movie of a digital female model which rotates 360 degrees on a computer screen for 3.8 seconds so that the subject can view the model from all directions. Poser 8 software (https://poser.en.softsonic.com/) was used to create the 3D models based on DAZ 3D's virtual female model Victoria 4.2 (https://www.daz3d.com/victoria-4-2-base). PhilC's tape measure tool (https://www.philc.net/PTB_page3.php) was used to produce the virtual physical measurements of bust, waist, and hip size. The use of this tool ensured that the virtual measurements corresponded to the actual physical dimensions desired in the study.

The 81 models vary systematically with respect to weight nested within a given waist size –hip size combination, and the resulting 27 combinations are crossed with bust size. The nesting of model weight within a given waist size and hip size combination is necessary to maintain the realistic proportions of the models and prevents them from appearing cartoon-like. The three levels of weight used in each waist by hip combination represented relatively lower, moderate, and higher weight conditions, but these levels were operationalized in a slightly different fashion for each waist by hip size combination to account for realistic body mass distributions. Figure: 1 shows one of these models with the measurements of 36 inch bust, 30 inch waist, 40 inch hips, and moderate overall

weight. The 81 stimuli represented a 3(3 x 3) x 3 nested design (i.e., weight (waist x hip) x bust design).

Figure 3

"Victoria" 36 inch bust, 30 inch waist, 40 inch hips, moderate overall weight.

2.1.2 Measurement & Procedure

In phase 1, data were collected in three parts. The first two parts were presented to each participant in a random order, followed by the third part in which all participants filled out demographic information.

The first part involved collecting paired comparisons judgments in which participants rated the similarity of two models side by side on the computer screen. One model rotates first followed by the other, and the participant then provided a response. Ratings for similarity were on a 9-point integer scale (anchored by 1=Very Dissimilar

and 9=Very Similar). Collection of all pairwise judgments from a single participant would require 3,240 paired comparisons trials. Due to the impracticality of this experimental design, participants instead make only 162 judgments constituting one "block", and their responses represented $1/20^{th}$ of the full matrix of 3,240 similarities. Data from 20 blocks of paired comparisons were assembled to form a full matrix of similarity judgments for one "virtual subject". Blocks are constructed prior to data collection, and counterbalanced using a matrix sampling procedure for incomplete paired comparison designs (Davison et al., 2012). This technique is based on a Ross ordering algorithm (Ross, 1934) which minimizes timing and spacing errors in delivery of the different sets of 162 stimulus pairs corresponding to a single virtual subject. Additionally, the assignment of particular stimuli to positions defined by the Ross ordering was randomized for each virtual subject. Data collected in the paired comparison phase is not central to the analyses of this project, although participants did complete this portion of the experiment.

During the second part of the behavioral portion, stimuli were presented to the participant one at a time in a random order. Participants made attractiveness judgments for each stimulus in an asymmetrical fashion (i.e. the responses are 1 = "Unattractive"; 2 = "Somewhat attractive"; 3 = "Attractive"; 4 = "Very attractive"). This response scale was chosen through initial analysis of the data during a pilot test of the project, when it was shown that participants generally find the models to be attractive, and category usage of a "very unattractive" option was quite low. As such, the symmetrical very unattractive – very attractive scale was abandoned to increase the quality of the data. Data from this

phase of the behavioral portion served as an initial input into the MGGUM model to locate the subject in the joint multidimensional latent space with the stimuli.

In the final part of the behavioral session, all participants answered basic demographic questions along with questions pertaining to dating history, sexual preference, the number of male and female siblings and guardians present in the home where they were raised, and their experience with digital media in general (see Table 1 for a full list of the demographic questions). All experimental sessions were conducted in a controlled laboratory environment with 1-5 subjects per session.

2.2 Data Screening (Inclusion Criterion)

A data screening procedure was implemented between the behavioral and fMRI sessions with the goals of 1) increasing the heterogeneity of the individual latent preference locations sampled, 2) ensuring that at least some of the dimensions defining the latent preference space are salient to all participants, and 3) ensuring that every participant is located close to at least one stimulus in the preference space. These goals ensured that the procedure developed here can be applied to all locations in this multidimensional space the same way. Under the assumption that neural signal is a function of $(\theta_{sd} - \delta_{id})$, it is critical that participants utilize information from these dimensions in their decision making process, and are located close to target stimuli in that space as defined by the covariate of interest developed in this project.

Several procedures were involved in determining the quality of the data and whether a participant met these inclusion criteria for the neuroimaging phase of the study. The data screening procedure was developed to be quick and seamless from the

perspective of the participant, and did not take more than two minutes of their time after the behavioral portion (phase 1) of the study was completed.

The metric distance of the participant to each stimulus in the latent multidimensional space is central to how preference is modeled under the MGGUM. The data from the individual ratings of attractiveness was used to estimate person location parameters under the MGGUM using EAP estimation in real time after the participants completed phase 1 of the study. These data were pulled into SAS scripts which performed two procedures. The first procedure modeled the preference data as a function of the stimulus characteristics in a weighted unfolding model (Davison, 1983). The weighted unfolding model can be written as:

$$y_{is} = \sum_{d} w_{ds}^{2}(x_{id} - x_{sd})^{2} + c_{s} \qquad (4)$$

where y_{is} is the reversed scored attraction rating (indicating a lack of preference) for the *sth* subject to the *ith* stimulus, x_{id} and x_{sd} are item and person locations on dimension *d*, respectively. The stimulus coordinates were calibrated with an MCMC algorithm using data from 657 participants who previously completed a physical attraction measurement study in which the same stimuli were used (Roberts, Barrett & King, 2017). These stimulus coordinates were treated as fixed and known in (4). The y_{is} values are regressed onto the squared stimulus-person coordinate differences. The slopes (i.e., w_{ds}^{2}) from (4) represent the salience of each dimension to the individual when making preference judgments. If the weight for a given dimension is not statistically different from zero, then the dimension is not salient to the individual when making attractiveness judgments. The w_{ds}^{2} weights for each dimension obtained from this regression procedure were

included into a new weighted distance metric that downplays coordinate differences between a person and stimulus on a non-salient dimension.

Under the MGGUM, one can use a weighted distance as a measure of proximity of the individual and stimulus as follows:

$$\pi_{si} = \sqrt{\sum_{d} \alpha_{id}^{2}(\theta_{sd} - \delta_{id})^{2}} \tag{5}$$

In (5), the squared distance between the locations of the *sth* person (θ_{sd}) and *ith* stimulus (δ_{id}) on the *dth* dimension of the latent space is weighted by the squared discrimination of the stimulus, α_{id}^{2}, on that same dimension. These quantities are then summed across all dimensions. Although this distance metric is suitable for comparisons across individuals, it assumes that the importance of a given dimension with respect to making attractiveness judgments is constant across individuals. Violations of this assumption may have a substantial impact when calculating the distance of a single subject from each stimulus in a latent preference space. Covariation involving this distance is central to the within-subject analyses in this project, and as such, a new distance metric is developed here by incorporating the person weights from Davison (1983) into the model of the distance which is otherwise based on MGGUM parameters:

$$\omega_{s} = \sqrt{\sum_{d} w_{sd}^{2}\alpha_{id}^{2}(\theta_{sd} - \delta_{id})^{2}} \tag{6}$$

This individualized weighted distance (IWD) metric in (6) now accounts for both the discrimination of the stimulus and the degree to which a person's preference judgments

depend on proximity along a given dimension (w_{sd}^2). The weighted unfolding model, weighted distance, and IWD calculations can be performed very quickly during the screening procedure. Due to the within-subject nature of the analysis procedure developed here, the IWD served as a criterion for inclusion, and as the covariate in the level-1 fMRI GLM analysis inside of matrix **D** in (3)**.**

The selection criteria for inclusion into the second phase of the study involved three things. First, the salience weights for the individual dimensions for each participant as defined by Carroll (1972) and (4) were evaluated. A participant must have two statistically significant weights on different dimensions for inclusion. In other words, at least two dimensions must be salient for inclusion into the fMRI portion of the study. Secondly, as distance is central to the MGGUM, a participant must be operationally "close" to a subset of stimuli that are used in the fMRI portion of the study. As mentioned above, data from 657 participants who previously completed a different physical attraction measurement study were used to derive normative values of discrimination and location coordinates under the MGGUM for each stimulus. Traditional weighted distance under the MGGUM was calculated using (5). For inclusion into phase 2, the participant must have a smaller weighted distance than the average as defined by the normed sample for at least half of the stimuli used in phase 2. A final criterion that was used is a simple one; a participant was included into phase 2 only if their θ_{sd} values were not too similar to other participants already included in the scanning phase of the study. In other words, they did not overlap in the preference space with participants already included into the second phase. This is an effort to further prevent redundancy in sampling from the preference space, but is otherwise a minor concern. This assessment was conducted in

real time after the participant completed phase 1, and if the inclusionary criteria are met, the participant received an invitation to phase 2 of the study involving data acquisition in the scanner on the same task.

2.3 Imaging Portion (Phase 2)

2.3.1 Experimental Design

2.3.1.1 Stimulus Presentation. A smaller subset of 24 stimuli were utilized in phase 2 for a few reasons. Firstly, due to time restrictions in the scanner, it was not feasible to present all 81 original stimuli multiple times in a scanning session. Secondly, multiple presentations of a stimulus were required to get a stable measure of signal change from the functional imaging session associated with that stimulus. The stimuli chosen here were a subset in the lattice of 81 stimuli that were maximally distinct and representative of a variety of physical body types. Specifically, these stimuli spanned all waist-hip combinations across 2 of 3 weight classes, and 2 of 3 bust sizes (smallest and largest for each category, leaving out the moderate sizes).

Stimuli were presented in a random order without replacement within a blocked event-related framework using a jittered interstimulus interval sampled from an exponential distribution of 2, 4, and 8 seconds. Jittering the onset of the stimuli in this manner maximized the amount of times a stimulus could be shown in a scanning session while maintaining the ability to extract the shape of the signal in full (Boynton et al., 1996; Ollinger et al., 2001) as opposed to non-jittered designs. The blocked nature of each run ensured that each stimulus was shown the same amount of times. The presentation order of the stimuli was further counterbalanced within each block to

sample from two separate lists calculated based on a median split of IWD to each stimulus for a subject as a function of (6) (accounting for the salience of each dimension unique to the individual). This presentation method ensures that after a stimulus categorized as "among most ideal" based on IWD, the next stimulus will always be one from a list that is "less ideal". In summary, each stimulus is shown in a blocked random order up to 12 times during the session while counterbalanced on the IWD metric for the subject[3]

The timing of the presentation of stimuli is important in order to correctly associate the IWD with each volume in which the stimuli is presented. This timing accounts for not only the time needed to present, view, and respond to the stimuli, but it also accounts for the peak duration of the hemodynamic response, typically around 8-10 seconds. This jittered-onset timing was chosen to isolate the neural response to each stimulus, as the hemodynamic response measured sums linearly with few exceptions (Glover, 1999; Wager et al., 2005). As such the IWD was logically expected to sum linearly in the same fashion, and was included into the first level GLM by associating it with each volume whenever the corresponding stimulus event occurred. Consider the presentation of two different stimuli that are separated by 4 seconds in time. Table 1 below illustrates the generation of the model for the time series at each image as a function of both events and their respective covariates.

[3] While it is ideal that all participants complete 12 blocks of the study, several factors such as technical difficulties of rebooting the scanner computer mid-session; participants showing up late; or electing to end the study early themselves [one participant; completed 6 blocks, data included] all affect the total number of potential blocks of stimuli delivered.

Table 1

Parameterization of BOLD response and IWD as a function of stimulus presentation

fMRI Image	1	2	3	4	5	6	7
Time	2	4	6	8	10	12	14
Event Onset	Stim1		Stim2				
Bold to 1st stim	η_{11} +γ_{11}	η_{12}+γ_{12}	η_{13}+ γ_{13}	η_{14}+ γ_{14}	η_{15}+ γ_{15}		
Bold to 2nd stim			η_{21}+ γ_{21}	η_{22}+ γ_{22}	η_{23}+ γ_{23}	η_{24}+ γ_{24}	η_{25}+ γ_{25}
Bold as function of TR (image)	η_{11} + γ_{11}	η_{12}+γ_{12}	η_{13}+η_{21}+ γ_{13} + γ_{21}	η_{14}+η_{22}+ γ_{14} + γ_{22}	η_{15}+η_{23}+ γ_{15}+γ_{23}	η_{24}+ γ_{24}	η_{25}+ γ_{25}

Note: Generation of BOLD response as a function of stimulus presentation. η_{kj} represents the modeled hemodynamic response for the kth stimulus at the jth image, or point in the time-series; γ_{kj} represents the kth stimulus's individualized distance covariate for the jth image, or point in the time series after stimulus onset. Note that the orthogonalization of events in fMRI GLM sets the covariance between columns in the design matrix to be zero, leading to an additive effect of modeling the signal.

This model for the bold response at any given image is generated through (3); the covariate is being added to the design matrix **D** and sums linearly across events in the same manner as the hemodynamic response. This is made possible due to the covariance structure of all regressors being set equal to zero across the entire design (Friston, 2003; Ashby, 2011).

2.3.1.2 Procedure. Upon arrival to the scanning site, participants were trained on how to respond to the task using the button boxes. Each button represents a rating on the same attractiveness scale utilized in phase 1 of the study; participants were trained on which finger to use for which rating. Participants were also trained on when to respond to each stimulus. During the imaging portion of the study, participants were able to provide ratings to each stimulus while the stimulus is rotating on the screen and up to one second after. This is optimal for saving valuable scanning time. Participants were also told about how to minimize head movement during the scanning session. Foam blocks were utilized

around the head area for the participants comfort and to minimize this potential confound. Total scanning time lasted no longer than 50 minutes for 12 presentations of each stimulus.

2.3.2 Scanning Parameters & Data Preprocessing

Data acquisition utilized the on-site 3-Tesla Siemens Trio Magnetic Resonance Imaging system using: gradient-echo T2*-weighted echo-planar images (EPI) to measure blood-oxygen-level-dependent (BOLD) contrasts; interleaved acquisition at a slice thickness of 3.5 mm with a repetition time (TR) of 2000 ms, and echo time (TE) of 30 ms; voxel resolution of approximately 3.2 x 3.2 x 3.2 mm.

Data preprocessing for this study followed a traditional approach. Preprocessing involved the inspection of the raw data for anomalies during the image reconstruction phase, slice timing correction for the interleaved acquisition, coregistration with the structural scan, and corrections for head motion. Data were manually rotated to a centered position on the anterior commissure after image construction, separately for each participant. Anterior commissure was chosen as a central neural structure to orient data rotation across participants for between subject analyses. A spatial smoothing kernel of $8mm^3$ was applied to the data, as the main measure of interest in the fMRI data for this project involves calculating signal change in regions of interest. This is useful to implement because without smoothing the changes in signal estimates across voxels can appear drastic and bias the estimates of signal change within a region. It is possible that any smoothing of the data will attenuate the amplitude of the signal to a degree, but employing no spatial smoothing of the signal at all could produce uninterpretable results (Stelzer et al., 2014).

2.4 Data Analysis

2.4.1 Regions of Interest Definition

Regions of interest (ROIs) were defined and masks were created for data analysis to reduce the search area for active voxels and increase the sensitivity for signal detection. Methods to construct the masks were derived from information-processing hypotheses related to the stimuli. It was thought that a participant could approach the situation in one of two ways: firstly that when viewing the stimulus, the person would have an automatic or 'quick' response to the stimulus and form their attractiveness rating without performing much conscious evaluation of the stimuli. The second hypothesis postulated that the participant would not have a 'quick' or automatic reaction to viewing the stimulus and instead would evaluate some physical characteristics about the stimuli in detail before forming their attractiveness rating. The first hypothesis represents a heuristic strategy that employs recruitment of one set of brain regions to activate the pleasure centers, while the second is a more bottom-up detail approach to formulate the same opinion. In essence these two strategies to formulate a rating would recruit different brain regions to perform the task. To satisfy these hypothesis, masks for data analyses were constructed from prior research on tasks involving the same type of judgment, as well as derived from comparisons of the physical characteristics of the stimuli to capture what these regions might be at the level of the individual subject.

2.4.1.1 I7 Anterior Cingulate Cortex ROI. The first ROI involved investigating brain structures that are commonly associated with attraction in neuroimaging research. Platek & Singh (2010) found patterns of activation in the right orbitofrontal cortex (rOFC), the anterior cingulate gyrus (ACG), and the lateral occipital cortex (LO) when showing stimuli portraying optimal waist-to-hip ratios to men during an fMRI session.

After initial investigation of the data, the I7 region of the ACG was chosen for analyses as other regions examined in the pilot study did not appear to be as consistently active, or share overlap with the region identified in Platek & Singh (2010). A template for the I7 region was sampled from the automatic anatomical labeling (AAL; Tzourio-Mazoyer et al., 2002) package for SPM12, which provides an ROI image based on data oriented in the standard MNI space (i.e., the standardized brain space developed from the Montreal Neurological Institute; Talairach & Tournoux, 1988; Evans, Collins, & Milner, 1992; Evans, et al., 1993; Mazziotta, et al., 1995) utilized in fMRI analyses. The exact ROI may be viewed in Appendix B.

2.4.1.2 Subject-level IWD Covariate ROI. A separate method for defining the regions of interest involved utilizing prior research on the theoretical framework of the unfolding response process to identify networks in the brain associated with the judgment. Utilizing the MGGUM as the response model, the IWD covariate corresponding to each stimulus was calculated using (6). The 24 stimuli were subsequently ranked based on this covariate and a median split was taken for each subject to form a contrast of the "most ideal" to "least ideal". A level-1 GLM was fit with no restrictions for threshold corrections ($p < .05$ uncorrected) with the exception that a minimum of 150 voxels must be active together in clusters for inclusion into the mask. This subject-level mask based on the covariate was accepted outright for this condition of the replication. Each subject mask may be viewed along with other ROI's in Appendix B.

2.4.1.3 Group-level WHR ROI. A second mask was established based on the comparisons made in Platek & Singh (2010). A level-2 GLM was conducted across subjects comparing smaller waist-to-hip ratios (WHR) to larger WHR's. Restrictions for

this mask included a mildly strict threshold correction ($p < .01$ uncorrected) with a minimum of 150 neighboring voxels being active to be considered a relevant cluster. This group-level mask was accepted outright for this condition of the replication and utilized across all 15 subjects. It follows then that the construction of this masks reflects the differential use of the waist and hip physical dimensions when forming attractiveness judgements of the stimuli. The group-level WHR mask may be viewed in Appendix B.

2.4.1.4 Masked Subject-level ROI. Another replication condition was analyzed in which the subject-level IWD mask discussed earlier was taken, and subsequently masked with relevant networks active when viewing the stimuli. In order to do this, a level-2 contrast was developed across subjects which compared stimuli "on" time to stimuli "off" time, with no regard for how ideal each stimulus was to each participant. Stimuli "on" time was defined as time occurring in the session in which a stimuli was presented with the same onset durations as other contrasts. The "off" time contrast modeled the time in between the stimuli. This contrast was performed with the criterion of $p < .01$ (uncorrected) and a minimum of 150 neighboring voxels to be considered a relevant cluster. This resulting SPM contained voxels primarily from the visual cortex but also contained some residual components in the limbic and motor systems (the full SPM may be viewed in Appendix B). MARSBAR (Brett et al., 2002) was utilized to combine the subject-level IWD ROI and the stimulus "on-off" ROI to produce a new ROI mask that contained only voxels involved with processing information about the stimulus in general, that were also unique to the subject. This replication was then performed at the subject-level with confidence that each ROI contained only voxels from networks

recruited when viewing the stimuli. All masked subject-level ROI's may be viewed in Appendix B.

2.4.1.5 M1 Motor Cortex ROI. A region of interest was defined as a control region for comparison to the hypothesized regions. The M1 motor cortex, also called the primary motor cortex region, was chosen due to its function being widely researched and identified. This region is responsible for controlling hand movement, and was chosen due to the signal extracted from the region could be reliably assumed to be unrelated to the preference judgment. The ROI was taken from Human Motor Area Template (HMAT; Mayaka, Corcos, Leurgans, & Vaillancourt, 2006) which contains separate ROIs based in standard MNI space for fMRI analyses for each component of the motor cortex. The M1 region was selected from this package for inclusion, and may be viewed in Appendix B.

2.4.2 Dependent Measures

2.4.2.1 – Percent Signal Change. The measure used to track a response to the stimulus in the fMRI session is percent signal change (PSC). The PSC is a reflection of the change in blood flow modeled by the hemodynamic response associated with a given event (i.e., presentation of stimulus). The calculation of PSC is as follows:

$$\beta(\%) = \beta_i * \left(\frac{\beta_{peak}}{b_m}\right) * 100 \qquad (7)$$

Where β_i is the beta relating the modeled hemodynamic response to the stimulus, β_{peak} is the maximum amplitude of the signal during the specified event, and b_m is the mean whole-brain signal derived from the constant associated with the run (block in which all stimuli are presented) during which the stimulus is shown. Therefore, a PSC value in (7) is obtained for each stimulus in every run. Since stimuli are shown up to 12 times (across

12 runs), up to 12 PSC values will be obtained and then averaged to get a more stable measure of PSC associated with each stimulus. This metric can be thought of as a measure of recruiting a particular brain region during information processing. As an example, a positive value for the PSC would indicate higher average blood-flow in the region, while a negative value would indicate a lower than average blood-flow. The when the hemodynamic function in response to a stimulus ends, there is a significant undershoot below the resting state as the signal 'fires' and moves to a new location in the brain. The theoretical leap is then made to determine what type of processing is occurring, which is usually associated with a common function or which the region is recruited. In the case of the present study, regions associated with processing information about waist-hip combinations, and bottom-up processing will be investigated (Corbetta & Shulman, 2002; Menon & Uddin, 2010 Platek & Singh, 2010).

Note that the PSC is the primary dependent measure in the second phase of the experiment. Participants will provide attractiveness ratings to stimuli while inside the scanner, and these ratings will provide partial evidence for validity of the selected brain regions by correlating the ratings with the PSC detected by the scanner. However, it is the relationship that PSC measures have with the IWD that is paramount. Moreover, the PSC is the physiological measure of blood flow in the brain that is being incorporated into the item response model. The attractiveness ratings provided by the participant during this fMRI portion of the experiment will instead be evidence of reliability and validity rather than a primary dependent measure of interest.

2.4.2.2 – Mean Square Error (fMRI GLM). The mean squared error term for the level-1 GLM was chosen as a way to monitor the quality of the signal change measured

as a function of the onset of the stimuli. As stated above, image quality can be measured as a function of the scanning session by calculating the average signal amplitude and dividing by the error term, or as a function of an individual image by taking the maximum amplitude of the image and dividing by the residual variance. One serves as a measure of signal detection quality for the session while the other serves at the level of the image. In either case, accounting for the residual variance is part of the function and the MSE used to calculate these statistics is considered here. The MSE is calculated within the search region of the ROI only, and thus is sensitive to not only viewing the stimulus but the spatial distribution of the network being examined as well. Larger values of the MSE indicate more residual variance in the model, and lower values of MSE indicate less.

2.4.2.3 – Regression Model Error Term. Another measure of how well the signal is being explained by the IWD covariate is to monitor the change in the error term of the regression equation during the iterative estimation procedure. The error term for PSC in the simultaneous equation procedure is modeled as:

$$\begin{aligned} \sigma_i &\sim \Gamma(.01, .01) \\ e_i &= {}^{1}\!/_{\sigma_i^2} \\ PSC &\sim N(\mu_i, e_i) \end{aligned} \tag{8}$$

Where μ_i is the mean value of signal change predicted by the regression equation for the stimulus, and e_i is the precision of that estimate. Due to the fact that e_i in (8) is a precision term in the OPENBUGS language, higher values represent more precision (less error) and smaller values represent less precision (more error).

2.4.3 Iterative Parameter Re-estimation Procedure

2.4.3.1 Overview. Initial data analysis includes getting the estimates of the participant's location in the latent space from the MGGUM using OpenBUGS software. The initial location estimates were derived from responses obtained from 81 stimuli in the laboratory section of the experiment. As such, the procedure outlined here aimed to improve upon this initial estimation through the addition of the external fMRI data. Following this, an initial GLM was also specified on the fMRI data to determine starting MSE values to assess signal-to-noise ratio (SNR) and contrast-to-noise ratio (CNR); tracking the general quality of the fMRI signal over the course of the procedure. The person location coordinates, and MSE values served as a starting point for an iterative parameter re-estimation procedure that was controlled via a batch command program in Windows.

The iterative parameter re-estimation procedure is shown schematically in Figure #4. The participant's initial EAP estimate was used to calculate a matrix of IWD values for all 24 stimuli using (6). These IWD values were calculated by MATLAB which were subsequently written into a level-1 within-subject GLM input file suitable for the SPM-12 program (Friston, 2003). Specifically, the IWD was associated with images in which the hemodynamic response for the stimulus occurred, and is then summed across events as shown in Table 1. Following the GLM, signal change in the ROI's were extracted using a MARSBAR (Brett et al., 2002) script, which derives this value based on the GLM parameter estimates from the preceding step.

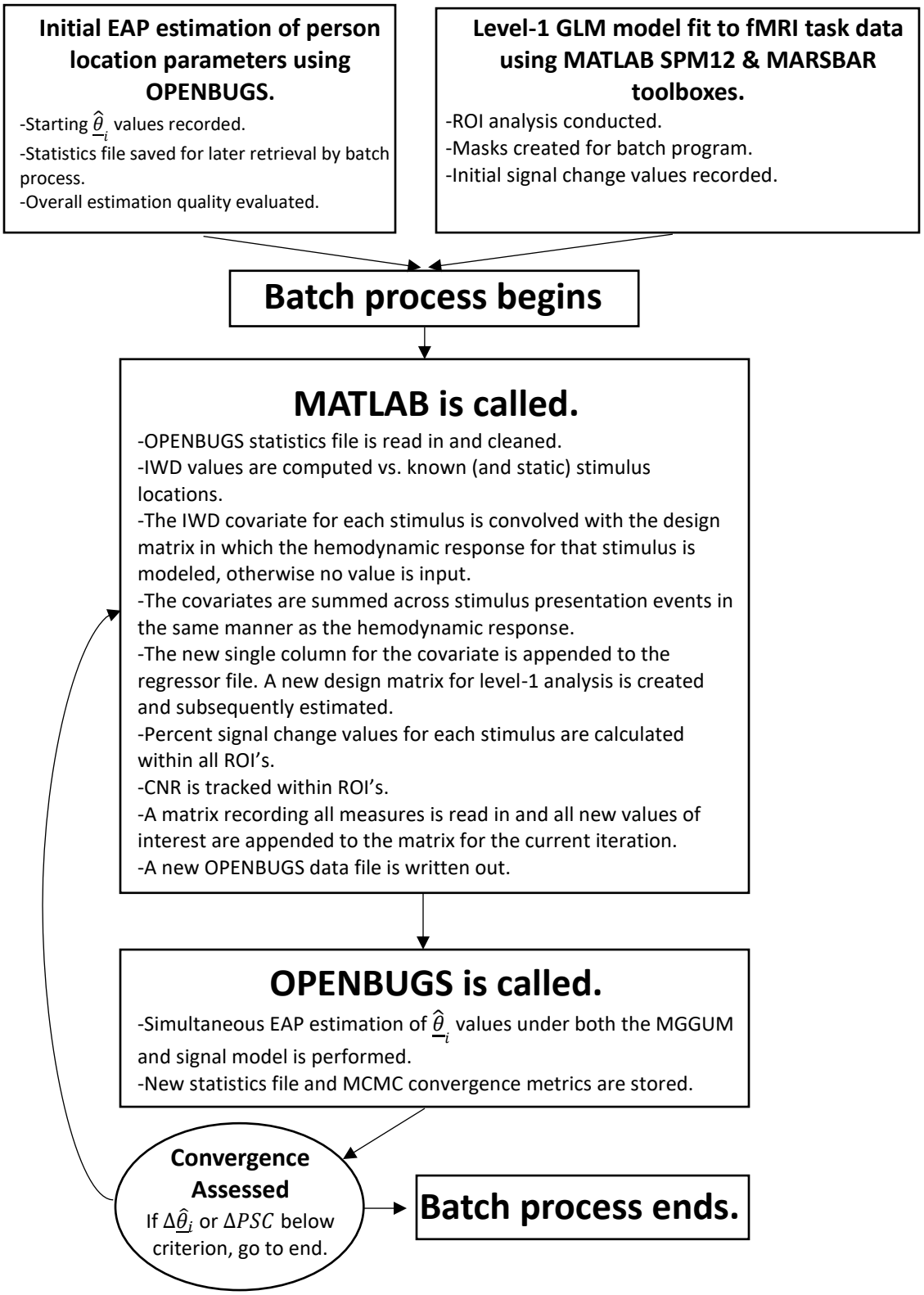

Figure 4

"Batch analysis procedure"

A MATLAB script then wrote out OpenBUGS code in the form of a text file containing the measures of percent signal change in addition to the participant's attraction ratings. The OpenBUGS code was then run by the parent script. It re-estimated the person's location in the latent space as a function of both the attractiveness ratings as modeled by the MGGUM and the signal change values derived from the fMRI data. The percent signal change values were then modeled as a function of the IWD values associated with each stimulus. The form of the second equation in this system is as follows:

$$\beta(\%)_s = \beta_0 + \beta_1\left(\sqrt{\sum_d w_{sd}^2\alpha_{id}^2(\theta_{sd}-\delta_{id})^2}\right) + \beta_2\left(\sqrt{\sum_d w_{sd}^2\alpha_{id}^2(\theta_{sd}-\delta_{id})^2}\right)^2 + \varepsilon_i \quad (9)$$

Where percent signal change is denoted as $\beta(\%)_s$. Note that, in (9), the known item parameters and person weights are fixed, and only θ_{sd} is estimated along with the regression weights used to predict $\beta(\%)_s$ in a linear and quadratic fashion. Initial testing on a single pilot subject suggested that the relationship between percent signal change with the individualized distance metric follows a quadratic trend across the brain regions discussed above. For four of the subjects, an additional cubic term was added to the model when the curvature of a smoothed spline plot for PSC and IWD indicated that it was appropriate. In this case, the corresponding regression weight was denoted as β_3.

A new latent trait estimate for the subject was calculated using the MGGUM simultaneously with (9), and then the estimate was used to recalculate IWD measures for each stimulus. These distances were again used in a GLM analysis followed by an

updated derivation of signal change. The process repeated until convergence is reached. Convergence was assessed by monitoring changes in the latent trait estimate on every iteration, and the algorithm terminated when the change in either the sum of the change across θ_{sd} or PSC for each stimulus was arbitrarily small (less than .05). For all participants, this procedure was run a minimum of two iterations after the starting values for the MGGUM location and level-1 GLM signal estimates were obtained.

2.4.3.2 MCMC Specifications. The MCMC procedure to produce EAP estimates of person location alongside estimates of regression parameters associating the PSC to the IWD covariate was performed with 5000 burn-in iterations before statistics were tracked. According to trace plots, estimates appeared to converge prior to the completion of the initial burn-in iterations, Five thousand more iterations were sampled in order to produce estimates for both the parameters of the MGGUM and the regression model parameters associating the IWD with PSC. An example trace plot is shown in Figure 5 below.

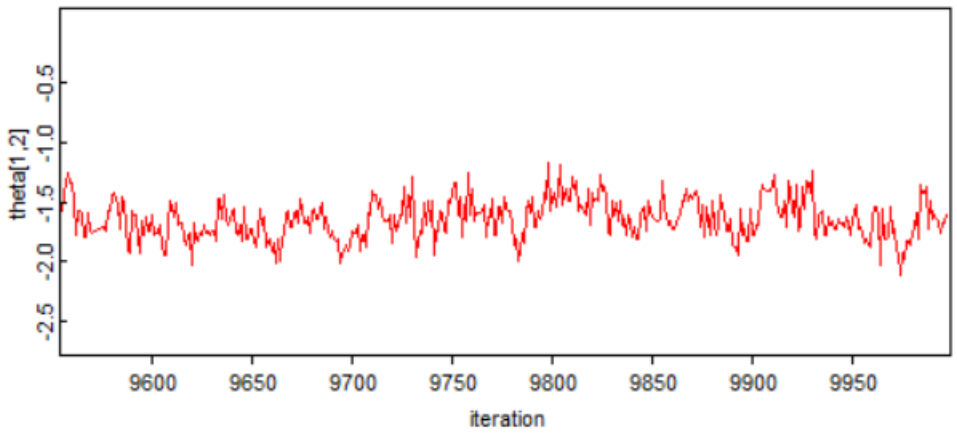

Figure 5

Example trace plot for estimation of θ_{sd}

When estimating the regression model parameters for the relationship between the IWD and PSC in the MCMC procedure, the loop only ran over the 24 stimuli shown during the fMRI portion of the experiment. Without this last safeguard, the mean value of signal change is substituted for each of the remaining stimuli and the regression parameters would be further flattened out towards zero. With this safeguard, the regression procedure is more similar to ordinary least squares regression.

Normal prior distributions for the MGGUM portion of the model were used for all θ_{sd} parameters (Roberts, Donoghue & Laughlin, 2000; Roberts & Shim, 2010), which were defined as:

$$\theta_{sd} \sim \mathrm{N}(0,1) \tag{10}$$

For the regression model, normal prior distributions were used for the beta weights relating PSC to the IWD covariate (Gelman, 2006), defined as:

$$\begin{aligned} \beta_0 &\sim \mathrm{N}(0,1) \\ \beta_1 &\sim \mathrm{N}(0,1) \\ \beta_2 &\sim \mathrm{N}(0,1) \\ \beta_3 &\sim \mathrm{N}(0,1) \end{aligned} \tag{11}$$

The signal change was derived in (7) above and modeled with the regression in (9).

CHAPTER 3. RESULTS & DISCUSSION OF PRIMARY ANALYSES OF DATA

3.1 Procedure overview

3.1.1 Participant Characteristics

Fifteen participants completed both the behavioral and fMRI portions of the experiment, and comprise the resulting data for the analyses presented in this section. Exactly 84 individuals were recruited to complete the behavioral portion of the experiment before the target of 15 subjects who met all of the inclusion criteria were accepted into the second phase. For the 15 persons who were accepted into the second phase, 14 completed demographic information; one subject's demographic information was lost due to a program crash in the behavioral portion of the study. Scanning sessions were scheduled as soon as time was available that matched the participants schedule; there was a range of 3 to 47 days (M = 17.53) between phase 1 and phase 2 of the study for these participants. The test-retest correlations for attraction ratings provided between the behavioral portion and the ratings provided in the first block of the fMRI portion ranged from -.13 to .79 (M = .39). Table 2 below shows these test-retest correlations alongside the number of days between each portion of the experiment, and how many fMRI blocks were completed in the second phase. The correlation between the test-retest values and days between session was .139 (NS). It should be noted that subject #6 had a uniform response vector in the fMRI portion of the experiment; all of their ratings were the highest category for every stimulus. The participant did however utilize multiple

response categories in the second block of the experiment. In order to calculate the test-retest correlation for this subject, data from the second block of the fMRI session was used instead.

Table 2

Subject Test-Retest Correlations, Time Between Sessions, and Blocks Completed in fMRI Portion of Study

Subject	Test-Retest Correlation	Days Between Sessions	Number of Blocks Completed in fMRI Portion
1	0.556	35	12
2	0.366	8	12
3	0.297	7	12
4	0.750	21	12
5	-0.132	34	12
6	.397	32	12
7	0.547	10	9
8	0.437	3	10
9	0.420	8	10
10	0.442	9	12
11	0.674	47	6
12	0.654	14	12
13	0.011	15	12
14	0.428	14	7
15	0.069	6	12

The test-retest of person location estimates from the MGGUM were evaluated between the laboratory and scanner sessions. Location estimates on four dimensions for each subject were calculated by performing EAP estimation of θ_{sd} using the MGGUM with the initial 81 responses in the laboratory, and then again with the response vector for the 24 stimuli taken from the first block of the fMRI session. The correlation of θ_{sd} across the trials was significant for the bust ($r = .36$, $p < .05$), waist ($r = .734$, $p < .01$), hip ($r = .54$, $p < .05$), and weight dimensions ($r = .463$, $p < .05$) suggesting a moderate level

of stability of the location of participants in the multidimensional space from the initial laboratory to the scanner sessions.

Participants ranged in age from 18 to 25 years old (mean age = 20.714), with five females and nine males reporting their information. There was a single freshman participant, four sophomores, five juniors, two seniors, and two graduate students. Fourteen of the participants were right handed, and one was left handed. All participants reported with normal to normal-corrected vision. The sample was predominantly Caucasian (57%) and Asian (21%) with one participant reporting Hispanic heritage and one reporting "other". Nine participants reported having at least one female sibling in the household while growing up, with two of those participants reporting more than one. The sample reported as predominantly "heterosexual" (85.7%) with one subject reporting as "bisexual" and one reporting as "homosexual". All participants reported having a female guardian in the household growing up. In addition to this, all participants reported "evaluating the attractiveness of other females in your daily life" at least "a moderate amount", with four participants reporting as "quite often". The sample characteristics did not exhibit any odd demographic patterns relative to the original physical attraction measurement study.

3.1.1.1 Inclusion Criterion & Starting Locations. All participants selected for inclusion into phase 2 of the study had a smaller than average MGGUM metric distance defined by (5) to at least 12 of the 24 stimuli used in phase two. The starting locations for the 15 participants used to calculate this distance to the stimuli utilized in the second phase are displayed below in Figure 6. The inclusion criterion of participants not overlapping in the preference space was assessed as data were collected. Some extreme

regions of the preference space on some dimensions were not represented in this study; neither were these same locations frequently seen in the 657 cases from the original physical attraction study. As such, the sample of 15 cases appeared to map well onto what was to be expected from a qualitative standpoint.

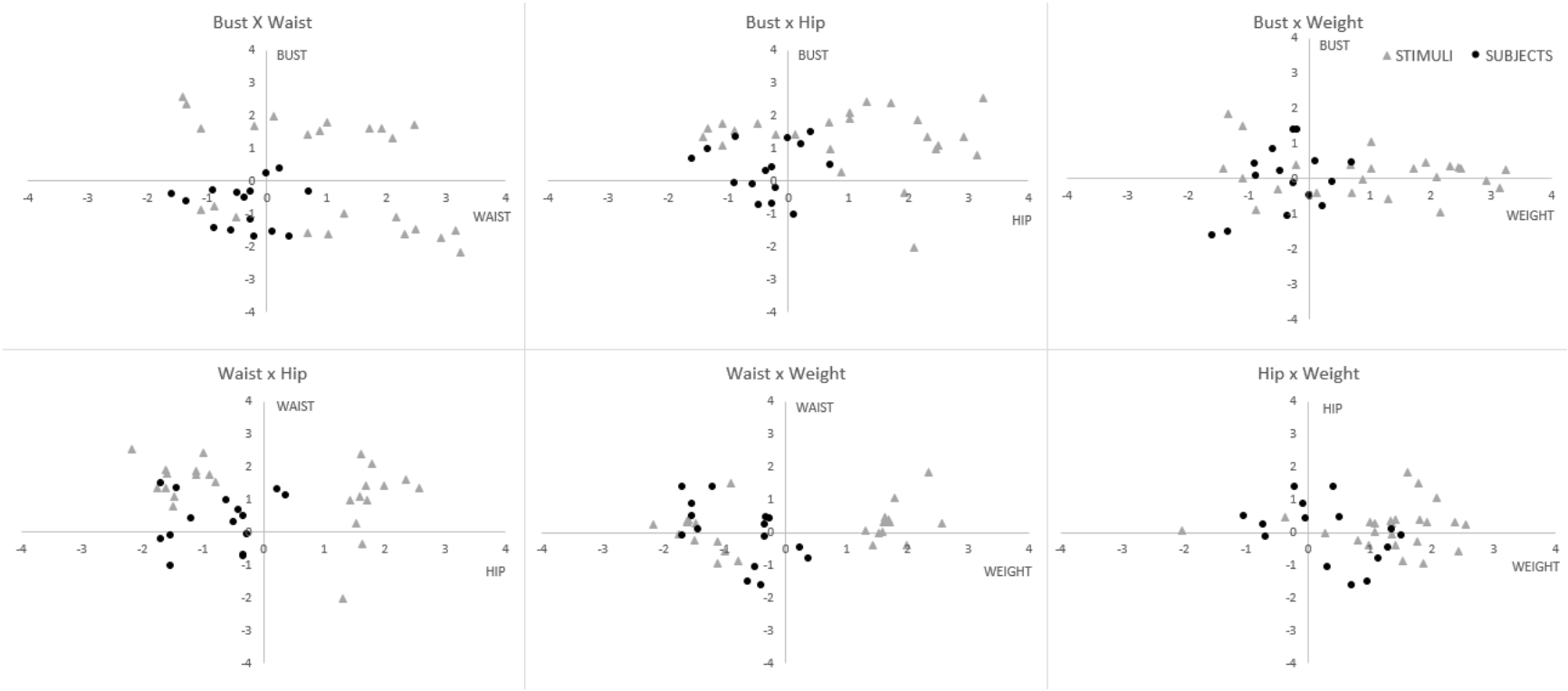

Figure 6

Starting locations for 15 participants (circles) relative to 24 stimuli utilized in phase 2 (triangles) across 4 dimensions.

Note: All subjects had a weighted distance defined by (5) that was smaller than the average to at least 12 stimuli.

For the 15 cases selected for inclusion into phase two of the study, all cases attended significantly to at least two dimensions according to the weighted unfolding model (Carroll, 1972; Davison, 1983). Within this, eight cases attended to two dimensions, five attended to three dimensions, and two cases attended to all four dimensions significantly. A visual display of dimensions attended to by subjects is shown here:

Table 3

Significant Dimensions Under Weighted Unfolding Model

Subject	**Bust**	**Waist**	**Hip**	**Weight**	**Total**
1		+	+	+	3
2		+		+	2
3		+	+	+	3
4	+			+	2
5	+		+		2
6	+	+			2
7		+	+	+	3
8		+		+	2
9		+	+	+	3
10			+	+	2
11	+	+	+	+	4
12		+	+	+	3
13	+	+	+	+	4
14	+			+	2
15			+	+	2
Total	6	10	10	13	

It is clear from Table 3 that there is appreciable variation in the set of dimensions that are attended to by each participant.

3.1.2 General Procedure Information

The iterative estimation procedure for simultaneous equations converged successfully across the multiple replications in which it was used. The procedure was repeated five times for each subject; once for each ROI. Ideally, this would yield a total of 75 replications (i.e., 15 subjects x 5 ROIs) of the estimation procedure, however, there were three participants (subjects 3; 5; 9) whose subject-level ROI's had no overlap with the network analysis from the group-level stimulus on/off contrast. Therefore, masks could not be created for these conditions and resulted in 72 total replications in which the estimation procedure could be performed. The estimation procedure converged successfully after the minimum number of iterations of 2 were performed for 67 out of 72 replications. Of the five that did not converge in the minimum number of iterations, all required one additional iteration. There were no major issues with running the procedure for any subject, and the program ran successfully each replication. The resulting overlay of predicted PSC values on top of observed PSC relationships with IWD generated as a result of the simultaneous equations procedure may be viewed in Appendix C.

3.2 In support of Hypothesis #1

3.2.1 Analyses of Residual Variance in fMRI GLM

In an effort to analyse the effect the procedure had on the fMRI quality metrics of signal-to-noise (SNR) and contrast-to-noise (CNR), the change in the mean square error

for the fMRI GLM was examined as the dependent variable. For all subjects, the value of the MSE was taken at both the start and the end of the procedure. Subsequently, a repeated measures analysis of variance was fit separately to each ROI to maximize the use of subject data as three subjects had no data for the 5th ROI. To account for this, a Bonferonni correction for multiple comparisons of (α / 5) was applied to each test.

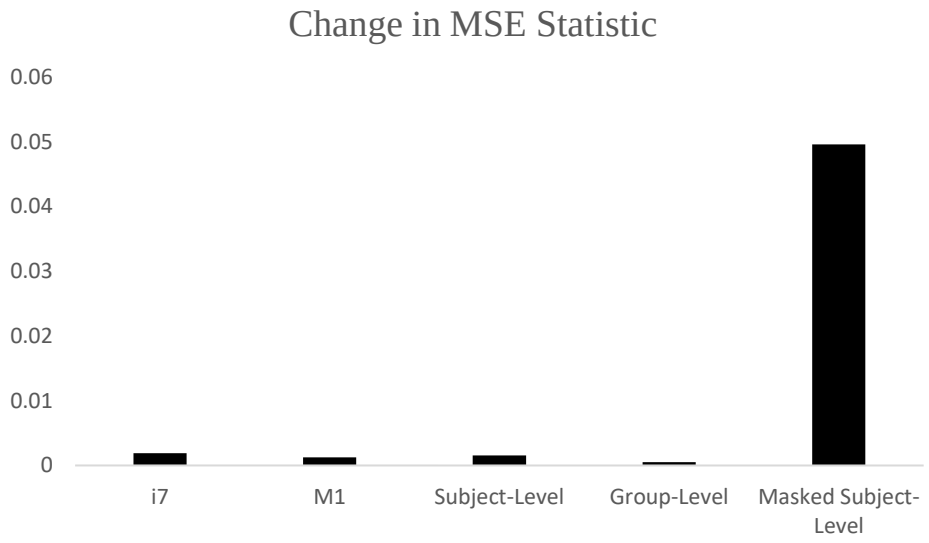

Figure 7

Average change of MSE statistic across five regions of interest

Note: Masked Subject-Level region driven by outlier.

Figure 7 above illustrates the scale and average change in the MSE statistic for the fMRI GLM's ran in the iterative estimation procedure. When examining the figure, it is clear that the scale of change is far too small (on the scale of only a few hundredths of a standard deviation) to highlight any effect the procedure might have had on the MSE and by extension, the SNR and CNR. No statistical differences were found in the i7 ROI ($F(1,14) = .75$, $p = .4011$); the M1 control ROI ($F(1,14) = 2.12$, $p = .1677$); the subject-level ROI ($F(1,14) = 1.00$, $p = .3343$); the group-level WHR ROI ($F(1,14) = .16$, $p =$

.6910); or the masked subject-level ROI (F(1,11) = .93, p = .3598). For the masked subject-level ROI region, the average change value was driven by a single outlier; when excluding the outlier, the distribution of the MSE statistic in this region was similar to the other four.

3.2.2 Analyses of Residual Variance in Regression Equation

A separate approach to analyse the effect the procedure had on the quality of estimation in the fMRI GLM is to look at how well the signal change for each stimulus is being explained by the IWD covariate. Under the assumption of hypothesis #1 that the signal from the onset of the stimulus is related to the subject's location in the multidimensional space, the signal should be explained better once the procedure converges to (more informed) parameter estimates. This, in turn, should be accompanied by an increase in the precision term (e_i) as defined by (8). The precision term represents the reciprocal of the residual variance in the regression, and serves as the dependent measure for this analysis. It is estimated as a byproduct of the Bayesian procedure implemented in the current model. Similar repeated measures GLM's were conducted on each ROI to assess this query and similar results were found.

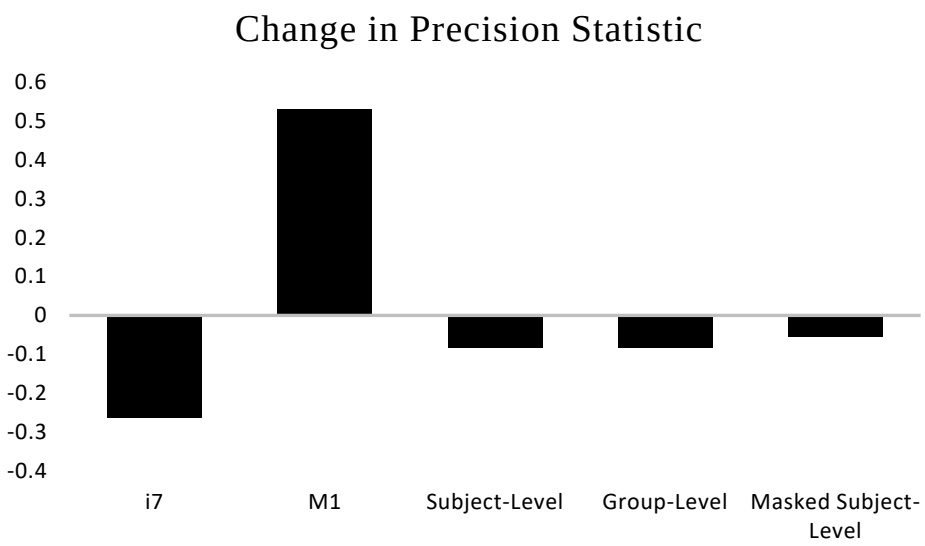

Figure 8

Average Change of Precision Term in Regression Component of Procedure

As can be seen in Figure 8 above, the average level of change in the precision statistic does not support the hypothesis. There was no significant difference observed in the i7 ROI ($F(1,14) = .90$, $p = .3574$); the M1 control ROI ($F(1,14) = 1.80$, $p = .2005$); the subject-level ROI ($F(1,14) = .35$, $p = .5617$); the group-level WHR ROI ($F(1,14) = .07$, $p = .7968$); or the masked subject-level ROI ($F(1,11) = .30$, $p = .5936$). On average, only the M1 control region saw an appreciable average change in the precision term in the direction of the hypothesis, albeit not significantly. For all other regions, the signal extracted from the ROI's was not explained better on average as a result of the procedure. A discussion on the M1 control region and its relationship to signal extracted from this region will be treated in the limitations to the study below at the end of chapter 4.

3.3 In Support of Hypothesis #2

3.3.1 Analyses of θ_{sd} Estimation Precision

To examine the effect that the iterative estimation procedure had on the precision of EAP estimates for the MGGUM portion of the experiment, the starting and ending values of standard errors for each θ_{sd} were utilized as the dependent measures in a series of repeated measures analyses. The same repeated measures GLM framework was applied to each ROI separately much like the analyses on the quality metrics for the fMRI portion of the experiment. Similar to the previous section, a Bonferonni correction of (α / 5) for multiple comparisons was applied to each of these tests to account for the fact that the same model was tested in each of the five ROI's. The principle difference here is that the dimension corresponding to each estimated theta coordinate was included as a within-subject factor. The design of this analysis was a 2 (time) x 4 (dimension) fully within-subjects repeated measures ANOVA on θ_{sd} standard errors. Therefore, a given dimension could be estimated more or less precisely, and it could interact with any change in standard error observed over the course of the estimation procedure.

There are two different approaches to take when examining the effect a within-subject factor, which is to utilize the multivariate approach instead of the univariate approach. The multivariate approach to repeated measures analysis has several advantages in this instance. Firstly it does not require the assumption of sphericity in the variance-covariance matrix for repeated measures (O'Brien & Kaiser, 1985). Secondly, as the violation of compound symmetry increases, the power of the multivariate approach increases relative to the univariate approach (Mendoza, Toothaker & Nicewander, 1974). In the results reported here, examining the sphericity assumption for each of the i7 (χ^2 (5) = 82.178, $p < .001$); M1(χ^2 (5) = 81.975, $p < .001$); subject-level (χ^2 (5) = 90.165, $p < .001$); group-level WHR (χ^2 (5) = 89.412, $p < .001$) and masked subject-level (χ^2 (5) =

55.542, $p < .001$) revealed that it was violated in each five ROI's analyses for the within subjects effect of theta dimension..

Given the evidence discovered in the initial examination of this within-subjects effect, and the violation of sphericity in the sample data, it is assumed that the sphericity does not hold in the population. Therefore, it is appropriate to assume that the Type I error rates of the corresponding univariate tests are inflated and inappropriate for examining these effects. Moving forward in these analyses, only the multivariate effect will be considered for the within-subjects factors of these designs: the time factor; the theta dimension; and the interaction of that factor with time were analyzed using the multivariate test Wilks' Lambda.

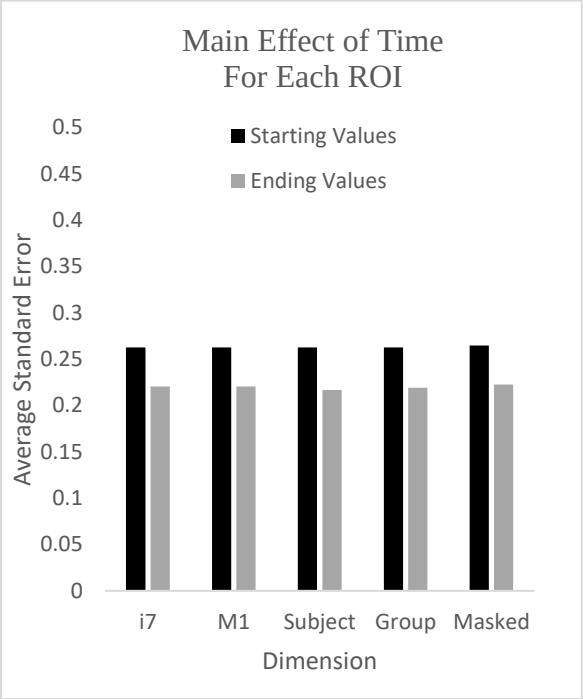

Figure 9

Main effect of time is significant while controlling for Type I error.

The average standard errors for θ_{sd} for each region of interest and dimension can be found in Table 4 below, and displayed graphically for the main effect of time in Figure 9 above. The reader will note that all ROI's have the same starting standard error values by design for the within-subjects effect. There were significant main effects of the within-subjects factor of Time (i.e., before vs. after the iterative estimation procedure) that held under the Bonferonni correction put in place for multiple comparisons across each of the ROI's. The i7 (Λ = .560, F(1,14) = 10.97, p = .0051); M1 (Λ = .540, F(1,14) = 11.91, p = .0039); subject-level ROI (Λ = .517, F(1,14) = 13.05, p = .0028); group-level WHR ROI (Λ = .558, F(1,14) = 11.09, p = .005); and the masked subject-level ROI (Λ = .488, F(1,11) = 11.52, p = .006) All exhibited an effect on the precision of estimation of theta across the time course of the procedure.

Table 4

Mean and standard deviation of θ_{sd} standard errors from the start and end of the procedure, for each ROI and dimension of theta.

ROI	Dimension	Start of procedure (Time 1)		End of procedure (Time 2)	
		MEAN	SD	MEAN	SD
I7 Hypothesized Region	Bust	0.212	0.021	0.208	0.025
	Waist	0.179	0.021	0.179	0.019
	Hip	0.283	0.177	0.240	0.126
	Weight	0.378	0.269	0.252	0.112
M1 Control Region	Bust	0.212	0.021	0.208	0.025
	Waist	0.179	0.021	0.178	0.020
	Hip	0.283	0.177	0.238	0.124
	Weight	0.374	0.269	0.256	0.114
Subject Level Cluster	Bust	0.212	0.021	0.205	0.024
	Waist	0.179	0.021	0.176	0.018
	Hip	0.283	0.177	0.237	0.132
	Weight	0.374	0.269	0.247	0.108
Group Level WHR	Bust	0.212	0.021	0.204	0.026
	Waist	0.179	0.021	0.175	0.017
	Hip	0.283	0.177	0.239	0.131
	Weight	0.374	0.269	0.257	0.107
Masked Subject Level	Bust	0.212	0.021	0.206	0.029
	Waist	0.178	0.021	0.174	0.018
	Hip	0.297	0.177	0.254	0.186
	Weight	0.369	0.269	0.255	0.114

Examining the multivariate effects for the within-subjects factor of theta dimension revealed a significant main effect in each of the i7 (Λ = .288, $F(3,12) = 4.87$, $p = .0015$); M1 (Λ = .283, $F(3,12) = 10.12$, $p = .0013$); subject-level (Λ = .260, $F(3,12) = 11.35$, $p = .0008$); group-level WHR (Λ = .270, $F(3,12) = 10.97$, $p = .0064$) and masked subject-level ROI's (Λ = .270, $F(3,9) = 8.08$, $p = .0064$) which held under correction for multiple ROIs using the Bonferonni correction on alpha. Figure 10 below illustrates the standard error for each theta dimension, averaged across the time course of the procedure,for each ROI. Each of the five ROI's have the same starting standard error contributing to the average, and the similarity in the resulting plots indicates that the main effect of theta dimension was comparable across ROI's.

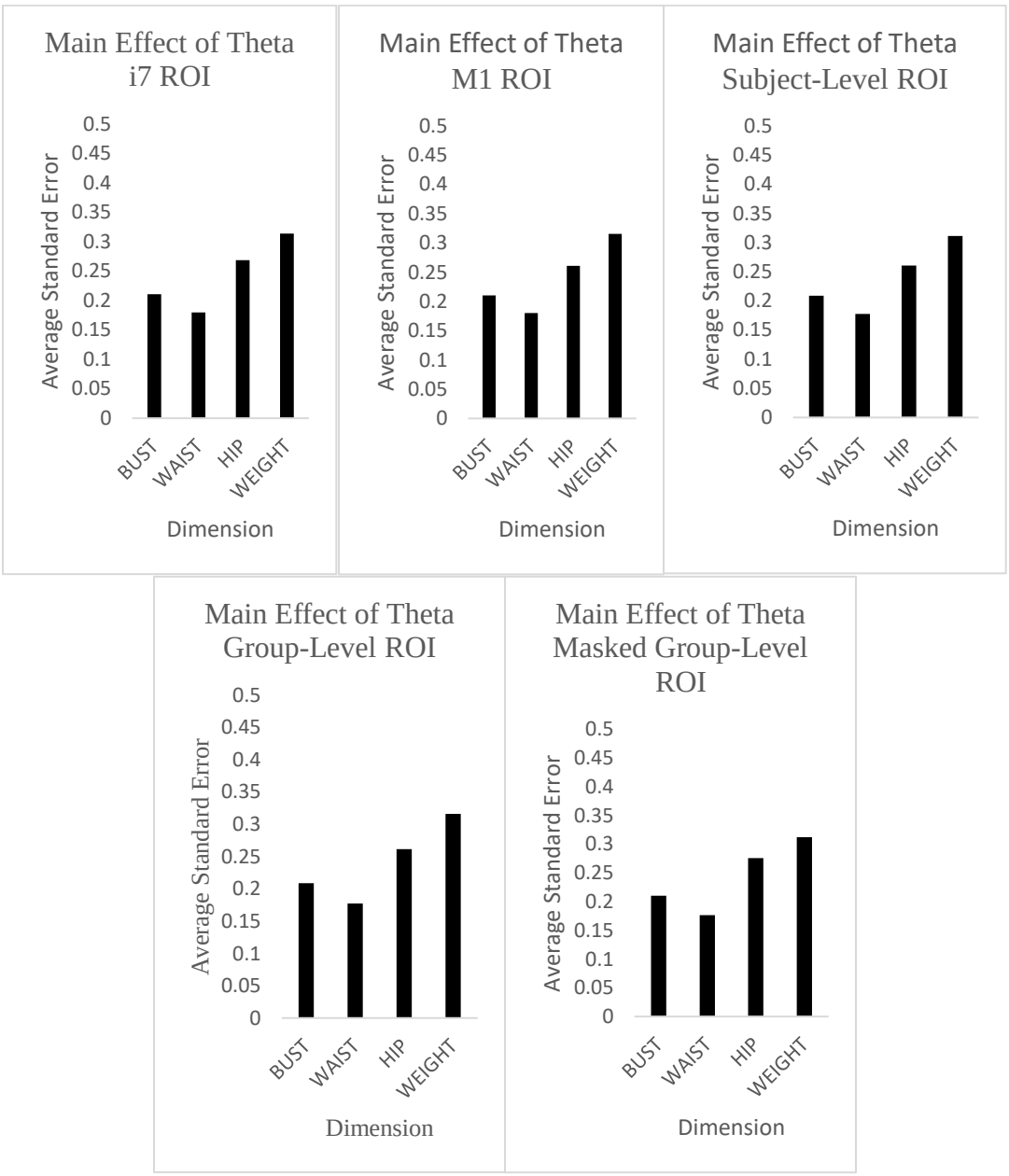

Figure 10

Significant main effect of the within-subjects factor of theta dimension for each ROI

In contrast to the within-subject main effects, the interaction between time x theta dimension was not statistically significant at the Bonferonni corrected Type I error rate. (i7 (Λ = .488, F(3,12) = 4.19, p = .0302); M1 (Λ = .517, F(3,12) = 3.73 p = .0420); subject-level (Λ = .433, F(3,12) = 5.22, p = .0155); group-level WHR (Λ = .506, F(3,12)

= 3.90, p = .0372) and masked subject-level ROI's (Λ = .448, F(3,9) = 3.68, p = .0554)) However, it should be noted that interaction effect for the i7, M1, subject-level and group-level WHR ROIs were associated with probabilities less than .05 and that for the masked subject-level ROI was less than .06. Across all ROIs, the reduction in standard errors for theta coordinates was highest for the hip and weight dimensions, and negligible for the bust and waist dimensions.

In general, it appears that the inclusion of the PSC data as collateral information in the MGGUM by way of estimation using simultaneous equations does improve the estimation accuracy of the theta dimensions, but does not appear to affect each of the dimensions differently in a statistically significant manner. However, this result is obviously a result of the Type I error control imposed across the five ROIs.

3.3.2 Analysis of change in θ_{sd} coordinates

It would not be expected that participants would receive updated theta parameters themselves that were radically dissimilar from their original coordinate. Nonetheless, a series of follow-up 2 (time) by 4 (theta dimension) fully within-subjects ANOVAs were conducted using the MGGUM person coordinate estimates as dependent measures. The multivariate approach was, again, utilized to test each within-subject effect. This analysis revealed no significant change in the θ_{sd} coordinates across the time course of the procedure. Significant main effects of the within-subjects theta dimension were found for θ_{sd} coordinates. This effect held under Bonferonni correction for each of the i7 (Λ = .286, F(3,12) = 9.95 p = .0014); M1 (Λ = .289, F(3,12) = 9.83, p = .0015); subject-level (Λ = .274, F(3,12) = 10.56, p = .0011); group-level WHR (Λ = .274, F(3,12) = 10.56, p =

.0011) and masked subject-level ROI's (Λ = .304, F(3,9) = 3.90, p = .0106). The main effect of theta dimension in this instance reflects a difference in the average of the starting and ending coordinate across dimensions, and this is expected given that subjects were initially chosen because their ideal points were located in qualitatively different areas if the multidimensional space. Lastly, no significant interactions with any of the theta dimensions across the time course of the procedure were found.

The lack of significance of any effect involving time on the θ_{sd} coordinates is encouraging in that it suggests that the behavioral responses themselves were enough to estimate reasonable person locations. The inclusion of the PSC data hypothesized to increase the precision of these estimates by way of decreasing standard errors, and this was observed. (Again, this may have occurred differentially to some degree across theta dimensions, but this was not statistically significant).

As mentioned above, there was no systematic change in theta coordinates from the beginning to end of the new estimation procedure. This simply means that the average change was not statistically different than zero. Furthermore, this finding was consistent across ROI, and it did not interact with theta dimension. However, this does not mean that any variability in the change of a given theta coordinate was random. Indeed, when the change in the theta estimate is examined as a function of starting theta value, there is some evidence that those individuals with more extreme theta coordinates at the start of the procedure experienced the most change by the end of the procedure. One potential explanation for this type of change is simply the fact that shrinkage often occurs in Bayesian estimation procedures. A select example of possible shrinkage can be

seen in Figure 11 below. (The remaining dimension by ROI combinations are located in Appendix D.)

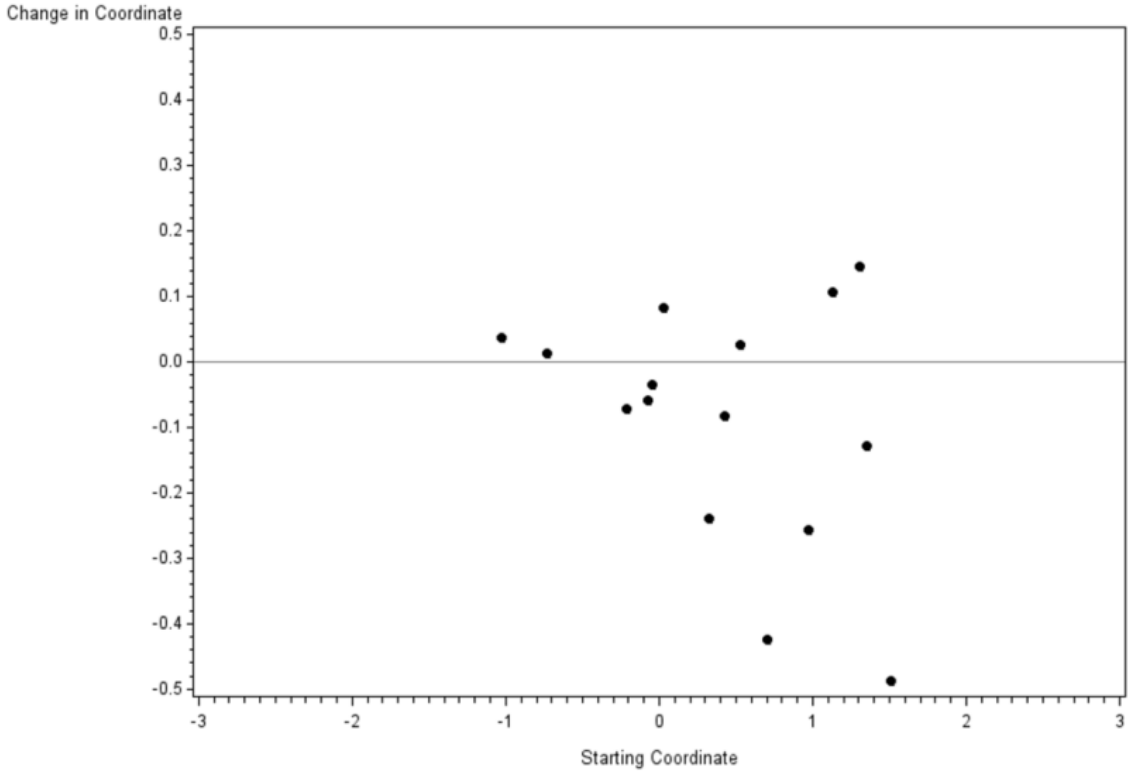

Figure 11

Change in hip coordinate as a result of the procedure in the Subject-level ROI. Possible shrinkage is observed.

Shrinkage can occur in instances when a parameter has a relatively high estimate with correspondingly high standard error; the updated estimate of the parameter may 'shrink' towards the mean of the prior distribution specified in the MCMC estimation procedure (zero, in this case). When examining the figure above, it can be seen that some degree of shrinkage is possibly occurring on the hip dimension for the subject-level ROI. Subjects whose coordinates were more positive tended to change more in the direction of the mean of the prior distribution. When examining the remaining plots in Appendix D, it can be seen that this trend occurs in each ROI for the hip dimension in roughly the same manner.

Although shrinkage may possibly account for some changes seen in theta estimates derived without and with additional neurological information, there is a logical reason to believe this is not the case. The theta estimates derived from item responses alone were already subject to shrinkage when the information contained in a subjects' item responses was not large enough to determine the corresponding coordinate with precision. Adding a second source of data should only improve the accuracy of these estimates because it would increase the information about each parameter to at least some extent, and thus, should counteract the sensitivity of an estimate to the prior distribution.

3.3.3 Analyses of Preference and Signal Change

A separate analyses of signal change observed in the fMRI portion of the experiment and its relation to preference for the stimuli was conducted. Given that some ROI's were chosen based on previous research on attractiveness, and others were constructed from attractiveness ratings provided by the participants themselves, we should expect to see a correlation between attractiveness ratings and signal change in

these regions to at least some degree. Furthermore, if the procedure does increase image resolution for detecting signal, it is possible that signal values increased overall as a result of the experiment.

A univariate repeated measures ANOVA was conducted using PSC for a given ROI as the dependent measure and time as the sole within-subjects factor.[4] A Bonferonni correction was applied to account for analysing each ROI separately with the same model. No significant change was detected in any of the i7($F(1,14) = .10$, $p = .7512$); M1 ($F(1,14) = .65$, $p = .4326$); subject-level ROI's ($F(1,14) = .38$, $p = .5486$); group-level WHR ROI ($F(1,14) = 1.40$, $p = .2562$) or masked subject-level ROI's ($F(1,11) = .07$, $p = .8019$).

Participant's attractiveness ratings for each of the stimuli were then averaged across all of the blocks that occurred for each subject, producing an average rating for each stimulus during the fMRI experimental session. These average ratings were then correlated with the PSC pulled from both the start and after the end of the iterative procedure.

[4] For within-subjects factors with a single degree of freedom, the sphericity assumption is not invoked and a univariate approach can be used.

Table 5

Correlation of attractiveness ratings during fMRI session and PSC values before and after the procedure.

ROI	Starting PSC	Ending PSC
1 – i7 ACG Region	0.15993	0.17524
2 – M1 Control Region	-0.07171	-0.06598
3 – Subject-level IWD Cluster	0.16696*	0.16971*
4 – Group-level Cluster	-0.09685	-0.1042
5 – Masked Subject-level Cluster	0.24705**	0.24757**

*Note: *p < .05 ** p <.001*

The correlations with the signal change for each stimulus were statistically significant in the subject-level ROI cluster, and the subject-level ROI cluster masked by the level-2 network SPM derived from comparing stimuli 'on' to stimuli 'off' time. Correlations for signal change with the attractiveness ratings in the I7 region of the anterior cingulate gyrus derived from Platek & Singh (2010) were correlated at a comparable rate both at the start and end of the new estimation procedure, although only trending towards significance. Correlations with attractiveness ratings in the M1 motor cortex region being used as a control region were effectively zero. Signal in the group-level cluster derived from waist-hip combinations were not significantly correlated with attractiveness ratings.

Recall that the subject-level and masked subject-level ROI's were created by contrasting the IWD for each stimulus separately for each subject. An important note about this manipulation check is that the correlations of attractiveness ratings and signal change observed over the course of the procedure were highest in these regions; highlighting the correlation between the reported attractiveness ratings for each stimulus

and signal in regions based on the underlying assumption that the MGGUM models preference for these stimuli. As such, the manipulation check appears to be satisfied.

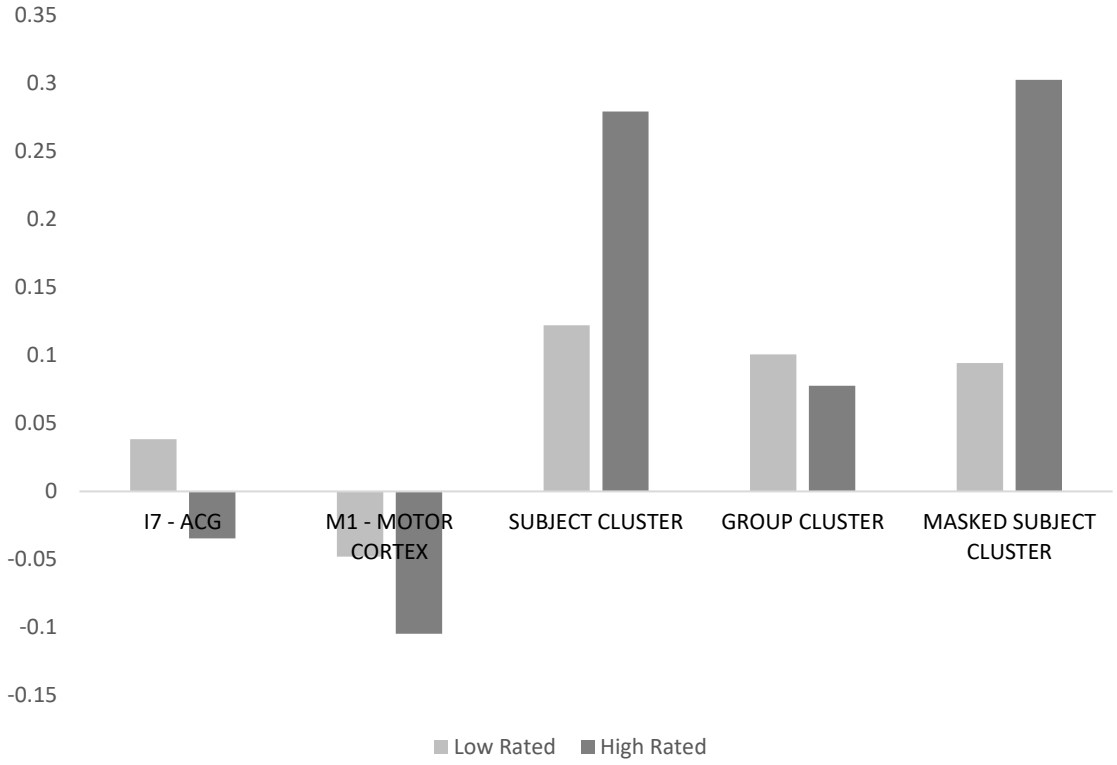

Figure 12

Signal change as a function of median-split stimulus attractiveness ratings and region of interest in the brain.

Lastly, Figure 12 above illustrates the signal change comparison by ROI for a median split of attractiveness ratings for each subject from the fMRI portion of the experiment. Similar to the previous results, all subject-level oriented regions of interest derived from attractiveness ratings produced, on average, higher signal change than other regions. It follows then that there is a measurable relationship between PSC in the regions of interest used in this analysis and attractiveness ratings for the 24 stimuli.

CHAPTER 4. RESULTS AND DISCUSSION OF ADDITIONAL ANALYSES PERFORMED

4.1 Latitude of acceptance

Additional exploratory analyses were performed on the data to examine the relationship between signal change in the brain and the response process modelled by the MGGUM. Specifically, post-hoc analyses of the relationship between percent signal change and the IWD covariate revealed points of interest worth further examination in this project.

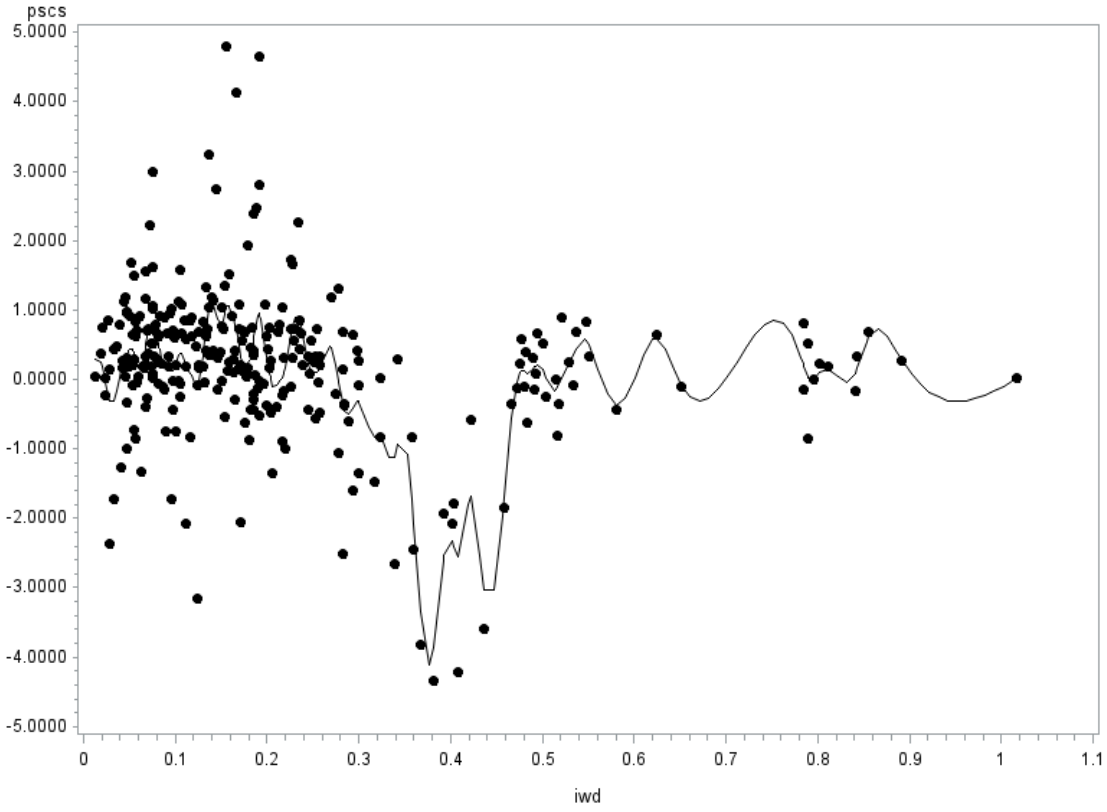

Figure 13
Plot of percent signal change (Y axis) versus IWD (X axis) for each stimulus in the masked subject-level ROI cross participants.

In Figure 13 above, there appears to be an interval along the IWD in which the signal change in the ROI for the stimulus dips. Under the MGGUM, when the IWD is small, the stimulus is more 'ideal' for the respondent, and when the IWD is large the stimulus departs substantially from this ideal. From an information processing theory perspective, when a stimulus is sufficiently close to or far from an individual's ideal, the response process is more automatic because the comparison to the individual's prototype is simpler (Barsalou, 1985; Chaplin, John, & Goldberg, 1988); the individual is capable of recruiting the heuristic required to make the less effortful judgment. Under the assumption of a proximity-based response process modelled by the MGGUM, the subject utilizes a heuristic which anchors their judgment to their ideal (Wyer, 1976; Roberts & Shim, 2010) and can easily tell when a stimulus is close to or far from that ideal. However, when the stimulus is sufficiently ambiguous (neither sufficiently close to nor far from their ideal) these types of heuristics for judgment around anchors or ideals are not useful (March & Simon, 1958). In this case, the stimulus is ambiguous and more effortful cognitive processing is required to evaluate the stimulus and form a judgment.

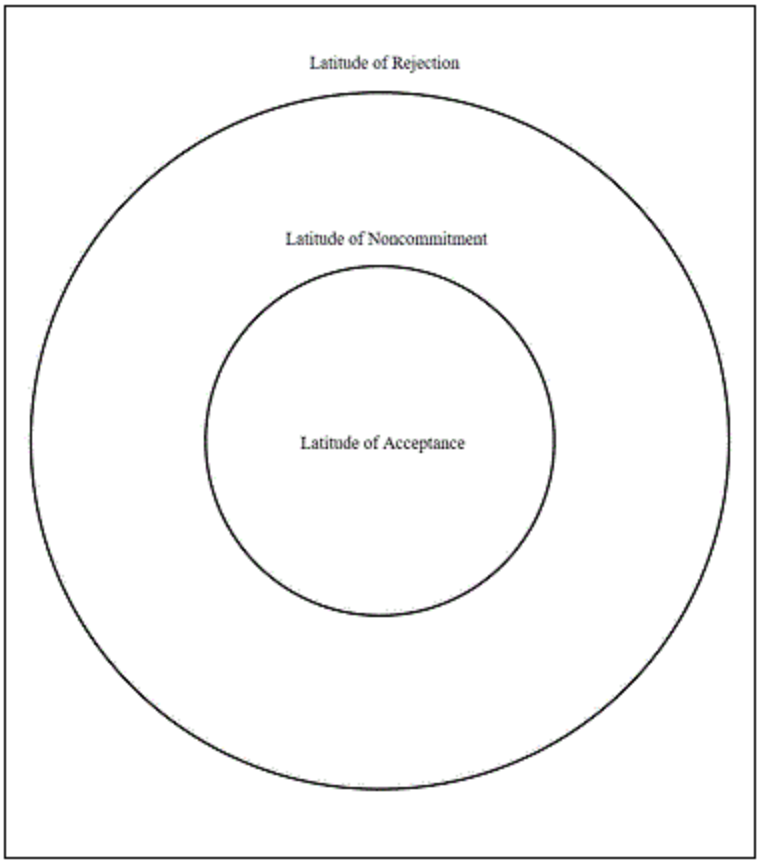

Figure 14

Illustration of the differences between the latitudes of acceptance, noncommitment, and rejection.

With respect to the MGGUM, one can think of a region around an ideal point where an individual responds positively to a stimulus in an almost automatic fashion. The individual is likely to prefer stimuli that are located in this region. This region in the space has been referred to as the "latitude of acceptance" in the social judgment theory literature (Sherif & Hovland, 1961; Sherif, Sherif, & Nebergall, 1965; Roberts, Rost, and Macready, 2010). At a more general level, it refers to a region of the preference space where the individual is certain that a stimulus is preferred. The stimuli adjacent to this

zone, in contrast, require more cognitive processing to determine whether they are preferred or not. This has been referred to as the "latitude of non-commitment." Farther still from the ideal point lies all the remaining area of an individual's preference space in which stimuli are not preferred. This is often called the "latitude of rejection." Figure 14 above illustrates an example of the differences between these three regions visually in a 2-dimensional latent space. Although the social judgment theory literature is tied to attitude measurement and attitude change, it is likely that these same concepts might be applicable to the general preference domain.

Given the previous findings in this paper that the attractiveness ratings were correlated with signal change in the subject-level and masked subject-level ROI's, the assumption can be made that signal change in these ROI's are related to preference for these stimuli to at least some degree. In the case of the figure above, the interval in which the signal change dips along the IWD indicates less information processing occurring in the target ROI (Mckeown, Hanse, & Sejnowski, 2003). It follows that when an individual encounters a stimulus with an IWD in this interval, recruitment of other regions in the brain occurs to make the attractiveness judgment. In essence, this observed dip in signal change may help locate the latitude of non-commitment for these stimuli with respect to IWD.

4.2 Methodology

4.2.1 Overview

The interval of interest for the boundaries of the latitude of acceptance was defined based on Figure 13 above. Seven subjects (1; 2; 7; 10; 11; 12; 13) with IWD to

stimuli in the observed range of the dip along the interval (.26 to .48) were selected for inclusion in an exploratory, post-hoc analysis to see if IWD values within the latitude of non-commitment were associated with more negative signal change than IWD values that were progressively outside of this interval (i.e., indicative of the most or least preferred stimuli). This analysis was conducted separately for the subject-level IWD cluster and the masked subject-level cluster. Analyses were limited to these two ROIs because they were the only ROIs so exhibit the dip in signal as the stimulus became more discrepant from the subjects' ideal. (Appendix F contains plots of percent signal change by IWD for each ROI to illustrate the presence or absence of the latitude of non-commitment.) As outlined in the previous chapter, these two regions also had significant positive correlations between signal change and attractiveness ratings. The IWD for each subject was centered at the midpoint of this interval associated with the dip in PSC (i.e., at .365), and then the absolute value of this recentered distance was calculated and stored. This measure was equal to zero when the IWD was at the center of the latitude of non-commitment and it took on higher positive values when the IWD represented situations in which the stimulus was close to the subject's ideal point (in the latitude of acceptance) or far away from it (in the latitude of rejection). This new measure will be referred to as the modified distance measure (MDM) to distinguish it from the original IWD.

The iterative estimation procedure outlined in this paper was adapted in two primary ways. First it was modified to estimate simultaneous equation parameters based on data from all subjects included in the analysis rather than one subject at a time. Second, the PSC for each subject-stimulus pairing was regressed on the MDM described

above. The regression model was an analysis of covariance model with a repeatedly measured covariate:

$$\beta(\%)_{si} \sim N(M_{si}, {}^{1}/_{\sigma^2}) \tag{12}$$

$$\sigma^2 \sim \Gamma(.01, .01) \tag{13}$$

$$M_{si} = \beta + \beta_s + \beta_{si}\left(\left|\sqrt{\sum_d w_{sd}^2 \alpha_{id}^2 (\theta_{sd} - \delta_{id})^2} - .365\right|\right) \tag{14}$$

Where in (14) β represents the grand mean of PSC ($\beta(\%)_{si}$) across all subject & stimulus combinations; β_s represents the effect of mean PSC level for a given subject s, and β_{si} is the regression coefficient relating the MDM to the conditional mean PSC for each of s subjects and i stimuli. The precision ($1/\sigma^2$) in (12) is the error component in this regression model and is estimated with a gamma distribution prior shown in (13). In short, this regression model predicted the conditional mean PSC for a given subject-stimulus pair using a repeatedly measured covariate (MDM).

A procedure similar to that described in the previous chapter was used to integrate the percent signal change from the fMRI portion of the experiment to the new system of simultaneous equations with the MDM. Each subject's fMRI GLM was fit at the level of the individual subject to obtain signal change estimates by inserting the resulting modified distance covariate from the simultaneous equations for the subject into the appropriate design matrix. The process was then continued by extracting the percent signal change from these individual fMRI GLM's and then inserting them into the simultaneous equation procedure for further iterations. The system of simultaneous

equations was estimated for all seven subjects together. Thus, one set of regression coefficients was estimated across these seven subjects on any iteration of the procedure. This is substantially different than the procedure from the original analysis reported earlier in this document.

4.3 Results

4.3.1 Results of Iterative Procedure on θ_{sd} Estimation Precision in the Group Model

The overall effect of the iterative estimation procedure for simultaneous equations was examined in the same manner outlined in the previous chapter. The precision of EAP estimates for the MGGUM portion of the experiment was evaluated using a 2 (time) by 4 (theta dimension) fully within subjects repeated measures GLM framework comparing the standard errors for each θ_{sd} across the procedure as the dependent measure. These were analyzed for multivariate effects given the previous issues with sphericity, and performed separately for the two regions of interest which exhibited the presence of the latitude interval along the IWD and PSC relationship.

Similar to the previous chapter, a significant main effect of theta dimension was detected in both the subject-level (Λ = .059, F(3,4) = 21.23, p = .0064) and masked subject-level ROI's (Λ = .061, F(3,4) = 20.29, p = .007). The significance of the main effect of theta dimension shows that the average of the starting and ending standard errors varied across dimensions. In Figures 15 and 16 below, the replication of the findings from the previous chapter can be seen; the hip and weight dimensions had the highest average standard errors across the time course of the procedure, and as such stood to potentially gain the most increase in precision of theta estimates on these dimensions.

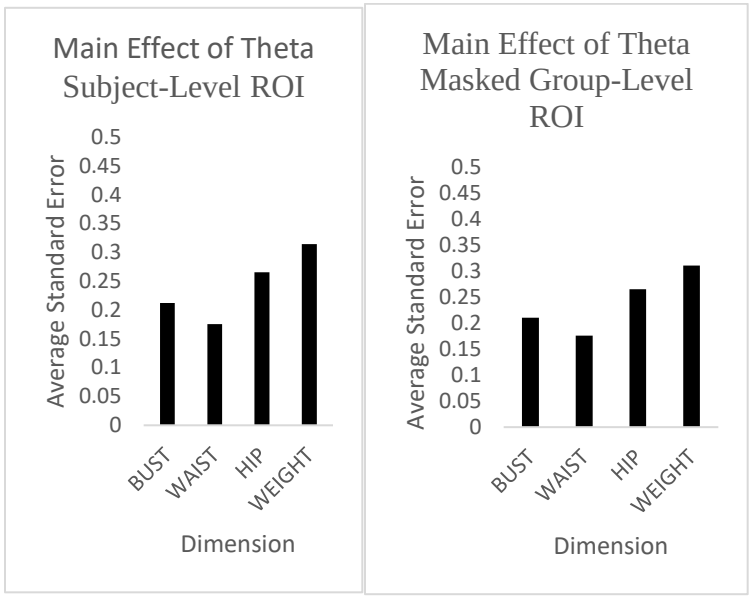

Figure 15

Replication of results from the initial portion of the study using the exploratory analysis. Significant main effect of theta dimension.

Also similar to the previous chapter, the main effect of time was detected in each of the subject-level (Λ =.426, $F(1,6) = 8.09$, $p = .029$) and masked subject-level ROI's (Λ =.429, $F(1,6) = 7.98$, $p = .03$) which could be considered significant using a Type I error rate of .05. (Given that this portion of the analysis is exploratory in nature, controlling Type I error across both ROIs with Bonferroni's procedure is not especially important.) In figure 18 below, it can be seen that, by design, the standard errors for the start of the procedure were the same for each ROI. Similarly, it can be noted that the effect was observed in each of the five ROI's, including the M1 control region. Some potential implications of this finding are treated in the discussion section 4.4 below.

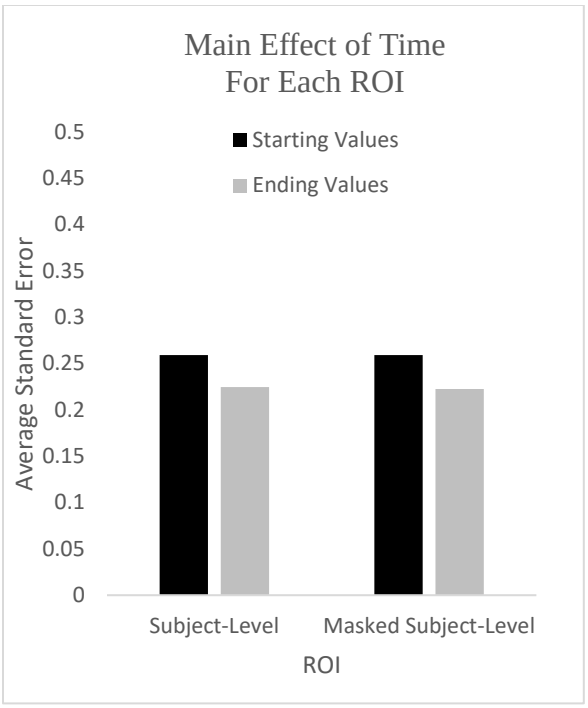

Figure 16

Replication of the main effect of time using the exploratory analysis.

Note: Significant at .05 level

There was no interaction detected between the within subject factors of time and theta dimension in the subject-level (Λ =.392, F(3,4) = 2.06, p = .247) or and masked subject-level ROI's (Λ =.391, F(3,4) = 2.07, p = .246). The lack of a significant interaction is a replication of the results found in chapter 3. This project was unable to detect a differential effect of the time course for the procedure across dimensions of theta.

4.3.2 Results of GLM Analyses on Latitude Intervals

The iterative procedure for estimating simultaneous equations produced relationships between the repeatedly measured MDM and PSC. Recall that the MDM is defined by first centering the IWD at the middle of latitude of non-commitment interval, and then taking the absolute value. This process 'folds' the IWD covariate and changes

its representation such that higher values on the MDM covariate represent leaving the non-commitment interval, and lower values represent an area within or near it. It is expected that as the MDM grows large (i.e., the stimulus begins to leave the latitude of non-commitment), less effortful cognitive processing will be recruited to form a judgment of the stimuli. Similarly, as the MDM shrinks, the stimulus falls within the latitude of non-commitment, and a more cognitively effortful response is expected. The regression of PSC on this repeatedly measured covariate for each stimulus taps into this potential effect. The regression models for each ROI contained parameters for the intercept (β), subject parameters (β_s) a slope relating the MDM covariate to PSC (β_{si}), and a precision estimate modelling the error variance for the overall model. In essence, the regression models the relationship of the repeatedly measured covariate with PSC while controlling for the individual subject effects.

The significance of the slope parameter relating PSD to MDM was evaluated by checking to see if the absolute value of the parameter was greater than two times the standard deviation of the estimate obtained from the OpenBUGS program used to estimate the regression model. A significant slope parameter was found for the subject-level ROI's (β_{si} = 1.312, SD = .667), but not for the masked subject-level ROI's (β_{si} = 1.142, SD = .649) although this latter effect approached the statistical criterion as well.

The subject-level ROI and masked subject-level ROI's had the highest positive correlations between signal change and attractiveness ratings, and also exhibited a significant or trending significant positive slope between signal change and MDM. This finding is consistent with the hypothesis that stimuli outside of the latitude of non-commitment invoke higher signal change than those within the interval. The masked

subject-level region also had a significant positive correlation between attractiveness ratings and signal change, but produced a positive slope that did not reach significance thresholds in this analysis. While these results are interesting from a theoretical perspective, the analyses reported here are entirely post-hoc and exploratory.

4.4 Discussion

4.4.1 Summary of Findings

The results from these regression equations highlight some differential functioning across the regions of interest examined in this paper. The subject-level region that was constructed by contrasting highly rated stimuli versus lower rated stimuli on attractiveness, and the masked version of this ROI contained an appreciable dip in signal along the interval of IWD, which suggested that these regions were sensitive to the latitude of non-commitment in these regions.

One of these regions, the subject-level ROI, produced a significant positive slope for MDM which supports the hypothesis that as the location of a stimulus moves outside of the latitude of non-commitment, signal change in this region increases. An additional piece of evidence from figure 14 in the previous chapter is that this same region had statistically different mean PSC values when stimuli were split by median attractiveness with those stimuli that were rated highest in attractiveness exhibiting the largest average signal change. Taken together, we can see that stimuli which are rated very low or very high on attractiveness by the participant, also elicit higher signal change in the subject-level region, and are more likely to be outside of the latitude of non-commitment for the subject. As a result, it can be inferred that participants recruit the heuristic to form

attractiveness judgements in this ROI for stimuli outside of this interval. This finding was not replicated for the masked subject-level ROI, although it was in the correct direction.

In the subject-level ROI's formed based on subject's attractiveness ratings, an effect of the latitude of non-commitment is present. The dip in the PSC means that less (indeed, negative) signal change is observed within this interval whereas more signal change is apparent to either side of this interval. The dip present in these relationships causes the slope to turn out positive when PSC is regressed on MDM; such that as a stimulus moves further from the center of the latitude of non-commitment in either direction, the PSC will increase. In other words, when the stimulus is clearly in the latitude of acceptance or the latitude of rejection, then it is no longer ambiguous and the corresponding PSC is higher. This is presumably due to less effortful cognitive processing in these situations.

The inference about the response process (whether deliberate or heuristic in its nature) invoked when the participant provides attractiveness ratings to the stimuli is captured by the fact that the subject-level and masked subject-level regions were constructed from the attractiveness ratings themselves. The observed relationships between the PSC and attractiveness ratings in the previous chapter, as well as PSC and MDM found here, supports the inference about differential recruitment brain regions for stimuli located in different places along the continuum of weighted ideal distance from the stimulus. Similar findings can be seen in Figure 18 below. Recent work from Sparks (2021) on reaction time when responding to attitude statements suggests that stimuli in

the latitude of non-commitment lead to slower reaction times relative to those in the latitudes of acceptance or rejection.

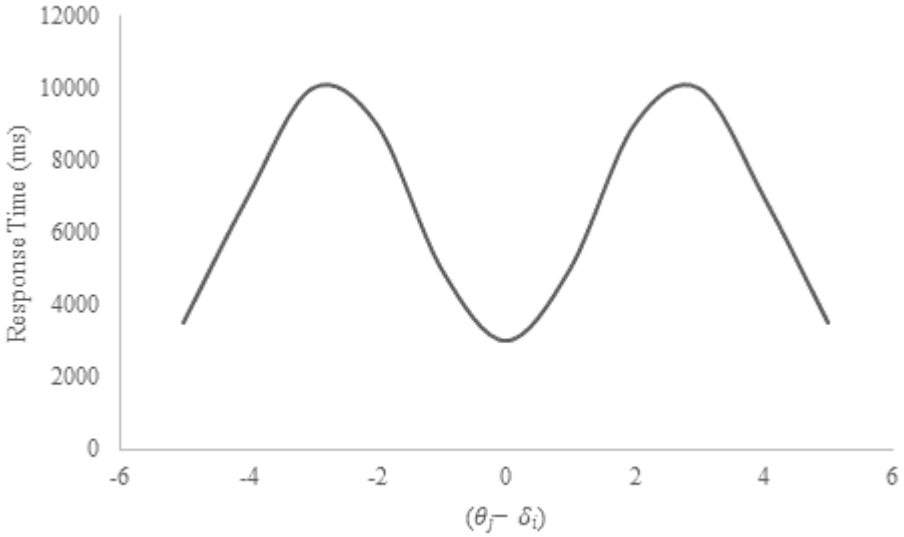

Figure 17

Response time plotted as a function of metric distance under the GGUM. Stimulus ambiguity causes increased response time.

The larger picture encapsulating these findings illustrates the interplay among the response process for attractiveness ratings modelled by the MGGUM, and signal change observed in the brain. The IWD constructed in this project is built from the metric distance in the MGGUM, providing a measure of how ideal each stimulus is expected to be for a given subject. Subject-level regions of interest were established on the basis of contrasting the highly rated stimuli to the lowest. Signal change in these resulting regions was not only positively related to attractiveness ratings, it also provided insight into the manner in which subjects produced attractiveness ratings by reflecting the latitude of non-commitment in the relationship with the IWD in these same regions via the MDM.

These findings suggest differential recruitment of brain regions in forming attractiveness judgments as a function of how ideal the stimulus is to the individual.

4.4.2 General Limitations and Recommendations for Future Research

One recommendation that is easy to make is to collect more measurements for each stimulus in the scanner session; it would be ideal to obtain anywhere from 30-60 measurements of each stimulus to more accurately model the PSC within the fMRI GLM framework. This is more than double the amount presented in this study, however given the limitations that accompany data collection, the researcher must sometimes make careful considerations of ways to balance their resources if deciding between more measurements for each stimulus, or more participants to obtain measurements from. In an ideal (and unrealistic) world for the researcher, both of these are maximized and the subject is willing to lie in the scanner for hours providing attractiveness ratings.

However, repeated exposure to stimuli during a scanning session for a single participant can pose an issue when they are asked to provide a rating for a single stimulus multiple times. If a participant recognizes a stimulus, it is possible that their response can be drawn from memory, rather than being the product of a genuine preference elicited experimentally from the session. A participant may form a response strategy to the stimuli over the time course of the scanning session when exposed to multiple stimuli of the same nature which operates at a higher cognitive level than traditionally observed neural adaptation to tasks (Poldrack & Farah, 2015). To this end, the researcher might prefer a larger number of subjects as opposed to a larger number of measurements within

a given subject to circumvent this issue. An analysis of block-to-block correlations of responses in this project revealed no pattern of increasing relationships across subjects.

When weighing the value of these factors, increasing the number of subjects allows further generalization of the findings of the relationship of the MGGUM and signal change, while an increased number of measurements furthers the measurement quality in the fMRI data collection process (i.e., the measurement of signal change), and consequently, the characterization of that relationship. These two things are inextricably intertwined as better PSC estimates provide a more stable metric to relate to the IWD from the MGGUM portion of the study. Both of these factors were bound by the limited time available for the scanning sessions, and the amount of each factor was carefully considered to try to optimize both generalization of findings and measurement sensitivity.

In addition to the number of measurements and number of subjects, this study withstood an additional challenge in utilizing short videos as stimuli. A specific recommendation would be to instead use pictures as stimuli. The use of a video as a stimulus creates a situation in which the researcher must control for the duration of the stimulus in their statistical model for the fMRI framework, averaging over more signal as a result. When the stimulus occurs over a longer duration of time compared to a picture, it can be more difficult to pinpoint the onset of cognitive processing related to the stimulus than it would be using a different medium. Coupled with the reduction in time to display the stimuli, utilizing pictures further allows the opportunity to display the stimuli more frequently within the same allocated time period. One reason this was not considered for this project is that there were no calibrated MGGUM item parameters available for pictures, but only for videos. Given that large data sets are required to estimate MGGUM

item parameters, these pre-existing item parameter estimates made examination of the relationship between MGGUM and PSC possible with a relatively small number of subjects.

One finding of note in this study was the replication of the within-subjects effect of time on standard errors of theta estimates in the M1 control region, which was not an expected finding. The Human Motor Area Template (HMAT; Mayaka, Corcos, Leurgans, & Vaillancourt, 2006) M1 ROI region used was contralateral to the left hand in which participants were instructed to respond to each stimulus. During the development of the procedures, recruitment of right hand participants was desired to minimize systematic variation associated with responses due to differential connectivity involving use of their non-dominant hand (Morris et al., 2018). However, due to the use of the contralateral M1 region, it stands to reason that there may be some systematic variation in signal detected that is related to the finger used to respond to each of the stimuli. As such, the data were revisited and an additional ROI was examined using the ipsilateral M1 on the left side of the brain in an attempt to resolve this confound.

Reanalyzing data from the ipsilateral M1 region with the same criterion as the previous chapter revealed a replication of the earlier findings for the contralateral region. Significant differences for the within-subjects effects of time (pre or post procedure) (Λ = .50, $F(1,14) = 13.96$, $p < .01$) and for the theta dimension ($\Lambda = .275$, $F(3,12) = 10.49$, $p < .01$) were detected that passed the Bonferroni threshold. The interaction of time with theta dimension ($\Lambda = .405$, $F(3,12) = 5.86$, $p = .0106$) did not meet the significance threshold. Additional findings for this region include a replication of the lack of a significant effect for both the fMRI residual GLM variance ($F(1,14) = 4.18$, $p = .06$) and

regression model error term explaining the signal with the IWD ($F(1,14) = 0.12$, $p = .7372$), both of which failed to arrive at the significance thresholds. Similar to the previous chapter, attractiveness ratings did not correlate with signal change extracted from this region ($r = .08$, $p = .09$). Additionally, the correlation between signal change and the IWD covariate in this new ipsilateral version of the M1 ROI was also not significant ($r = .09$, $p = .06$). Each of the effects described here hold the same relative magnitude and direction as the contralateral M1 region findings outlined in the previous chapter.

The replication of the within-subject effects of time for the additional ipsilateral M1 ROI raises additional questions about why the standard errors for theta estimates are benefiting from the procedure in ROI's not posited to be related to the task. Mean differences in the standard error of θ_{sd} as a result of the procedure for each subject seen in Table 4 show that two subjects had higher overall improvement compared to the other 13 subjects. A replication of the analyses performed with these two subjects removed shows a main effect of time that persists, likely a consequence of losing additional subject variance.

The persistence of this main effect points to the fact that the estimates of theta are being informed more accurately, likely from the addition of the regression equation from the simultaneous procedure. It is possible that slope estimates are being leveraged by random variation in signal within each subject on which the regression is performed. To examine this, a series of regression models were fit within each subject for each ROI; the PSC was regressed against the IWD covariate, both obtained from the end of the procedure, and leverage statistics in the form of Cook's D (Cook, 1977) were examined.

Appendix C contains the plots of all of these relationships for all subjects with the prediction from the regression model in the procedure overlaid on top of it. A select few cases are presented here for purposes of illustration.

A cutoff of 4/n was chosen as a significant leverage point for any observation in which the PSC was an outlier in the relationship with IWD (Muller & Mok, 1977; Das & Gogoi, 2015). For the i7 ROI 73% of subjects contained at least 1 leverage point with a maximum of 2. For the contralateral M1 ROI 80% of subjects contained at least 1 leverage point with a maximum of 3. For the subject-level ROI 93% of subjects contained at least 1 leverage point with a maximum of 3. For the group-level WHR ROI 80% of subjects contained at least 1 leverage point with a maximum of 3. For the masked subject-level ROI 92% of subjects contained at least 1 leverage point with a maximum of 4. Lastly, for the ipsilateral M1 ROI, 80% of subjects had at least 1 leverage point with a maximum of 2.

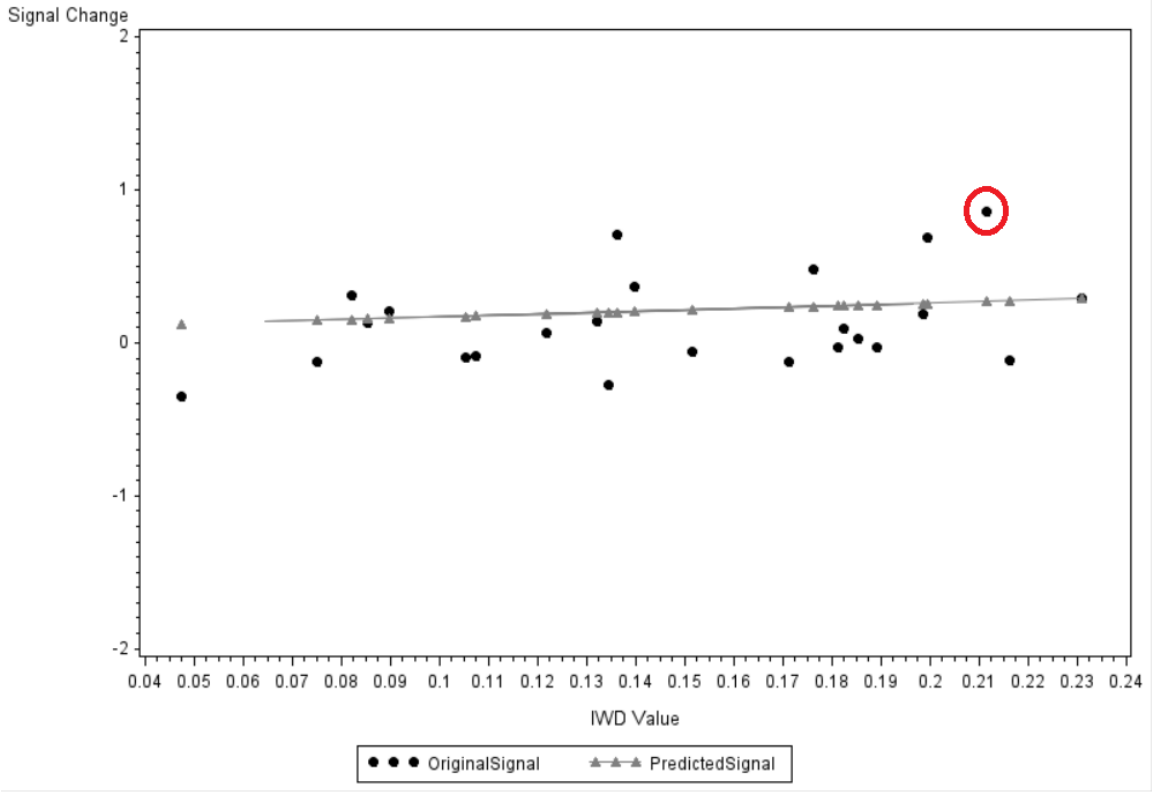

Figure: 18

PSC & IWD Relationship with Prediction Overlay. Contralateral M1 ROI, Subject 14.

Note: Identified leverage point is highlighted.

In Figure 18 above, a leverage point is present within this subject's contralateral M1 ROI which influences the final regression coefficient of the model. A similar example can be seen for the ipsilateral M1 ROI below in Figure 19. In this example, one particularly extreme negative value is influencing the final estimated slope of the regression equation.

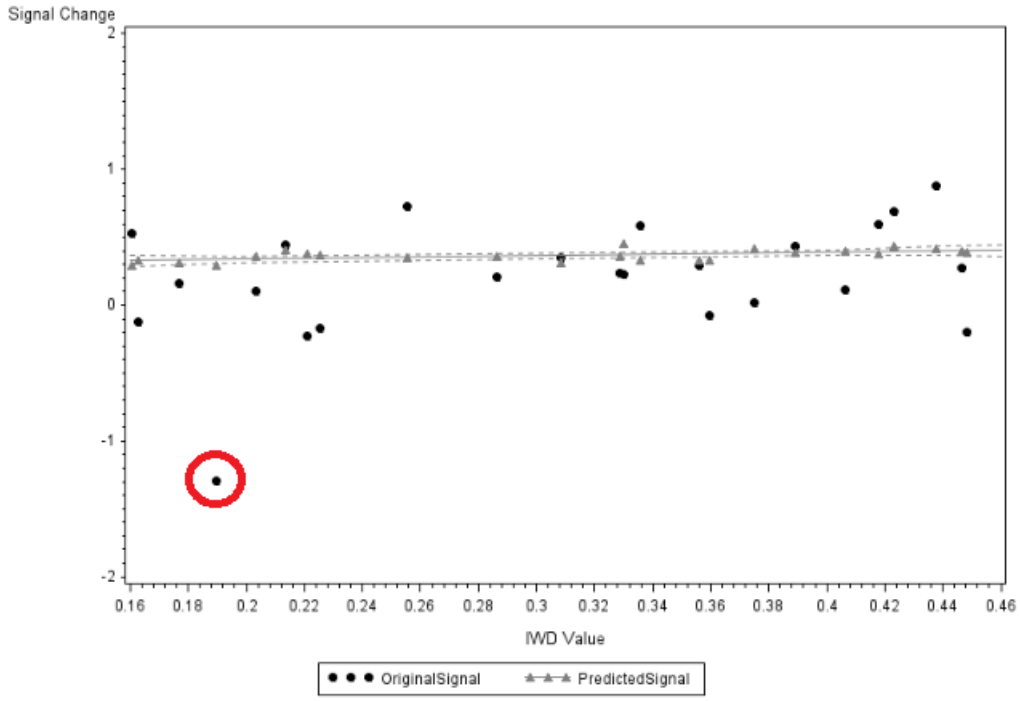

Figure 19

PSC & IWD Relationship with Prediction Overlay: Ipsilateral M1 ROI, Subject 9.

Note: Identified leverage point is highlighted.

In both of these examples, the final regression equation contains a non-zero beta coefficient relating PSC to IWD. Instances in which leverage points occur create a situation in which more variation in signal change is explained by IWD. Furthermore, these leverage points are occurring within a majority of the subjects for each ROI. The theta parameter in turn gains more precision in its estimate for its role in the IWD component of an equation for a line that would otherwise be more precisely flat. When the regression model included in the system of simultaneous equations explains a non-zero amount of variance in signal. Ultimately, theta is estimated with more precision due to this effect, however small it may be. Another possible explanation for the reduction in standard errors in the M1 region (and perhaps others) is that the model for the global

signal in the brain may have been insufficient to capture all task-related variance in this study. Efforts to remove global signal in fMRI data analyses are implemented due to the fact that seemingly innocuous things such as head movement, respiratory function, and heartbeat may be correlated with task variance on the whole (See: Aquino et al., 2020 for a recent review of the problem). It stands to reason that there could be similar physiological functions that correlate with responses when making attractiveness ratings, as individuals can conflate the perception of a physically attractive characteristic with a physical feeling including changes in breathing or heart rate (Swami & Furnham, 2008). The fMRI GLM procedures implemented here attempted to account for this signal by utilizing a set of head motion parameters and a separate intercept parameter for each of the ROI's and subjects tested. Thus, it is possible that reduction of theta standard errors when incorporating PSC from the M1 and other regions is a result of remaining global signal in both of the M1 regions correlated with the task that is unaccounted for by the GLM intercept parameter in these regions.

Another use of statistical methods in this project to consider is the controlling of type I error rate for ROI's and other analyses in the fMRI framework. In many cases for neuroimaging studies, the ROI selection process is considered to be a priori, and Type I error rate is not controlled across these comparisons (Hayasaka & Nichols, 2003; Bennet et al., 2009; Poldrack & Mumford, 2009). It can be argued that even in these cases, the planned & unplanned distinction is not a justifiable means of controlling Type I error rates when multiple tests are performed. By controlling for Type I error rates across multiple tests, the false positive rate is objectively lower and the results are more likely to be replicated. Furthermore, many ad-hoc decisions were made after the data were

collected to test, and re-test additional regions of interest both for experimental and exploratory analyses in this project. Lastly, even if this restriction were lifted, it would not affect the results in this project in any meaningful way. The interactions between theta dimension and time could be considered significant at this threshold for some ROI's, but this finding would be easily explained by the much larger starting standard error values of theta for the dimensions interacting with time.

While this study highlighted differential utilization of brain regions in forming attractiveness judgments, it did so by way of individualized subject-level ROI's which were substantially different from one another. Future research into this topic should explore construction of additional regions that are common across subjects. The group-level WHR ROI was one example of an attempt to construct a common region based on a prototypical feature related to attractiveness ratings. Previous research on this topic suggests that an ideal point for attractiveness of WHR is .7$\pm$.02, and WHR values more distant are perceived to be less attractive (Henss, 1995; Tassinary & Hansen, 1998; Henss, 200; Markey et al., 2002; Forestell et al., 2004). Stimulus measurements for WHR in this study ranged from .65 to .83. The ROI utilized in this study was constructed by running a level-2 GLM across all subjects contrasting lower WHR stimuli to higher WHR stimuli based on a median split. This split contrasted 12 stimuli with measurements ranging from .65 to .72 in the lower portion, and 12 stimuli with measurements ranging .75 to .83 in the higher portion. As such, the WHR region that was common across subjects captured the ranges documented in the literature as most commonly being attractive to those that are not.

Another general region hypothesized to be related to attractiveness across subjects was tested in this project, the anterior cingulate cortex (i7) ROI, which Platek & Singh (2010) found to be related to attractiveness ratings of still photos of female torsos with variable waist-to-hip ratio measurements. This project failed to replicate their findings, however there exist clear confounds when comparing these projects in that the stimuli and methods used were very different. Platek & Singh (2010) utilized photographs of women who have undergone surgery to change their proportions, and tested to see which regions were most active in the contrast between these photos. While the stimuli in the present study exhibit these same differences of physical measurement, they were videos of computer generated models, and not still photos of real women.

The current project stands out from past research as it is the first of its kind to pair neuroimaging data with the observed responses using an item response theory framework. The variance in the spatial distribution of active voxels across subjects for the subject-level ROI's raises some questions about the neuroanatomical configuration of structures involved in forming these types of judgments. The lack of a replication of findings in Platek & Singh (2010), and the variance observed in subject-level regions paint a need for further research into the potentially individualized nature of different brain regions in forming attractiveness judgments. The individual nature of the ideal point modelled by the MGGUM is a concept familiar in IRT paradigms, and may also be reflected in a process corresponding to an individualized neuroanatomical structure. The distributed nature of information processing may be affected by not only what the person is forming a judgment on, but the manner in which they form that judgment. The subject-level ROI's found in this project from contrasting attractiveness ratings could instead

serve as an informative starting point to continue the advancement of neuroimaging research on perceptions of attractiveness.

Further along the definition of the ROI's to consider is their relative size. When the ROI's were constructed from initial runs, a relatively strict family-wise error control of $p < .01$ was paired with the criterion of a minimum of 150 neighboring voxels being active to consider it a valid 'cluster' for inclusion into the ROI. This criterion was applied in the same way for the subject-level, masked subject-level, and group-level WHR ROI's. The selection of which voxels to pull time series data from is something that directly impacts many outcomes in this study as the percent signal change from these voxels are one of the primary measures of interest. It could be argued that this criterion was too strict, and that the resulting clusters might be larger than what neuroanatomical region might correspond to the task. In this project, exploratory data analyses on the size of the clusters showed more distinct regions when the threshold was higher. For lower thresholds, the regions appeared more distributed and random.

There are two points to consider here. Firstly, the subject-level ROI's (i.e., masked-subject-level ROI's) were defined using experimental comparisons from subject response data (e.g., IWD covariate), and in the case of the WHR ROI the virtually measured WHR. Secondly, these subject-level ROI's varied in size across subjects. Valid PSC data can be pulled from ROI's of any size (Poldrack & Mumford, 2009); furthermore evidence of the latitude of non-commitment was present in ROI's of varying sizes for 7 subjects. Lastly, effects of time were replicated (if even by leverage) in ROI's that were extremely large (M1 control, Ipsilateral M1 control regions) relative to other ROI's used in this study. In short, while changing the ROI definitions can impact the

signal pulled, there is no reason to believe that they were inherently invalid in this project as currently defined.

Improvements in the identification of neurological correlates of physical attraction might be achieved with a different analytical framework as well. This study implemented a relatively common method of analyzing fMRI data in the form of GLM contrasts. No framework was established to link processing in specific regions together. Alternative methods such as independent components analysis, multi-voxel pattern analysis, and sliding window correlations which can leverage the temporal component of the data more fully could be used to better characterize the exact flow of processing in, and out of the latitude of non-commitment observed on the MDM interval and across regions of the brain. These methods would require a minimum of 20-30 subjects to approach stable estimates of components required for temporal inferences between brain regions (Pajula & Tohka, 2016). While the goal of identifying common regions of interest for forming attractiveness judgments played a small role in this project, the goal of profiling their temporal relationships to one another during processing was outside of the original scope of the project.

4.5 Conclusions

This project has contributed to the scientific literature in several ways. From a methodological perspective, the simultaneous equation method implemented in this dissertation is novel. It provides a new means to model data from different domains at the person-stimulus level as long as the data sources follow models that involve common parameters. Integration of external information into IRT models has been accomplished

before with other approaches, however, the inclusion of information from latent trait measures in IRT into fMRI GLM, and the inclusion of neuroimaging data into IRT models is unique.

This study provided an opportunity to assess the degree to which traditional fMRI analyses can be improved via inclusion of results from a related external behavior task as a covariate of a stimulus feature, extending previous research on the topic (Woolrich et al., 2001; Johnstone et al., 2006; Spisak et al., 2014; Bezdek et al., 2015). Furthermore, it extended the use of PSC as an external variable in alternative research paradigms for analysis of behavior outside the fMRI framework.

Likewise, this study extended research on parameter estimation in MIRT models that are augmented by external data modalities (of which, fMRI has never been attempted). To this author's knowledge, there is no readily available research in the area of integrating physiological information from the brain into item response models. Researchers have integrated external processes such as response time into these models, but little to no effort has been put forward to investigate the amount of information that can be utilized from physiological processes. This project could serve as a valuable source of information for those researchers interested in incorporating neural signal or other physiological measures into IRT models.

This project also established use of an individualized version of metric distance under the MGGUM with individual subject parameters. Use of this IWD metric was critical in identifying relationships between signal change in the brain when viewing a stimulus and an individual's location in the multidimensional continuum. Furthermore, this IWD metric helped reveal the presence of the boundaries of the latitude of acceptance, non-

commitment, and rejection, manifesting in the form of differential signal change for stimuli along this IWD continuum.

Lastly, while the findings outlined in chapter 3 of this paper show that the precision of θ_{sd} estimation improved regardless of the ROI utilized for the source of the PSC, there was no sign of a dip in PSC within the latitude of non-commitment for the M1 control region. This suggests the relationships between PSC and IWD observed in ROI's that were constructed from attractiveness ratings highlight interplay between the location of an individual in the multidimensional continuum and signal change in the brain.

APPENDIX: A – Demographic Questions

Questions:

1. What is your gender?
2. What is your age in years?
3. What is your class standing?
4. How many female siblings did you have in your household growing up?
5. How many male siblings did you have in your household growing up?
6. Have you played video games with lifelike models before?
7. What was your age in years when you first started dating?
8. Was there a male adult parent/guardian in your household during a majority of time that you lived at home?
9. Was there a female adult parent/guardian in your household during a majority of time that you lived at home?
10. Do you consider yourself to be more of an introvert or an extrovert?
11. Do you consider yourself to be talented with respect to artistic endeavors such as drawing, painting, sculpting, etc.?
12. Do you find yourself subjectively evaluating the attractiveness of other females in your everyday life?
13. Do you enjoy watching movies or television shows with lifelike computer generated imagery (CGI)?

Table: 1: Demographic questions.

APPENDIX: B – Regions of Interest

i7

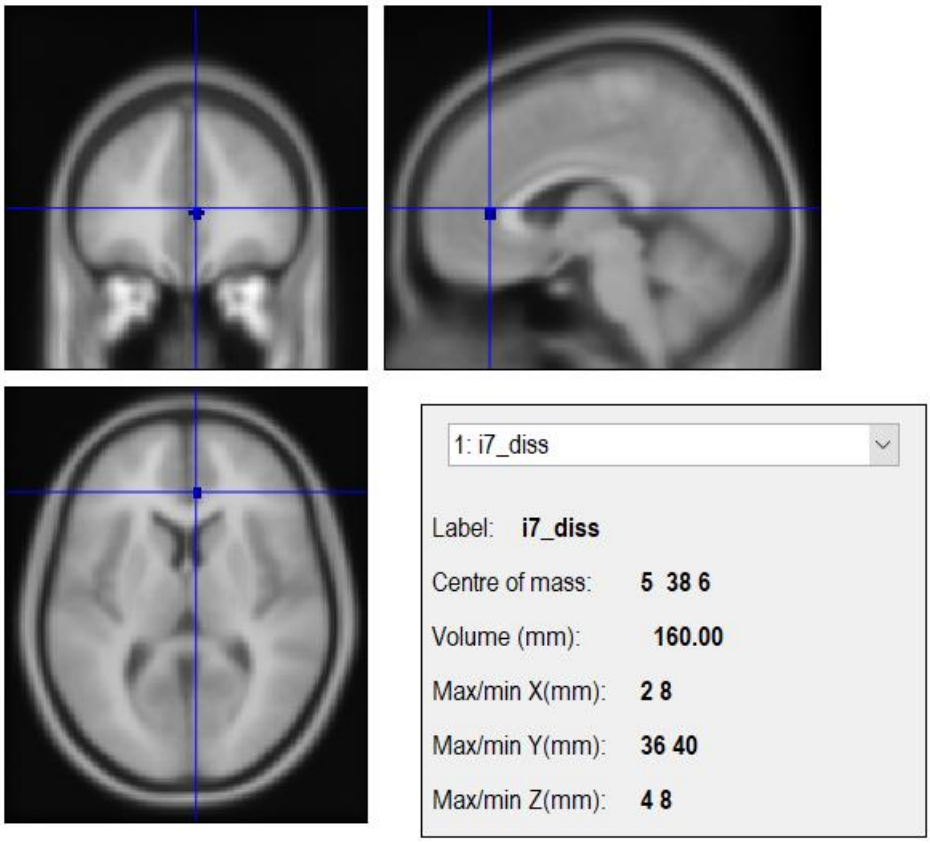

M1

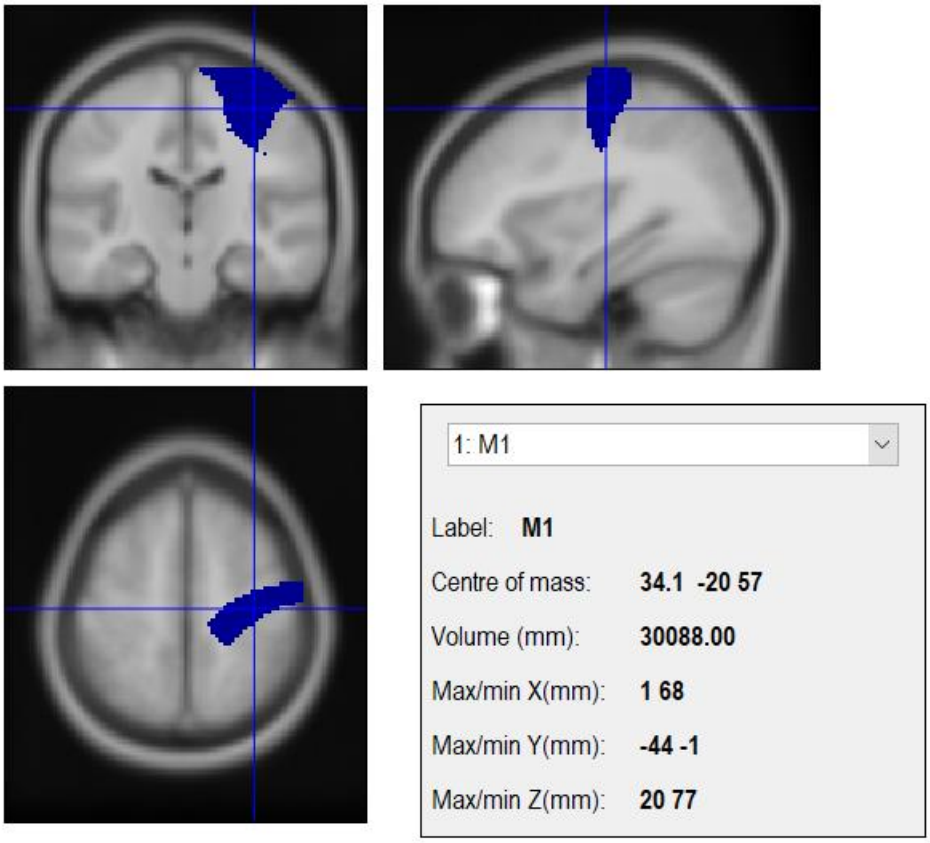
1: M1
Label: M1
Centre of mass: 34.1 -20 57
Volume (mm): 30088.00
Max/min X(mm): 1 68
Max/min Y(mm): -44 -1
Max/min Z(mm): 20 77

Group-level WHR

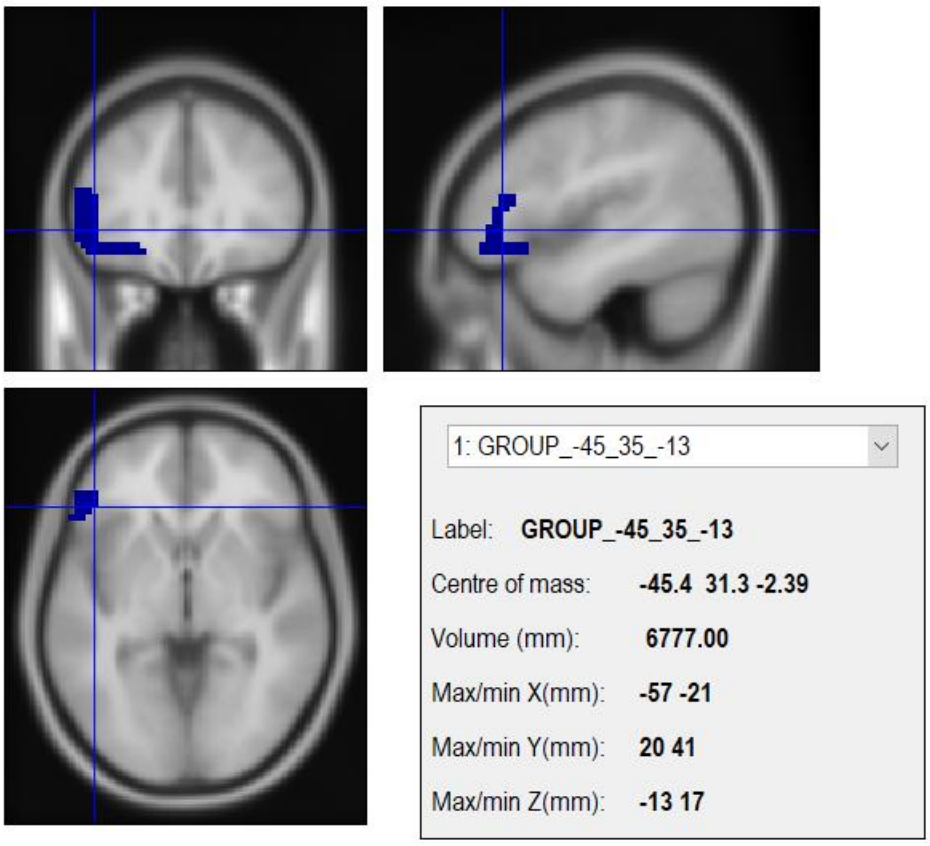

Subject-level ROI's

Subject 1

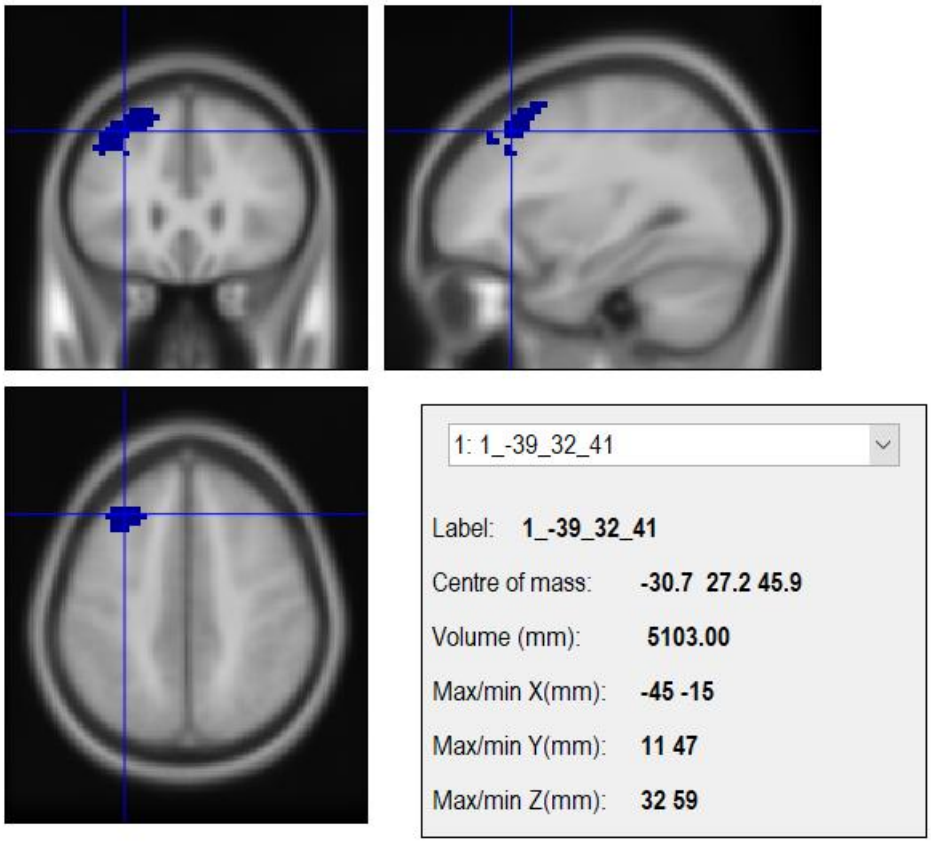

Subject 2

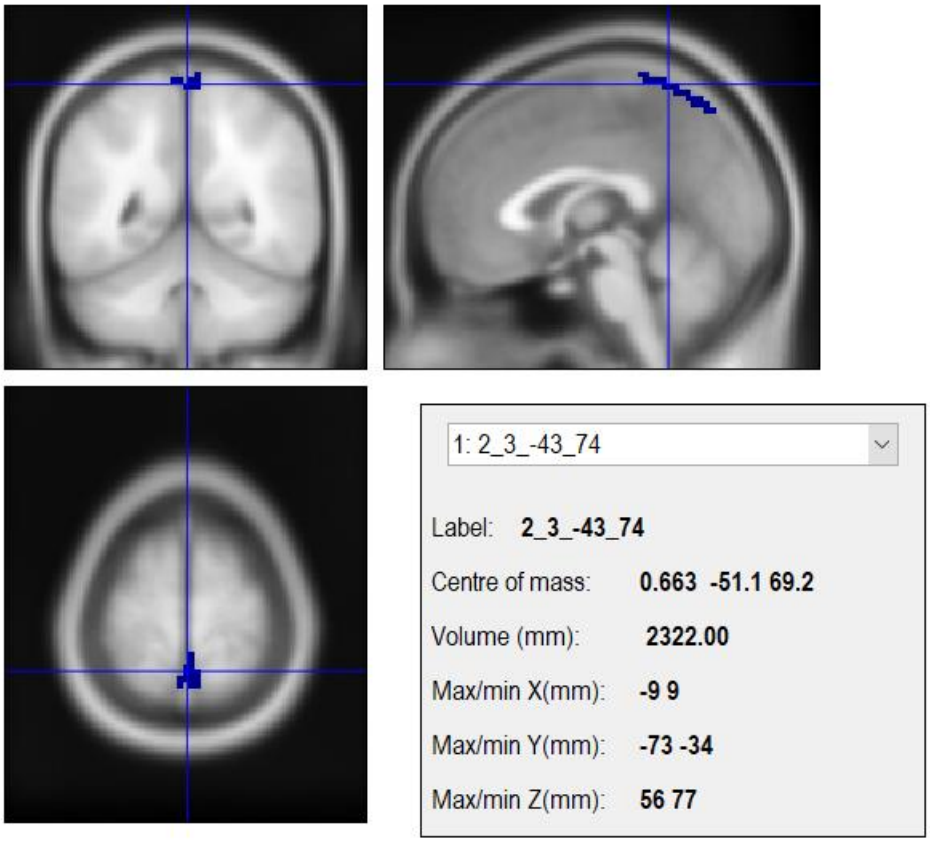
1: 2_3_-43_74
Label: 2_3_-43_74
Centre of mass: 0.663 -51.1 69.2
Volume (mm): 2322.00
Max/min X(mm): -9 9
Max/min Y(mm): -73 -34
Max/min Z(mm): 56 77

Subject 3

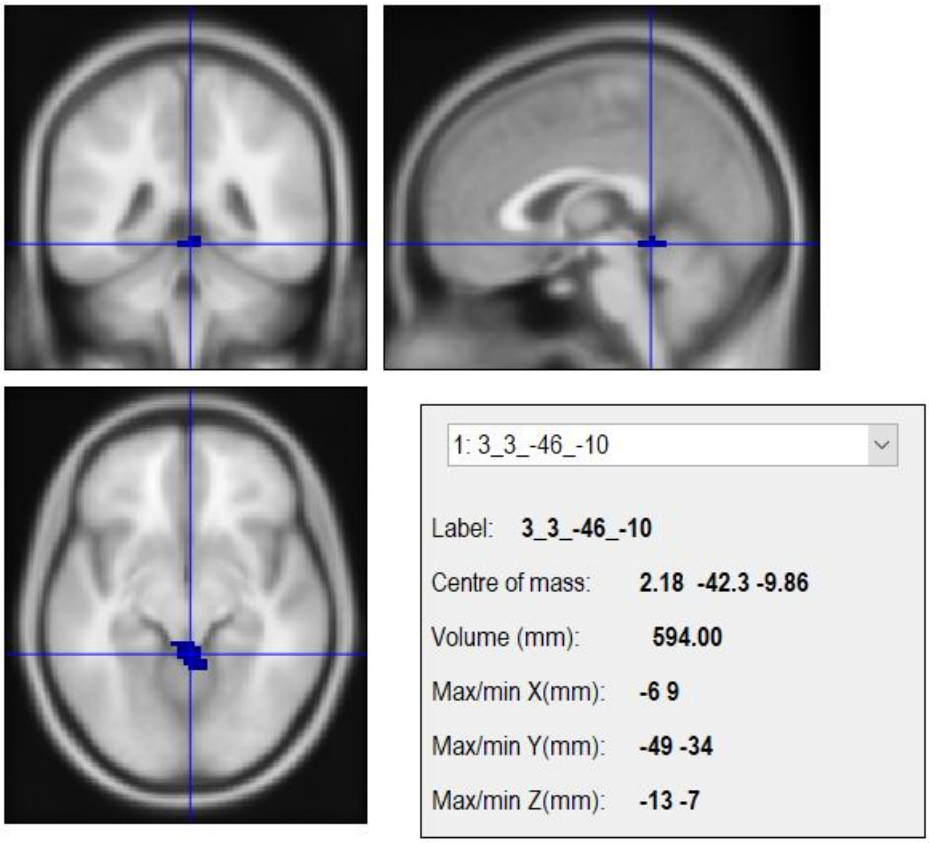
1: 3_3_-46_-10
Label: 3_3_-46_-10
Centre of mass: 2.18 -42.3 -9.86
Volume (mm): 594.00
Max/min X(mm): -6 9
Max/min Y(mm): -49 -34
Max/min Z(mm): -13 -7

Subject 4

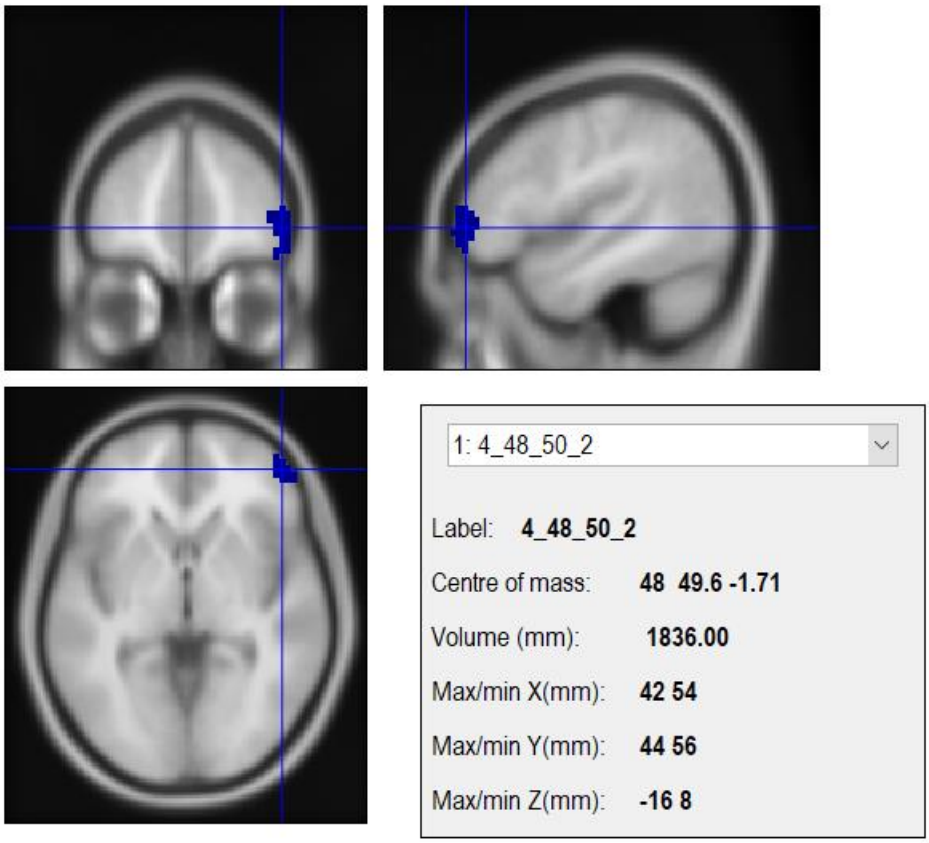
1: 4_48_50_2
Label: 4_48_50_2
Centre of mass: 48 49.6 -1.71
Volume (mm): 1836.00
Max/min X(mm): 42 54
Max/min Y(mm): 44 56
Max/min Z(mm): -16 8

Subject 5

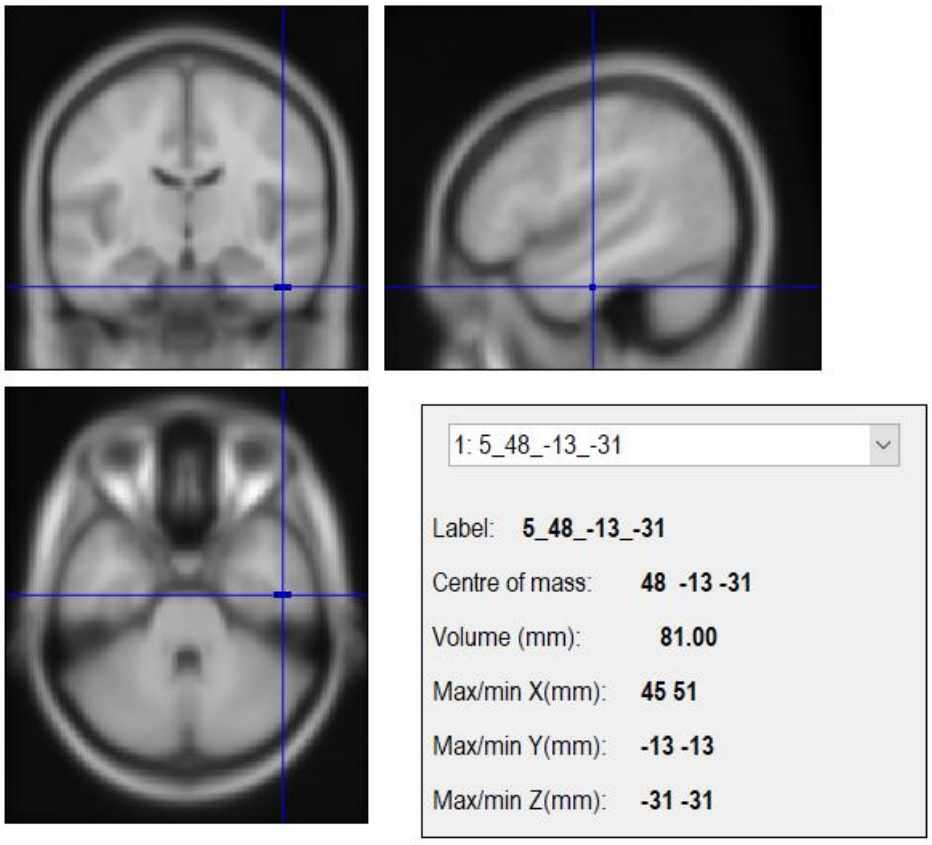
1: 5_48_-13_-31
Label: 5_48_-13_-31
Centre of mass: 48 -13 -31
Volume (mm): 81.00
Max/min X(mm): 45 51
Max/min Y(mm): -13 -13
Max/min Z(mm): -31 -31

Subject 6

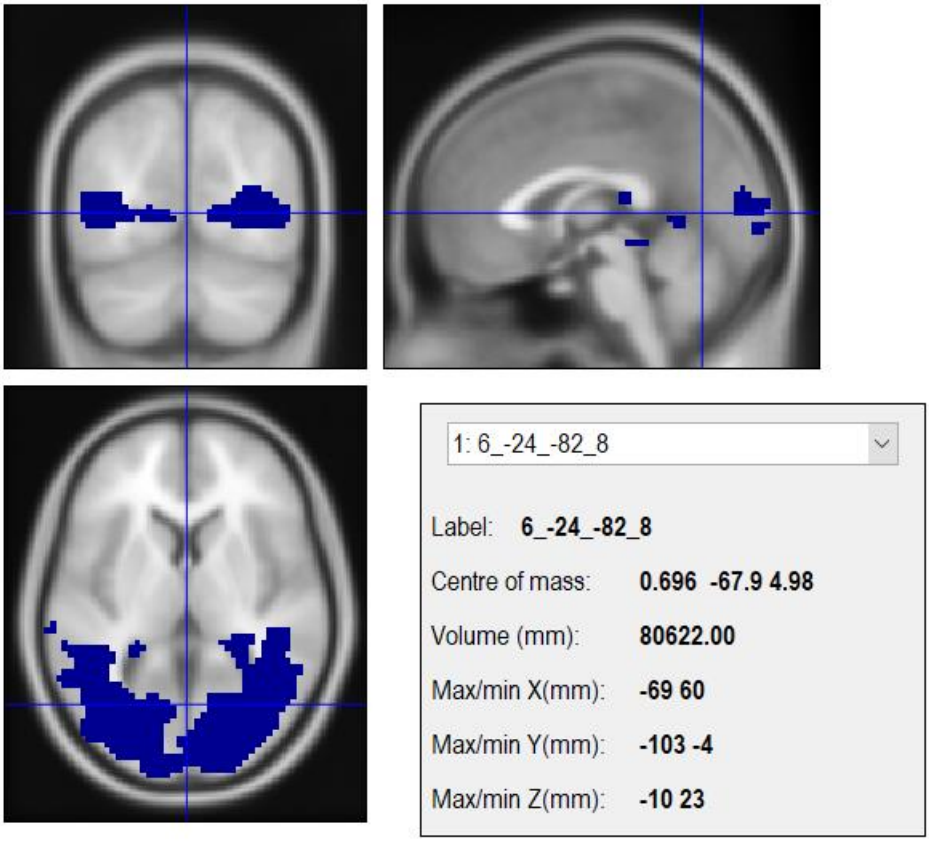
1: 6_-24_-82_8
Label: 6_-24_-82_8
Centre of mass: 0.696 -67.9 4.98
Volume (mm): 80622.00
Max/min X(mm): -69 60
Max/min Y(mm): -103 -4
Max/min Z(mm): -10 23

Subject 7

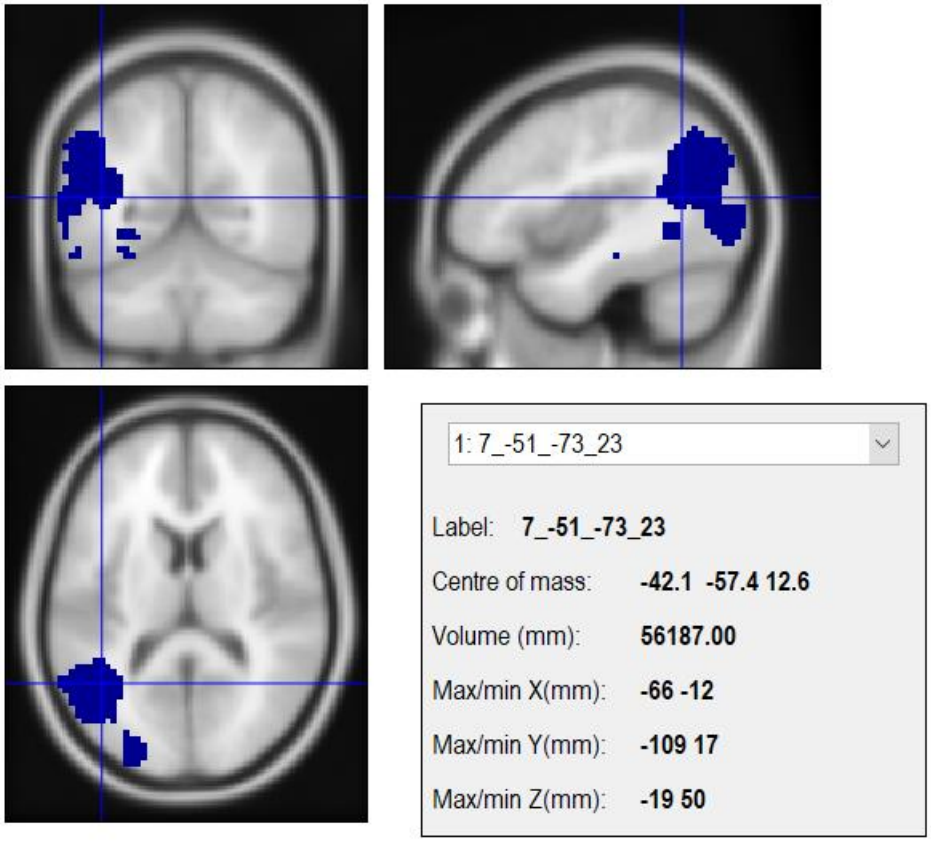
1: 7_-51_-73_23
Label: 7_-51_-73_23
Centre of mass: -42.1 -57.4 12.6
Volume (mm): 56187.00
Max/min X(mm): -66 -12
Max/min Y(mm): -109 17
Max/min Z(mm): -19 50

Subject 8

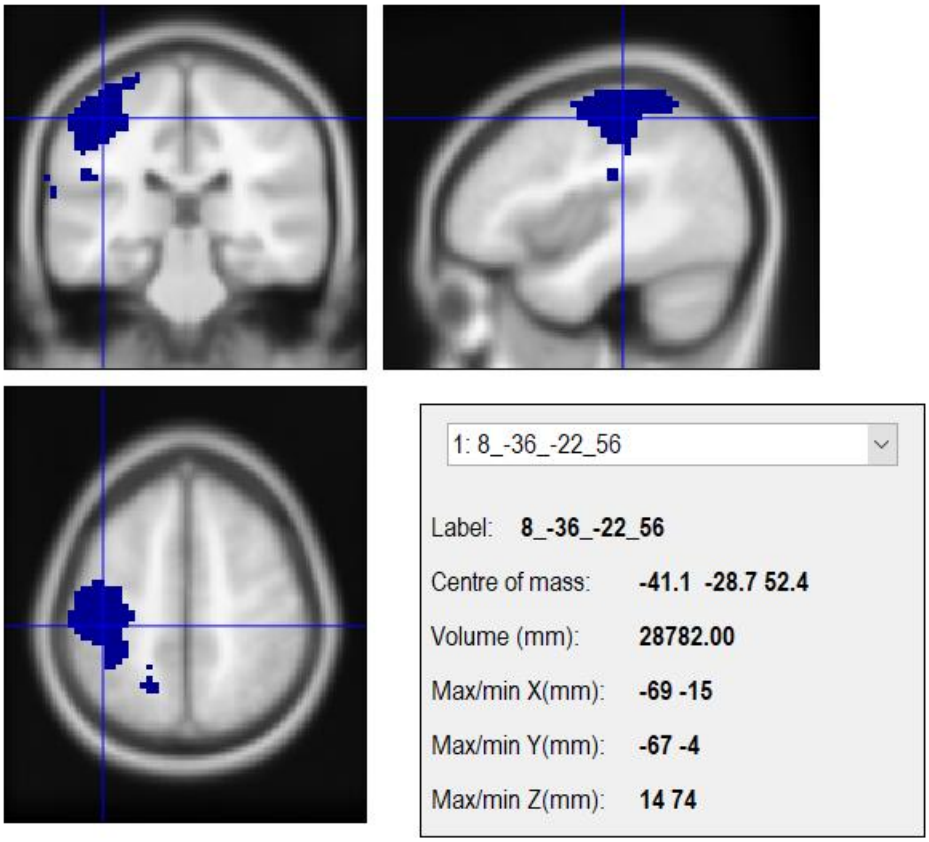
1: 8_-36_-22_56
Label: 8_-36_-22_56
Centre of mass: -41.1 -28.7 52.4
Volume (mm): 28782.00
Max/min X(mm): -69 -15
Max/min Y(mm): -67 -4
Max/min Z(mm): 14 74

Subject 9

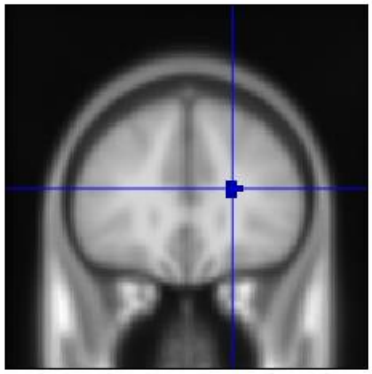

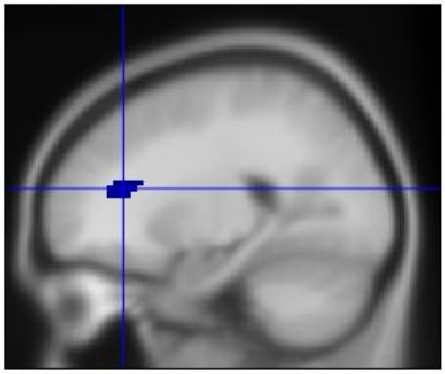

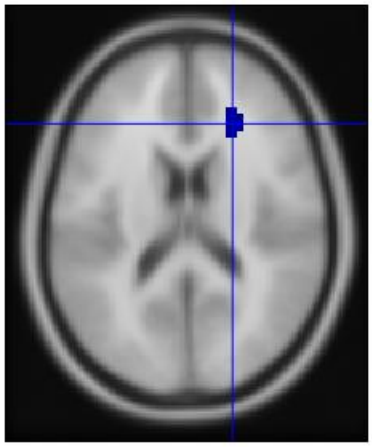

1: 9_24_32_17

Label: **9_24_32_17**

Centre of mass: **22.9 31.4 17.2**

Volume (mm): **837.00**

Max/min X(mm): **21 27**

Max/min Y(mm): **23 38**

Max/min Z(mm): **14 20**

Subject 10

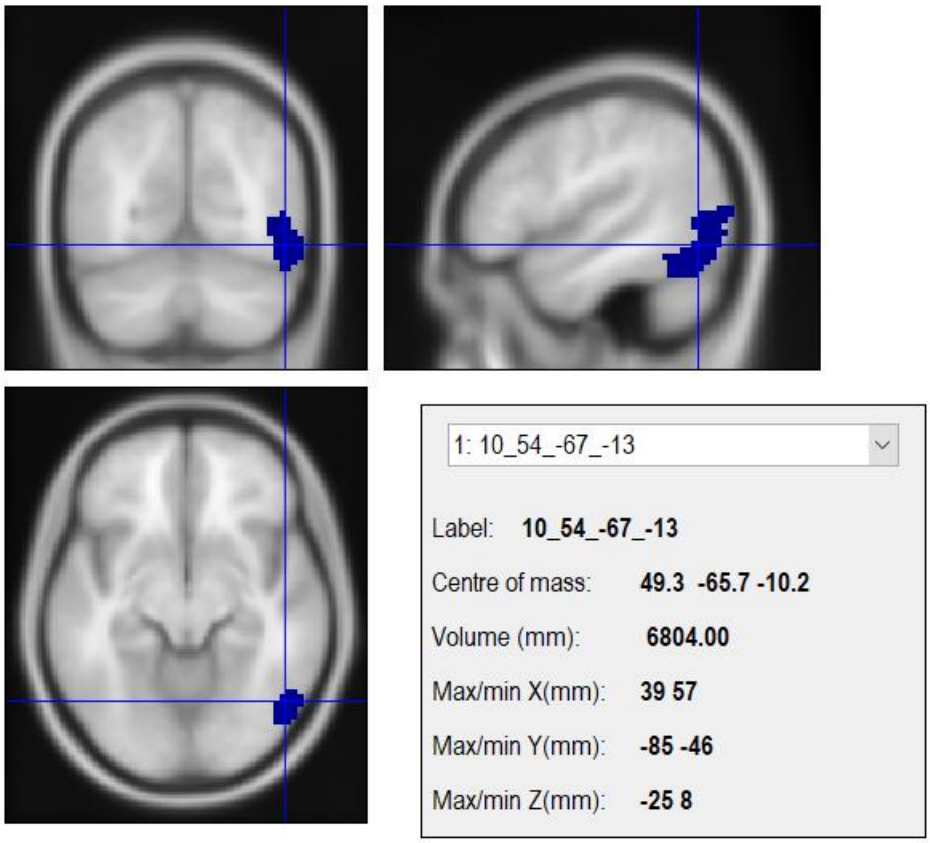
1: 10_54_-67_-13
Label: 10_54_-67_-13
Centre of mass: 49.3 -65.7 -10.2
Volume (mm): 6804.00
Max/min X(mm): 39 57
Max/min Y(mm): -85 -46
Max/min Z(mm): -25 8

Subject 11

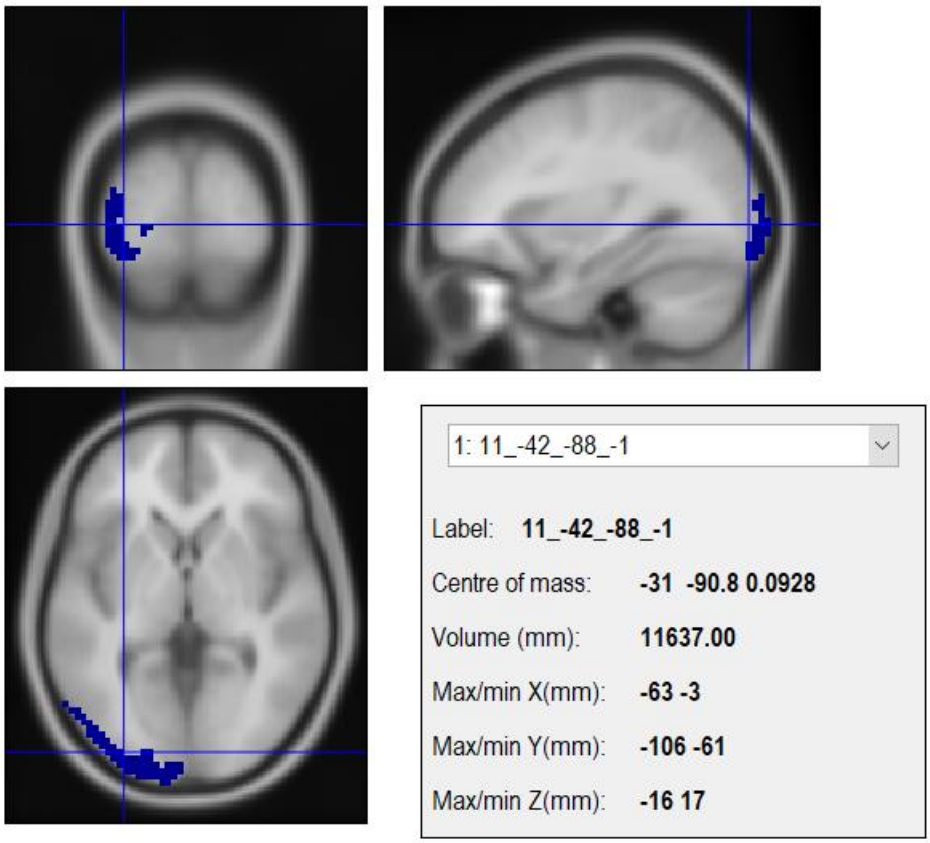
1: 11_-42_-88_-1
Label: 11_-42_-88_-1
Centre of mass: -31 -90.8 0.0928
Volume (mm): 11637.00
Max/min X(mm): -63 -3
Max/min Y(mm): -106 -61
Max/min Z(mm): -16 17

Subject 12

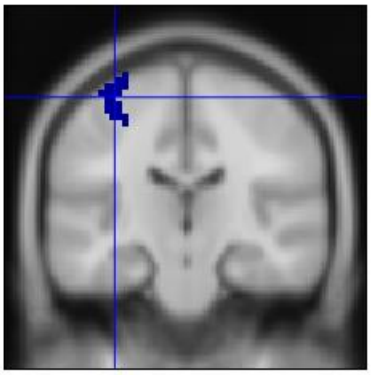

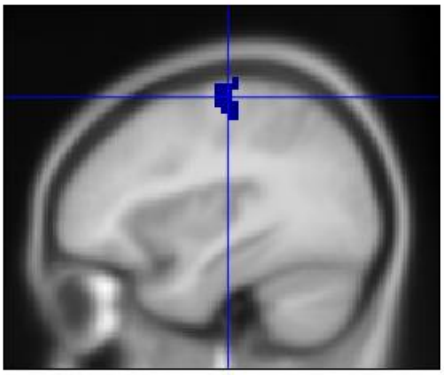

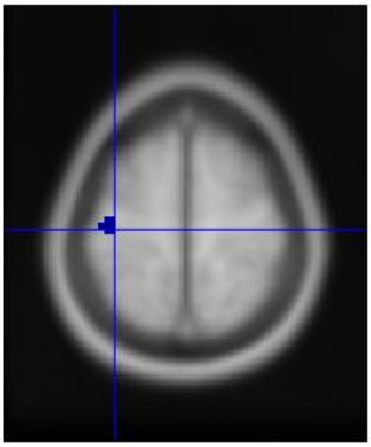

1: 12_-33_-22_71

Label: **12_-33_-22_71**

Centre of mass: **-35.2 -21.1 62.6**

Volume (mm): **1755.00**

Max/min X(mm): **-42 -30**

Max/min Y(mm): **-25 -16**

Max/min Z(mm): **50 74**

Subject 13

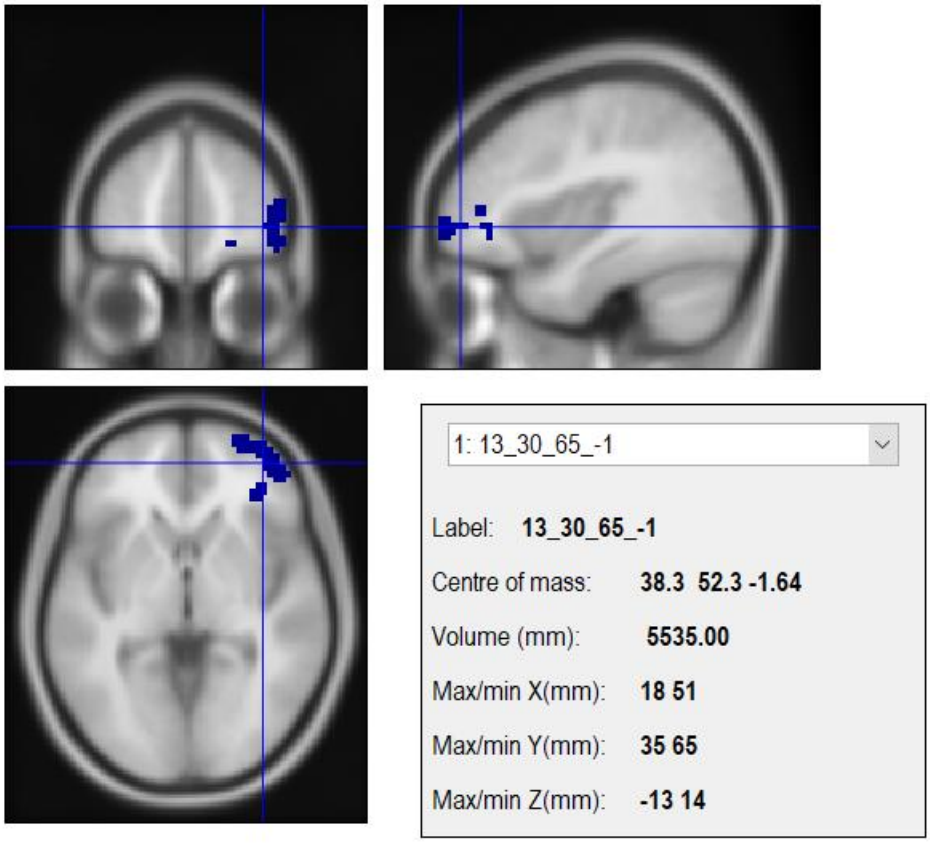
1: 13_30_65_-1
Label: 13_30_65_-1
Centre of mass: 38.3 52.3 -1.64
Volume (mm): 5535.00
Max/min X(mm): 18 51
Max/min Y(mm): 35 65
Max/min Z(mm): -13 14

Subject 14

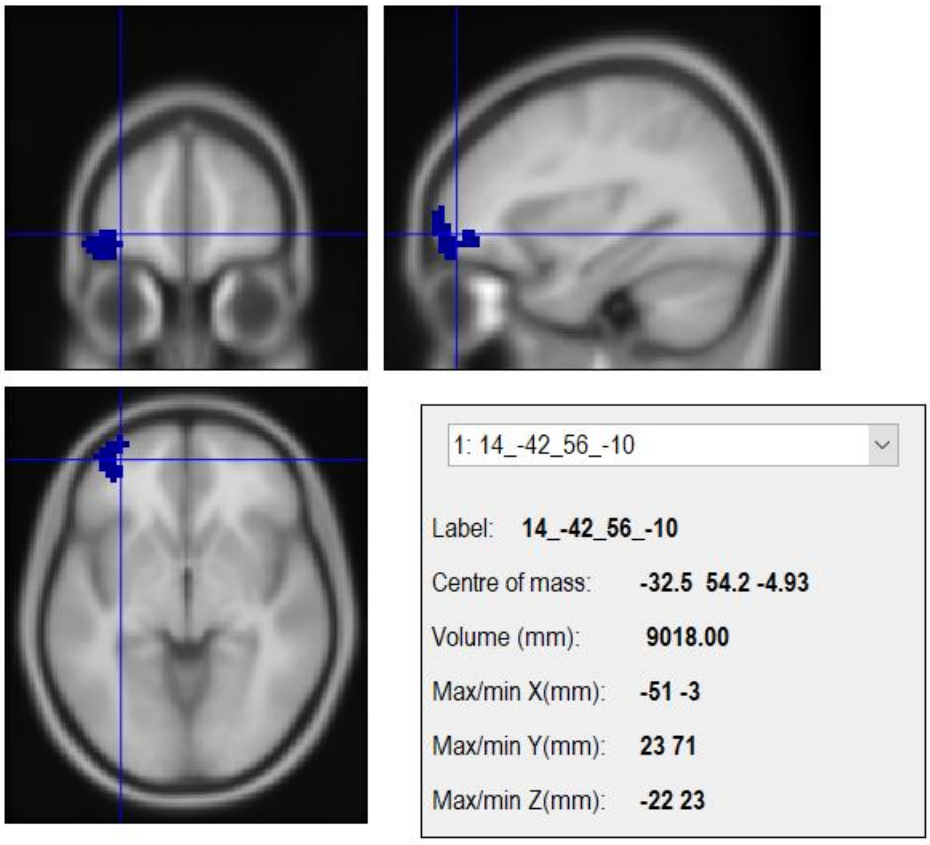
1: 14_-42_56_-10
Label: 14_-42_56_-10
Centre of mass: -32.5 54.2 -4.93
Volume (mm): 9018.00
Max/min X(mm): -51 -3
Max/min Y(mm): 23 71
Max/min Z(mm): -22 23

Subject 15

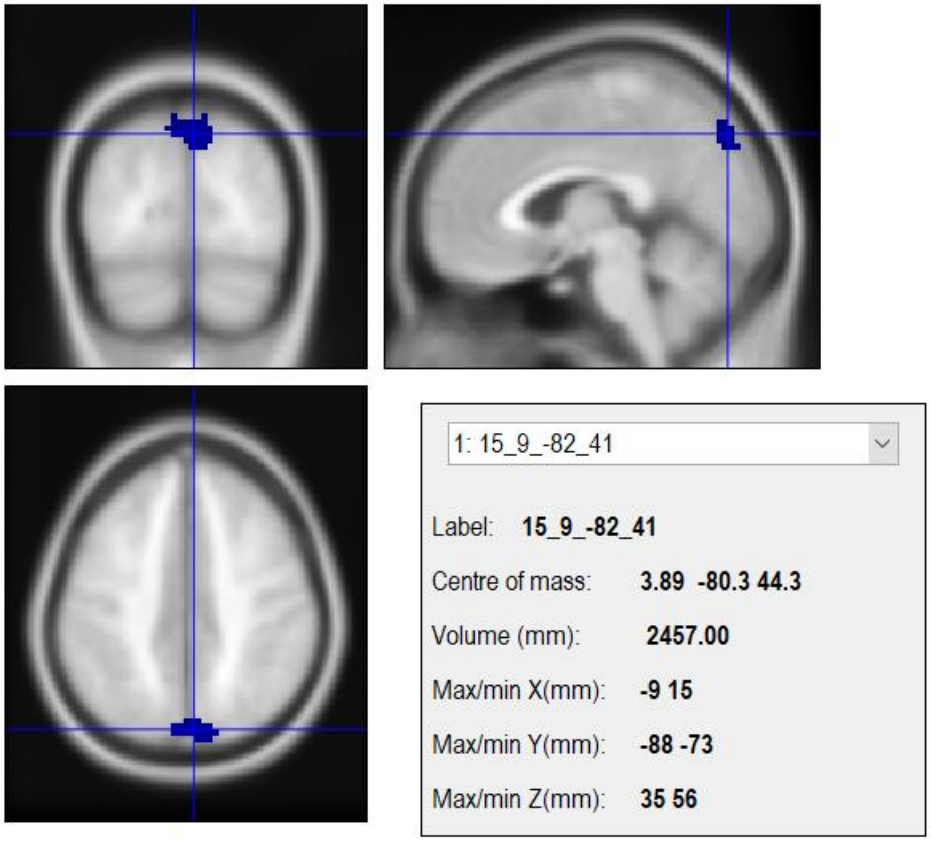
1: 15_9_-82_41
Label: 15_9_-82_41
Centre of mass: 3.89 -80.3 44.3
Volume (mm): 2457.00
Max/min X(mm): -9 15
Max/min Y(mm): -88 -73
Max/min Z(mm): 35 56

Masked Subject-level ROI's

Subject 1

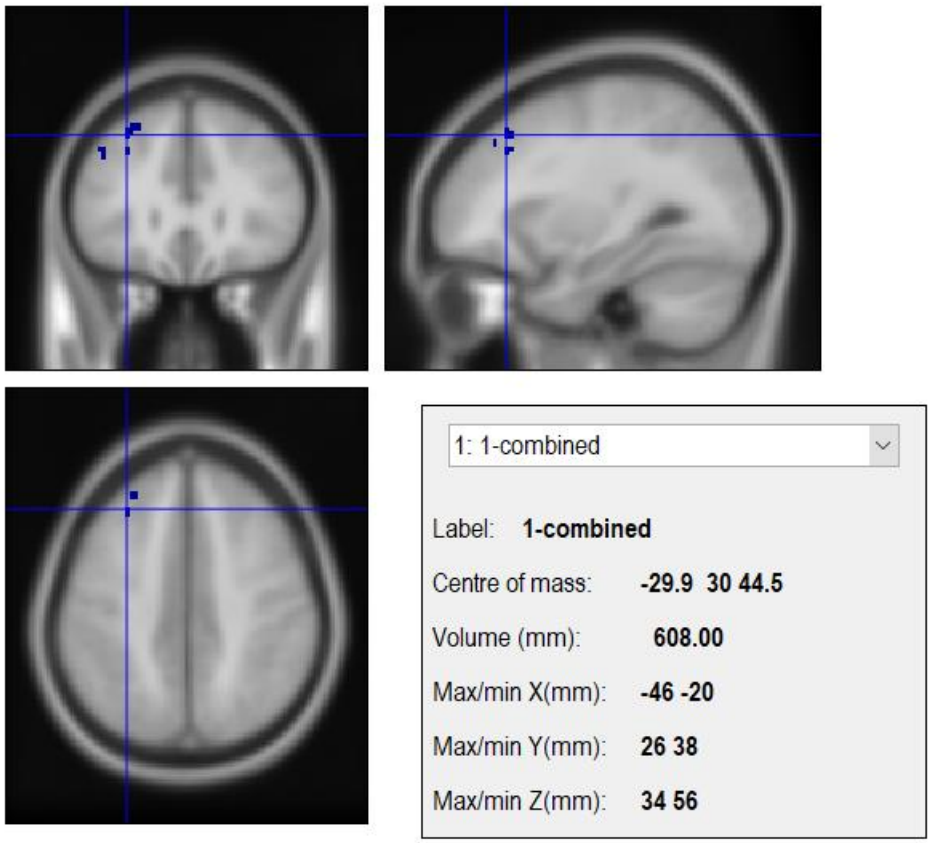

Subject 2

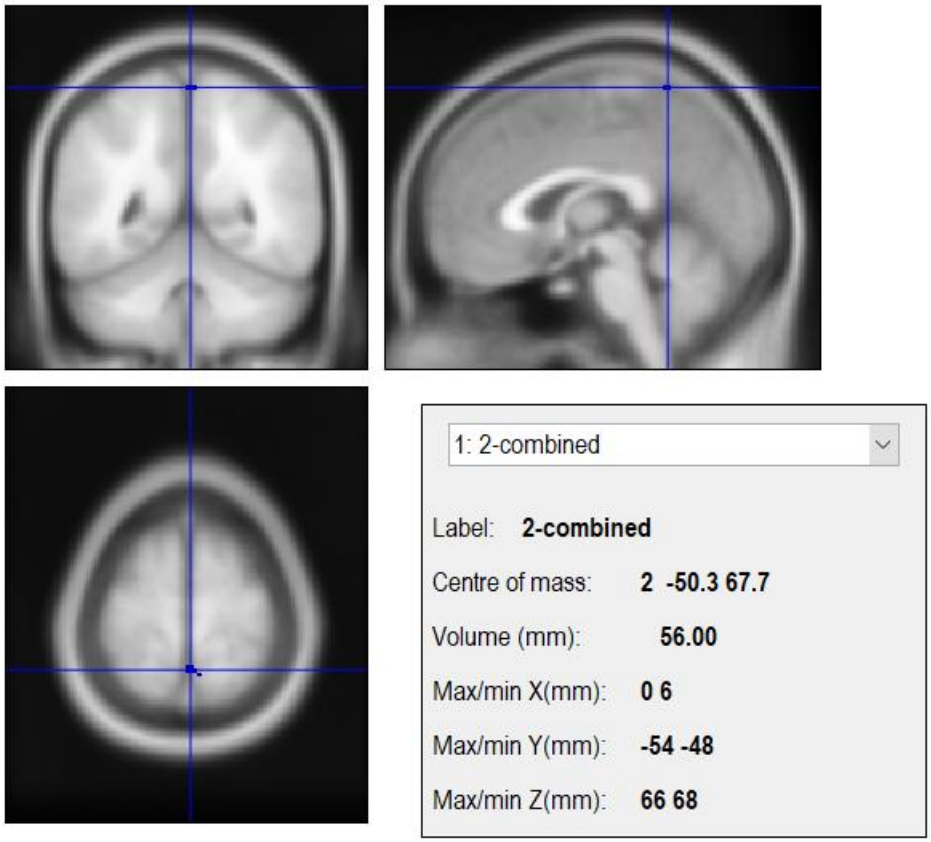
1: 2-combined
Label: 2-combined
Centre of mass: 2 -50.3 67.7
Volume (mm): 56.00
Max/min X(mm): 0 6
Max/min Y(mm): -54 -48
Max/min Z(mm): 66 68

Subject 4

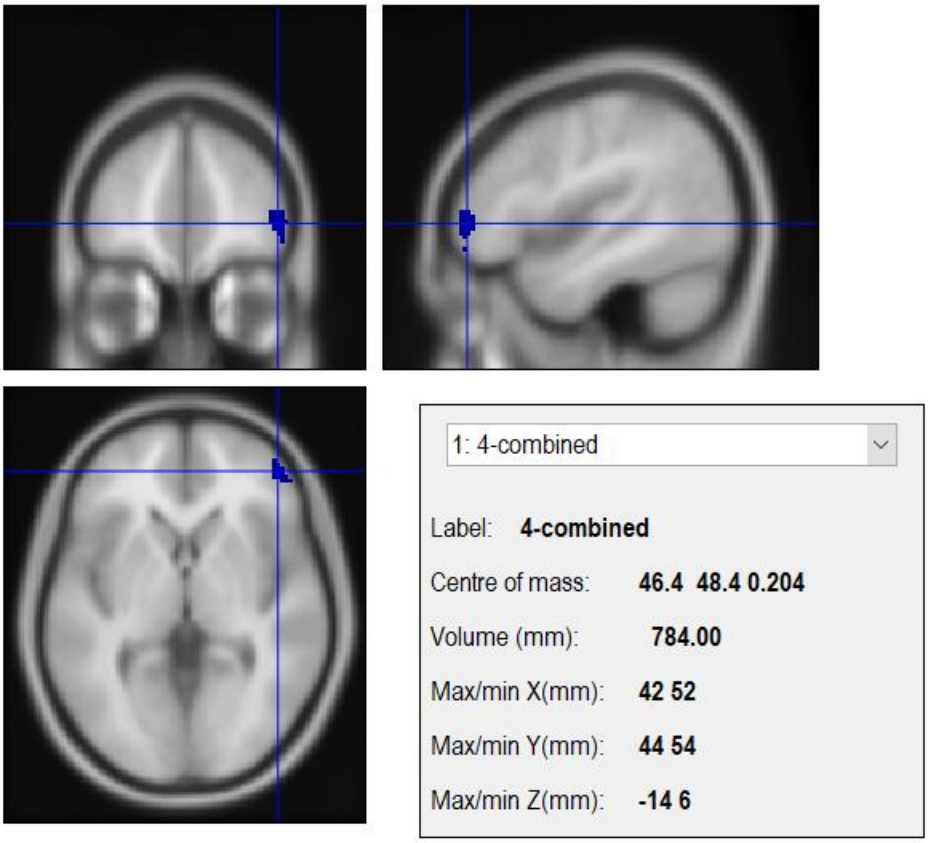
1: 4-combined
Label: 4-combined
Centre of mass: 46.4 48.4 0.204
Volume (mm): 784.00
Max/min X(mm): 42 52
Max/min Y(mm): 44 54
Max/min Z(mm): -14 6

Subject 6

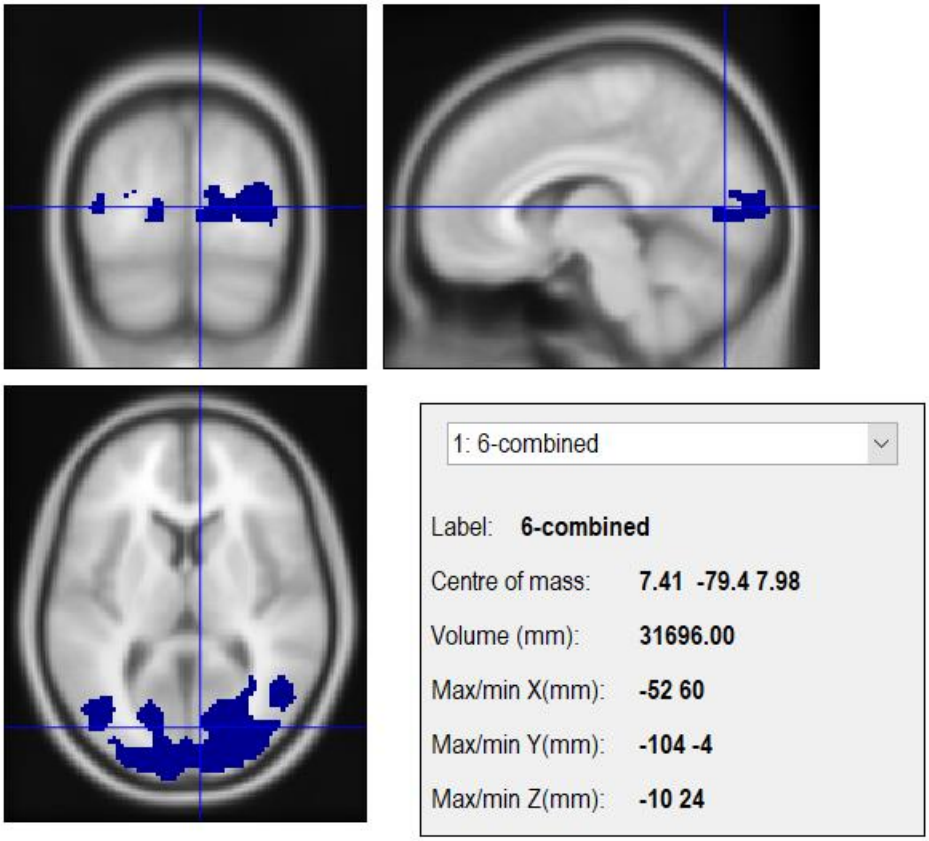
1: 6-combined
Label: 6-combined
Centre of mass: 7.41 -79.4 7.98
Volume (mm): 31696.00
Max/min X(mm): -52 60
Max/min Y(mm): -104 -4
Max/min Z(mm): -10 24

Subject 7

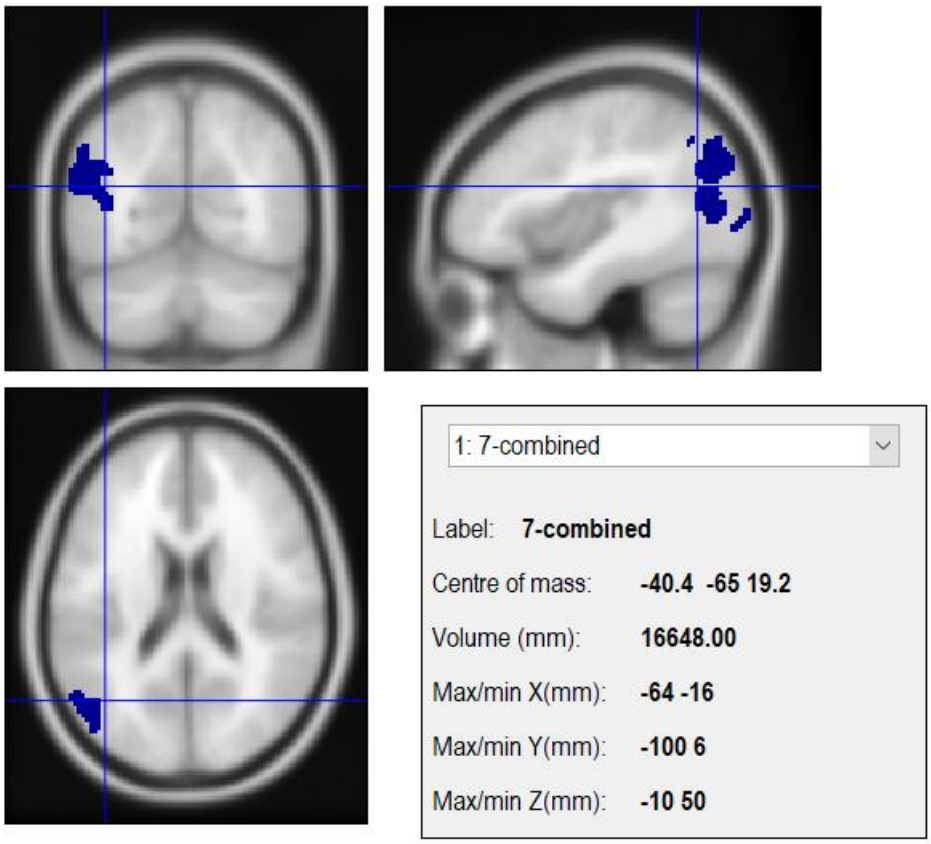
1: 7-combined
Label: 7-combined
Centre of mass: -40.4 -65 19.2
Volume (mm): 16648.00
Max/min X(mm): -64 -16
Max/min Y(mm): -100 6
Max/min Z(mm): -10 50

Subject 8

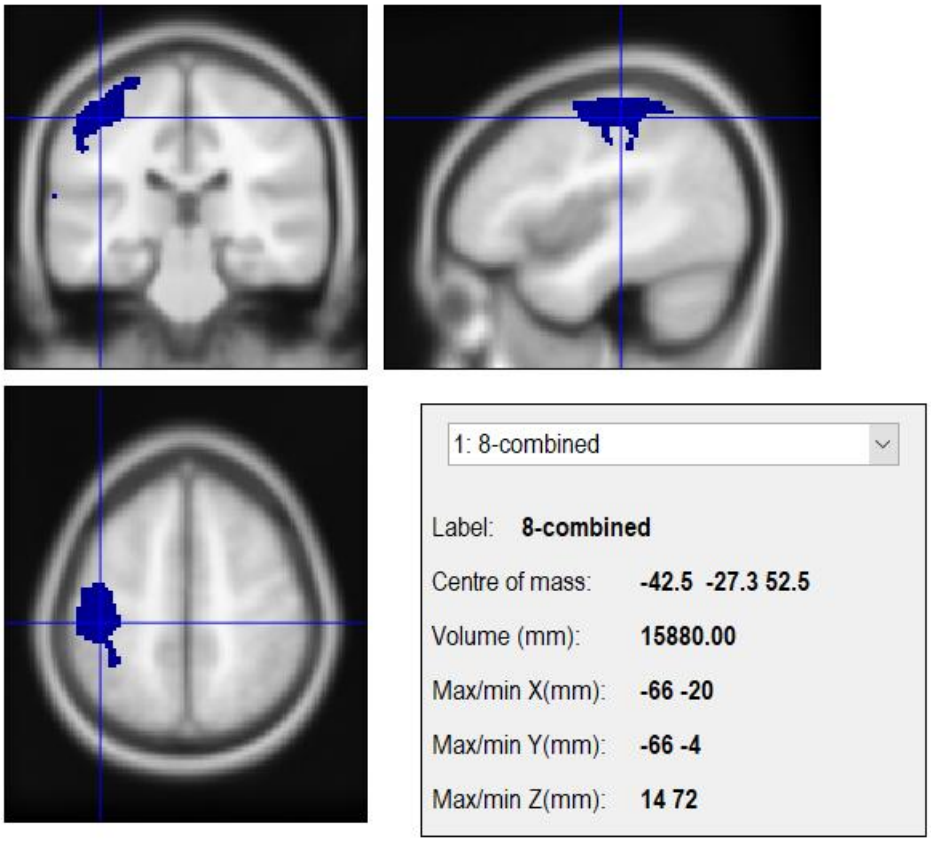
1: 8-combined
Label: 8-combined
Centre of mass: -42.5 -27.3 52.5
Volume (mm): 15880.00
Max/min X(mm): -66 -20
Max/min Y(mm): -66 -4
Max/min Z(mm): 14 72

Subject 10

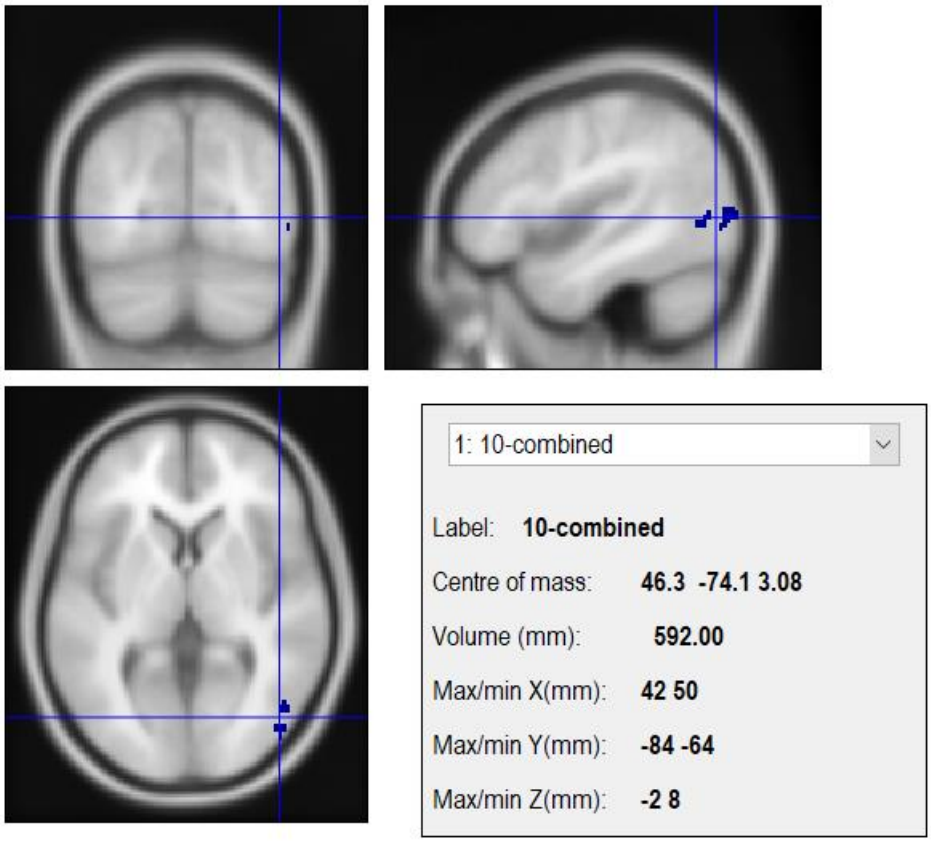
1: 10-combined
Label: 10-combined
Centre of mass: 46.3 -74.1 3.08
Volume (mm): 592.00
Max/min X(mm): 42 50
Max/min Y(mm): -84 -64
Max/min Z(mm): -2 8

Subject 11

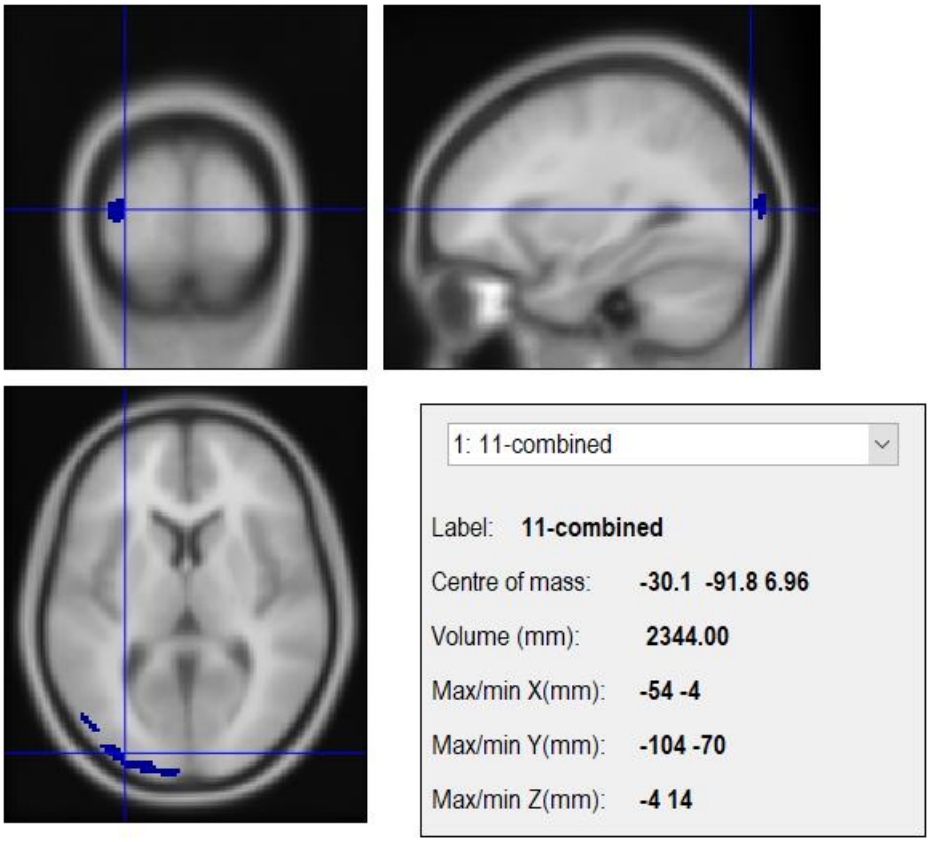
1: 11-combined
Label: 11-combined
Centre of mass: -30.1 -91.8 6.96
Volume (mm): 2344.00
Max/min X(mm): -54 -4
Max/min Y(mm): -104 -70
Max/min Z(mm): -4 14

Subject 12

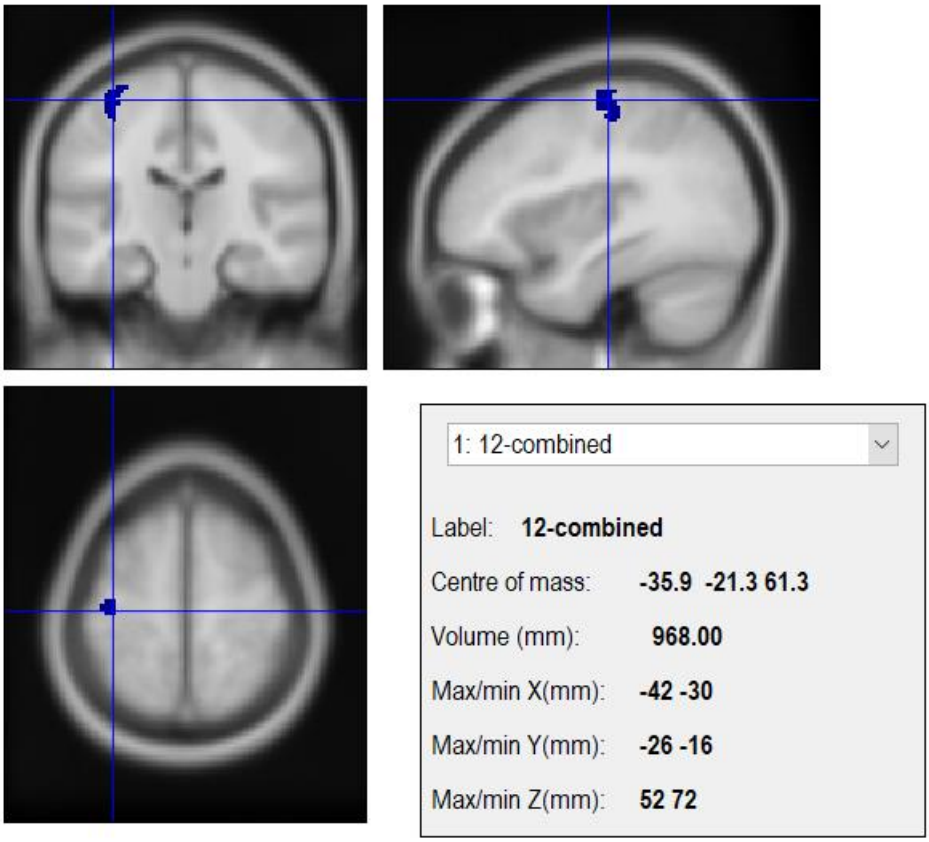
1: 12-combined
Label: 12-combined
Centre of mass: -35.9 -21.3 61.3
Volume (mm): 968.00
Max/min X(mm): -42 -30
Max/min Y(mm): -26 -16
Max/min Z(mm): 52 72

Subject 13

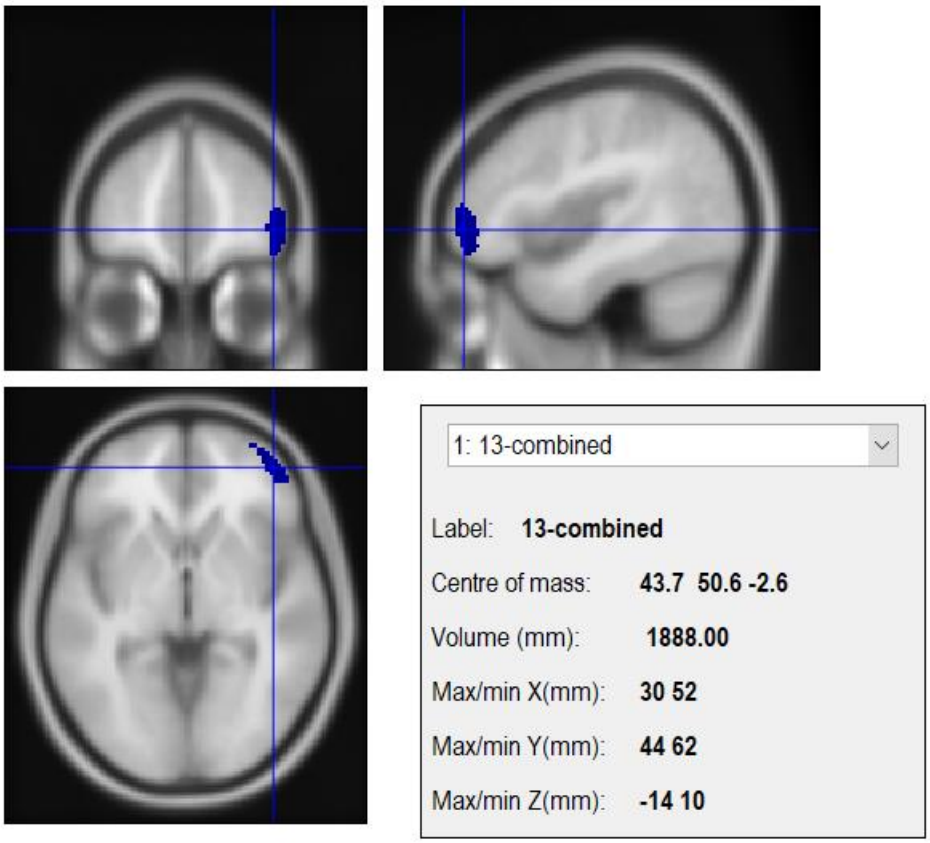
1: 13-combined
Label: 13-combined
Centre of mass: 43.7 50.6 -2.6
Volume (mm): 1888.00
Max/min X(mm): 30 52
Max/min Y(mm): 44 62
Max/min Z(mm): -14 10

Subject 14

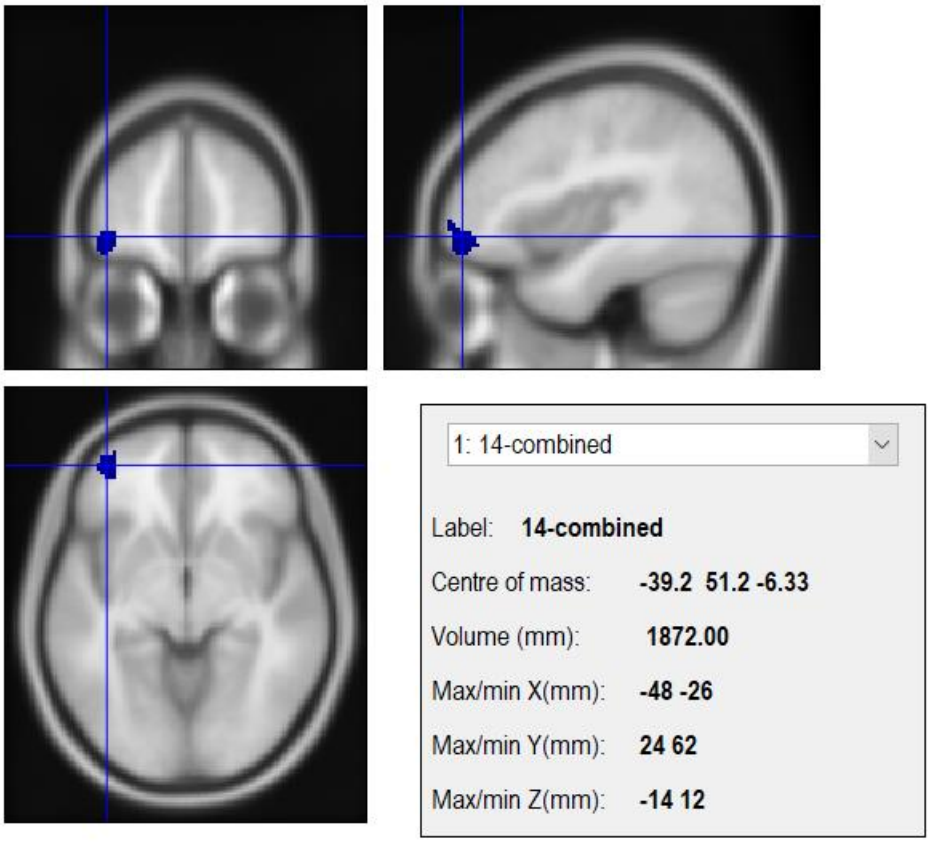
1: 14-combined
Label: 14-combined
Centre of mass: -39.2 51.2 -6.33
Volume (mm): 1872.00
Max/min X(mm): -48 -26
Max/min Y(mm): 24 62
Max/min Z(mm): -14 12

Subject 15

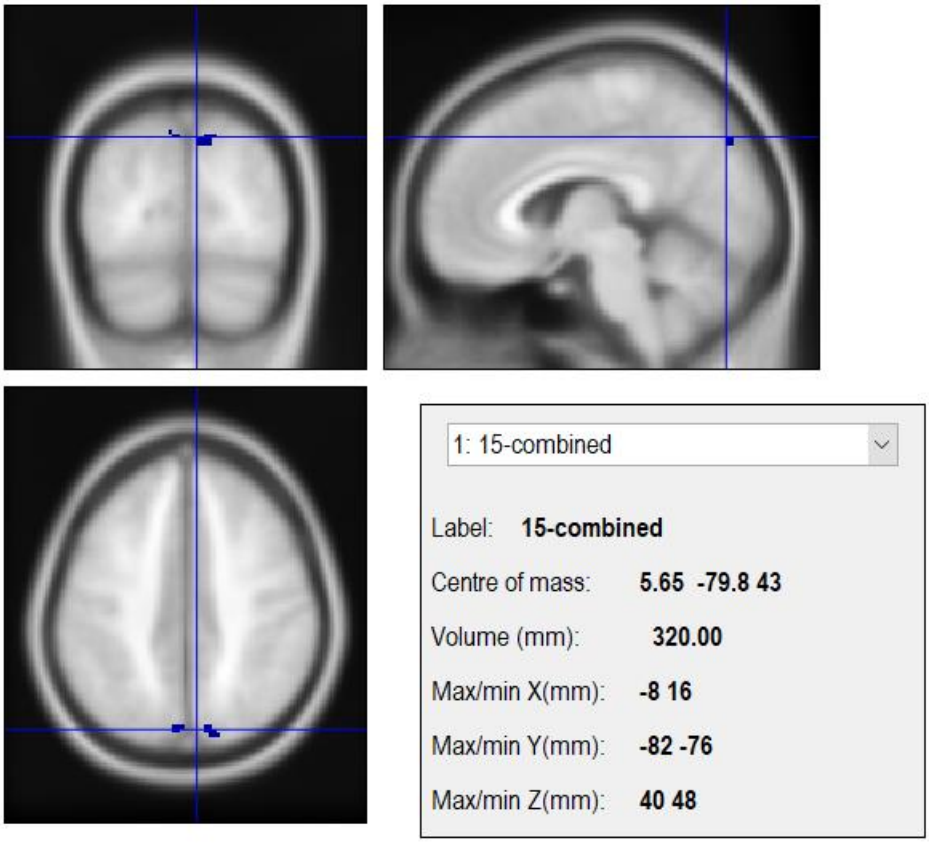
1: 15-combined
Label: 15-combined
Centre of mass: 5.65 -79.8 43
Volume (mm): 320.00
Max/min X(mm): -8 16
Max/min Y(mm): -82 -76
Max/min Z(mm): 40 48

APPENDIX: C – Overlay of PSC Prediction on Ending PSC & IWD Relationship

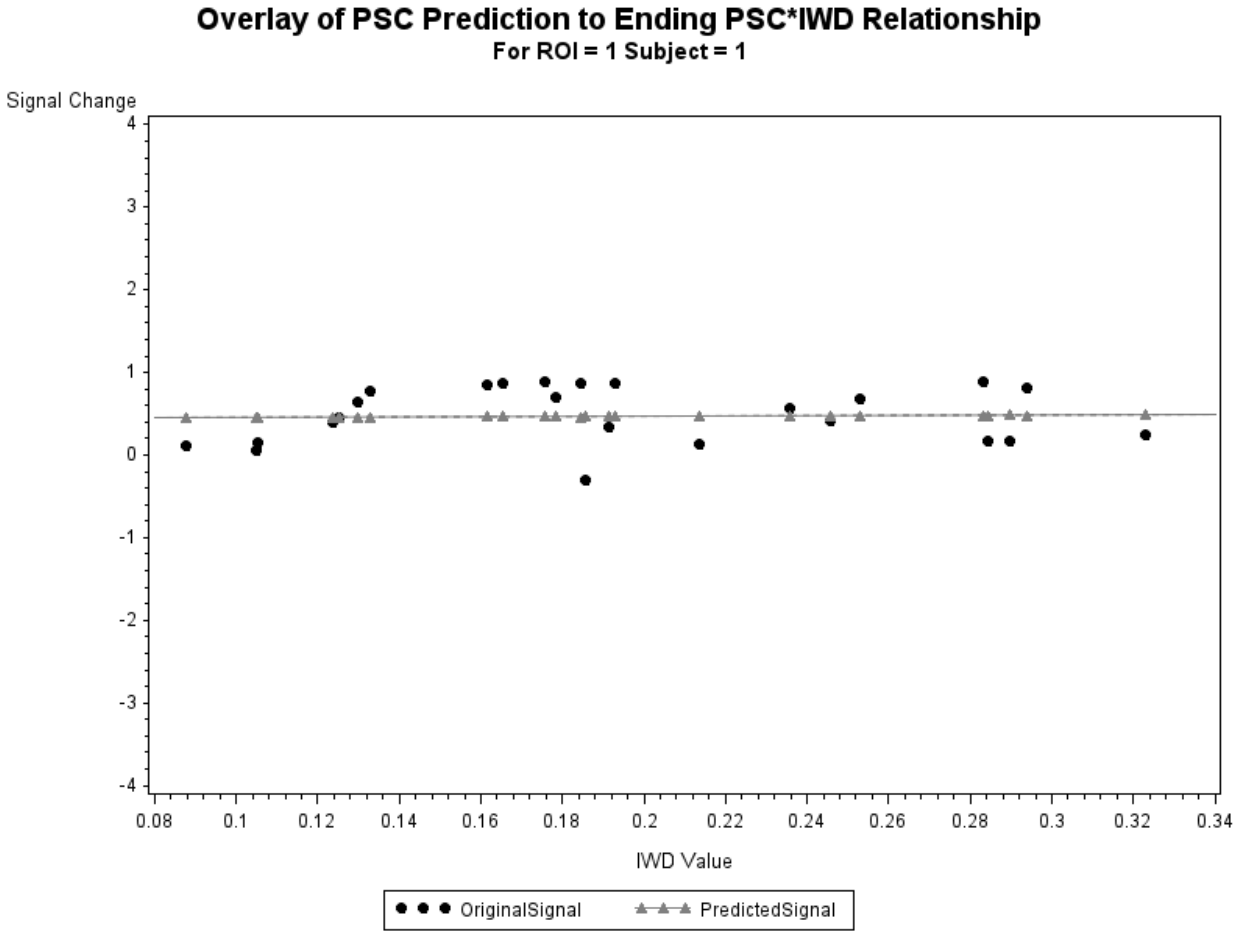

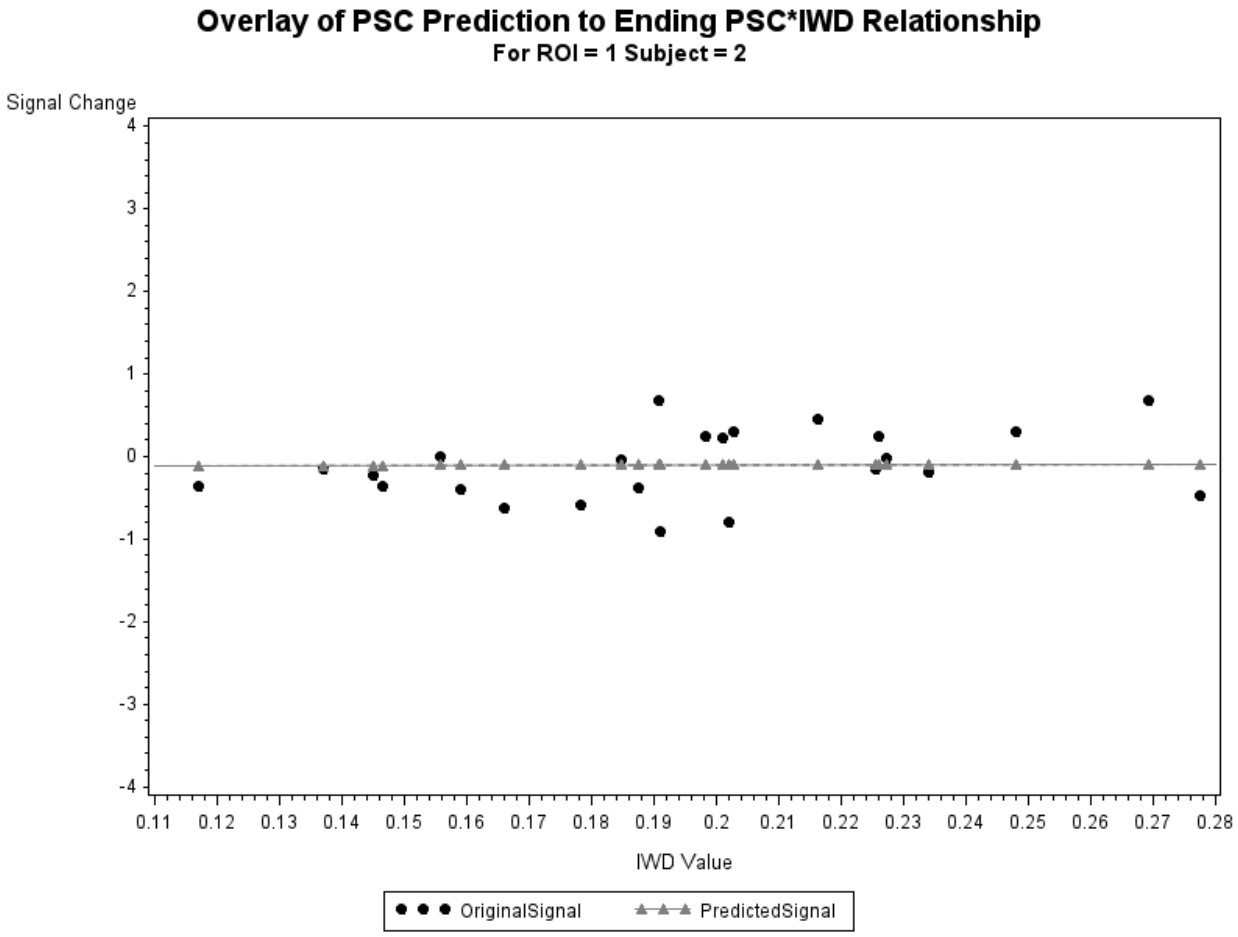
Overlay of PSC Prediction to Ending PSC*IWD Relationship
For ROI = 1 Subject = 2
Signal Change
4
3
2
1
0
-1
-2
-3
-4
0.11
0.12
0.13
0.14
0.15
0.16
0.17
0.18
0.19
0.2
0.21
0.22
0.23
0.24
0.25
0.26
0.27
0.28
IWD Value
OriginalSignal
PredictedSignal

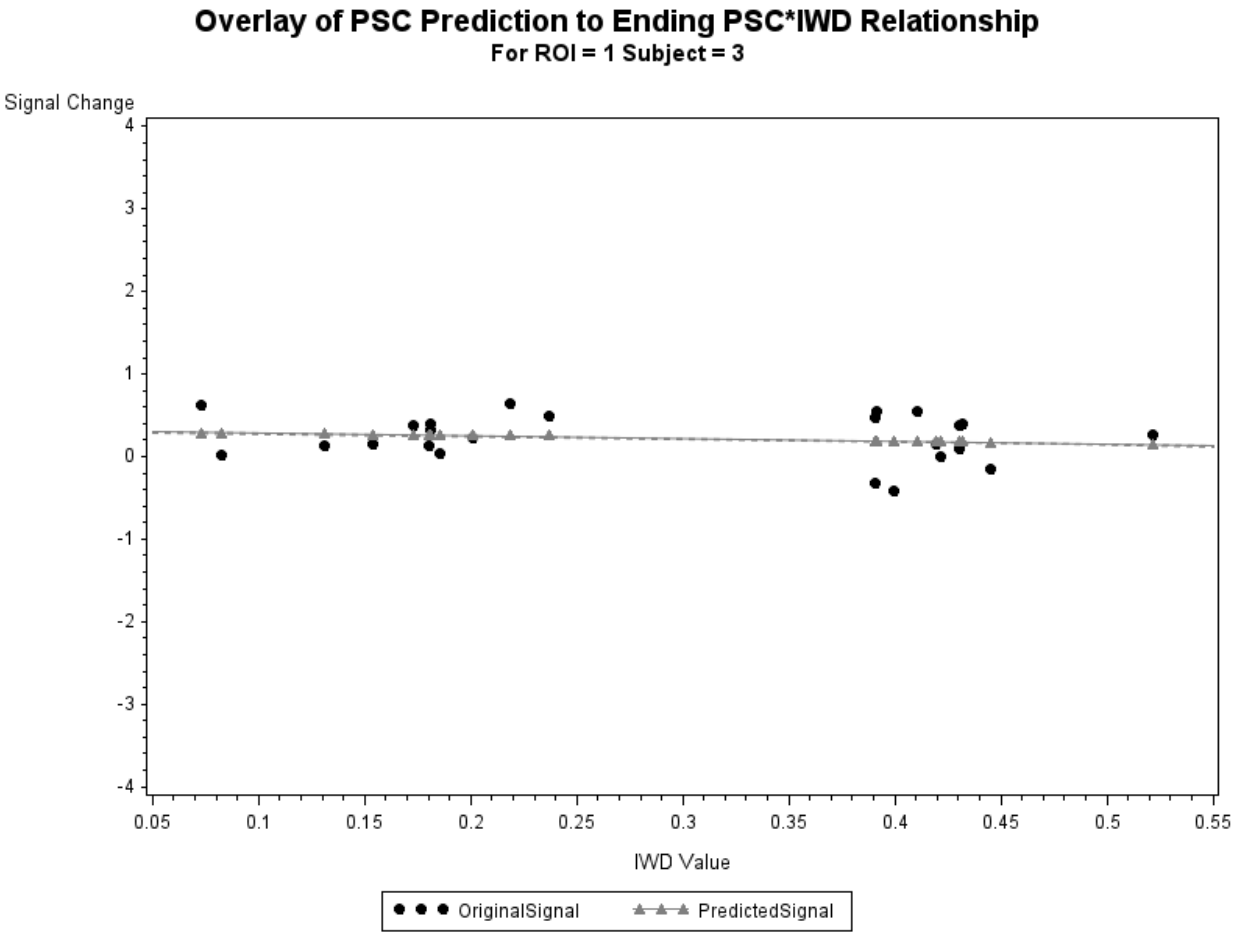
Overlay of PSC Prediction to Ending PSC*IWD Relationship
For ROI = 1 Subject = 3
Signal Change
4
3
2
1
0
-1
-2
-3
-4
0.05
0.1
0.15
0.2
0.25
0.3
0.35
0.4
0.45
0.5
0.55
IWD Value
OriginalSignal
PredictedSignal

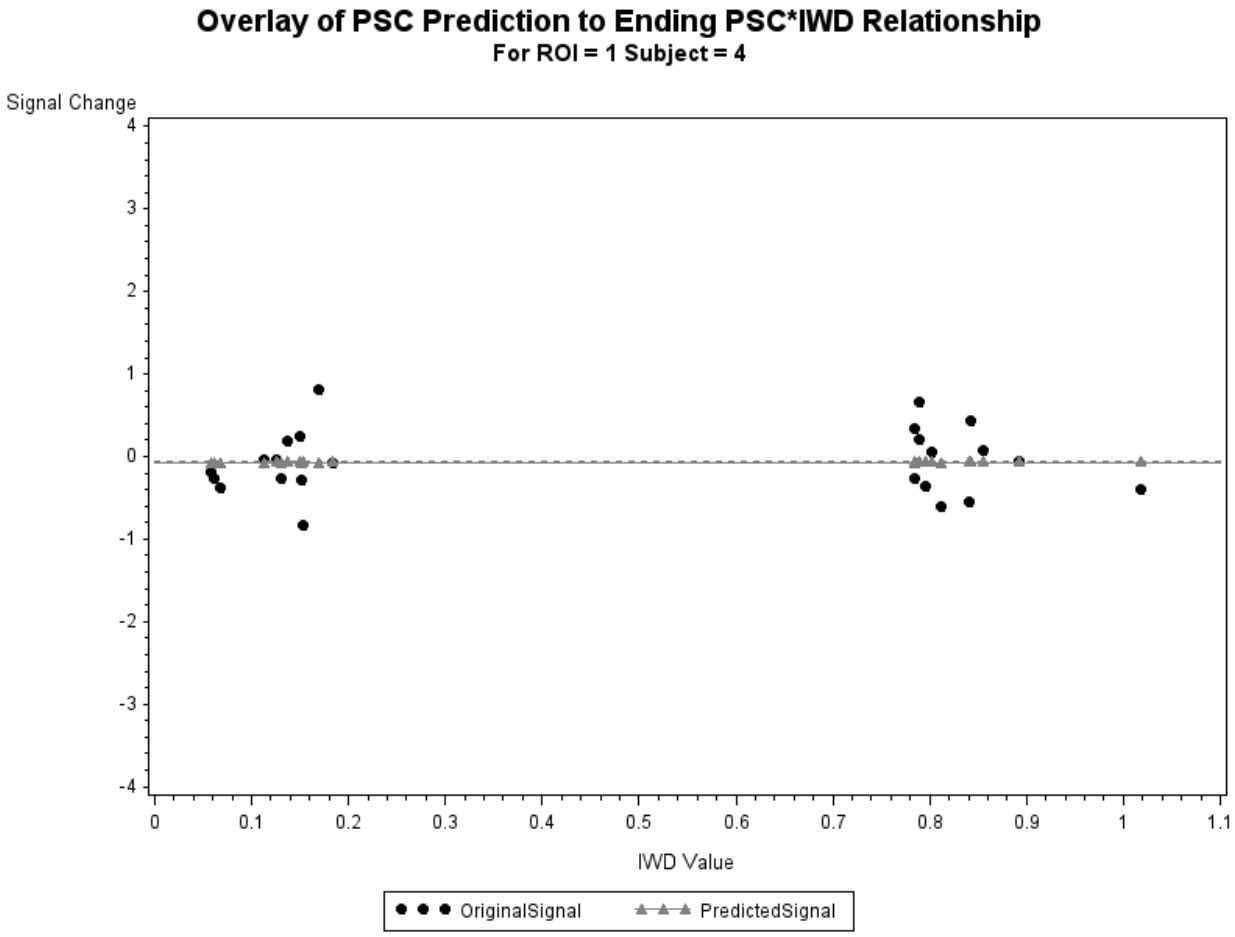
Overlay of PSC Prediction to Ending PSC*IWD Relationship
For ROI = 1 Subject = 4
Signal Change
4
3
2
1
0
-1
-2
-3
-4
0
0.1
0.2
0.3
0.4
0.5
0.6
0.7
0.8
0.9
1
1.1
IWD Value
OriginalSignal
PredictedSignal

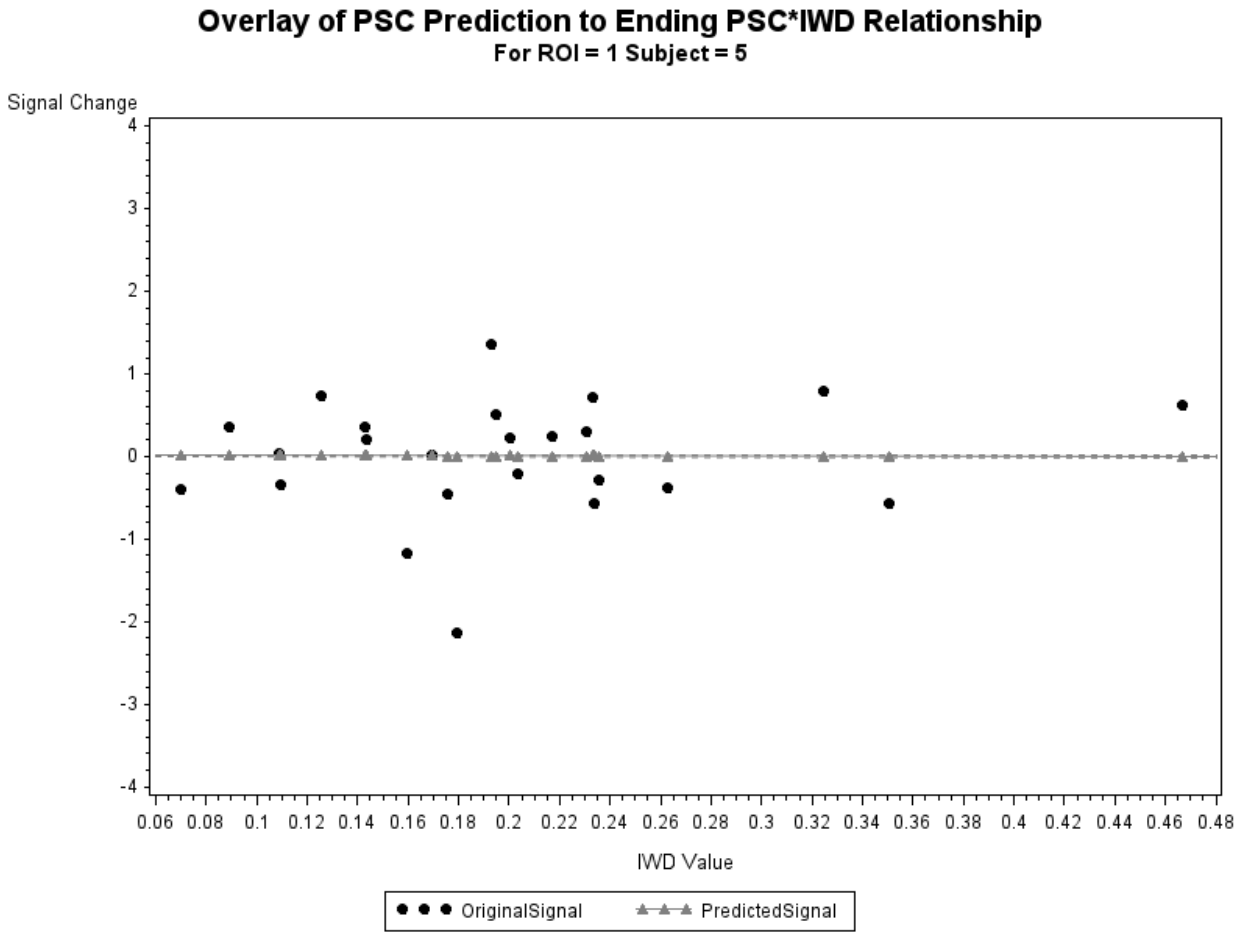
Overlay of PSC Prediction to Ending PSC*IWD Relationship
For ROI = 1 Subject = 5
Signal Change
4
3
2
1
0
-1
-2
-3
-4
0.06 0.08 0.1 0.12 0.14 0.16 0.18 0.2 0.22 0.24 0.26 0.28 0.3 0.32 0.34 0.36 0.38 0.4 0.42 0.44 0.46 0.48
IWD Value
OriginalSignal
PredictedSignal

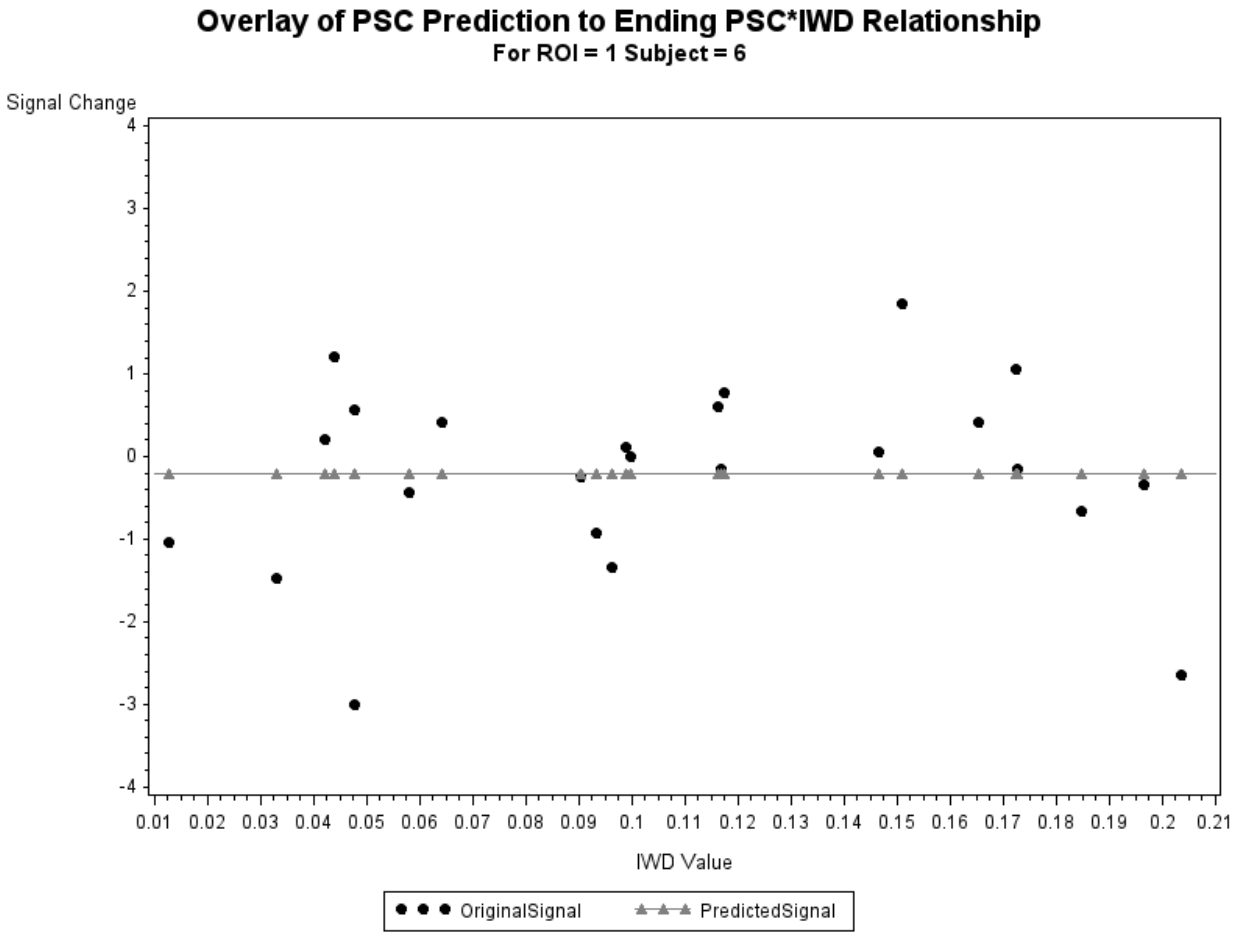
Overlay of PSC Prediction to Ending PSC*IWD Relationship
For ROI = 1 Subject = 6
Signal Change
4
3
2
1
0
-1
-2
-3
-4
0.01 0.02 0.03 0.04 0.05 0.06 0.07 0.08 0.09 0.1 0.11 0.12 0.13 0.14 0.15 0.16 0.17 0.18 0.19 0.2 0.21
IWD Value
OriginalSignal
PredictedSignal

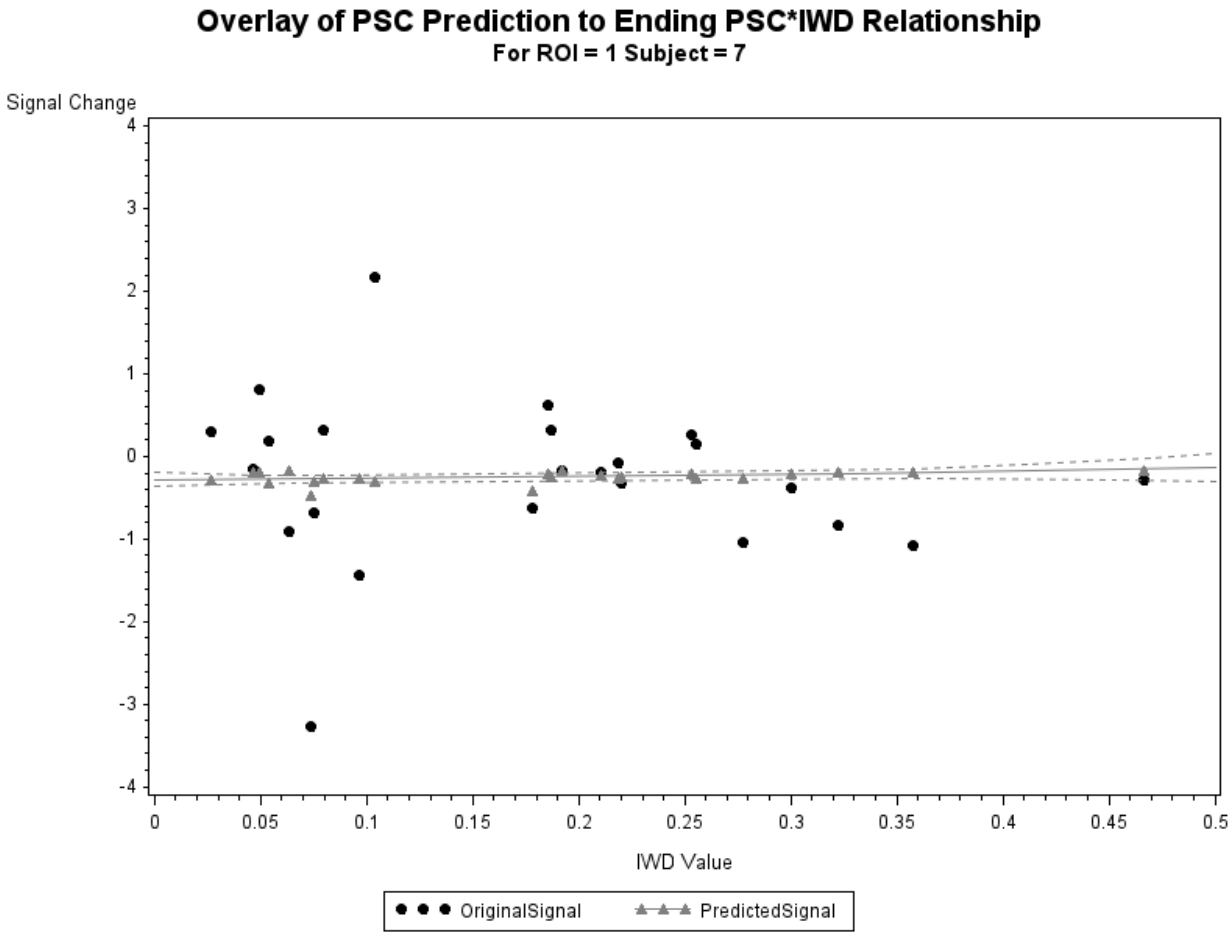
Overlay of PSC Prediction to Ending PSC*IWD Relationship
For ROI = 1 Subject = 7
Signal Change
4
3
2
1
0
-1
-2
-3
-4
0
0.05
0.1
0.15
0.2
0.25
0.3
0.35
0.4
0.45
0.5
IWD Value
OriginalSignal
PredictedSignal

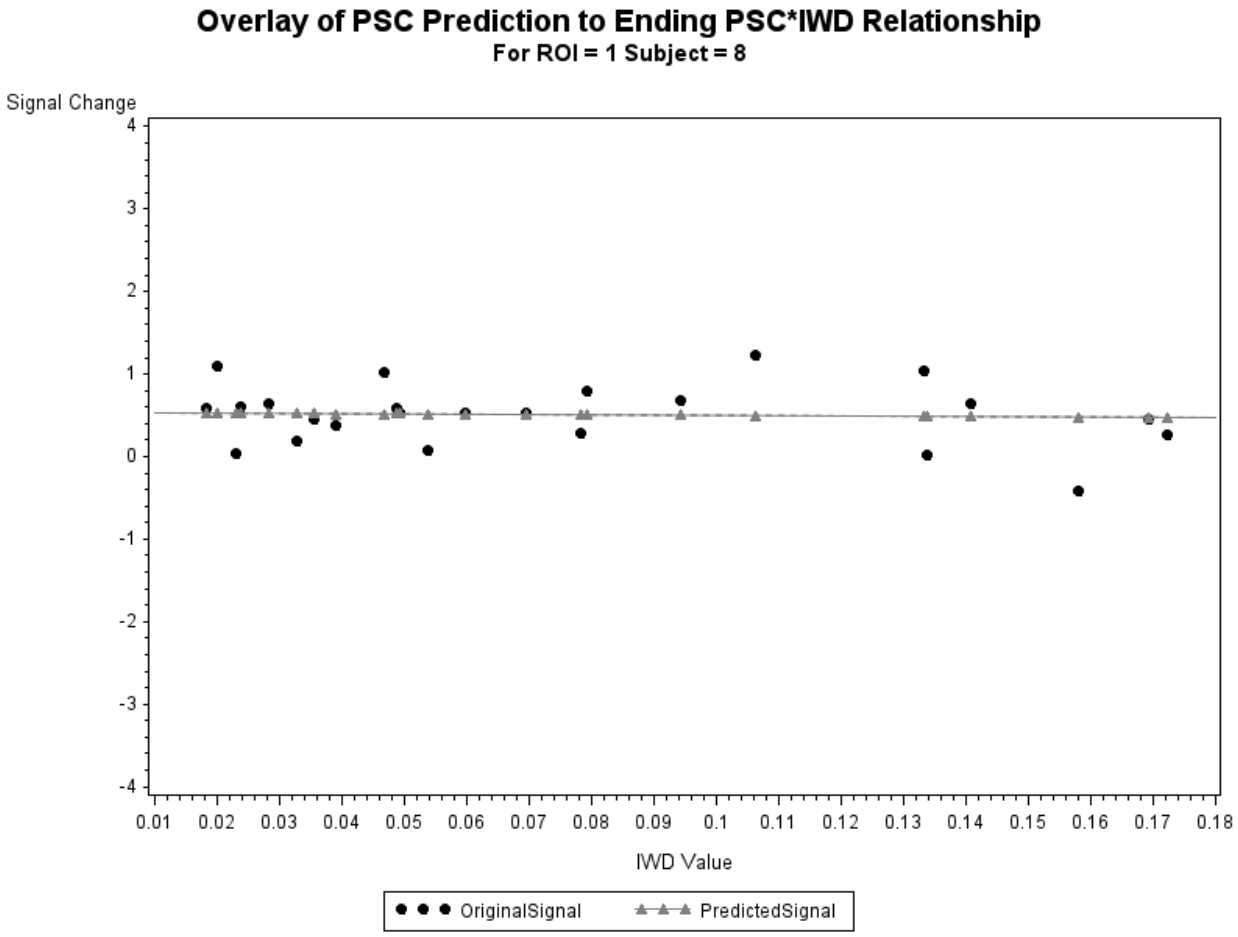
Overlay of PSC Prediction to Ending PSC*IWD Relationship
For ROI = 1 Subject = 8
Signal Change
4
3
2
1
0
-1
-2
-3
-4
0.01
0.02
0.03
0.04
0.05
0.06
0.07
0.08
0.09
0.1
0.11
0.12
0.13
0.14
0.15
0.16
0.17
0.18
IWD Value
OriginalSignal
PredictedSignal

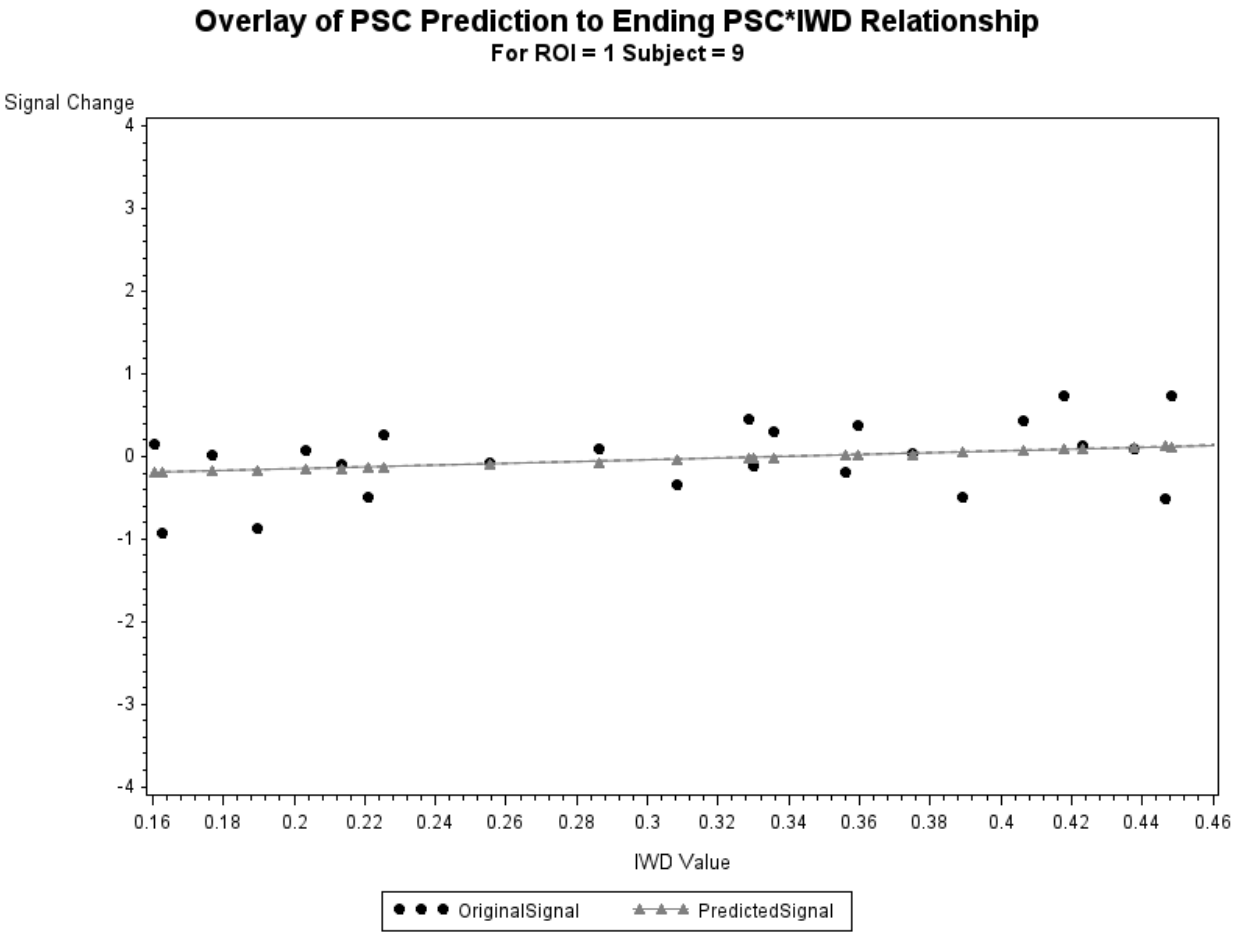
Overlay of PSC Prediction to Ending PSC*IWD Relationship
For ROI = 1 Subject = 9
Signal Change
4
3
2
1
0
-1
-2
-3
-4
0.16
0.18
0.2
0.22
0.24
0.26
0.28
0.3
0.32
0.34
0.36
0.38
0.4
0.42
0.44
0.46
IWD Value
OriginalSignal
PredictedSignal

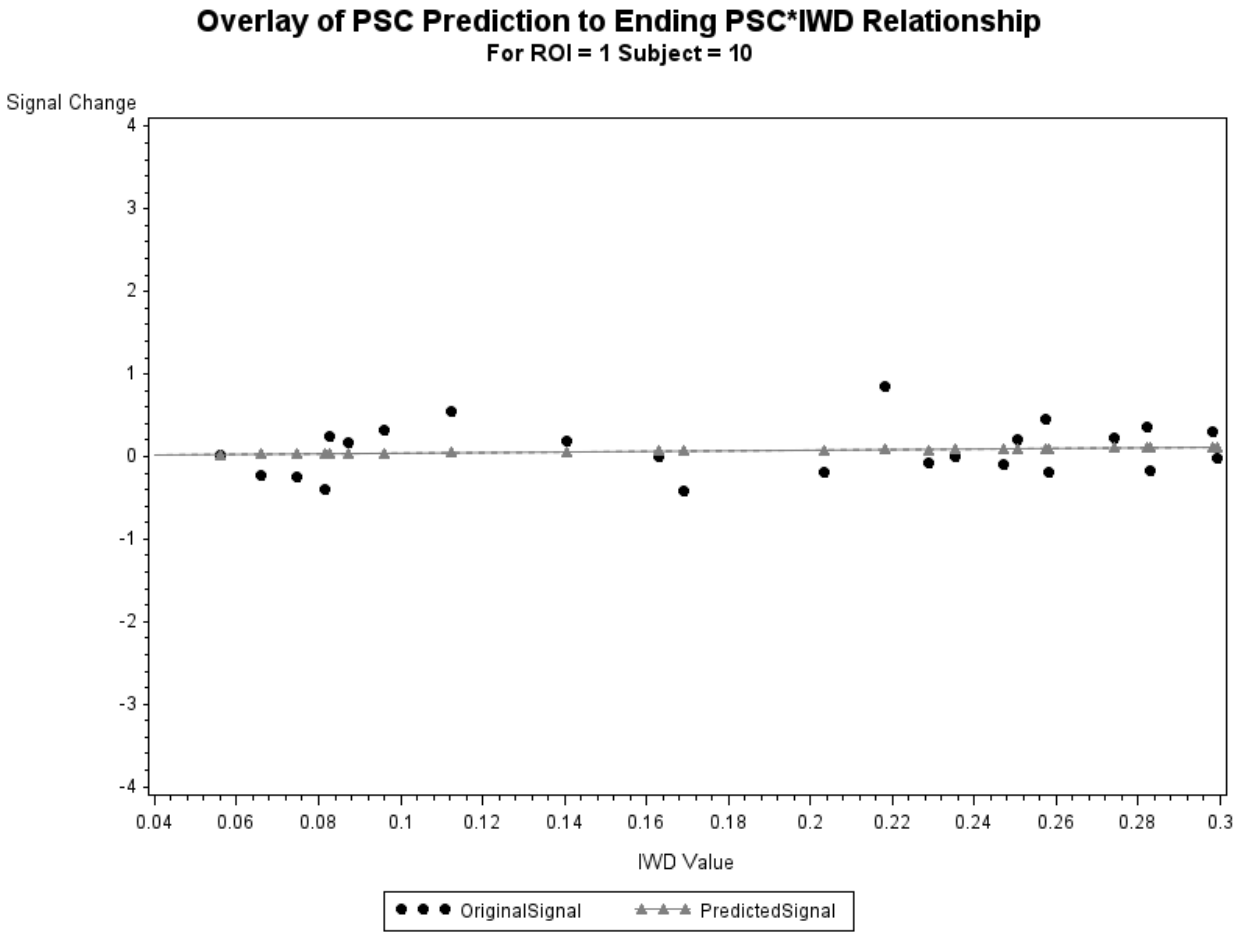
Overlay of PSC Prediction to Ending PSC*IWD Relationship
For ROI = 1 Subject = 10
Signal Change
4
3
2
1
0
-1
-2
-3
-4
0.04
0.06
0.08
0.1
0.12
0.14
0.16
0.18
0.2
0.22
0.24
0.26
0.28
0.3
IWD Value
OriginalSignal
PredictedSignal

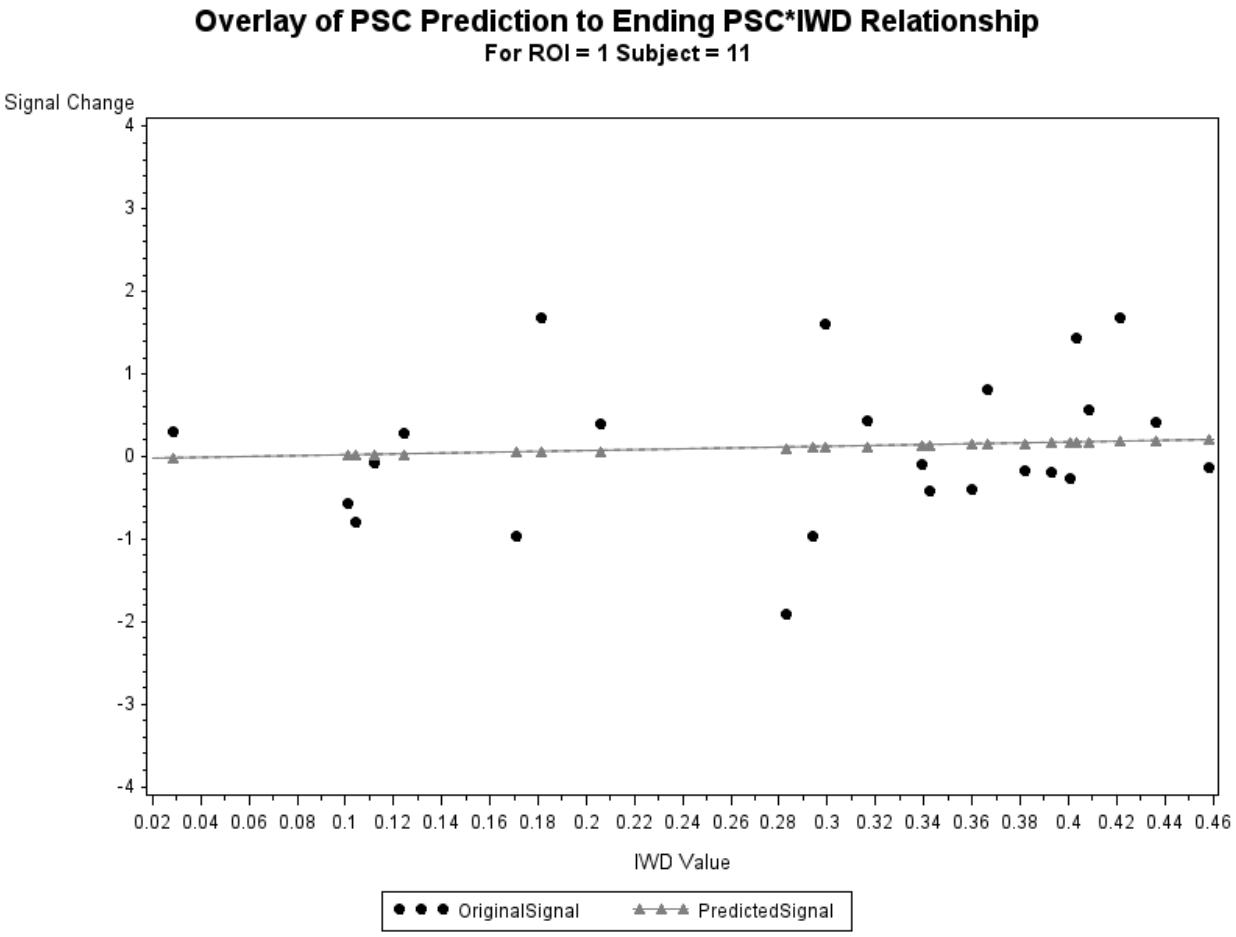
Overlay of PSC Prediction to Ending PSC*IWD Relationship
For ROI = 1 Subject = 11
Signal Change
4
3
2
1
0
-1
-2
-3
-4
0.02 0.04 0.06 0.08 0.1 0.12 0.14 0.16 0.18 0.2 0.22 0.24 0.26 0.28 0.3 0.32 0.34 0.36 0.38 0.4 0.42 0.44 0.46
IWD Value
OriginalSignal
PredictedSignal

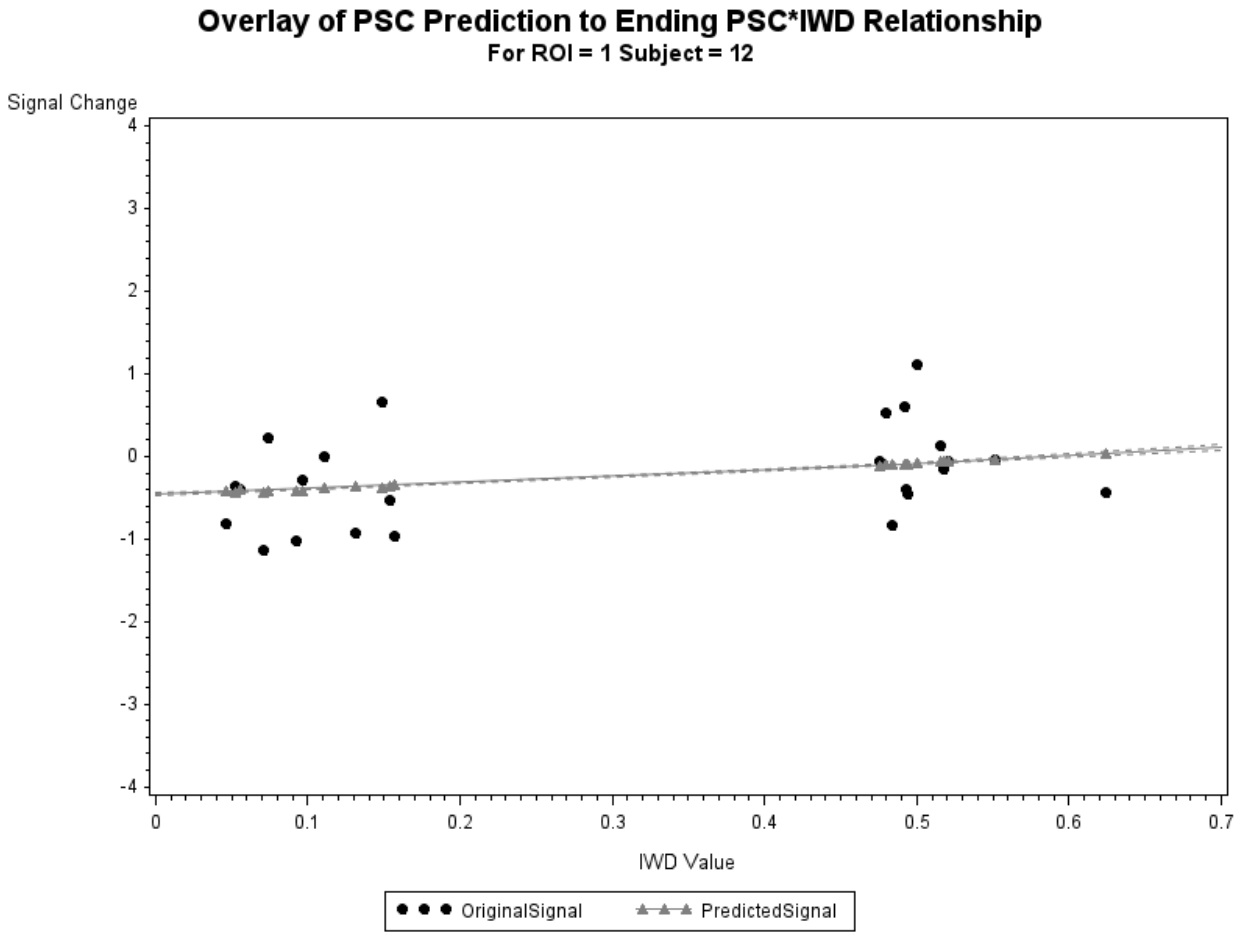
Overlay of PSC Prediction to Ending PSC*IWD Relationship
For ROI = 1 Subject = 12
Signal Change
4
3
2
1
0
-1
-2
-3
-4
0
0.1
0.2
0.3
0.4
0.5
0.6
0.7
IWD Value
OriginalSignal
PredictedSignal

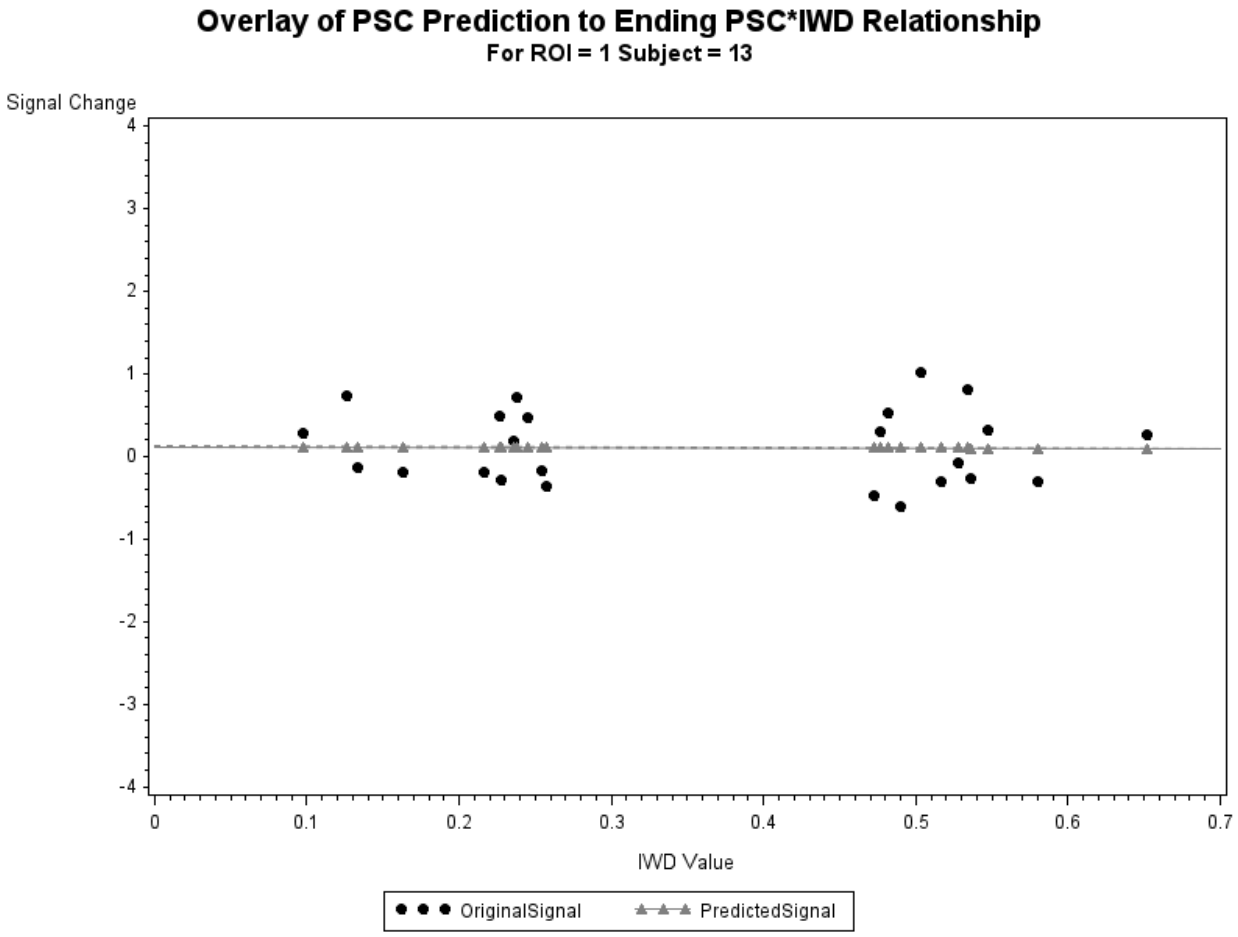
Overlay of PSC Prediction to Ending PSC*IWD Relationship
For ROI = 1 Subject = 13
Signal Change
4
3
2
1
0
-1
-2
-3
-4
0
0.1
0.2
0.3
0.4
0.5
0.6
0.7
IWD Value
OriginalSignal
PredictedSignal

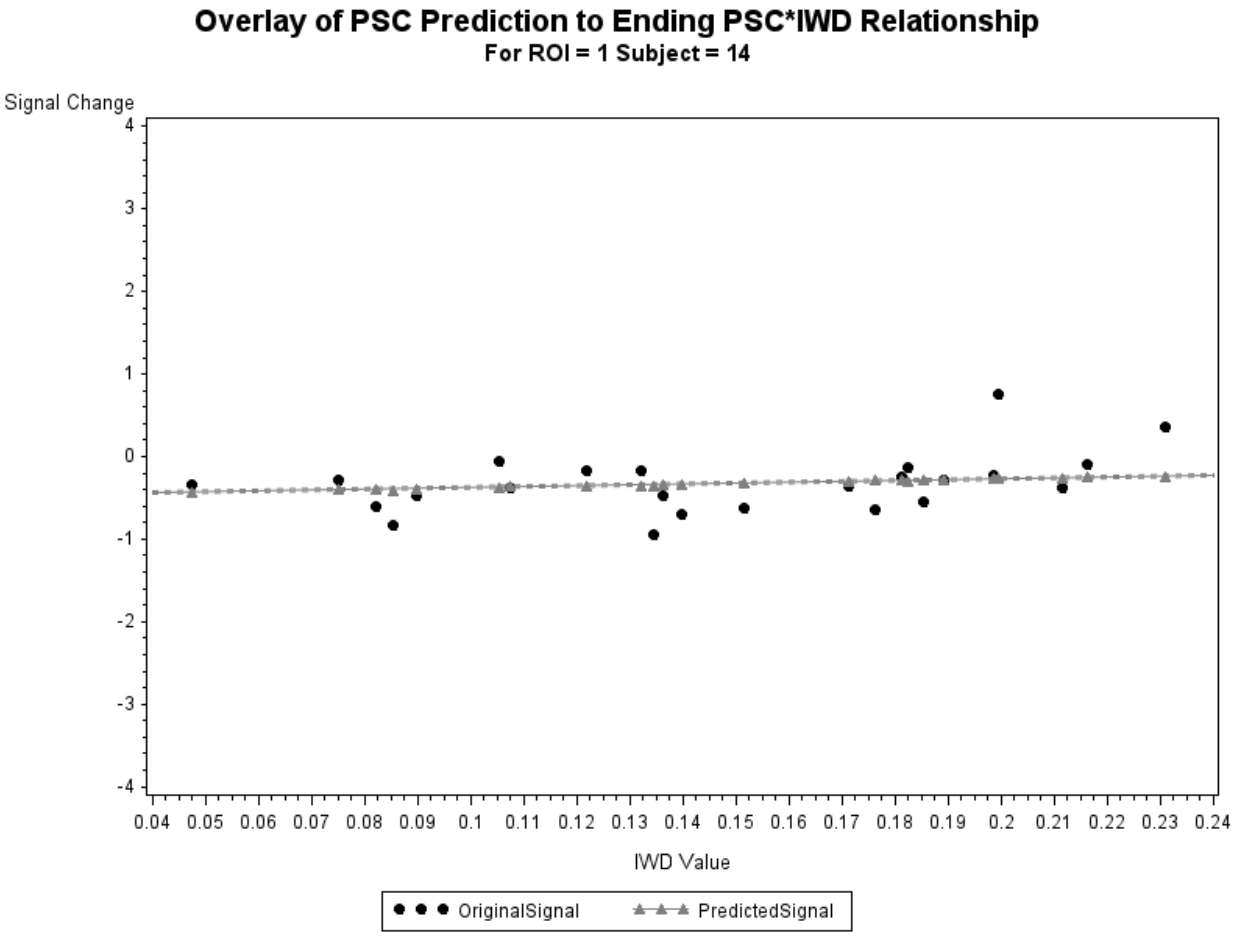
Overlay of PSC Prediction to Ending PSC*IWD Relationship
For ROI = 1 Subject = 14
Signal Change
4
3
2
1
0
-1
-2
-3
-4
0.04 0.05 0.06 0.07 0.08 0.09 0.1 0.11 0.12 0.13 0.14 0.15 0.16 0.17 0.18 0.19 0.2 0.21 0.22 0.23 0.24
IWD Value
OriginalSignal
PredictedSignal

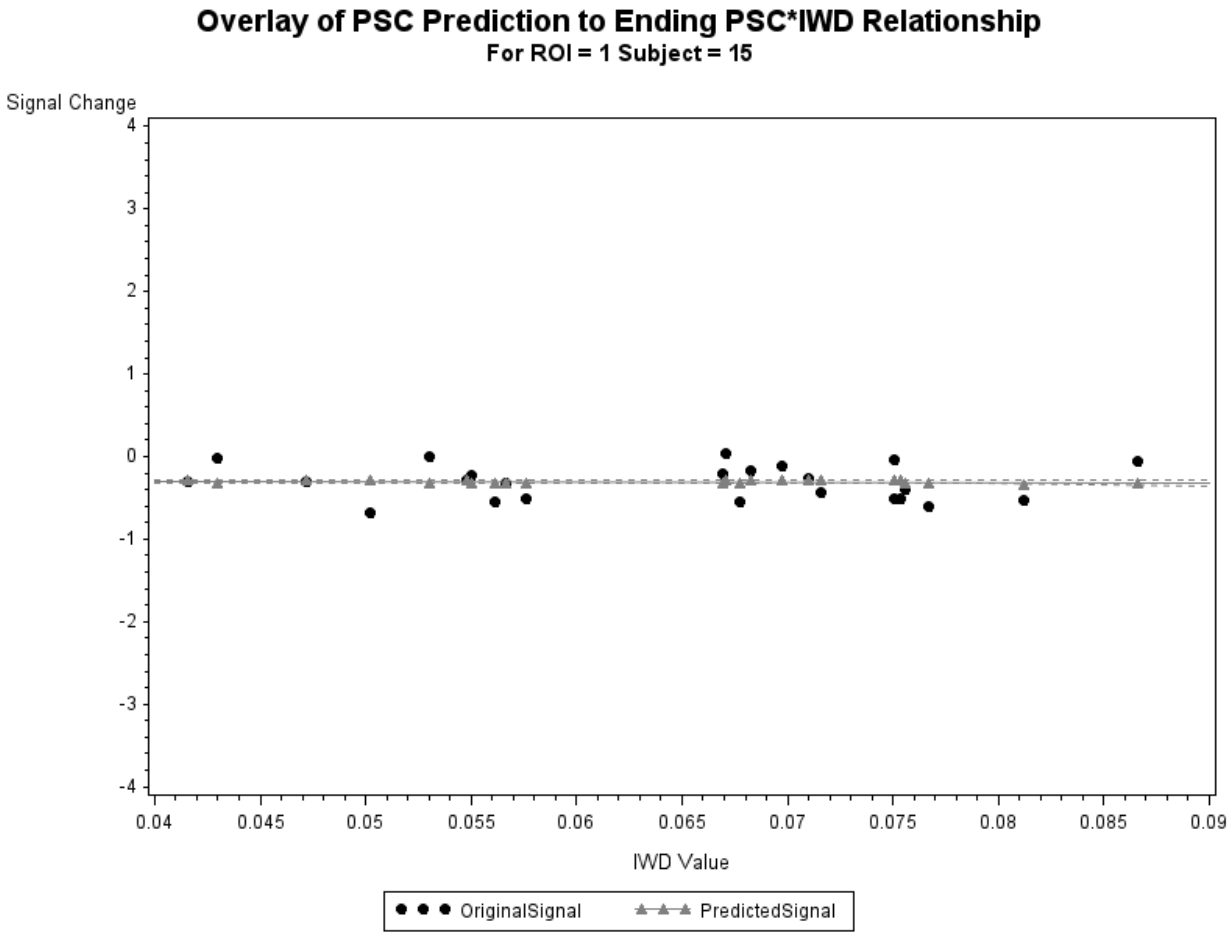
Overlay of PSC Prediction to Ending PSC*IWD Relationship
For ROI = 1 Subject = 15
Signal Change
4
3
2
1
0
-1
-2
-3
-4
0.04
0.045
0.05
0.055
0.06
0.065
0.07
0.075
0.08
0.085
0.09
IWD Value
OriginalSignal
PredictedSignal

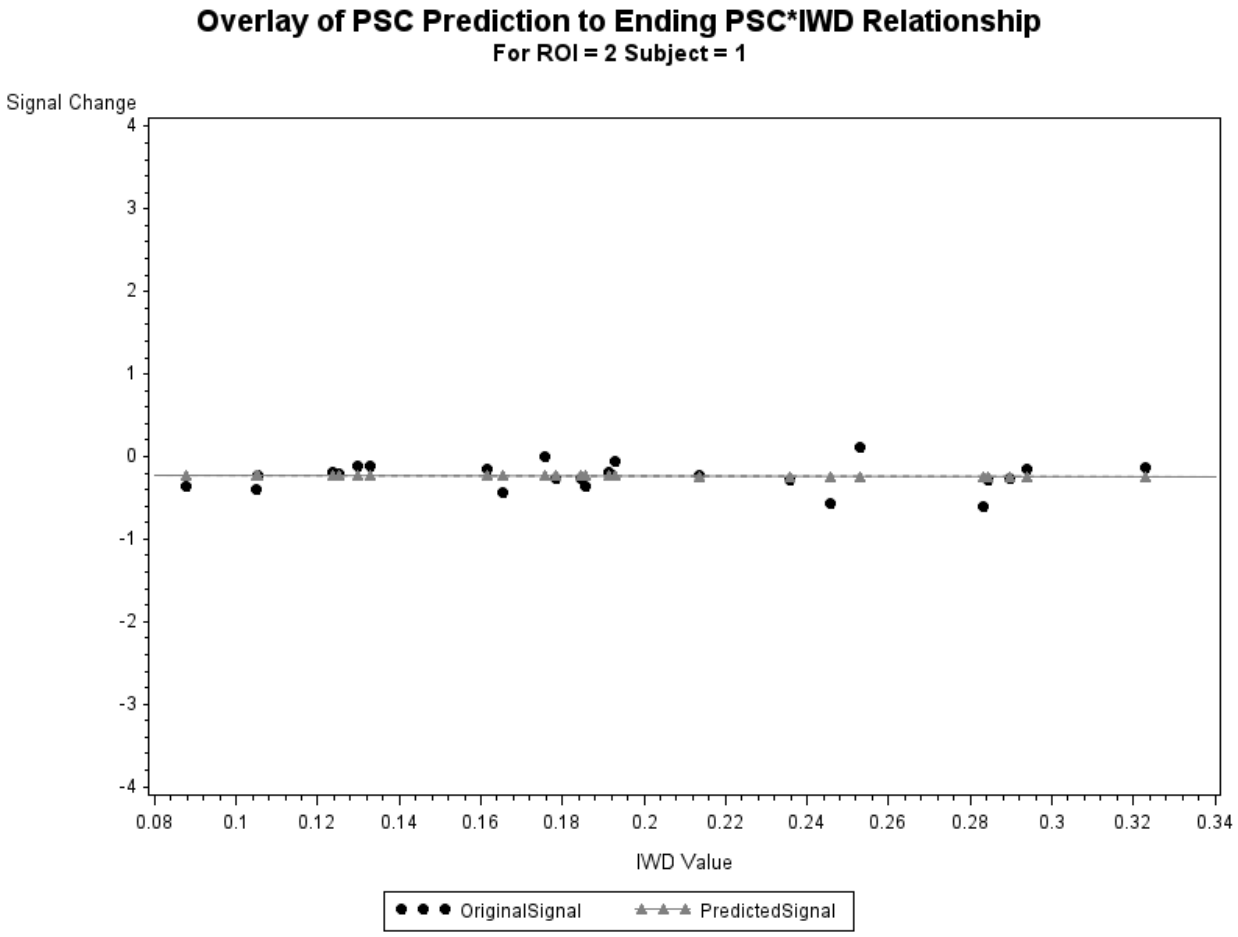
Overlay of PSC Prediction to Ending PSC*IWD Relationship
For ROI = 2 Subject = 1
Signal Change
4
3
2
1
0
-1
-2
-3
-4
0.08
0.1
0.12
0.14
0.16
0.18
0.2
0.22
0.24
0.26
0.28
0.3
0.32
0.34
IWD Value
OriginalSignal
PredictedSignal

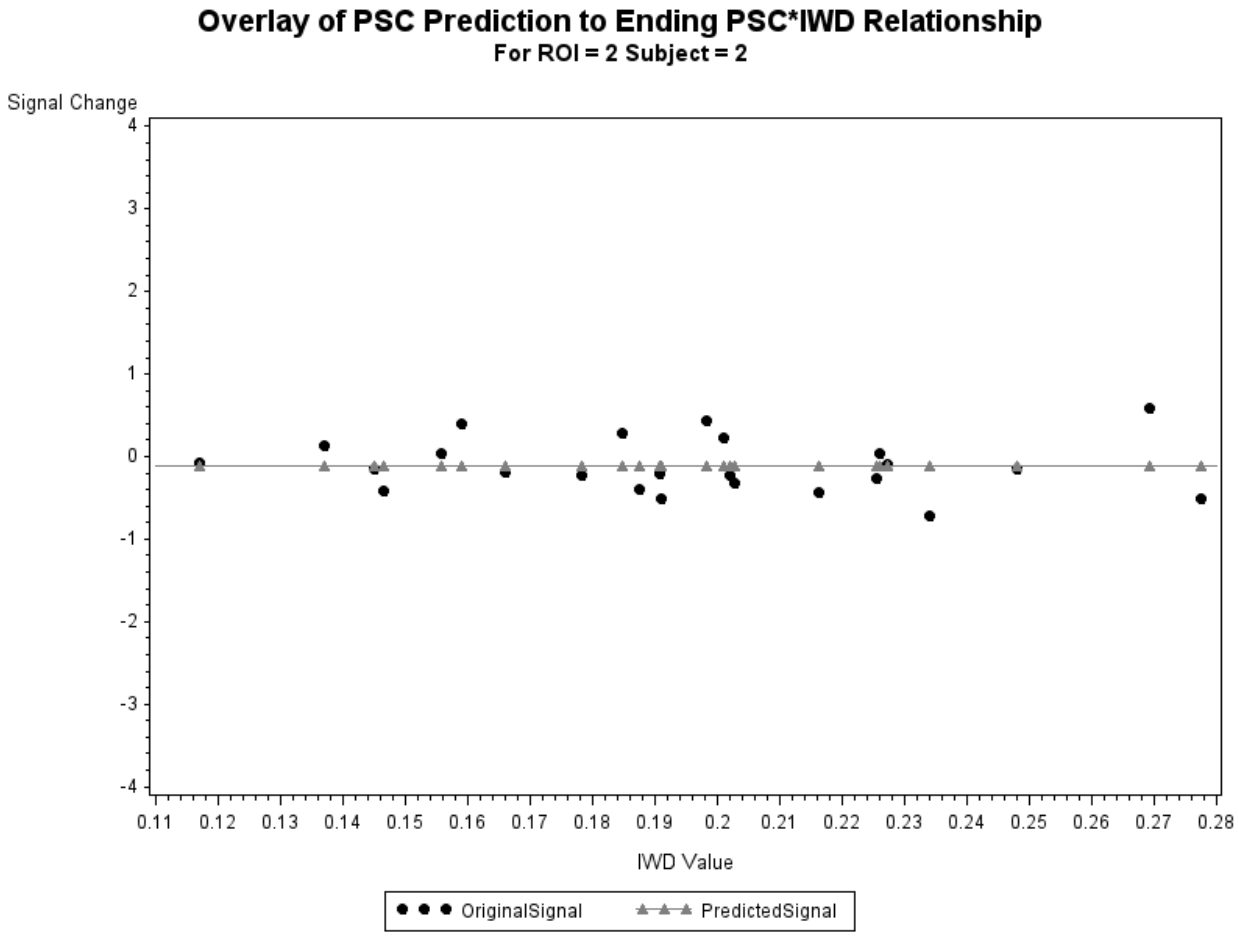
Overlay of PSC Prediction to Ending PSC*IWD Relationship
For ROI = 2 Subject = 2
Signal Change
4
3
2
1
0
-1
-2
-3
-4
0.11
0.12
0.13
0.14
0.15
0.16
0.17
0.18
0.19
0.2
0.21
0.22
0.23
0.24
0.25
0.26
0.27
0.28
IWD Value
OriginalSignal
PredictedSignal

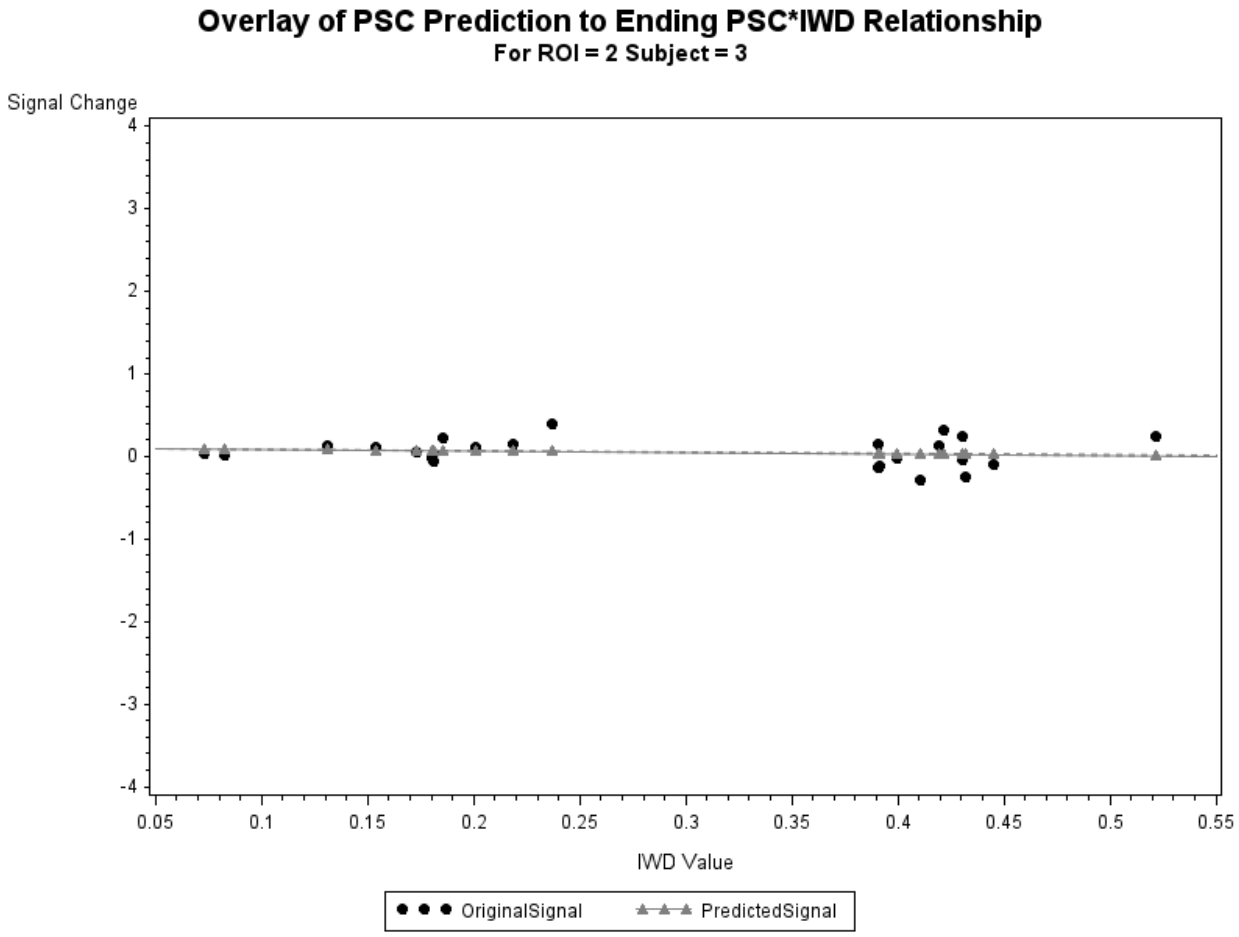
Overlay of PSC Prediction to Ending PSC*IWD Relationship
For ROI = 2 Subject = 3
Signal Change
4
3
2
1
0
-1
-2
-3
-4
0.05
0.1
0.15
0.2
0.25
0.3
0.35
0.4
0.45
0.5
0.55
IWD Value
OriginalSignal
PredictedSignal

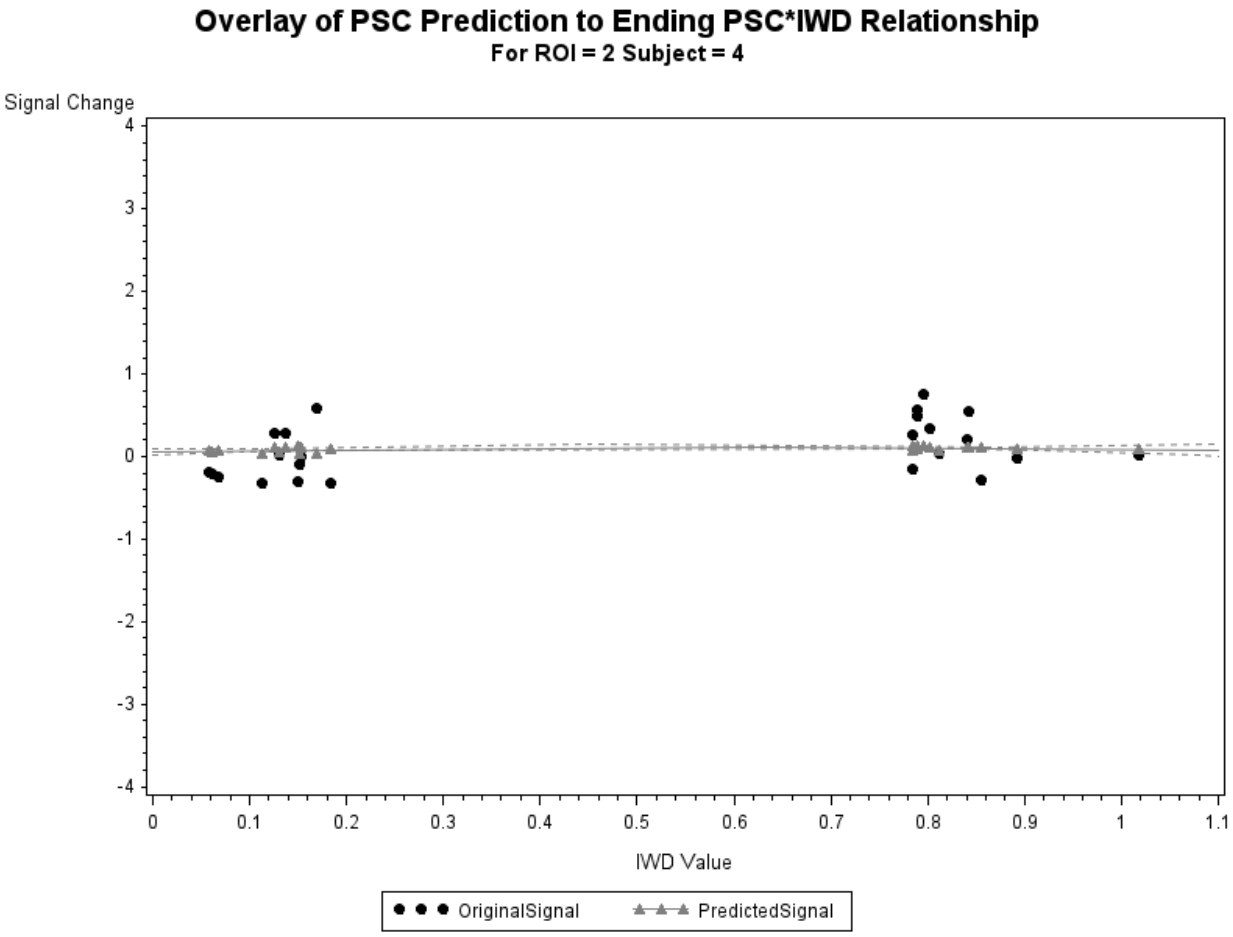
Overlay of PSC Prediction to Ending PSC*IWD Relationship
For ROI = 2 Subject = 4
Signal Change
4
3
2
1
0
-1
-2
-3
-4
0
0.1
0.2
0.3
0.4
0.5
0.6
0.7
0.8
0.9
1
1.1
IWD Value
OriginalSignal
PredictedSignal

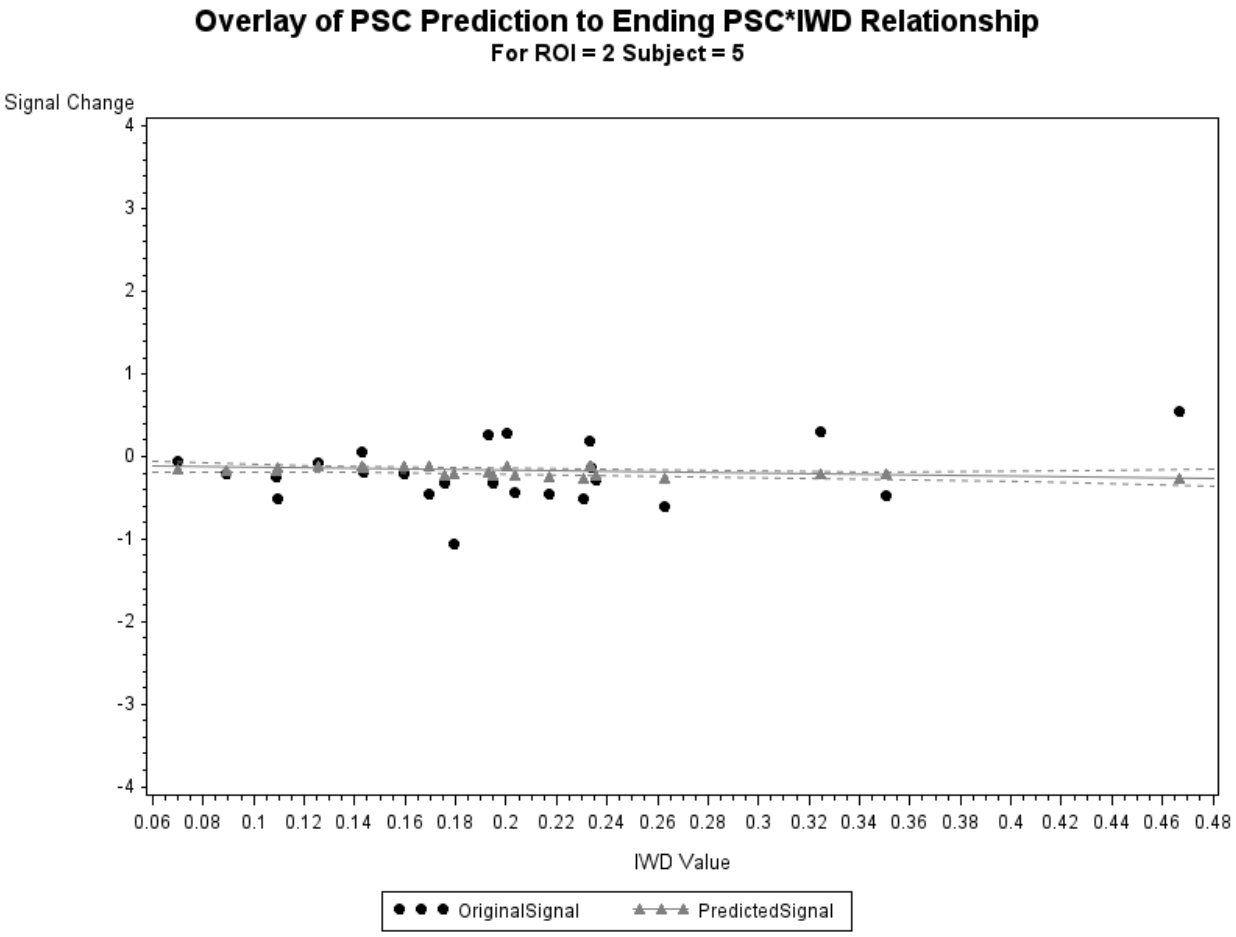
Overlay of PSC Prediction to Ending PSC*IWD Relationship
For ROI = 2 Subject = 5
Signal Change
4
3
2
1
0
-1
-2
-3
-4
0.06 0.08 0.1 0.12 0.14 0.16 0.18 0.2 0.22 0.24 0.26 0.28 0.3 0.32 0.34 0.36 0.38 0.4 0.42 0.44 0.46 0.48
IWD Value
OriginalSignal
PredictedSignal

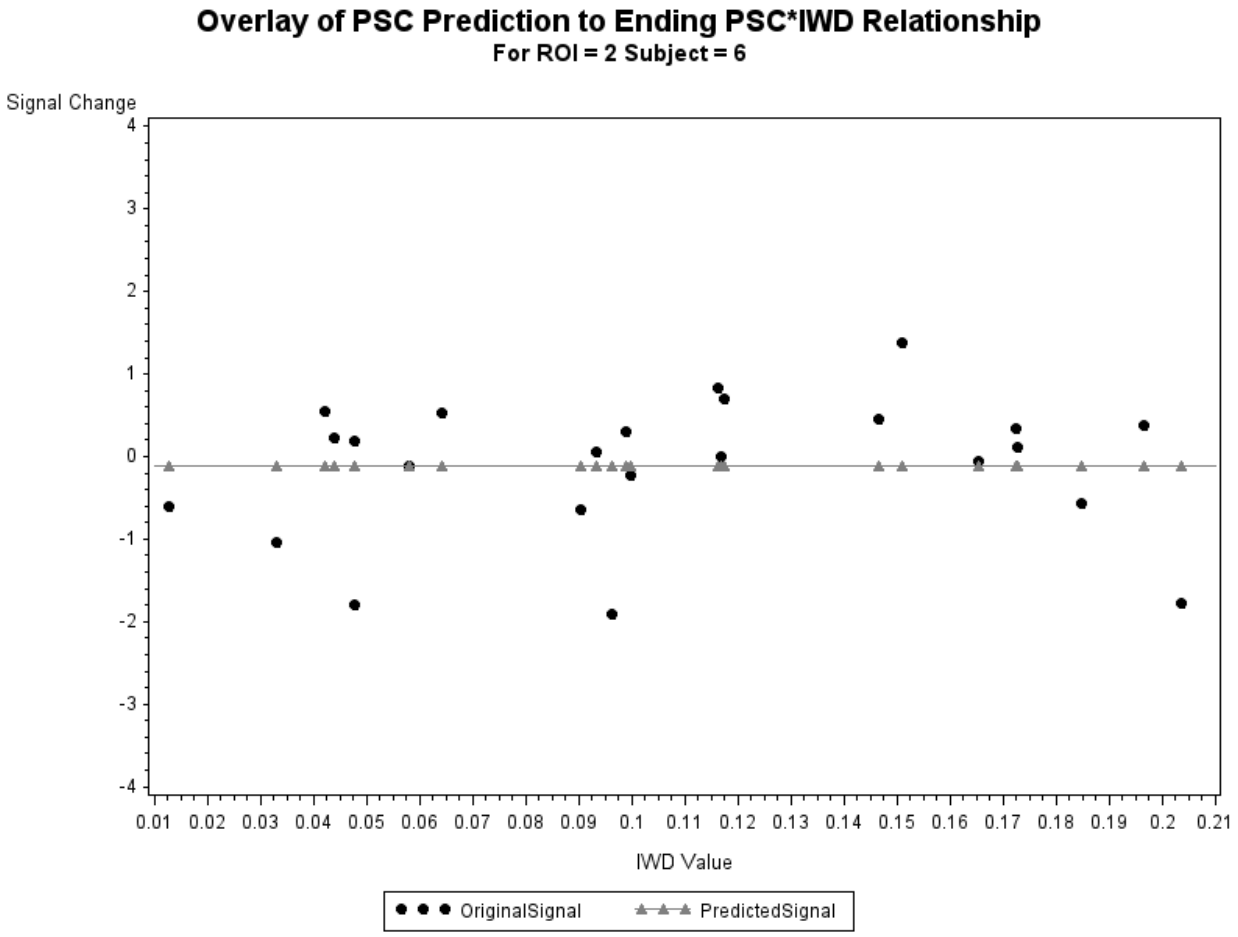
Overlay of PSC Prediction to Ending PSC*IWD Relationship
For ROI = 2 Subject = 6
Signal Change
4
3
2
1
0
-1
-2
-3
-4
0.01 0.02 0.03 0.04 0.05 0.06 0.07 0.08 0.09 0.1 0.11 0.12 0.13 0.14 0.15 0.16 0.17 0.18 0.19 0.2 0.21
IWD Value
OriginalSignal
PredictedSignal

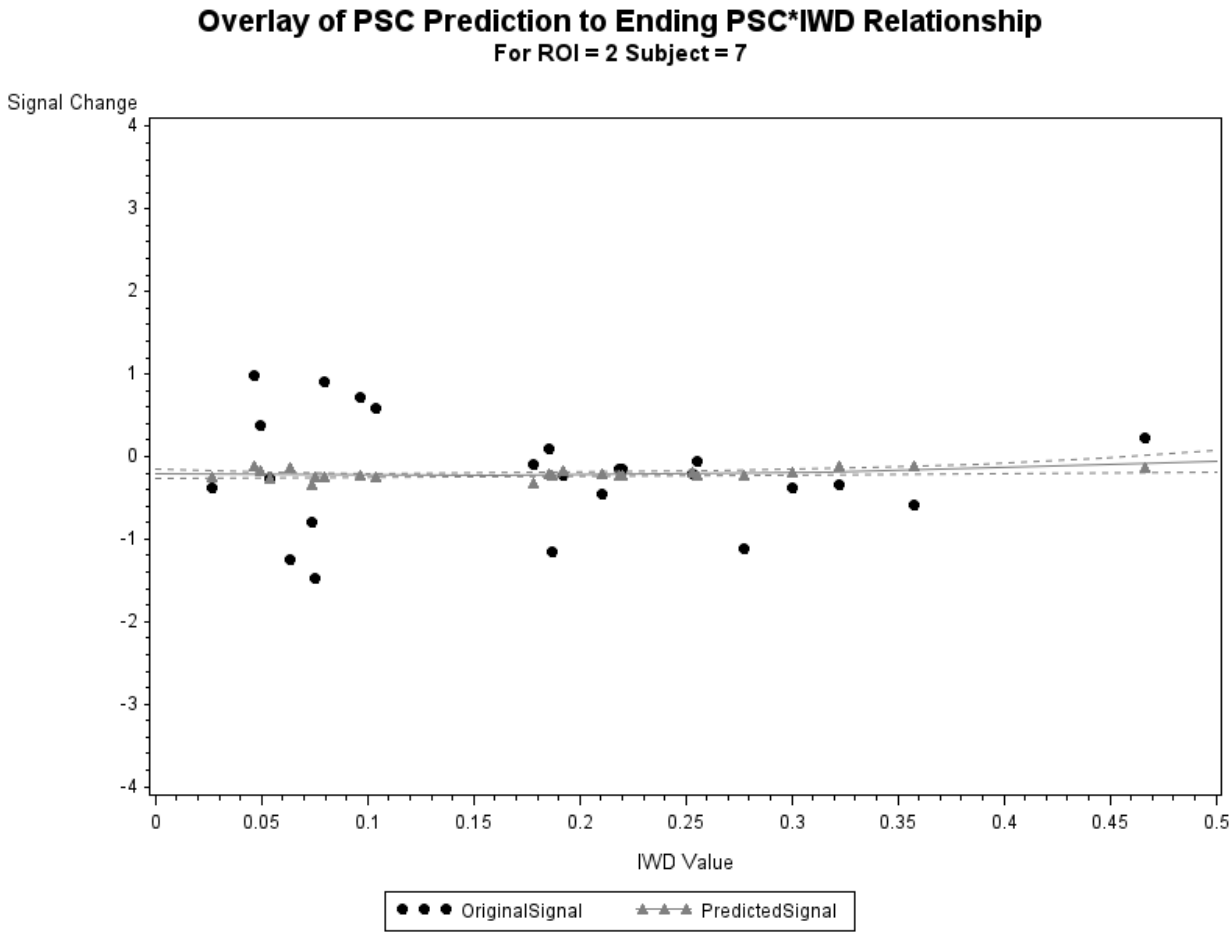
Overlay of PSC Prediction to Ending PSC*IWD Relationship
For ROI = 2 Subject = 7
Signal Change
4
3
2
1
0
-1
-2
-3
-4
0
0.05
0.1
0.15
0.2
0.25
0.3
0.35
0.4
0.45
0.5
IWD Value
OriginalSignal
PredictedSignal

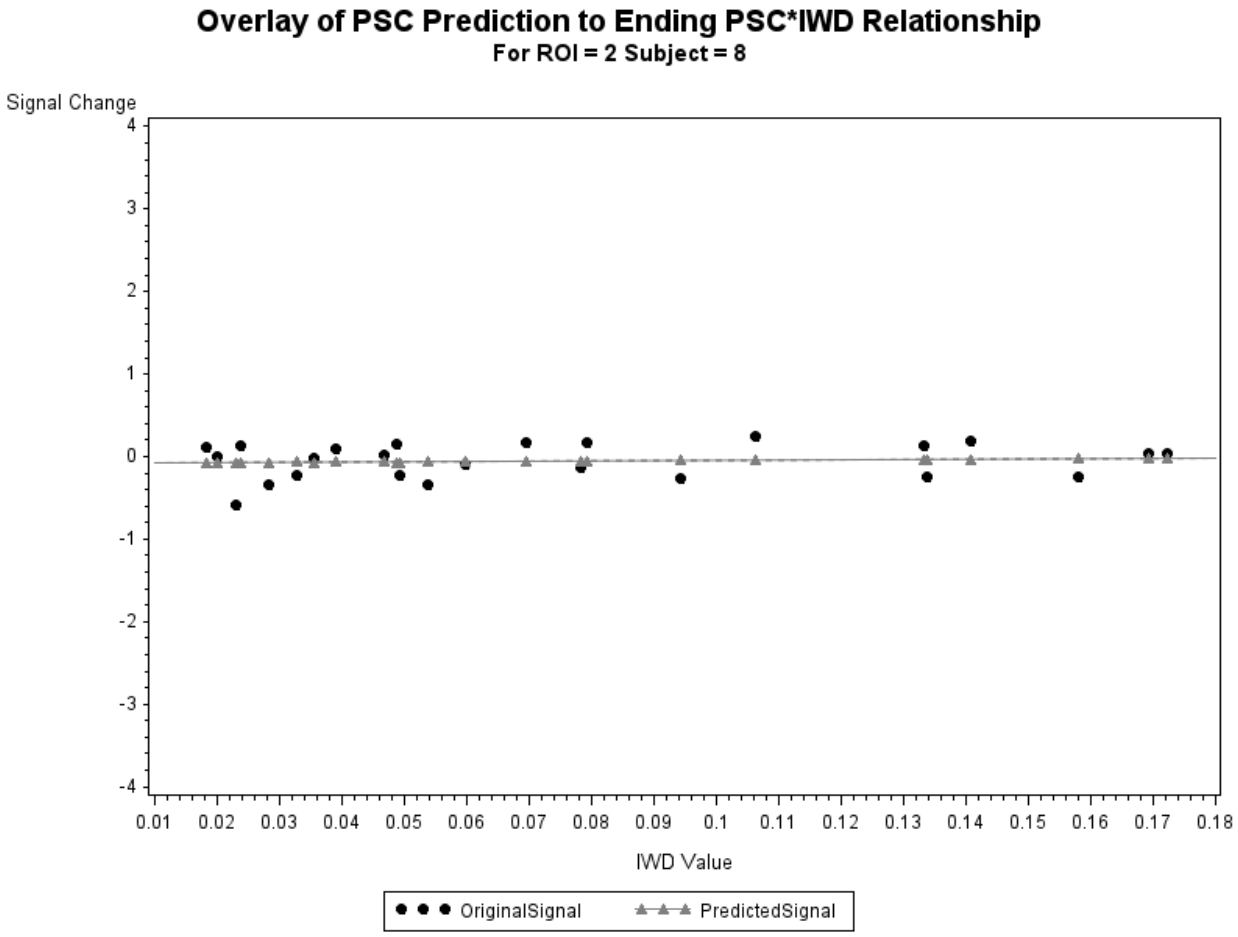
Overlay of PSC Prediction to Ending PSC*IWD Relationship
For ROI = 2 Subject = 8
Signal Change
4
3
2
1
0
-1
-2
-3
-4
0.01
0.02
0.03
0.04
0.05
0.06
0.07
0.08
0.09
0.1
0.11
0.12
0.13
0.14
0.15
0.16
0.17
0.18
IWD Value
OriginalSignal
PredictedSignal

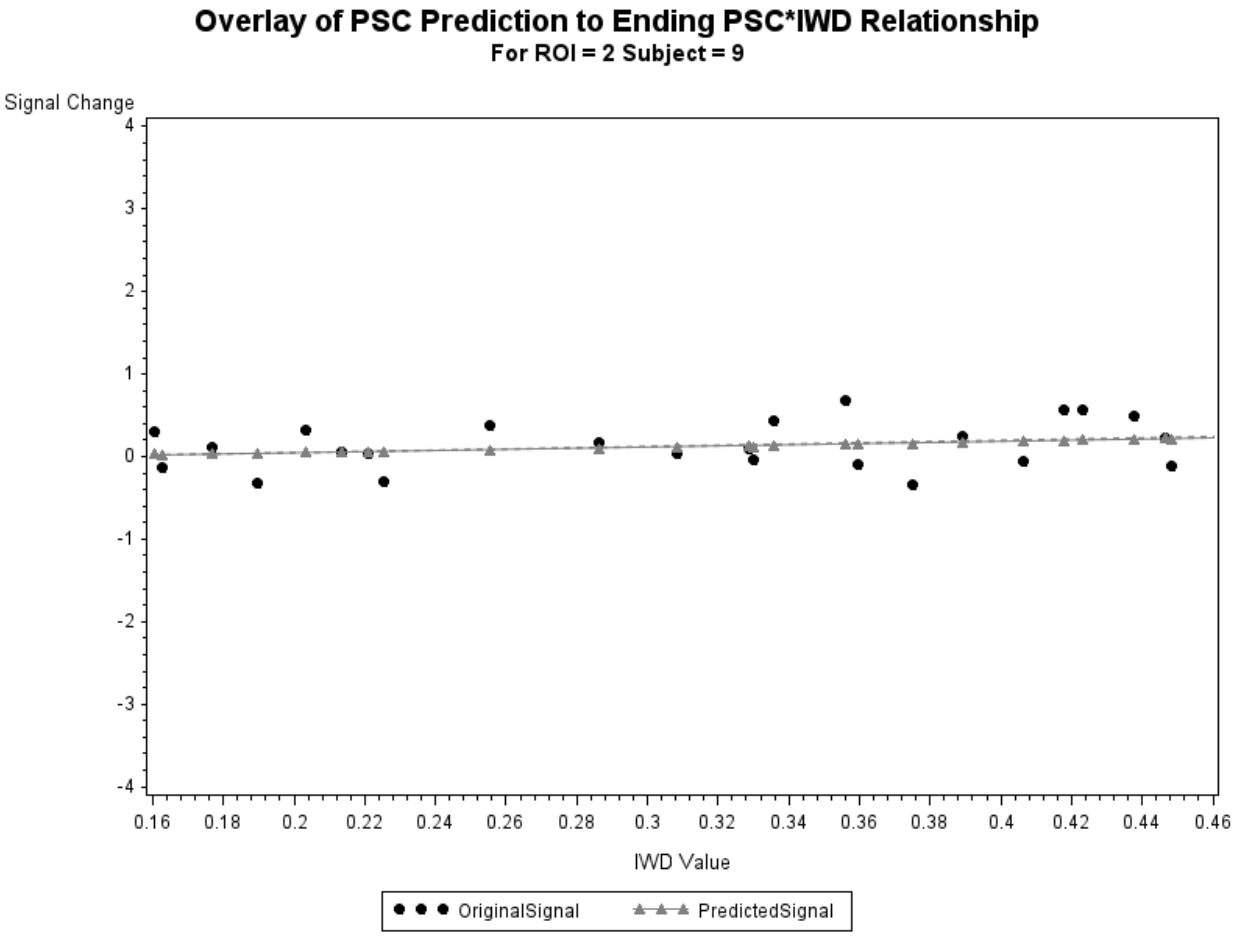
Overlay of PSC Prediction to Ending PSC*IWD Relationship
For ROI = 2 Subject = 9
Signal Change
4
3
2
1
0
-1
-2
-3
-4
0.16
0.18
0.2
0.22
0.24
0.26
0.28
0.3
0.32
0.34
0.36
0.38
0.4
0.42
0.44
0.46
IWD Value
OriginalSignal
PredictedSignal

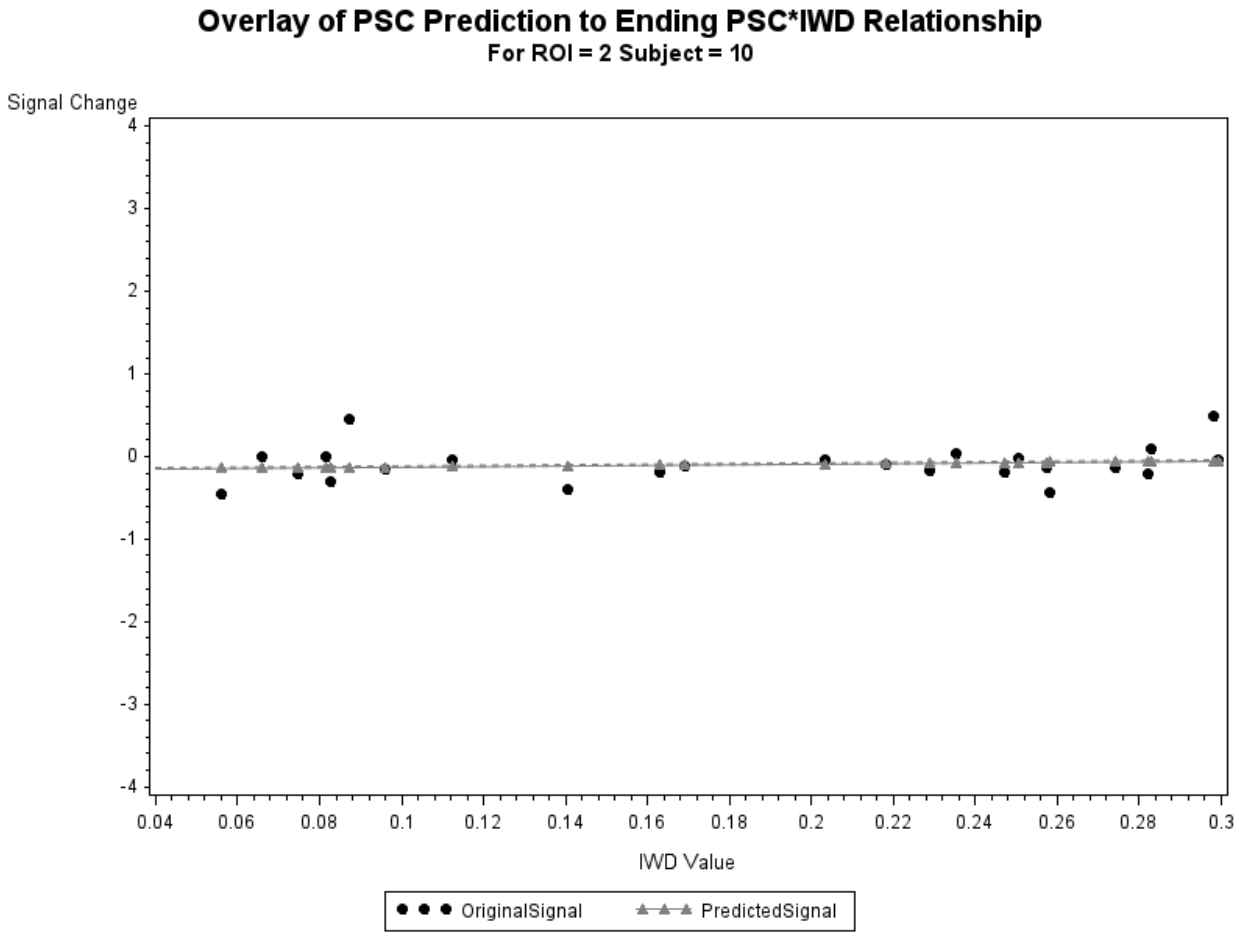
Overlay of PSC Prediction to Ending PSC*IWD Relationship
For ROI = 2 Subject = 10
Signal Change
4
3
2
1
0
-1
-2
-3
-4
0.04
0.06
0.08
0.1
0.12
0.14
0.16
0.18
0.2
0.22
0.24
0.26
0.28
0.3
IWD Value
OriginalSignal
PredictedSignal

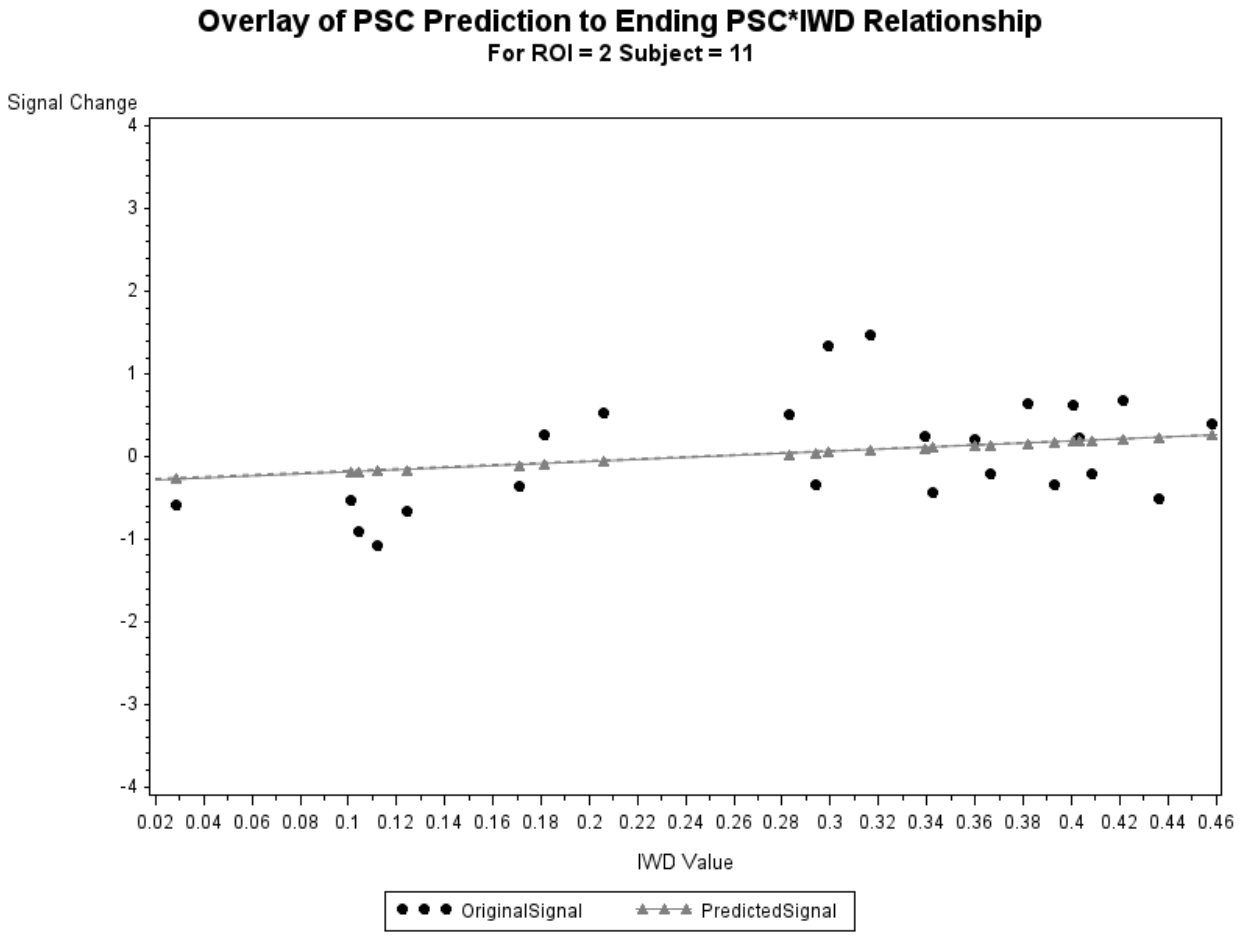
Overlay of PSC Prediction to Ending PSC*IWD Relationship
For ROI = 2 Subject = 11
Signal Change
4
3
2
1
0
-1
-2
-3
-4
0.02 0.04 0.06 0.08 0.1 0.12 0.14 0.16 0.18 0.2 0.22 0.24 0.26 0.28 0.3 0.32 0.34 0.36 0.38 0.4 0.42 0.44 0.46
IWD Value
OriginalSignal
PredictedSignal

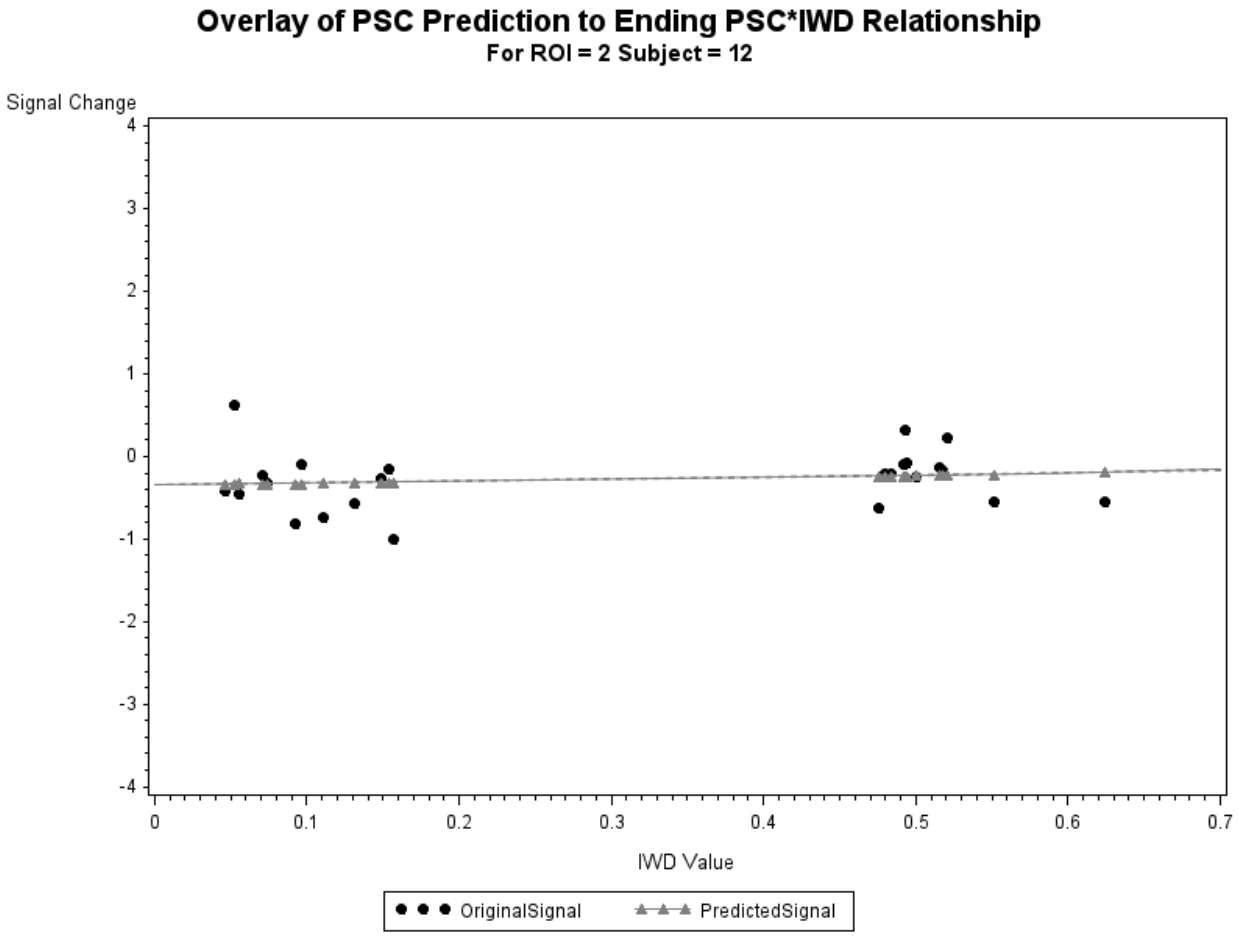
Overlay of PSC Prediction to Ending PSC*IWD Relationship
For ROI = 2 Subject = 12
Signal Change
4
3
2
1
0
-1
-2
-3
-4
0
0.1
0.2
0.3
0.4
0.5
0.6
0.7
IWD Value
OriginalSignal
PredictedSignal

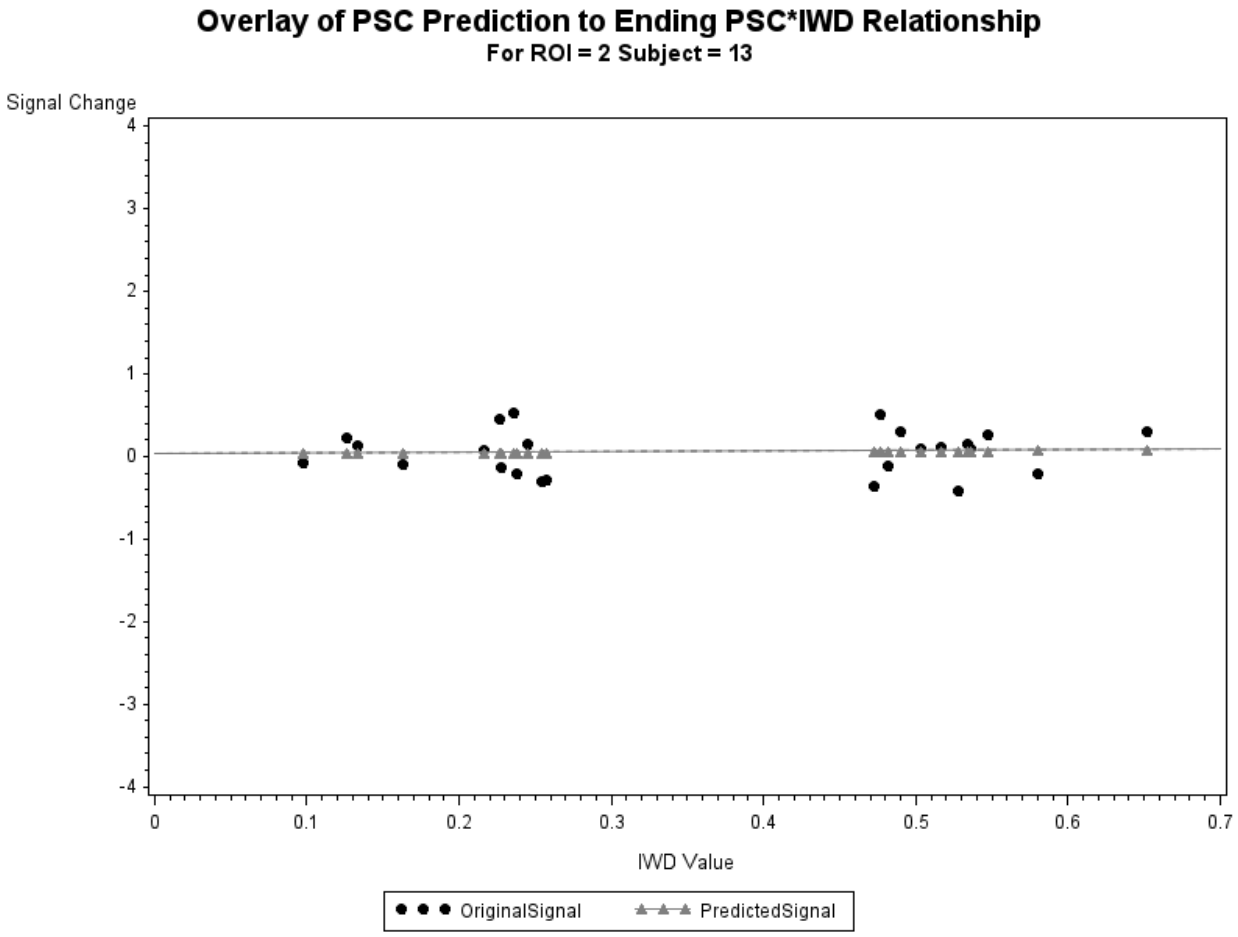
Overlay of PSC Prediction to Ending PSC*IWD Relationship
For ROI = 2 Subject = 13
Signal Change
4
3
2
1
0
-1
-2
-3
-4
0
0.1
0.2
0.3
0.4
0.5
0.6
0.7
IWD Value
OriginalSignal
PredictedSignal

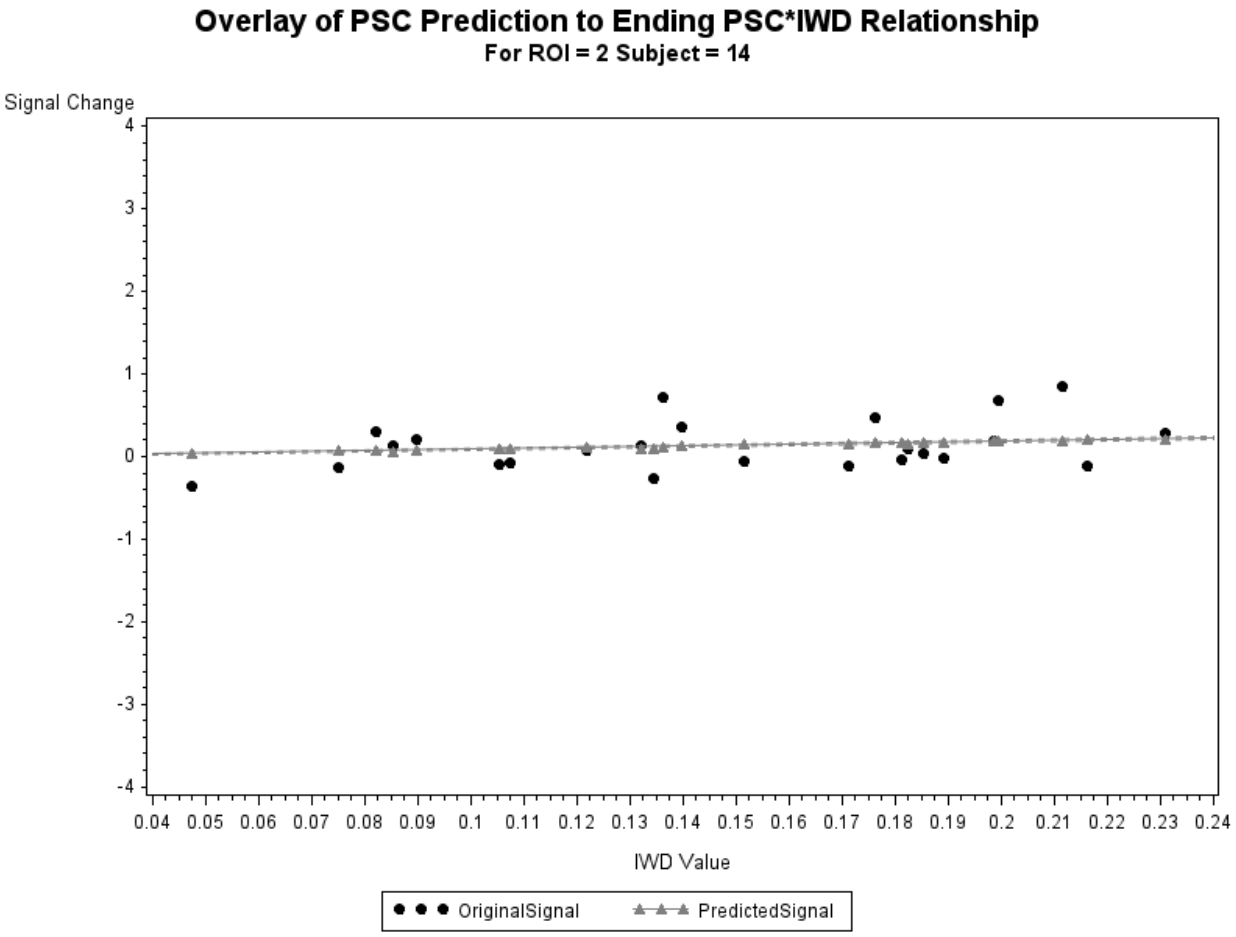
Overlay of PSC Prediction to Ending PSC*IWD Relationship
For ROI = 2 Subject = 14
Signal Change
4
3
2
1
0
-1
-2
-3
-4
0.04 0.05 0.06 0.07 0.08 0.09 0.1 0.11 0.12 0.13 0.14 0.15 0.16 0.17 0.18 0.19 0.2 0.21 0.22 0.23 0.24
IWD Value
OriginalSignal
PredictedSignal

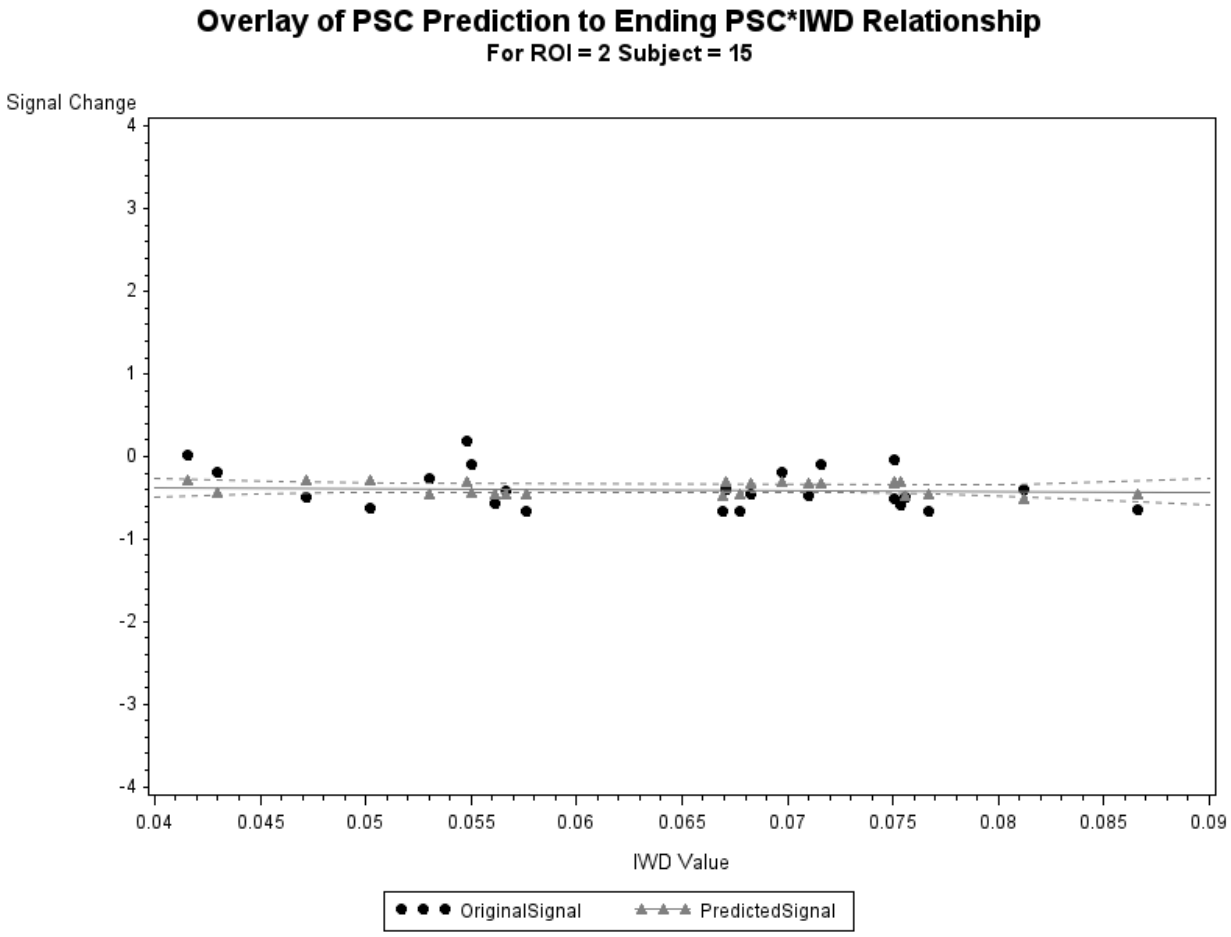
Overlay of PSC Prediction to Ending PSC*IWD Relationship
For ROI = 2 Subject = 15
Signal Change
4
3
2
1
0
-1
-2
-3
-4
0.04
0.045
0.05
0.055
0.06
0.065
0.07
0.075
0.08
0.085
0.09
IWD Value
OriginalSignal
PredictedSignal

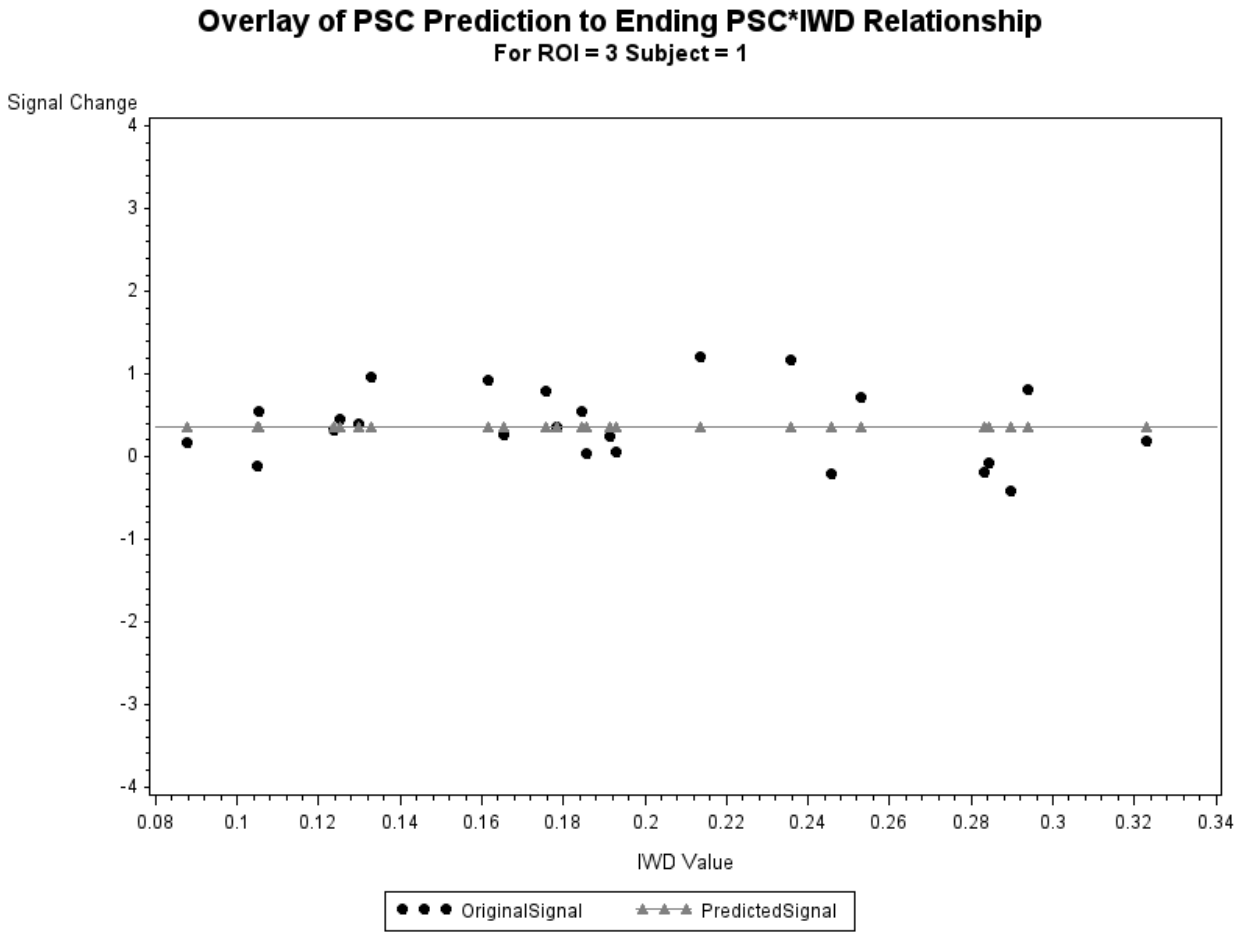
Overlay of PSC Prediction to Ending PSC*IWD Relationship
For ROI = 3 Subject = 1
Signal Change
4
3
2
1
0
-1
-2
-3
-4
0.08
0.1
0.12
0.14
0.16
0.18
0.2
0.22
0.24
0.26
0.28
0.3
0.32
0.34
IWD Value
OriginalSignal
PredictedSignal

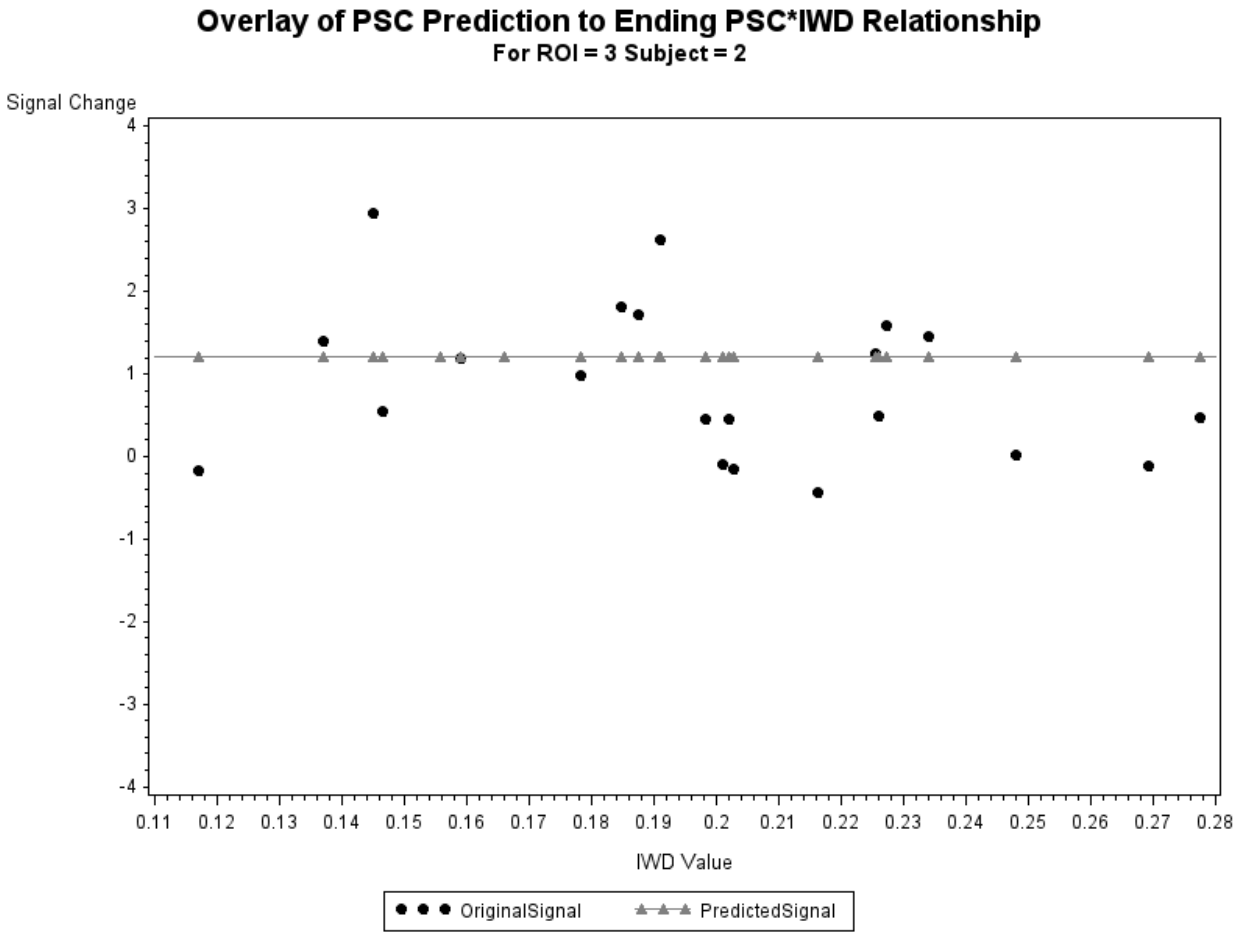
Overlay of PSC Prediction to Ending PSC*IWD Relationship
For ROI = 3 Subject = 2
Signal Change
4
3
2
1
0
-1
-2
-3
-4
0.11
0.12
0.13
0.14
0.15
0.16
0.17
0.18
0.19
0.2
0.21
0.22
0.23
0.24
0.25
0.26
0.27
0.28
IWD Value
OriginalSignal
PredictedSignal

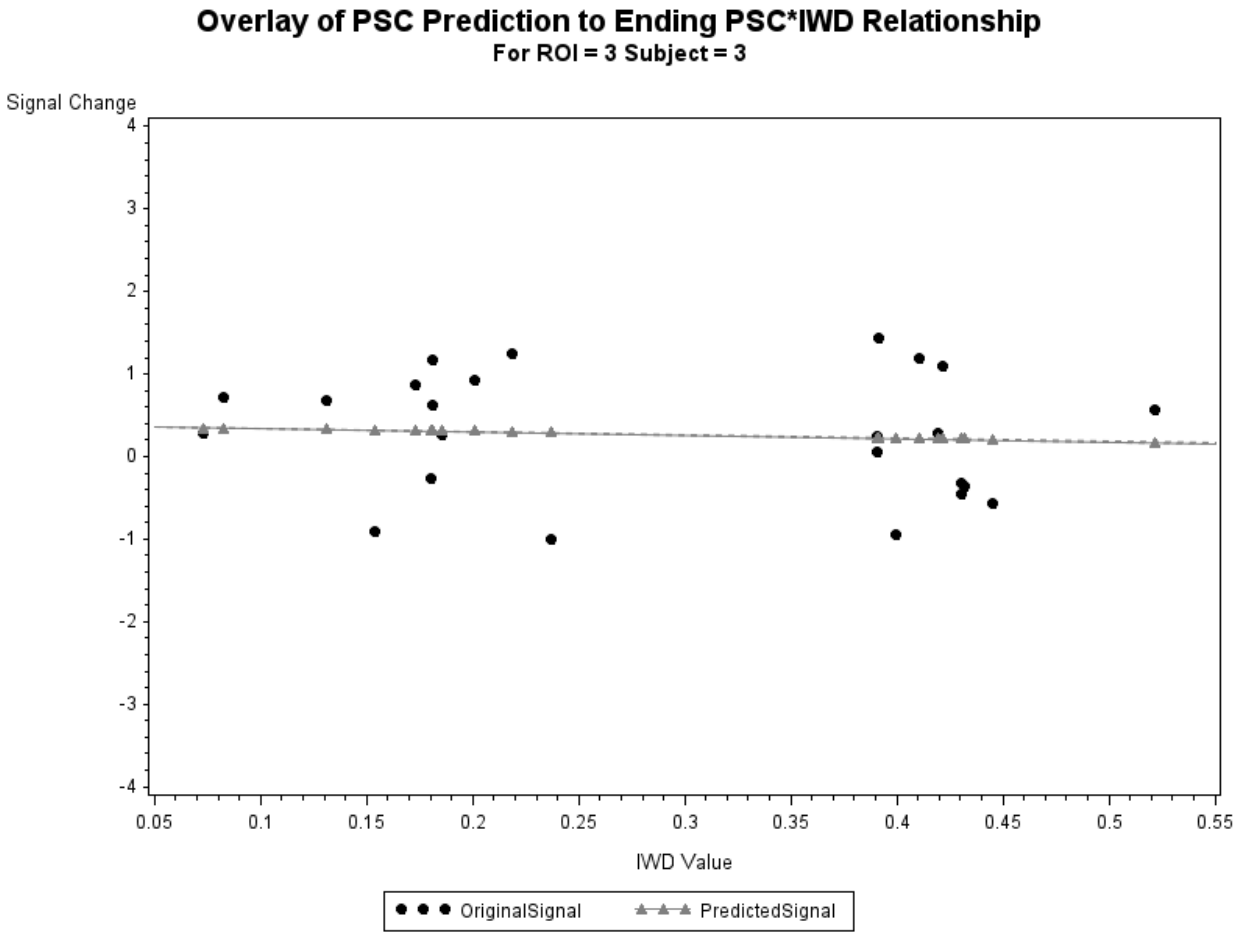
Overlay of PSC Prediction to Ending PSC*IWD Relationship
For ROI = 3 Subject = 3
Signal Change
4
3
2
1
0
-1
-2
-3
-4
0.05
0.1
0.15
0.2
0.25
0.3
0.35
0.4
0.45
0.5
0.55
IWD Value
OriginalSignal
PredictedSignal

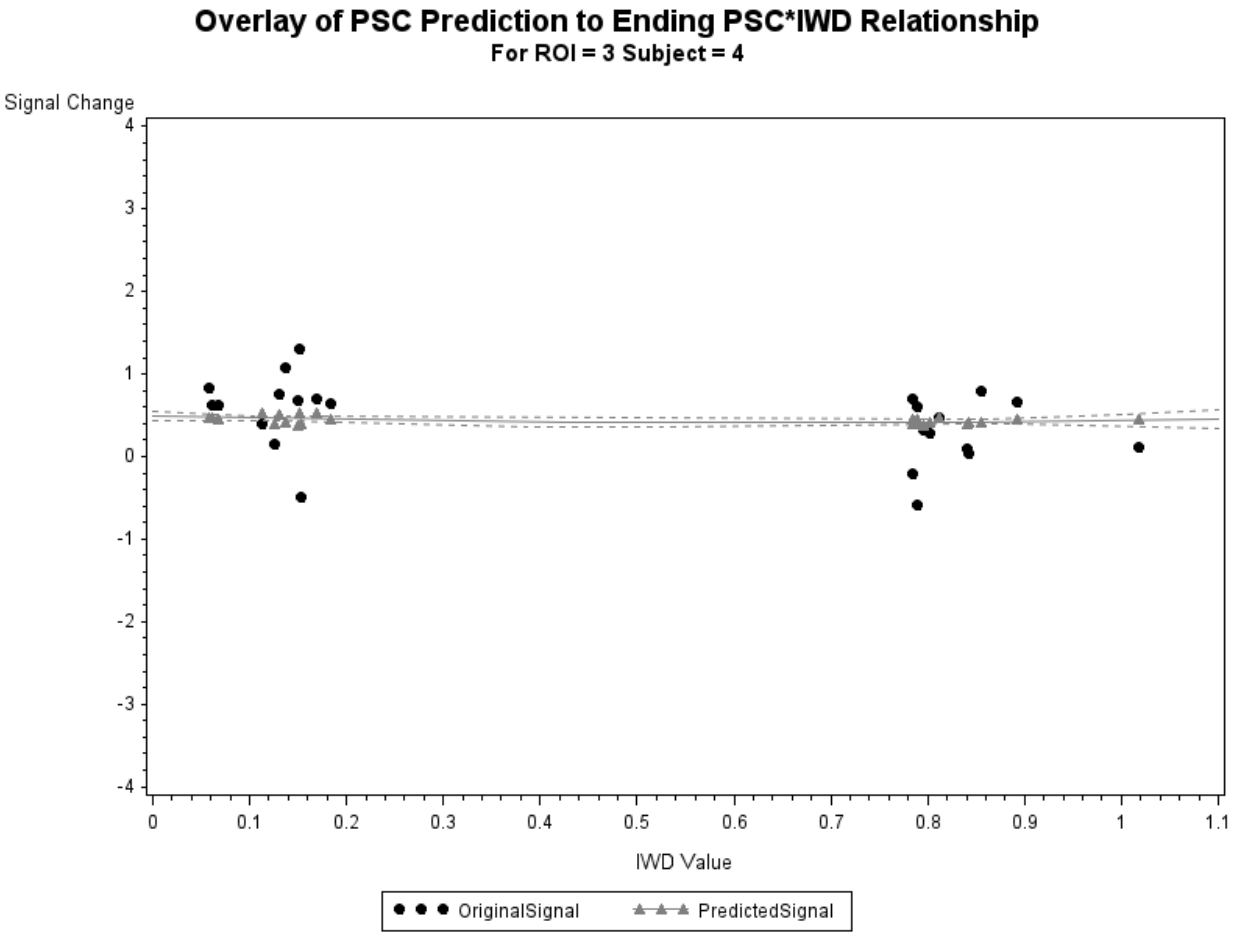
Overlay of PSC Prediction to Ending PSC*IWD Relationship
For ROI = 3 Subject = 4
Signal Change
4
3
2
1
0
-1
-2
-3
-4
0
0.1
0.2
0.3
0.4
0.5
0.6
0.7
0.8
0.9
1
1.1
IWD Value
OriginalSignal
PredictedSignal

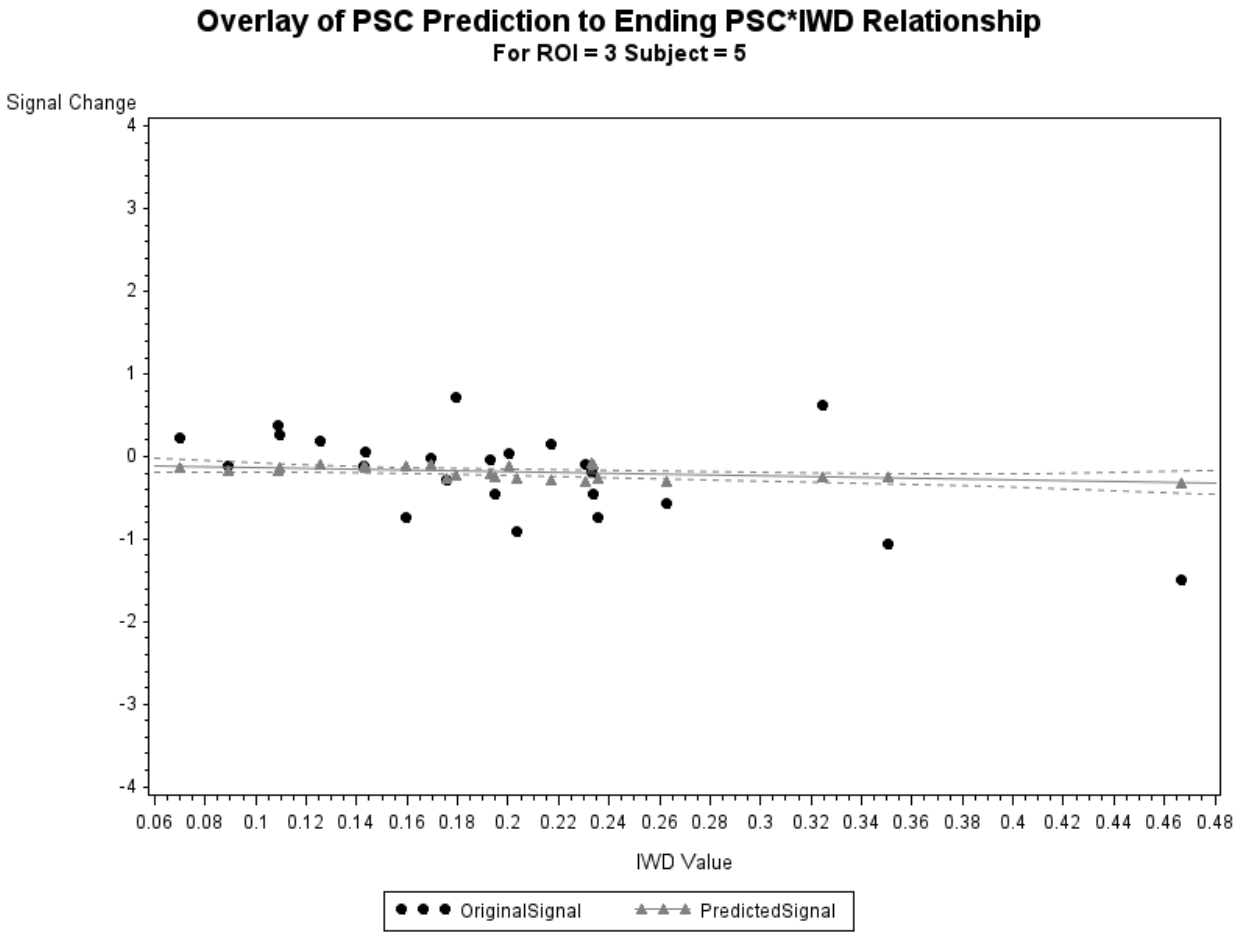
Overlay of PSC Prediction to Ending PSC*IWD Relationship
For ROI = 3 Subject = 5
Signal Change
4
3
2
1
0
-1
-2
-3
-4
0.06 0.08 0.1 0.12 0.14 0.16 0.18 0.2 0.22 0.24 0.26 0.28 0.3 0.32 0.34 0.36 0.38 0.4 0.42 0.44 0.46 0.48
IWD Value
OriginalSignal
PredictedSignal

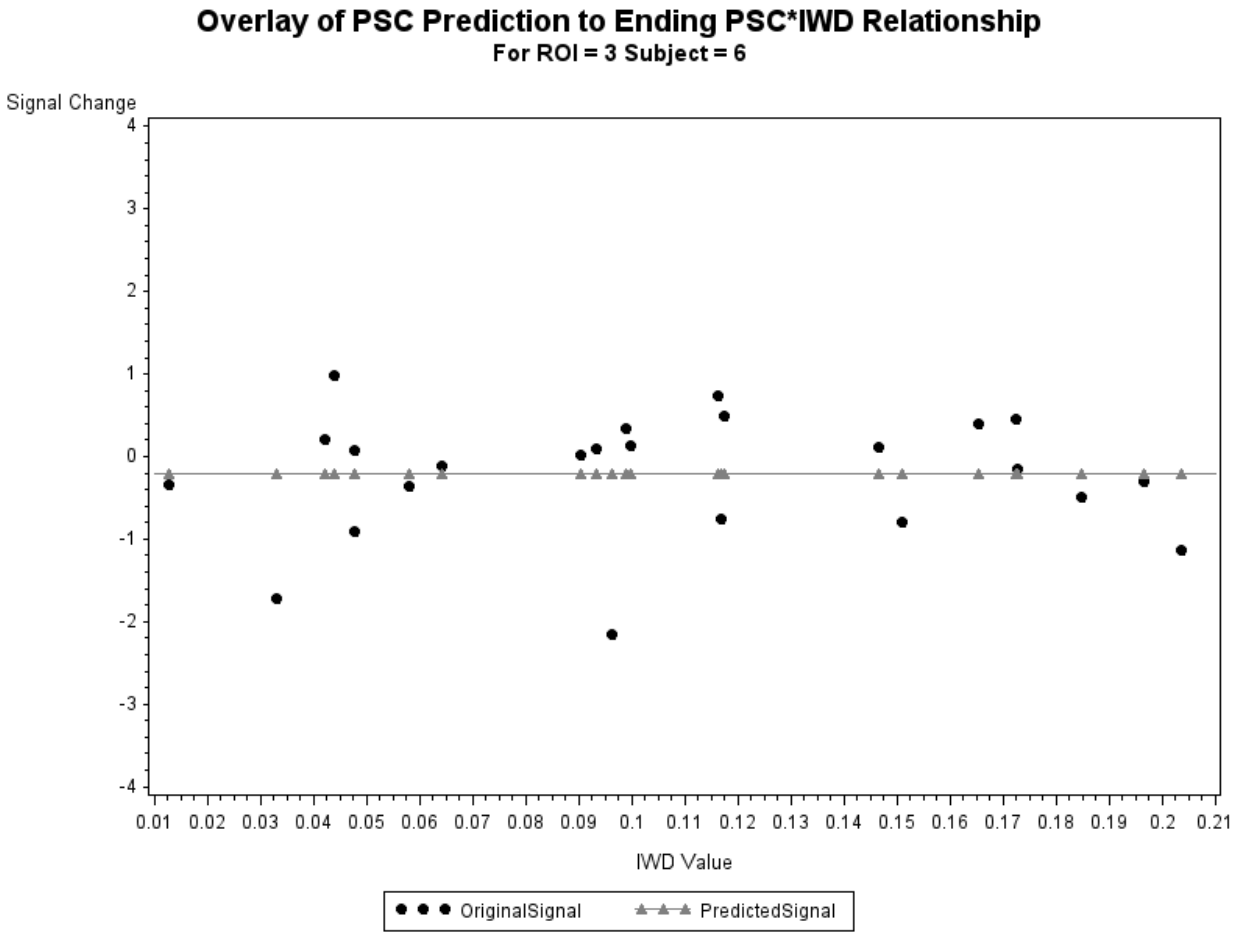
Overlay of PSC Prediction to Ending PSC*IWD Relationship
For ROI = 3 Subject = 6
Signal Change
4
3
2
1
0
-1
-2
-3
-4
0.01 0.02 0.03 0.04 0.05 0.06 0.07 0.08 0.09 0.1 0.11 0.12 0.13 0.14 0.15 0.16 0.17 0.18 0.19 0.2 0.21
IWD Value
OriginalSignal
PredictedSignal

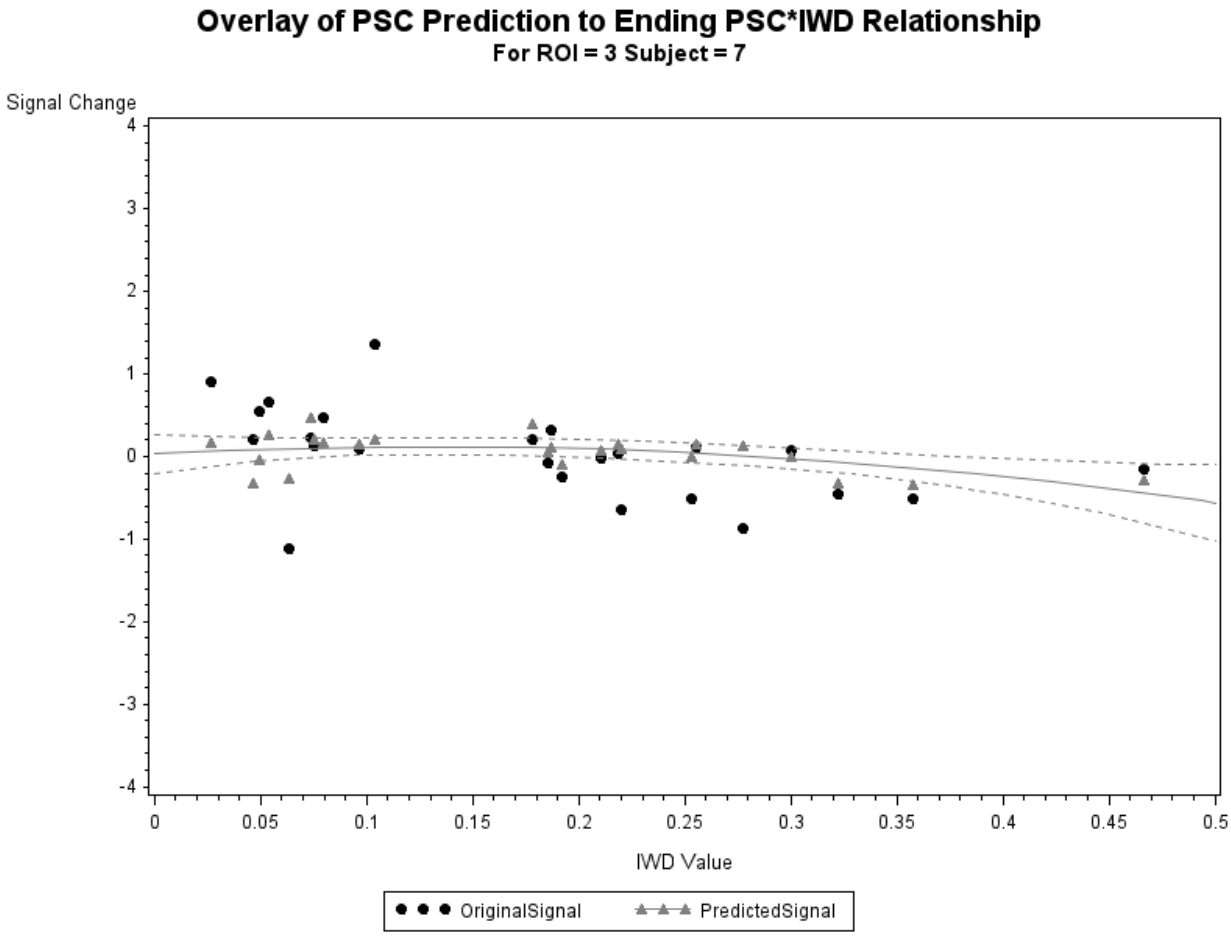
Overlay of PSC Prediction to Ending PSC*IWD Relationship
For ROI = 3 Subject = 7
Signal Change
4
3
2
1
0
-1
-2
-3
-4
0
0.05
0.1
0.15
0.2
0.25
0.3
0.35
0.4
0.45
0.5
IWD Value
OriginalSignal
PredictedSignal

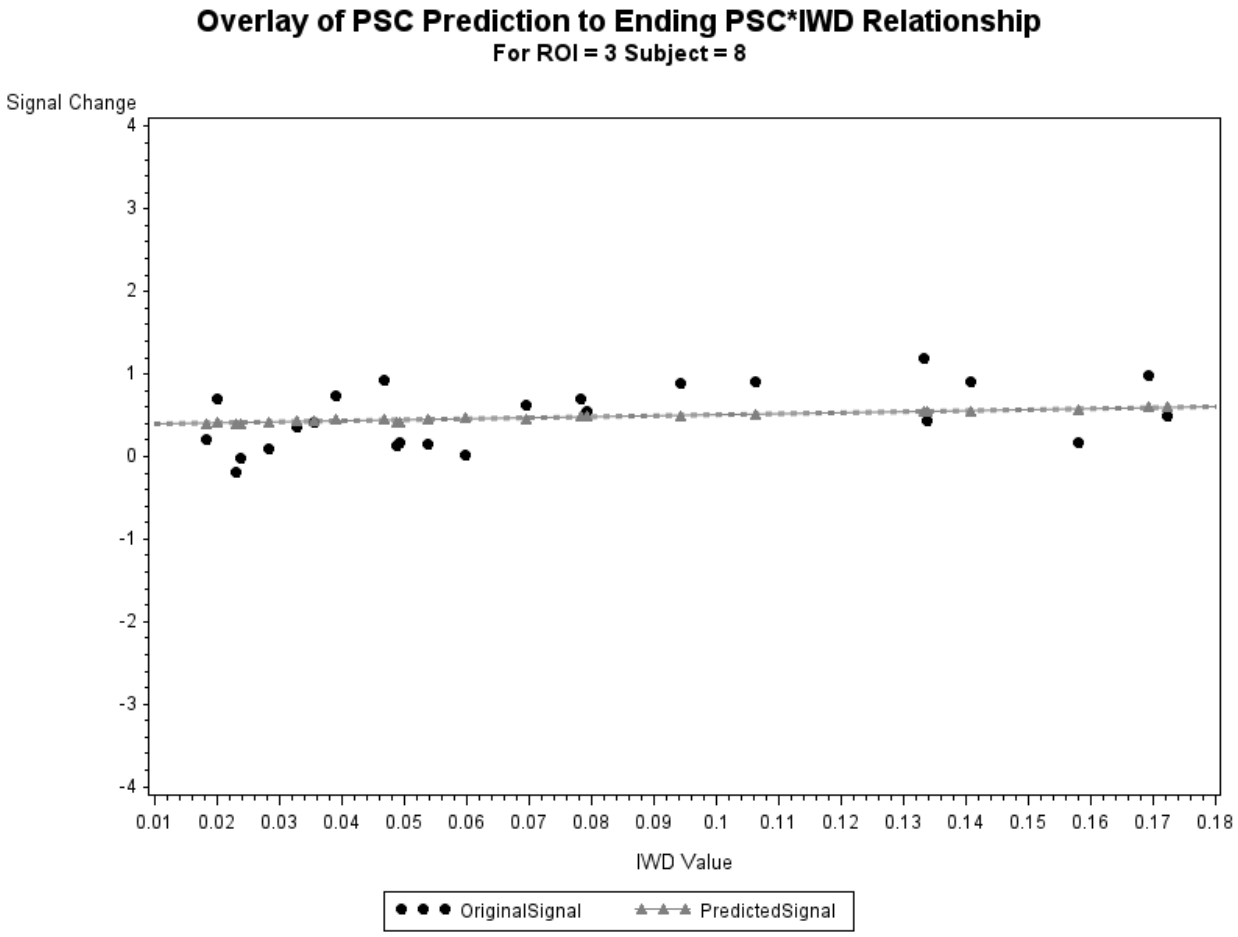
Overlay of PSC Prediction to Ending PSC*IWD Relationship
For ROI = 3 Subject = 8
Signal Change
4
3
2
1
0
-1
-2
-3
-4
0.01
0.02
0.03
0.04
0.05
0.06
0.07
0.08
0.09
0.1
0.11
0.12
0.13
0.14
0.15
0.16
0.17
0.18
IWD Value
OriginalSignal
PredictedSignal

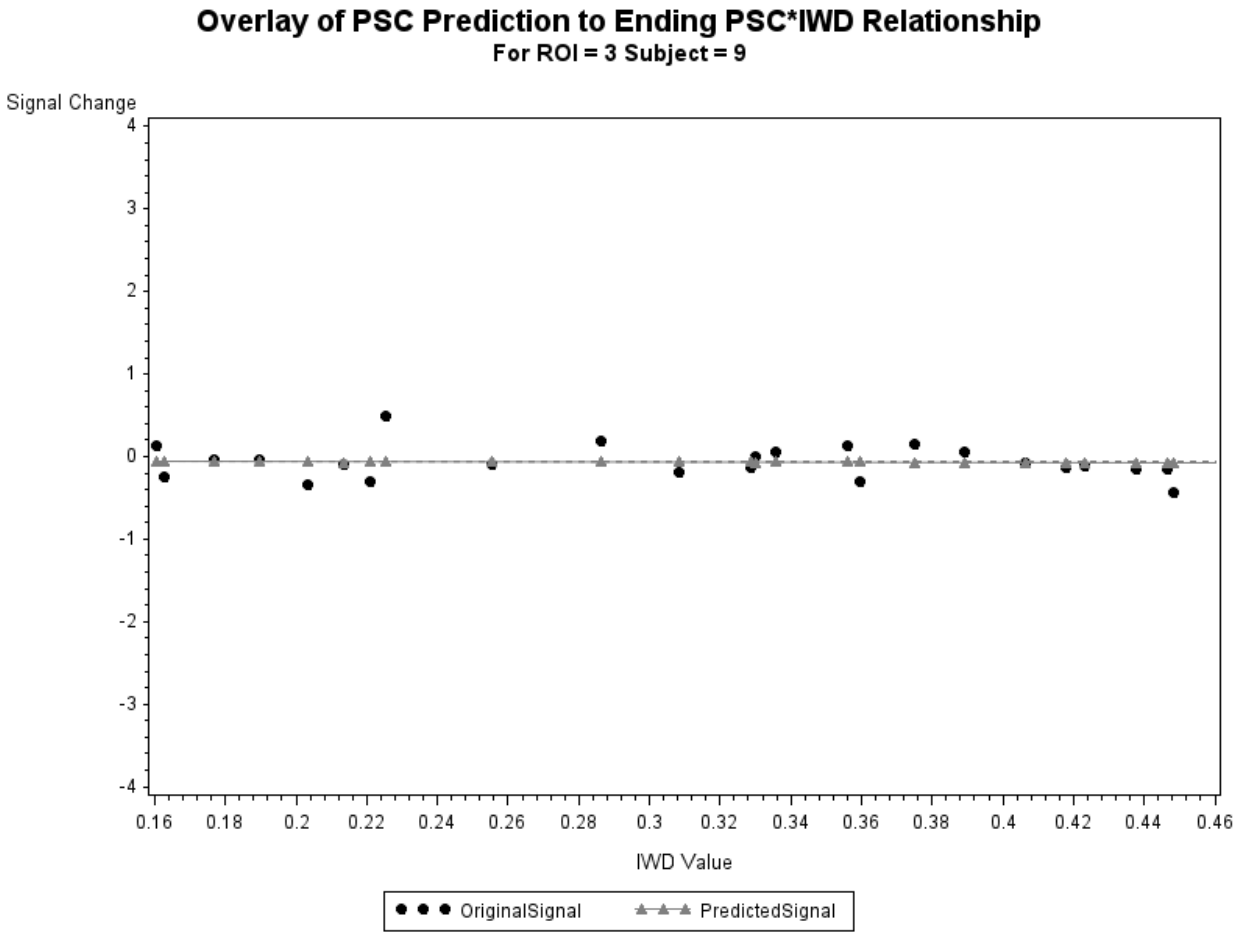
Overlay of PSC Prediction to Ending PSC*IWD Relationship
For ROI = 3 Subject = 9
Signal Change
4
3
2
1
0
-1
-2
-3
-4
0.16
0.18
0.2
0.22
0.24
0.26
0.28
0.3
0.32
0.34
0.36
0.38
0.4
0.42
0.44
0.46
IWD Value
OriginalSignal
PredictedSignal

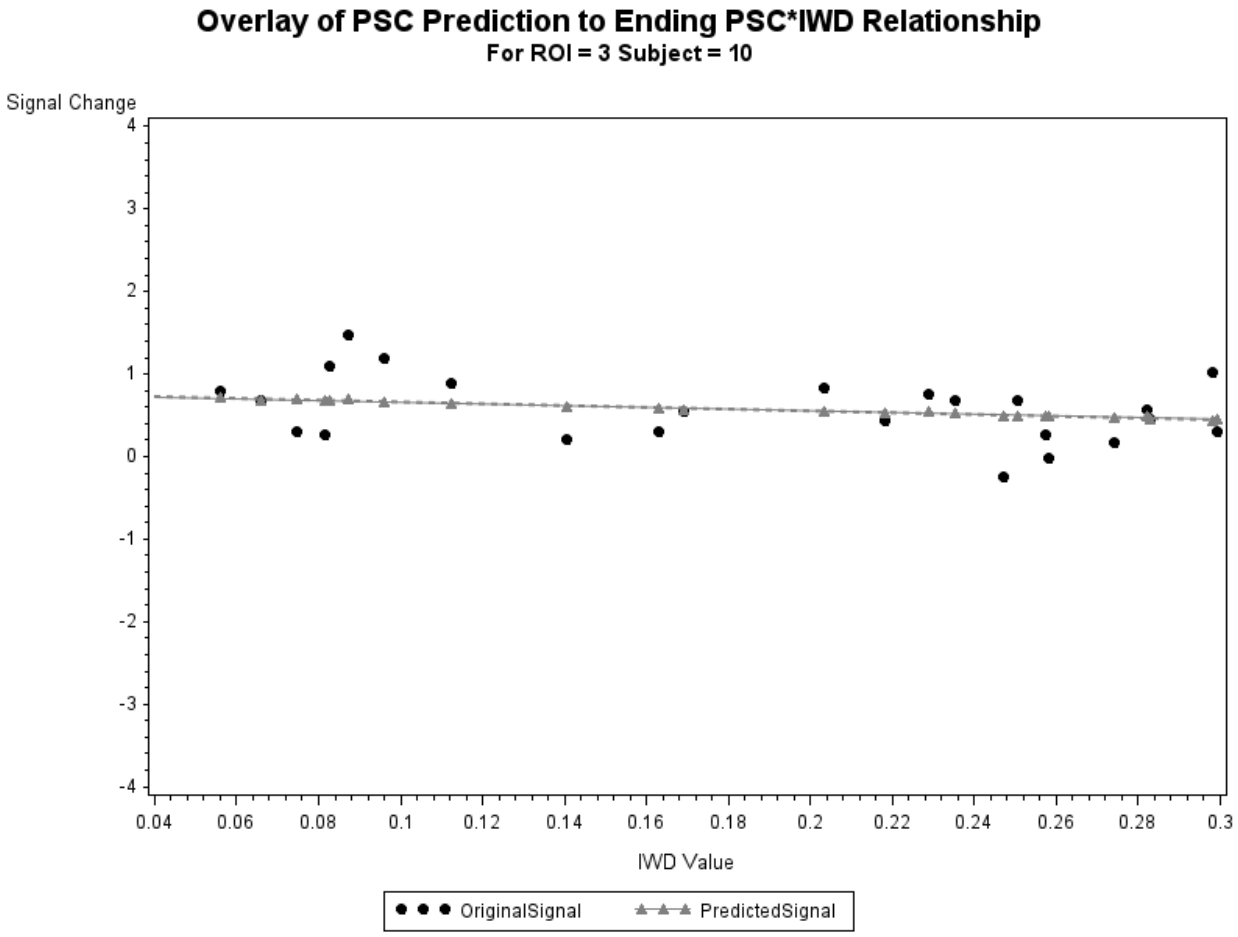
Overlay of PSC Prediction to Ending PSC*IWD Relationship
For ROI = 3 Subject = 10
Signal Change
4
3
2
1
0
-1
-2
-3
-4
0.04
0.06
0.08
0.1
0.12
0.14
0.16
0.18
0.2
0.22
0.24
0.26
0.28
0.3
IWD Value
OriginalSignal
PredictedSignal

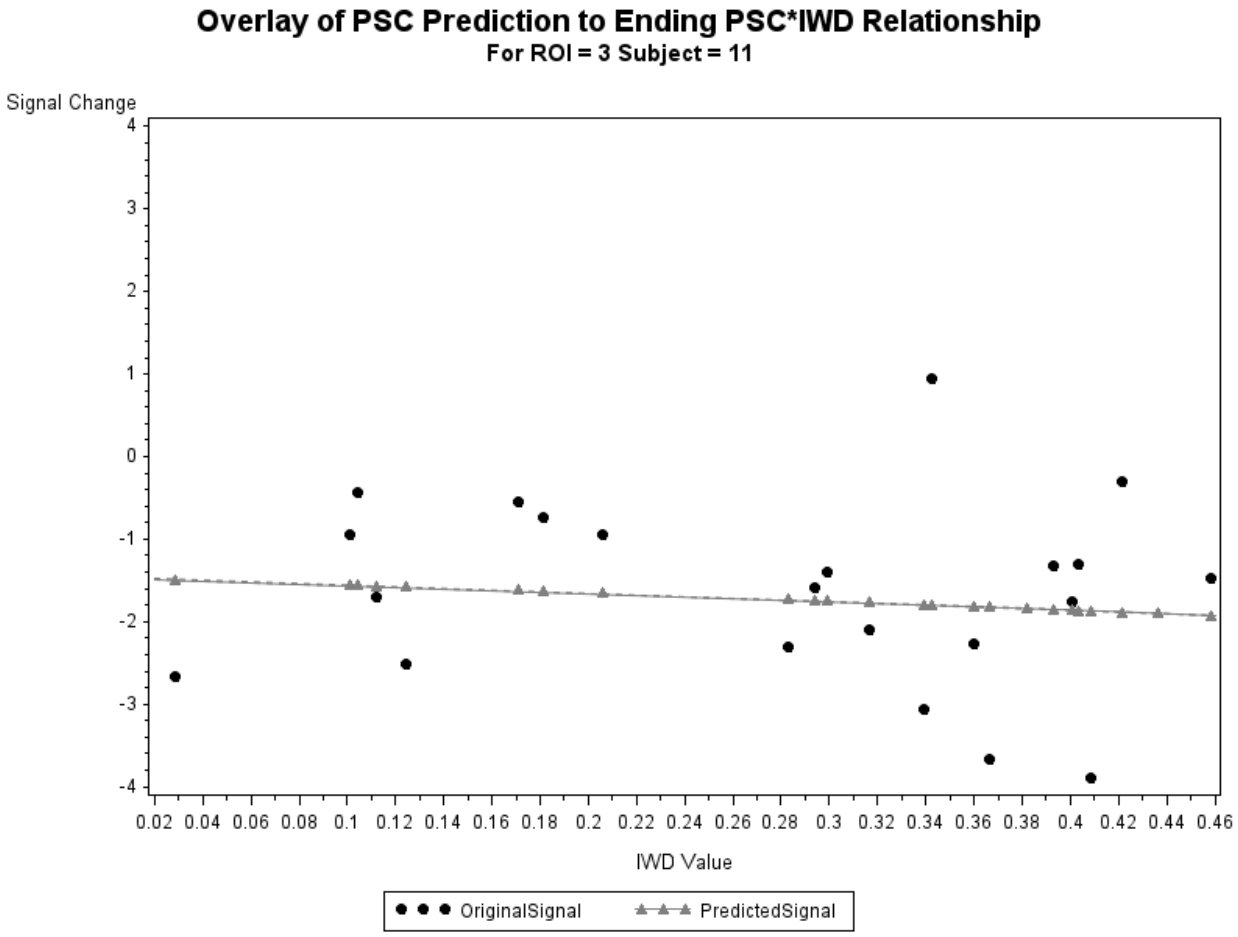
Overlay of PSC Prediction to Ending PSC*IWD Relationship
For ROI = 3 Subject = 11
Signal Change
4
3
2
1
0
-1
-2
-3
-4
0.02 0.04 0.06 0.08 0.1 0.12 0.14 0.16 0.18 0.2 0.22 0.24 0.26 0.28 0.3 0.32 0.34 0.36 0.38 0.4 0.42 0.44 0.46
IWD Value
OriginalSignal
PredictedSignal

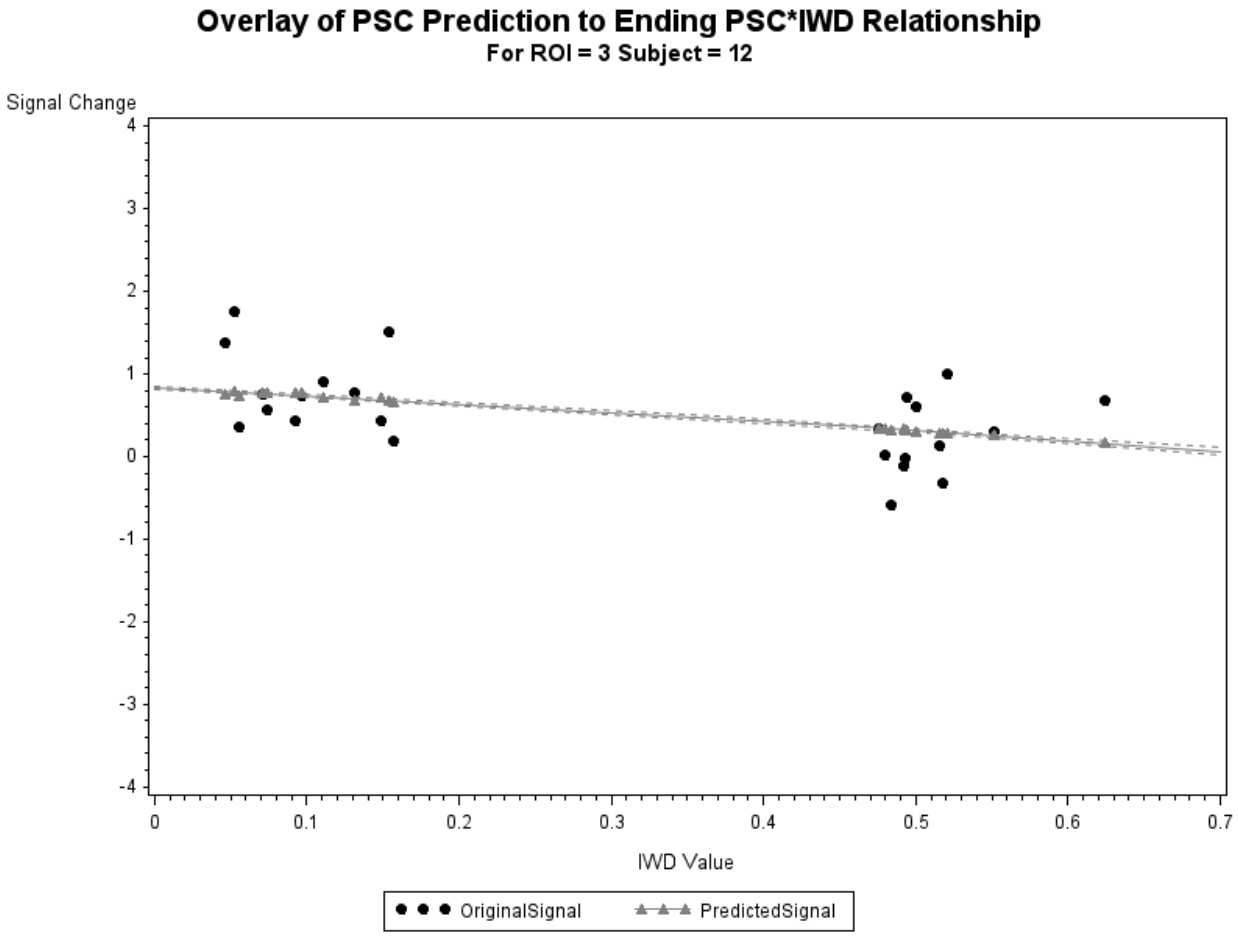
Overlay of PSC Prediction to Ending PSC*IWD Relationship
For ROI = 3 Subject = 12
Signal Change
4
3
2
1
0
-1
-2
-3
-4
0
0.1
0.2
0.3
0.4
0.5
0.6
0.7
IWD Value
OriginalSignal
PredictedSignal

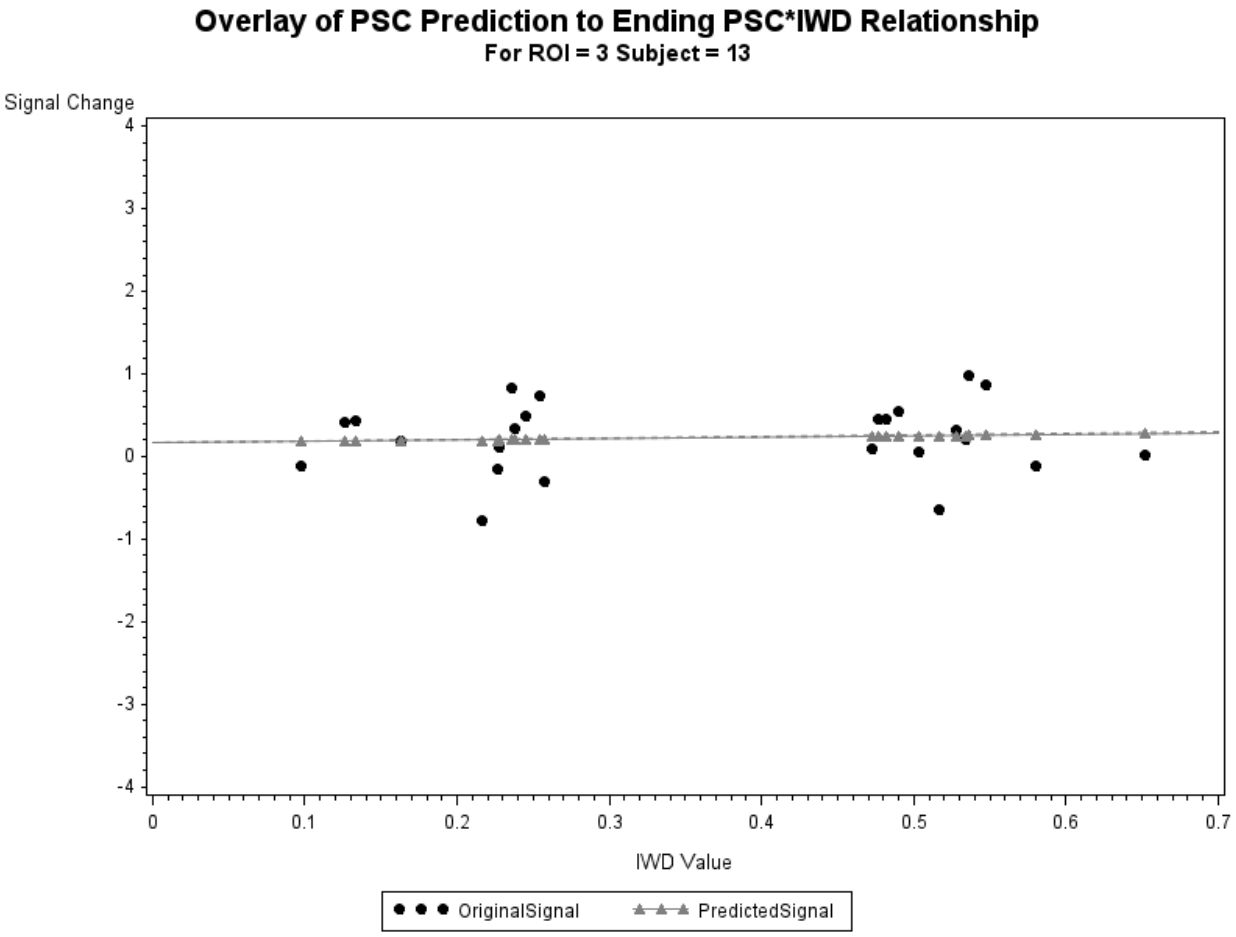
Overlay of PSC Prediction to Ending PSC*IWD Relationship
For ROI = 3 Subject = 13
Signal Change
4
3
2
1
0
-1
-2
-3
-4
0
0.1
0.2
0.3
0.4
0.5
0.6
0.7
IWD Value
OriginalSignal
PredictedSignal

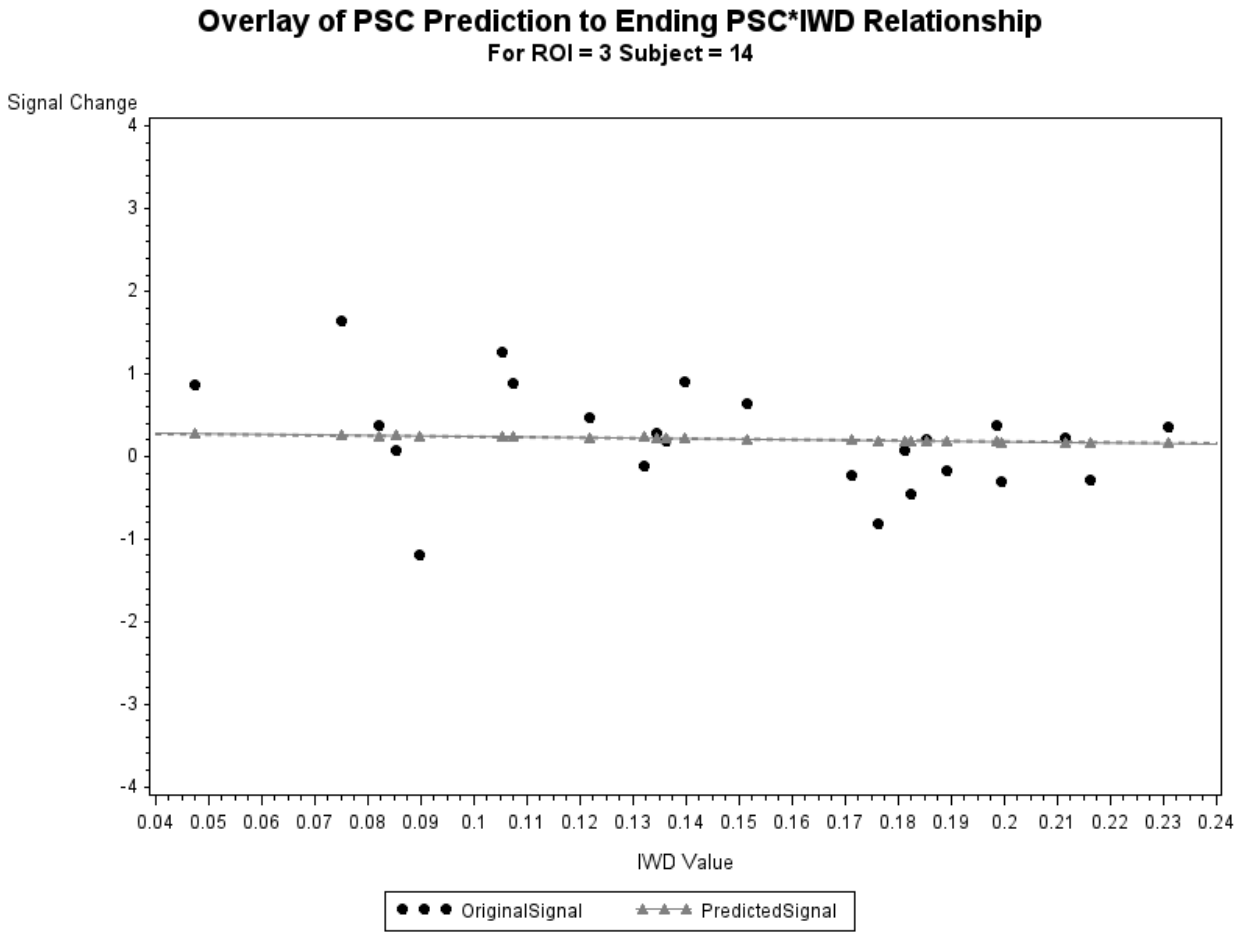
Overlay of PSC Prediction to Ending PSC*IWD Relationship
For ROI = 3 Subject = 14
Signal Change
4
3
2
1
0
-1
-2
-3
-4
0.04 0.05 0.06 0.07 0.08 0.09 0.1 0.11 0.12 0.13 0.14 0.15 0.16 0.17 0.18 0.19 0.2 0.21 0.22 0.23 0.24
IWD Value
OriginalSignal
PredictedSignal

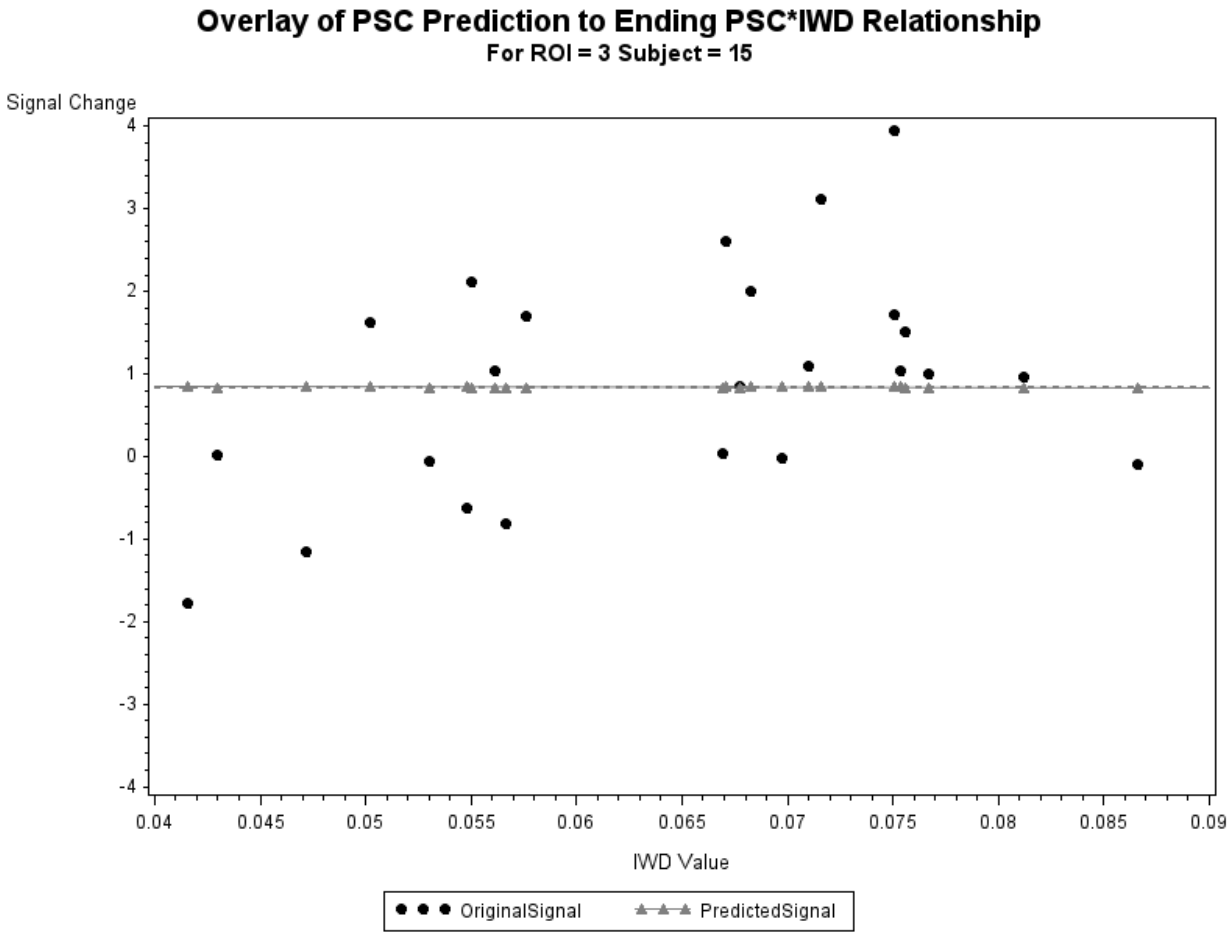
Overlay of PSC Prediction to Ending PSC*IWD Relationship
For ROI = 3 Subject = 15
Signal Change
4
3
2
1
0
-1
-2
-3
-4
0.04
0.045
0.05
0.055
0.06
0.065
0.07
0.075
0.08
0.085
0.09
IWD Value
OriginalSignal
PredictedSignal

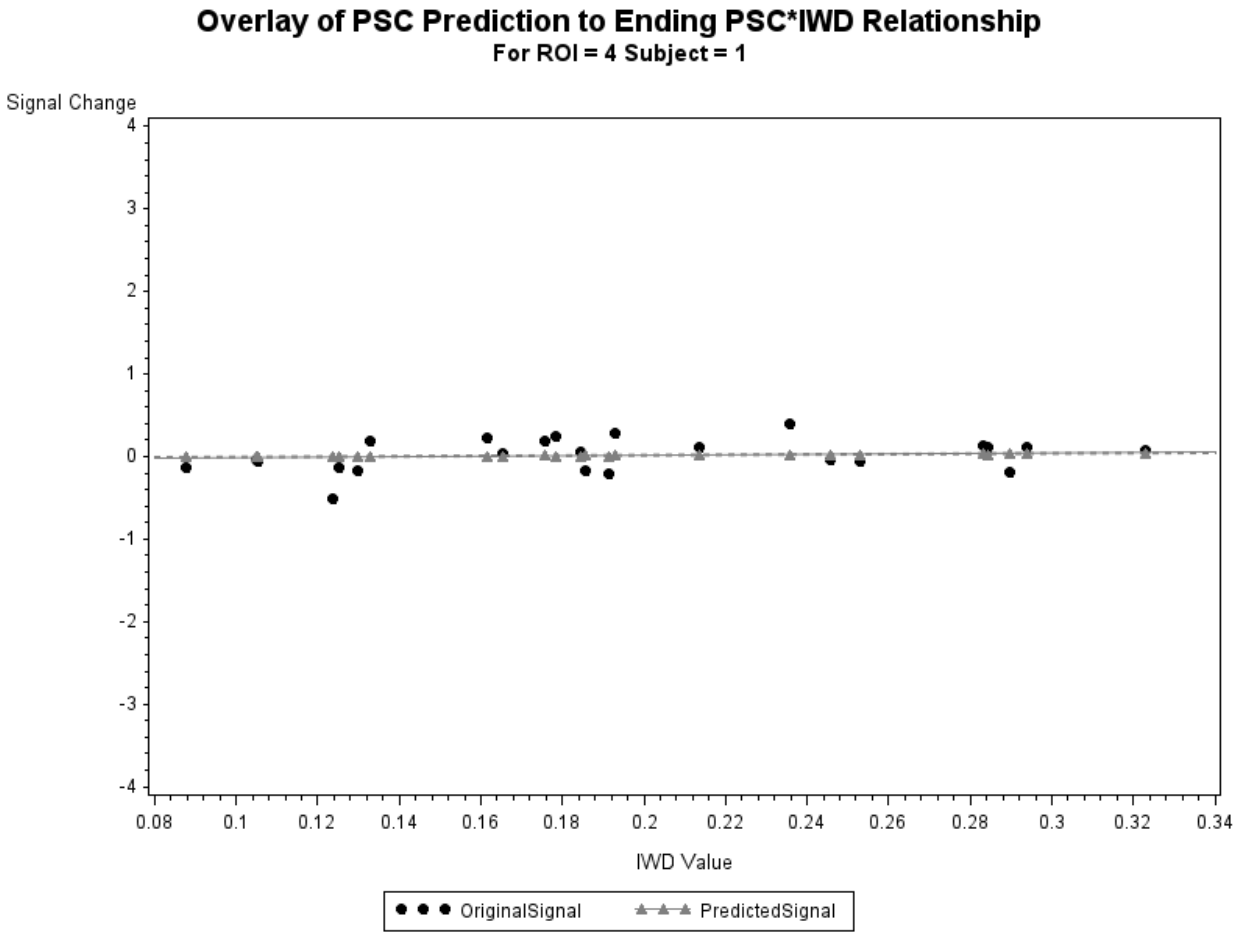
Overlay of PSC Prediction to Ending PSC*IWD Relationship
For ROI = 4 Subject = 1
Signal Change
4
3
2
1
0
-1
-2
-3
-4
0.08
0.1
0.12
0.14
0.16
0.18
0.2
0.22
0.24
0.26
0.28
0.3
0.32
0.34
IWD Value
OriginalSignal
PredictedSignal

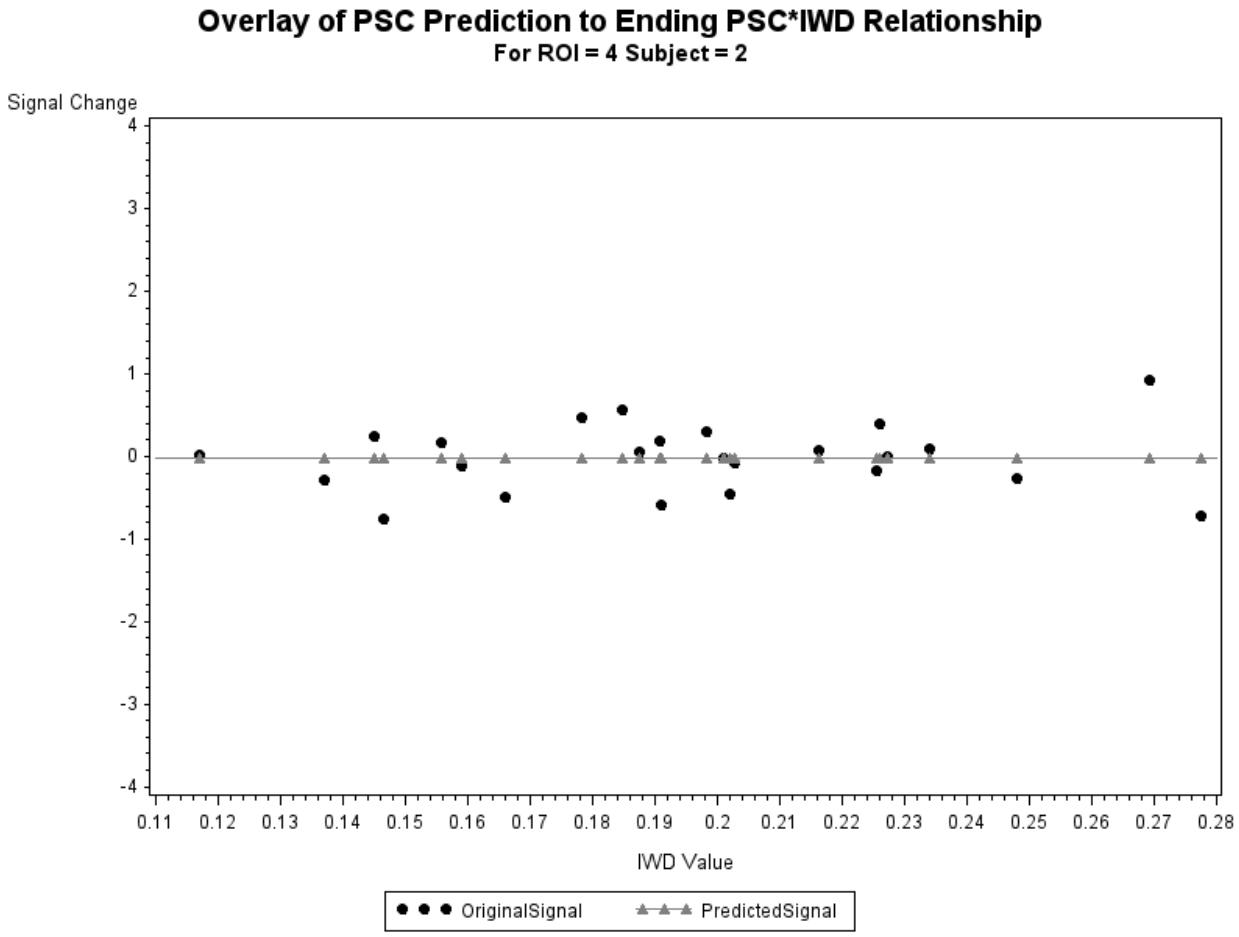
Overlay of PSC Prediction to Ending PSC*IWD Relationship
For ROI = 4 Subject = 2
Signal Change
4
3
2
1
0
-1
-2
-3
-4
0.11
0.12
0.13
0.14
0.15
0.16
0.17
0.18
0.19
0.2
0.21
0.22
0.23
0.24
0.25
0.26
0.27
0.28
IWD Value
OriginalSignal
PredictedSignal

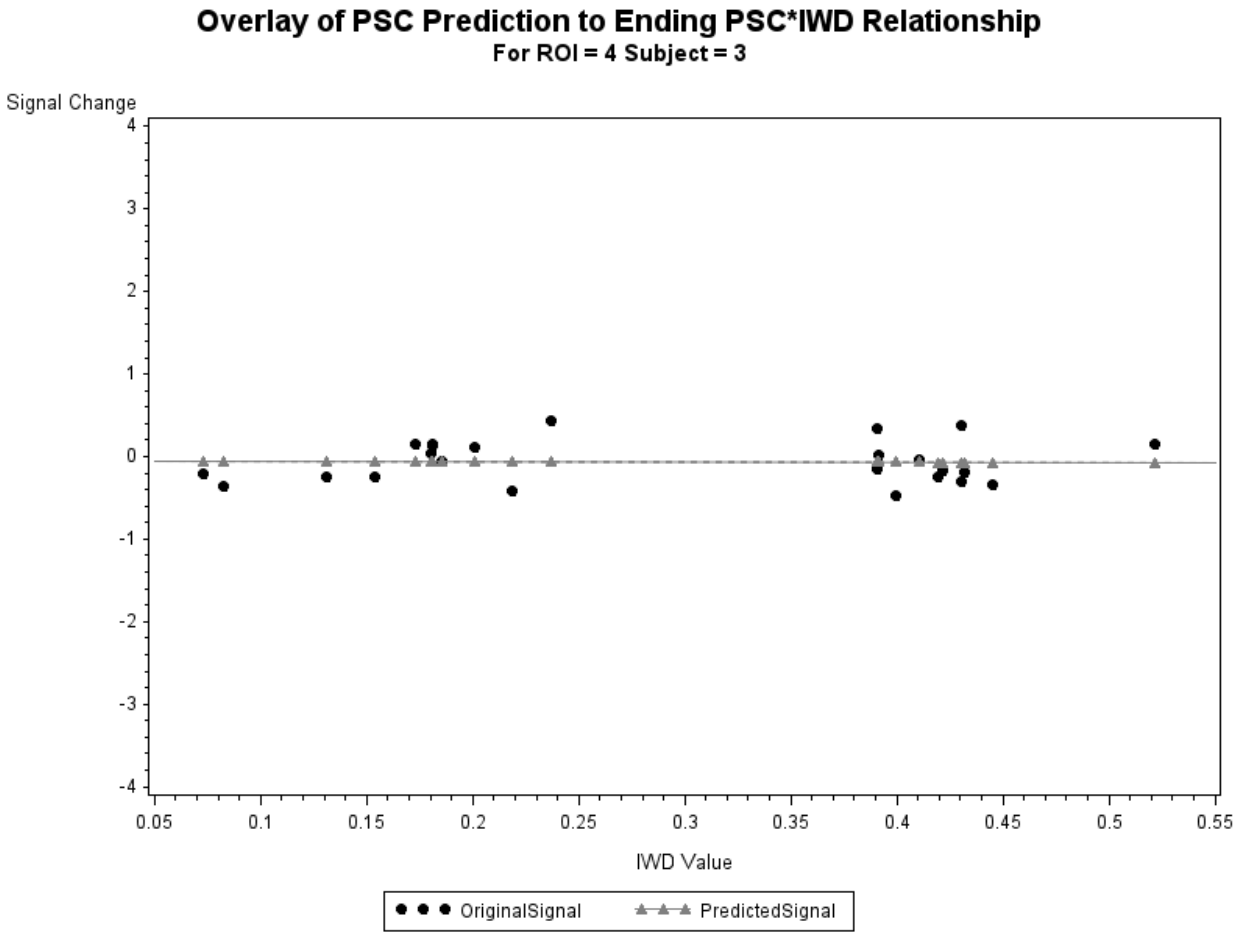
Overlay of PSC Prediction to Ending PSC*IWD Relationship
For ROI = 4 Subject = 3
Signal Change
4
3
2
1
0
-1
-2
-3
-4
0.05
0.1
0.15
0.2
0.25
0.3
0.35
0.4
0.45
0.5
0.55
IWD Value
OriginalSignal
PredictedSignal

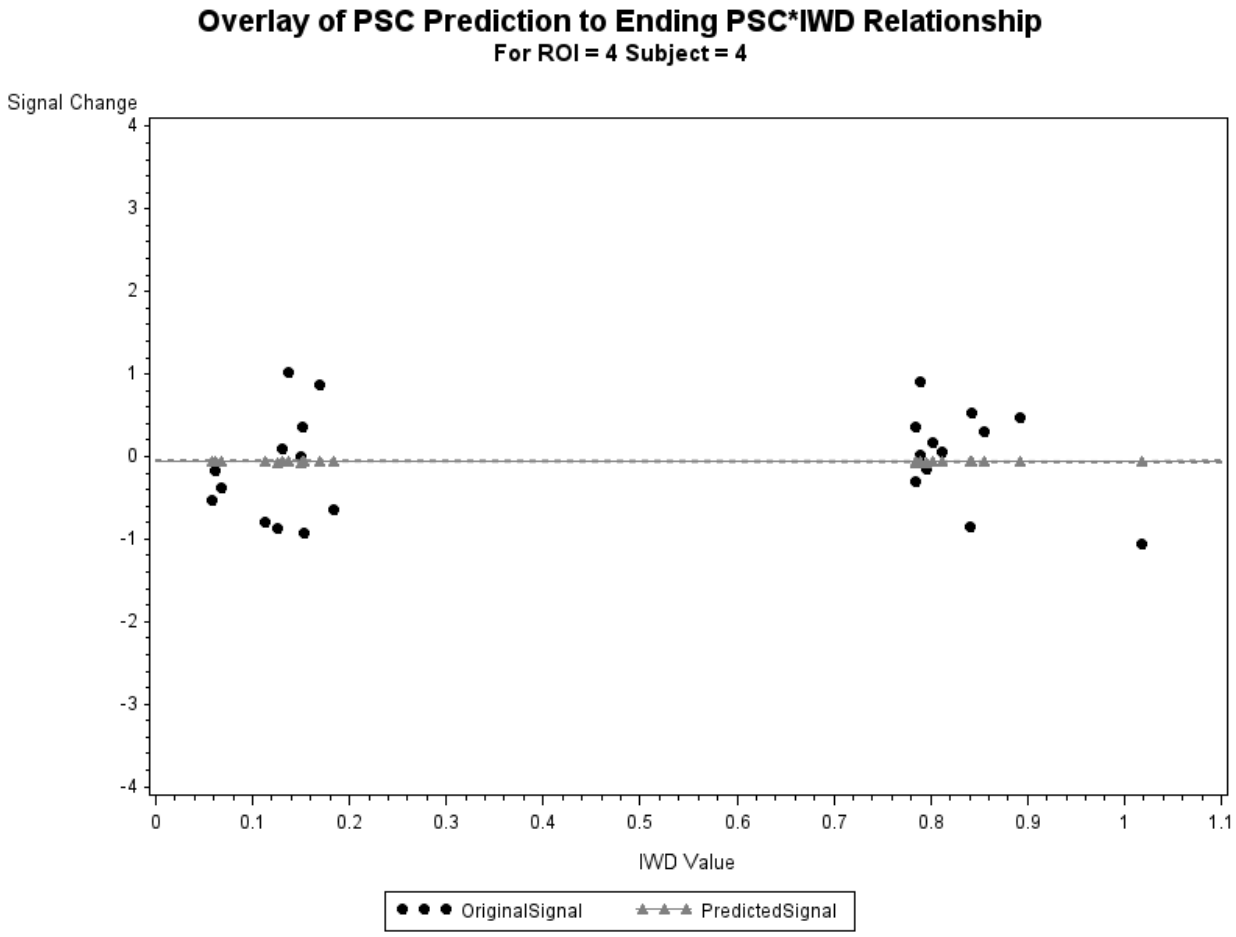
Overlay of PSC Prediction to Ending PSC*IWD Relationship
For ROI = 4 Subject = 4
Signal Change
4
3
2
1
0
-1
-2
-3
-4
0
0.1
0.2
0.3
0.4
0.5
0.6
0.7
0.8
0.9
1
1.1
IWD Value
OriginalSignal
PredictedSignal

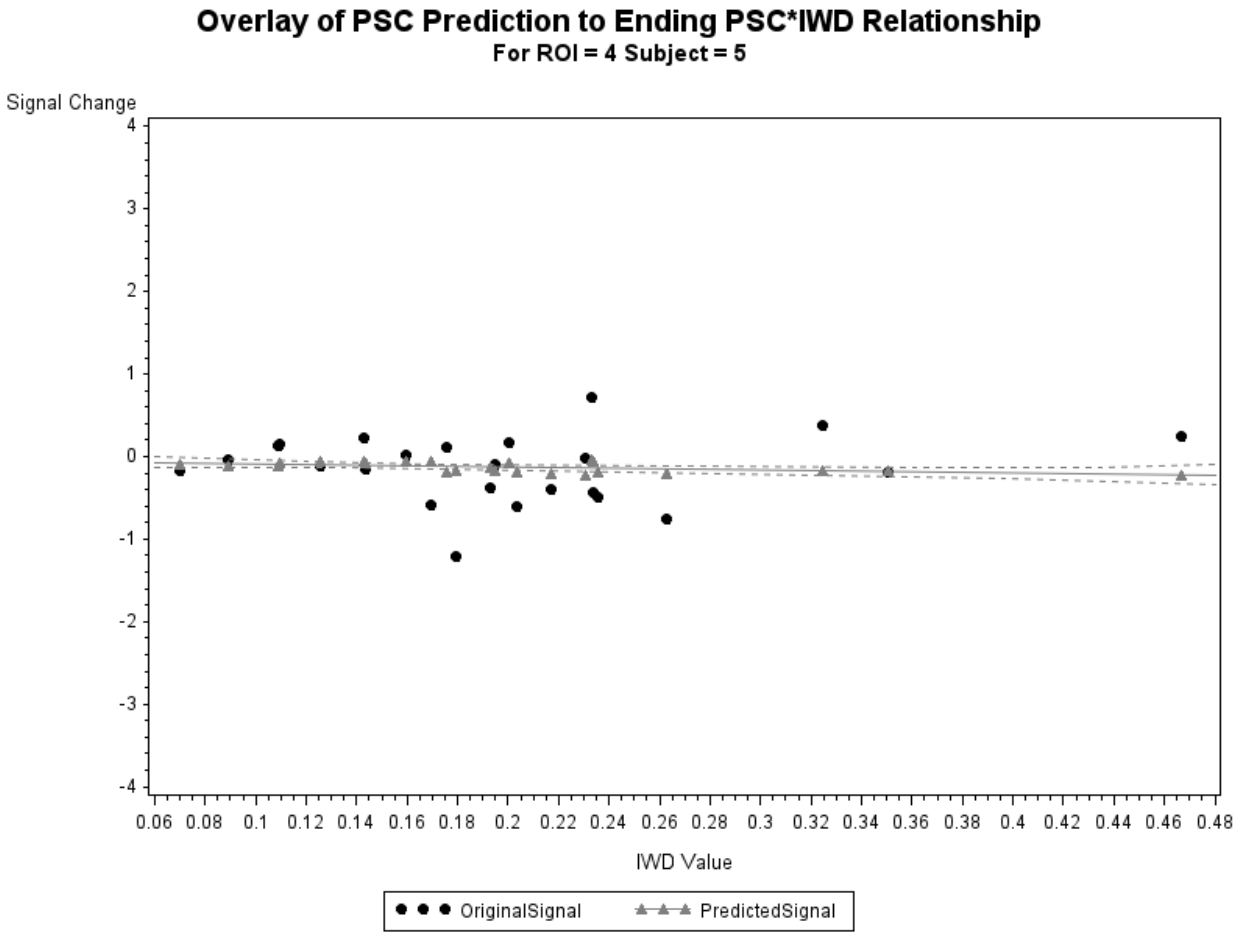
Overlay of PSC Prediction to Ending PSC*IWD Relationship
For ROI = 4 Subject = 5
Signal Change
4
3
2
1
0
-1
-2
-3
-4
0.06 0.08 0.1 0.12 0.14 0.16 0.18 0.2 0.22 0.24 0.26 0.28 0.3 0.32 0.34 0.36 0.38 0.4 0.42 0.44 0.46 0.48
IWD Value
OriginalSignal
PredictedSignal

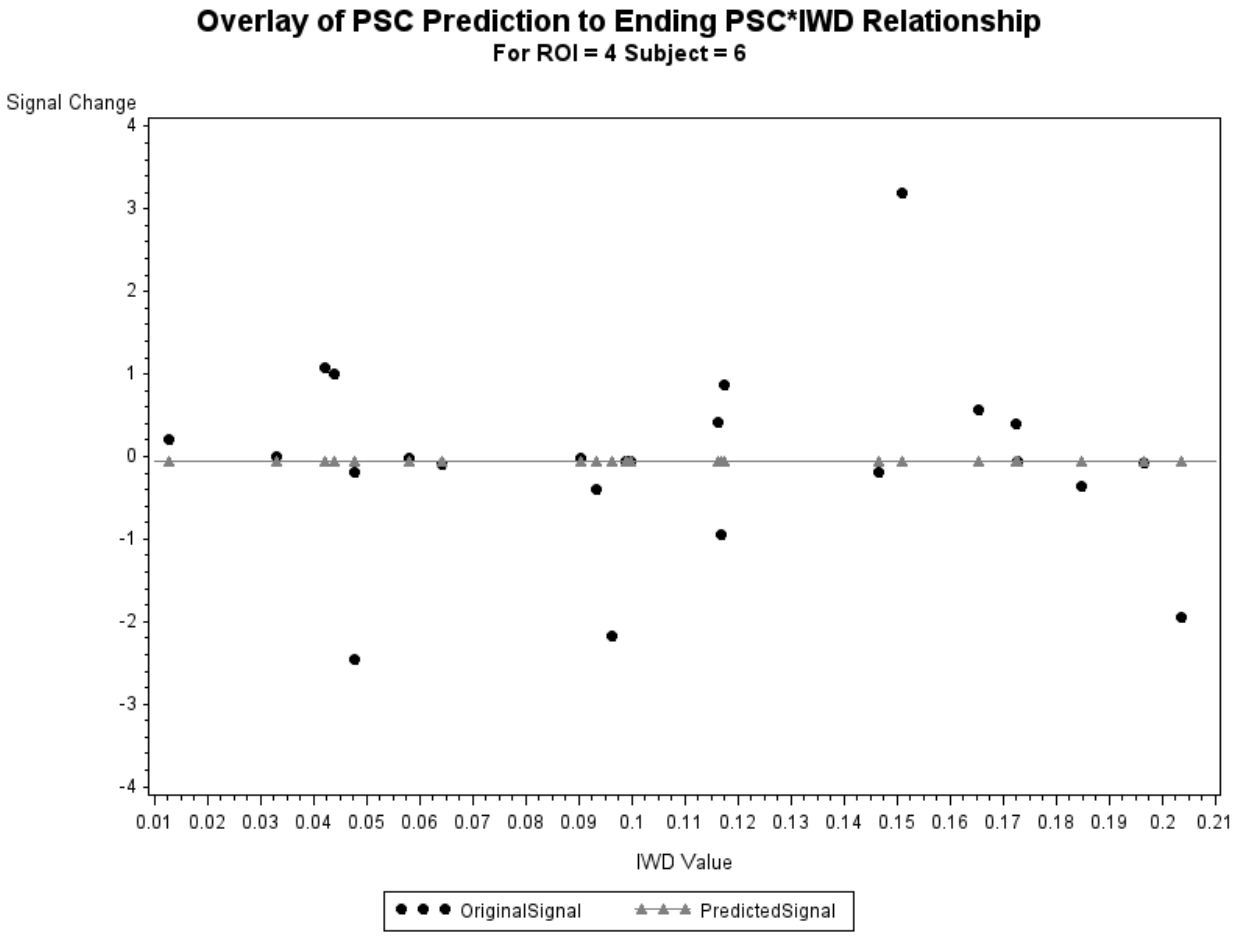
Overlay of PSC Prediction to Ending PSC*IWD Relationship
For ROI = 4 Subject = 6
Signal Change
4
3
2
1
0
-1
-2
-3
-4
0.01 0.02 0.03 0.04 0.05 0.06 0.07 0.08 0.09 0.1 0.11 0.12 0.13 0.14 0.15 0.16 0.17 0.18 0.19 0.2 0.21
IWD Value
OriginalSignal
PredictedSignal

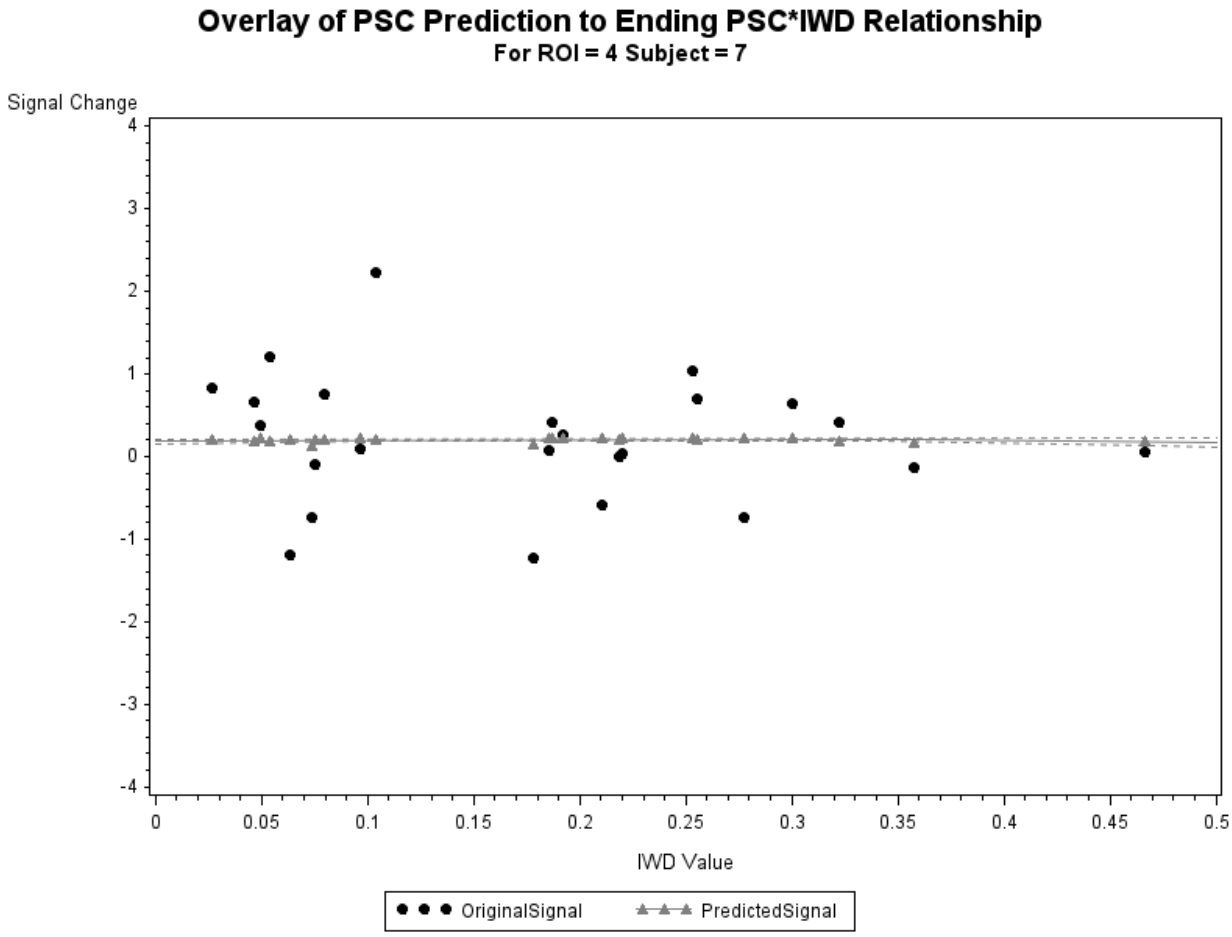
Overlay of PSC Prediction to Ending PSC*IWD Relationship
For ROI = 4 Subject = 7
Signal Change
4
3
2
1
0
-1
-2
-3
-4
0
0.05
0.1
0.15
0.2
0.25
0.3
0.35
0.4
0.45
0.5
IWD Value
OriginalSignal
PredictedSignal

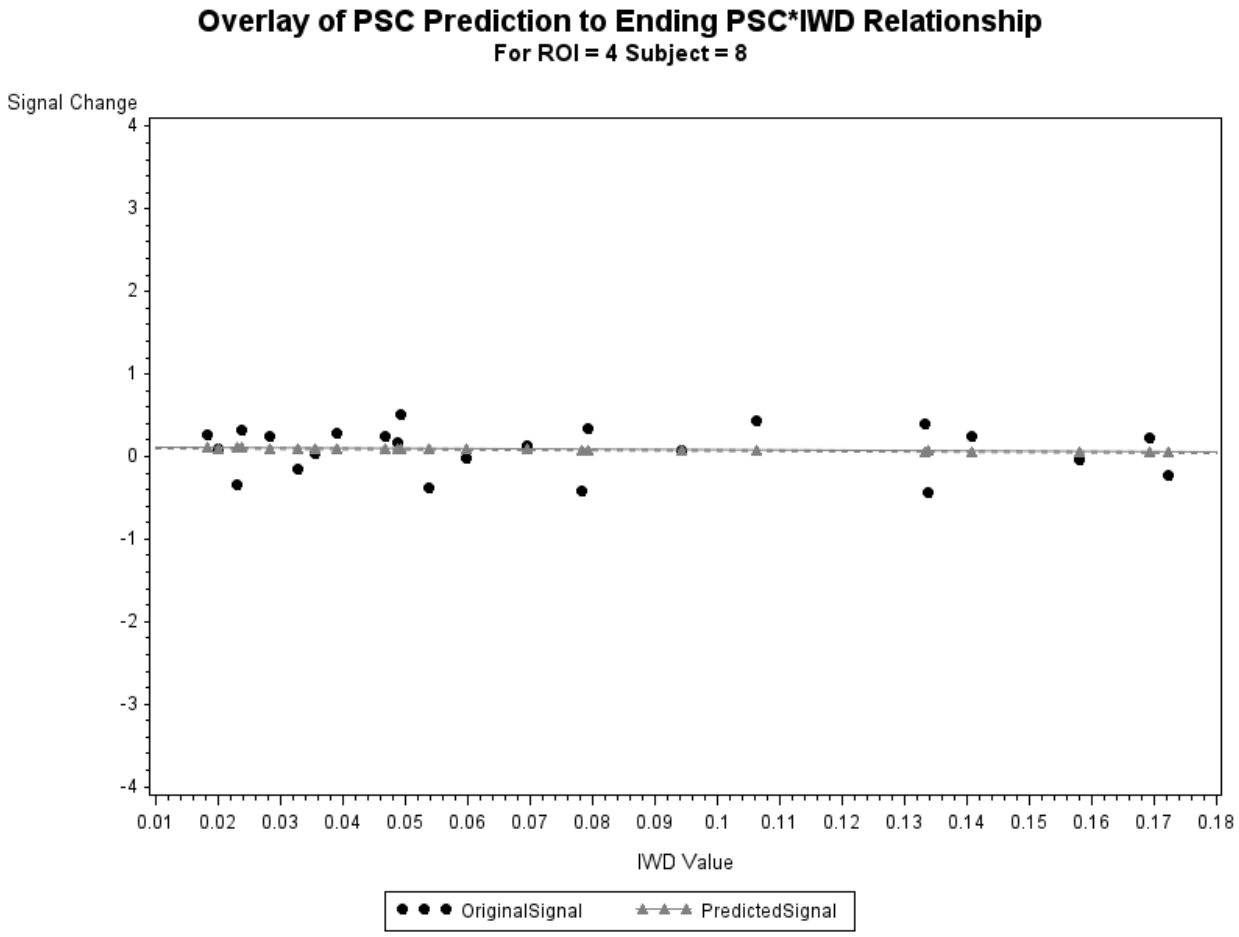
Overlay of PSC Prediction to Ending PSC*IWD Relationship
For ROI = 4 Subject = 8
Signal Change
4
3
2
1
0
-1
-2
-3
-4
0.01
0.02
0.03
0.04
0.05
0.06
0.07
0.08
0.09
0.1
0.11
0.12
0.13
0.14
0.15
0.16
0.17
0.18
IWD Value
OriginalSignal
PredictedSignal

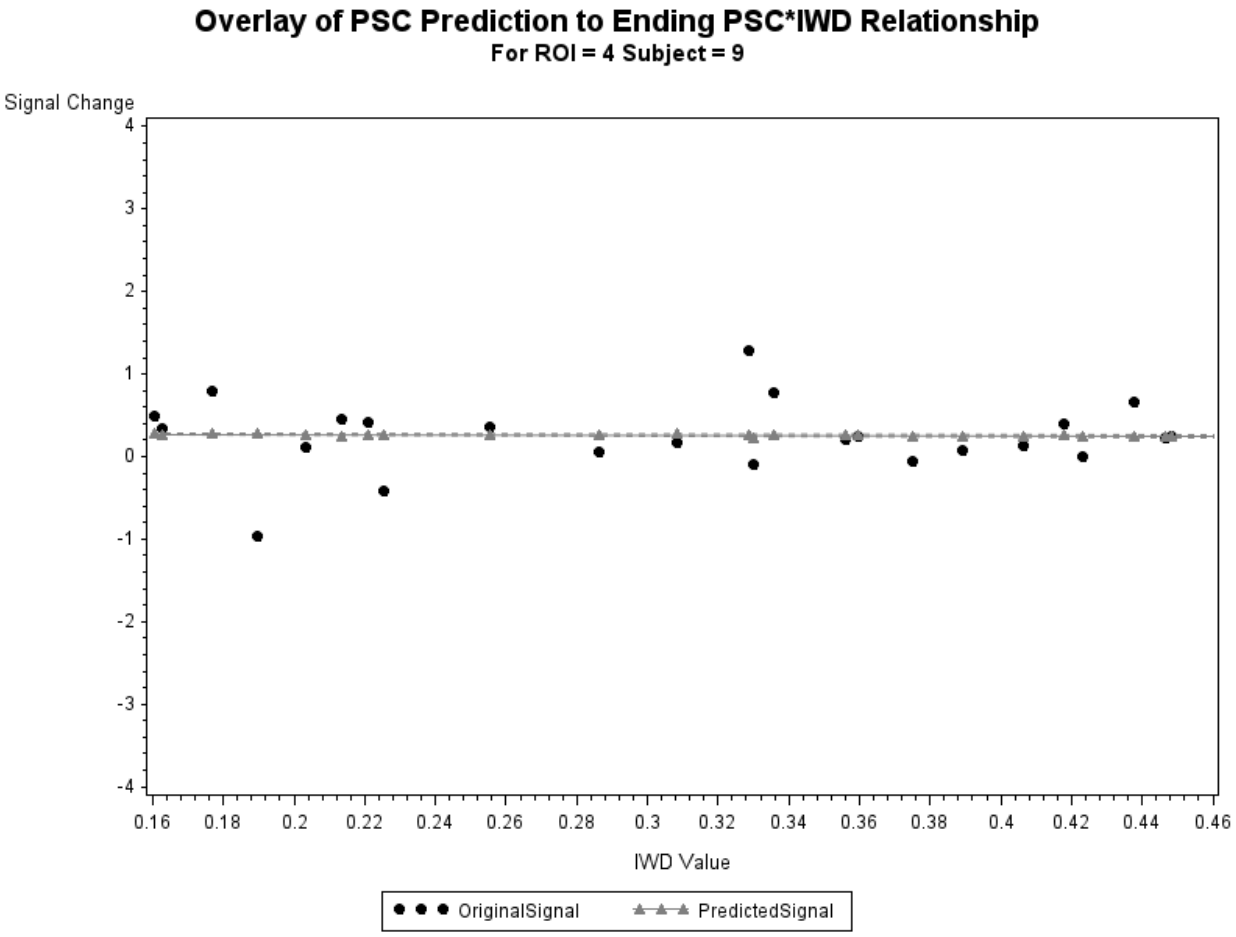
Overlay of PSC Prediction to Ending PSC*IWD Relationship
For ROI = 4 Subject = 9
Signal Change
4
3
2
1
0
-1
-2
-3
-4
0.16
0.18
0.2
0.22
0.24
0.26
0.28
0.3
0.32
0.34
0.36
0.38
0.4
0.42
0.44
0.46
IWD Value
OriginalSignal
PredictedSignal

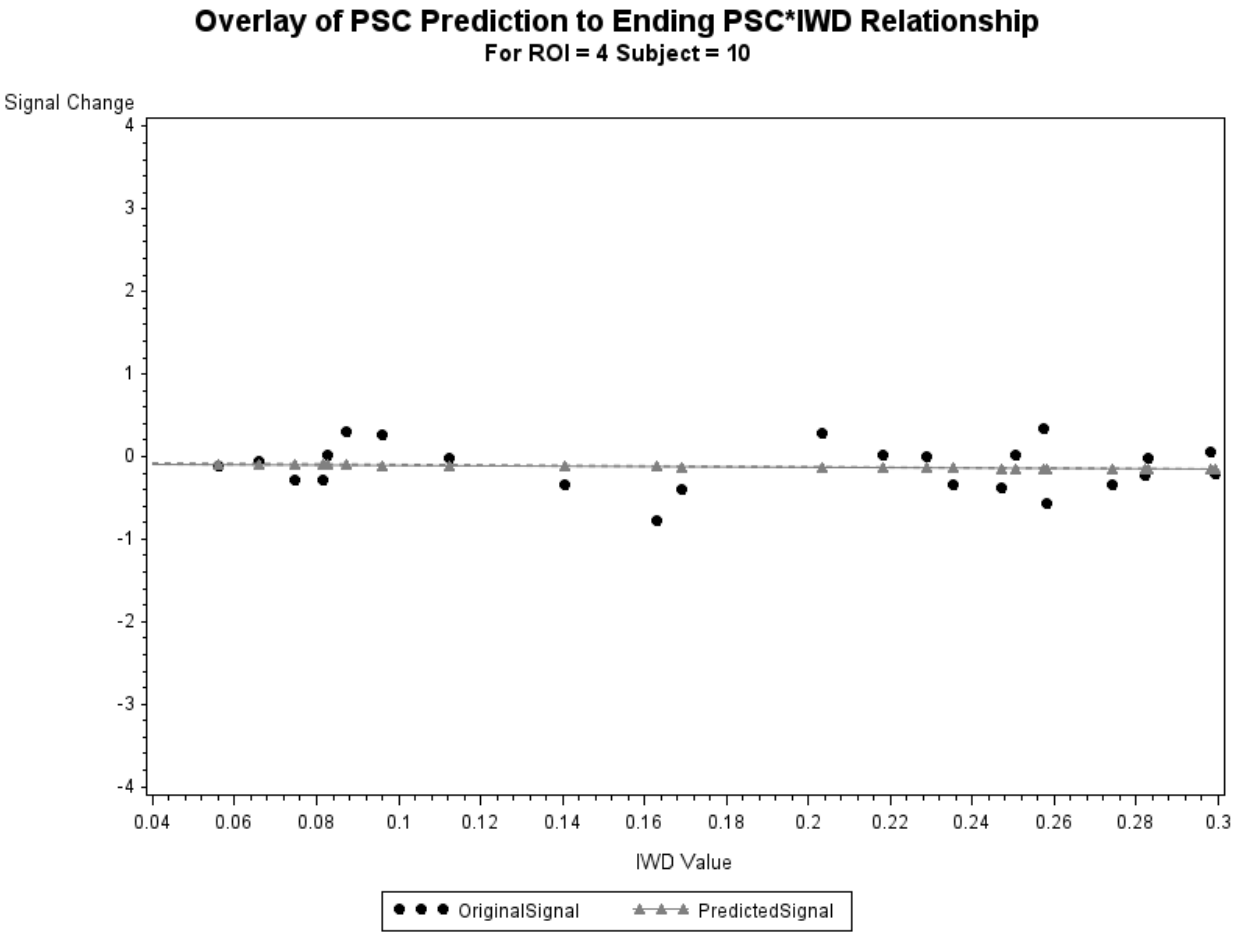
Overlay of PSC Prediction to Ending PSC*IWD Relationship
For ROI = 4 Subject = 10
Signal Change
4
3
2
1
0
-1
-2
-3
-4
0.04
0.06
0.08
0.1
0.12
0.14
0.16
0.18
0.2
0.22
0.24
0.26
0.28
0.3
IWD Value
OriginalSignal
PredictedSignal

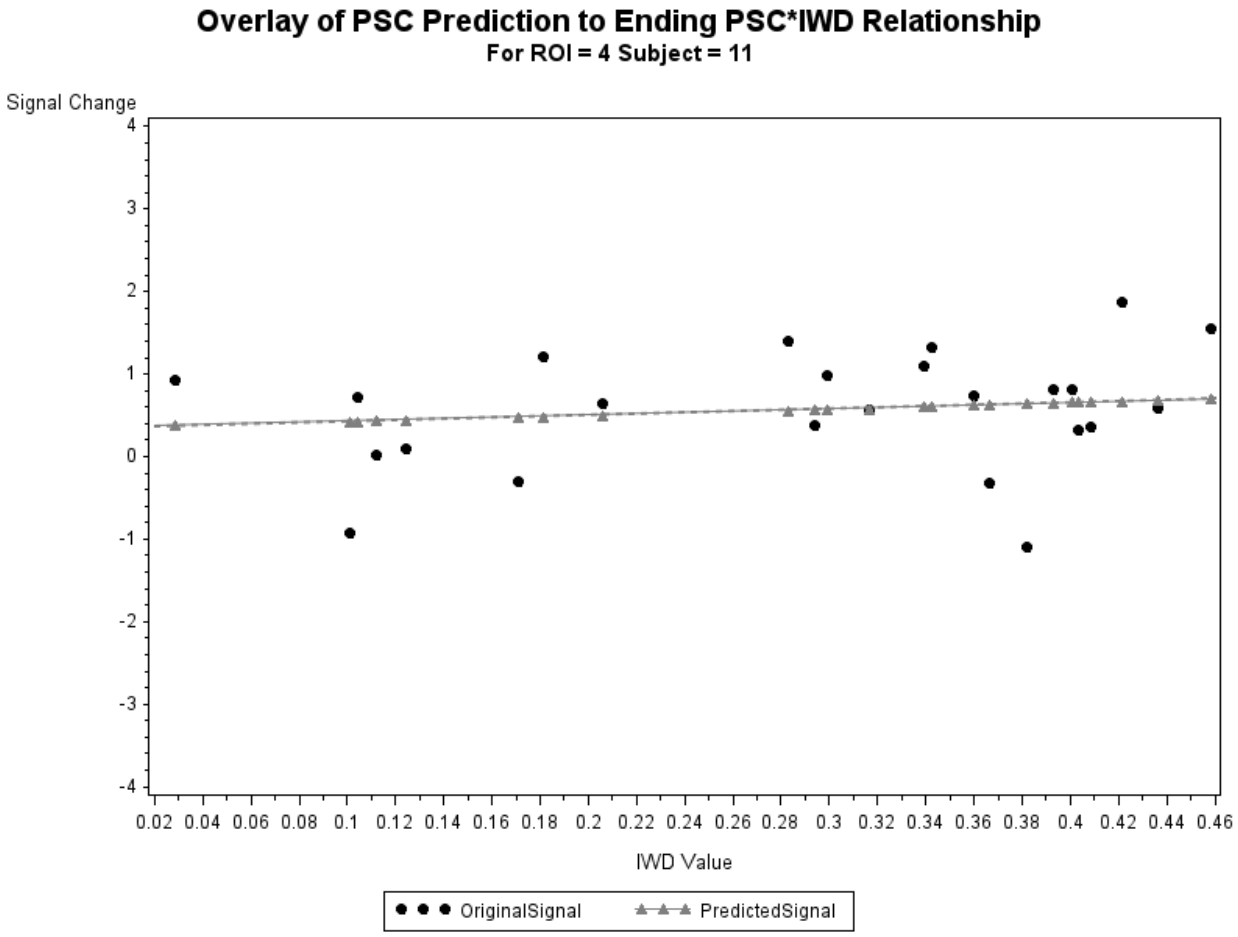
Overlay of PSC Prediction to Ending PSC*IWD Relationship
For ROI = 4 Subject = 11
Signal Change
4
3
2
1
0
-1
-2
-3
-4
0.02 0.04 0.06 0.08 0.1 0.12 0.14 0.16 0.18 0.2 0.22 0.24 0.26 0.28 0.3 0.32 0.34 0.36 0.38 0.4 0.42 0.44 0.46
IWD Value
OriginalSignal
PredictedSignal

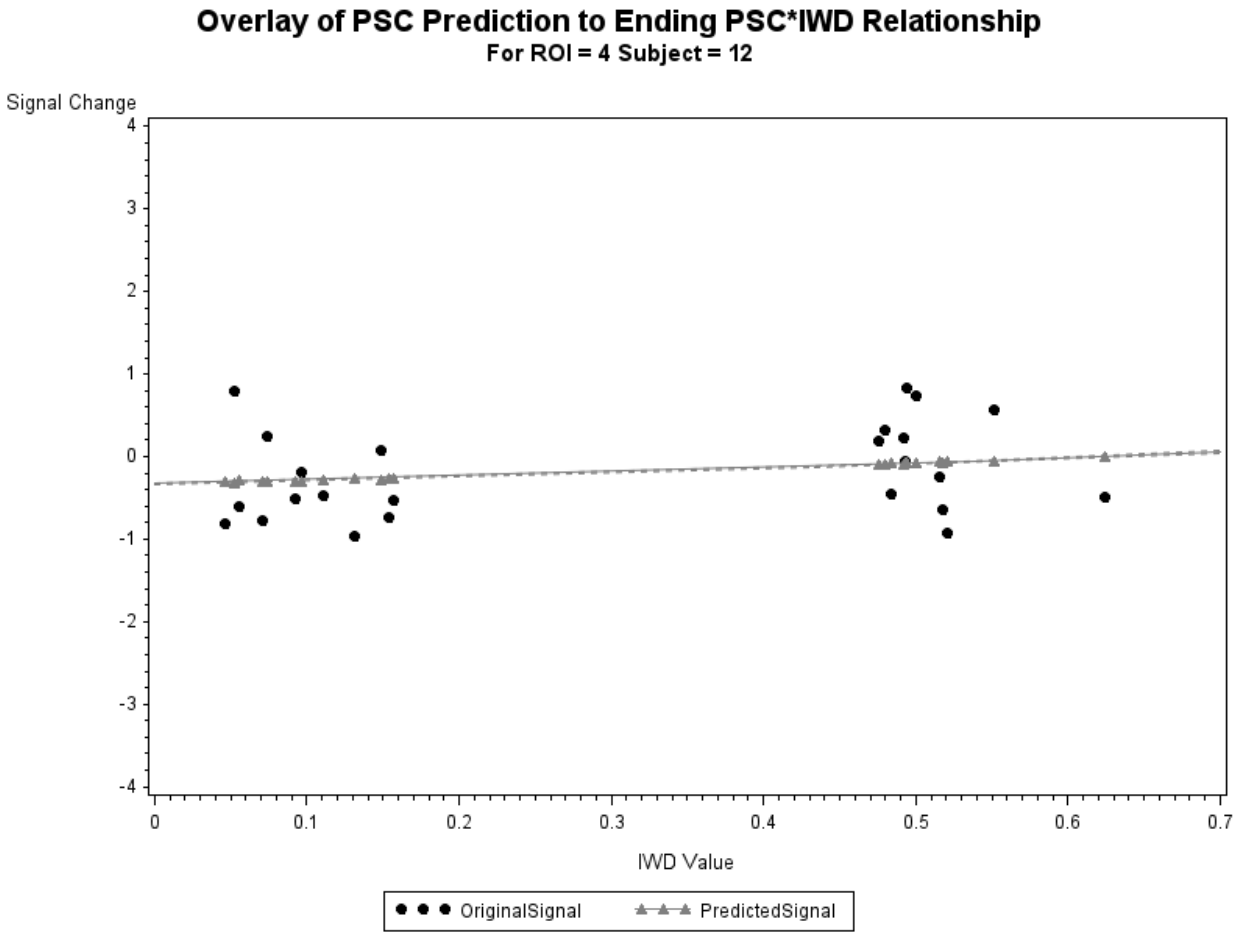
Overlay of PSC Prediction to Ending PSC*IWD Relationship
For ROI = 4 Subject = 12
Signal Change
4
3
2
1
0
-1
-2
-3
-4
0
0.1
0.2
0.3
0.4
0.5
0.6
0.7
IWD Value
OriginalSignal
PredictedSignal

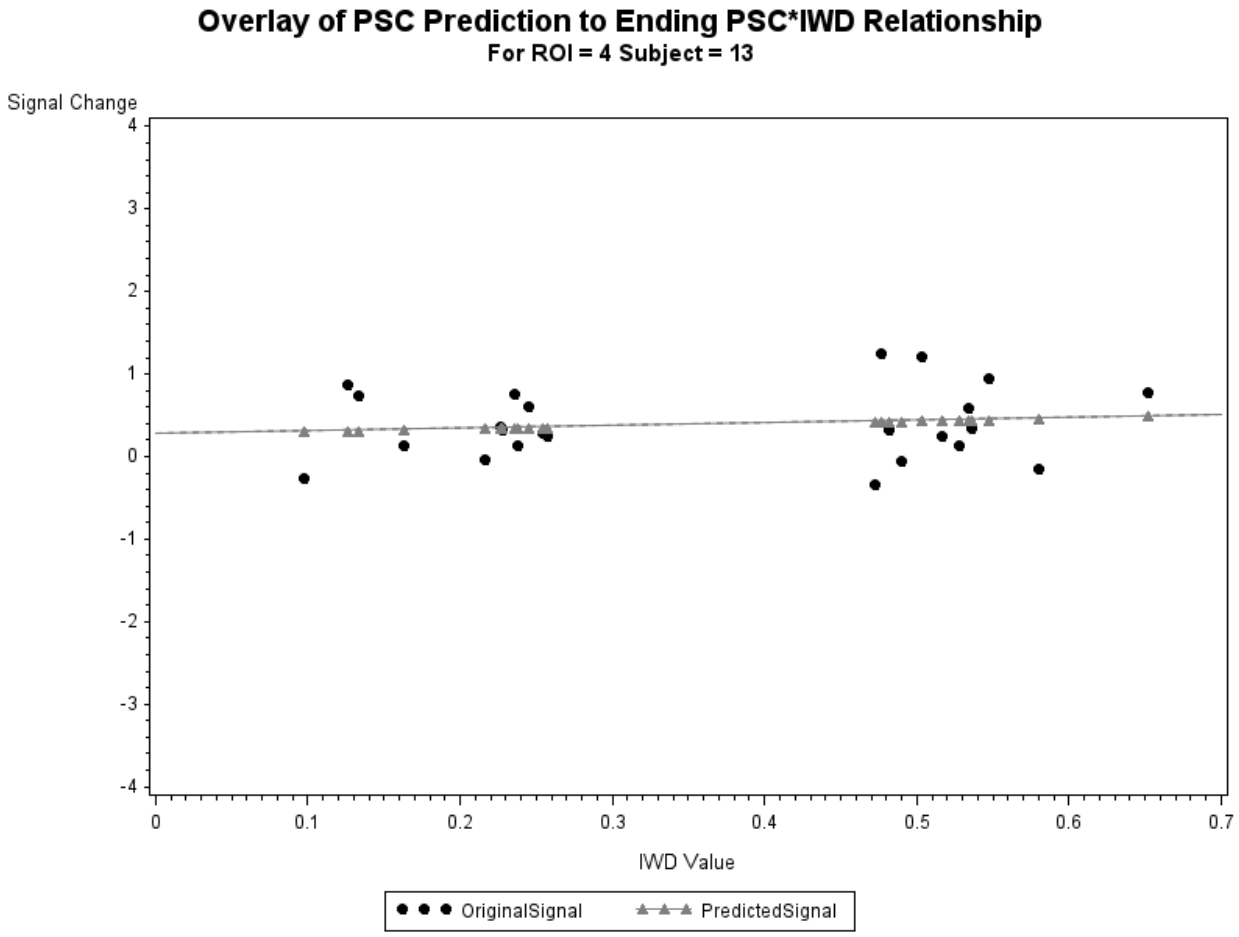
Overlay of PSC Prediction to Ending PSC*IWD Relationship
For ROI = 4 Subject = 13
Signal Change
4
3
2
1
0
-1
-2
-3
-4
0
0.1
0.2
0.3
0.4
0.5
0.6
0.7
IWD Value
OriginalSignal
PredictedSignal

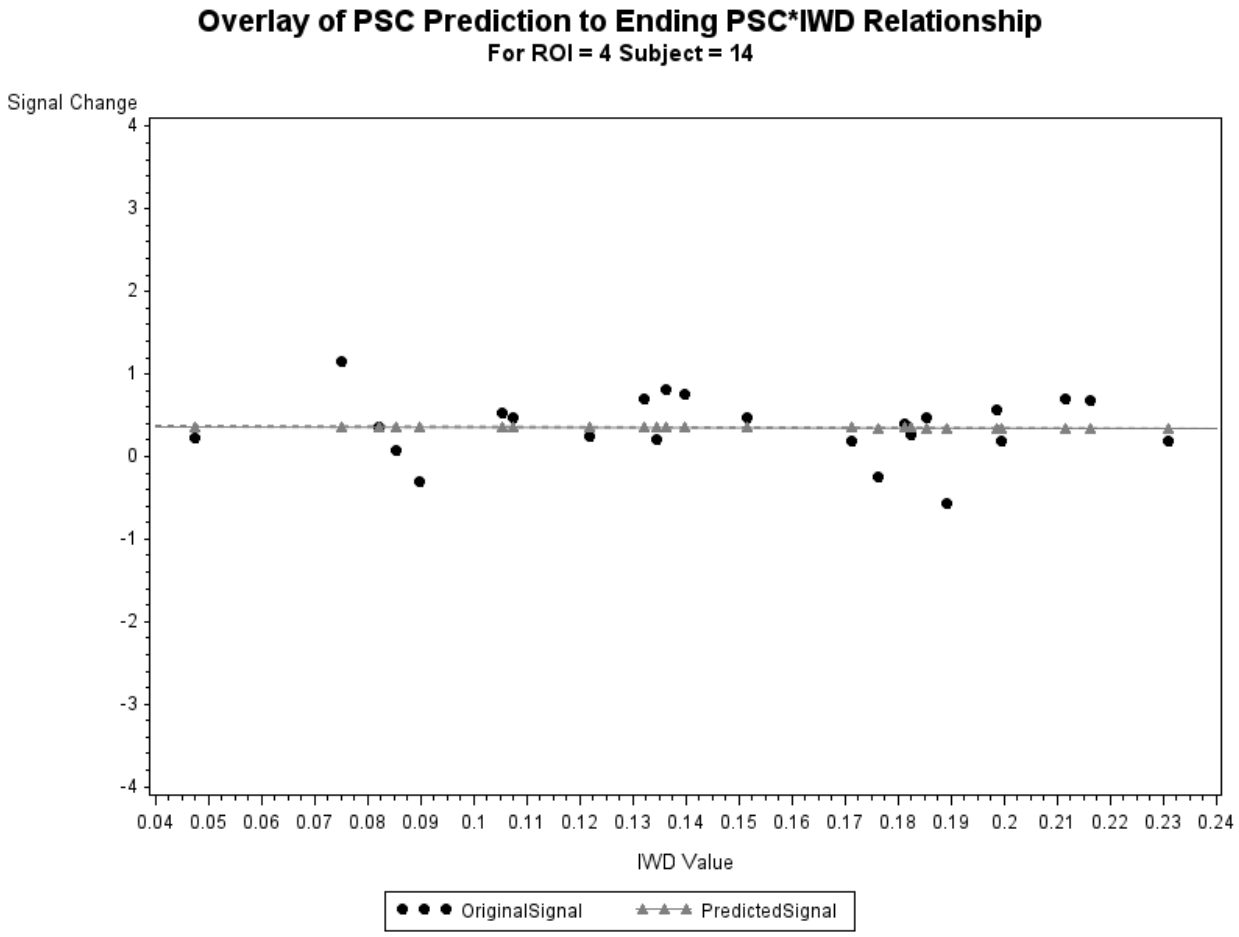
Overlay of PSC Prediction to Ending PSC*IWD Relationship
For ROI = 4 Subject = 14
Signal Change
4
3
2
1
0
-1
-2
-3
-4
0.04 0.05 0.06 0.07 0.08 0.09 0.1 0.11 0.12 0.13 0.14 0.15 0.16 0.17 0.18 0.19 0.2 0.21 0.22 0.23 0.24
IWD Value
OriginalSignal
PredictedSignal

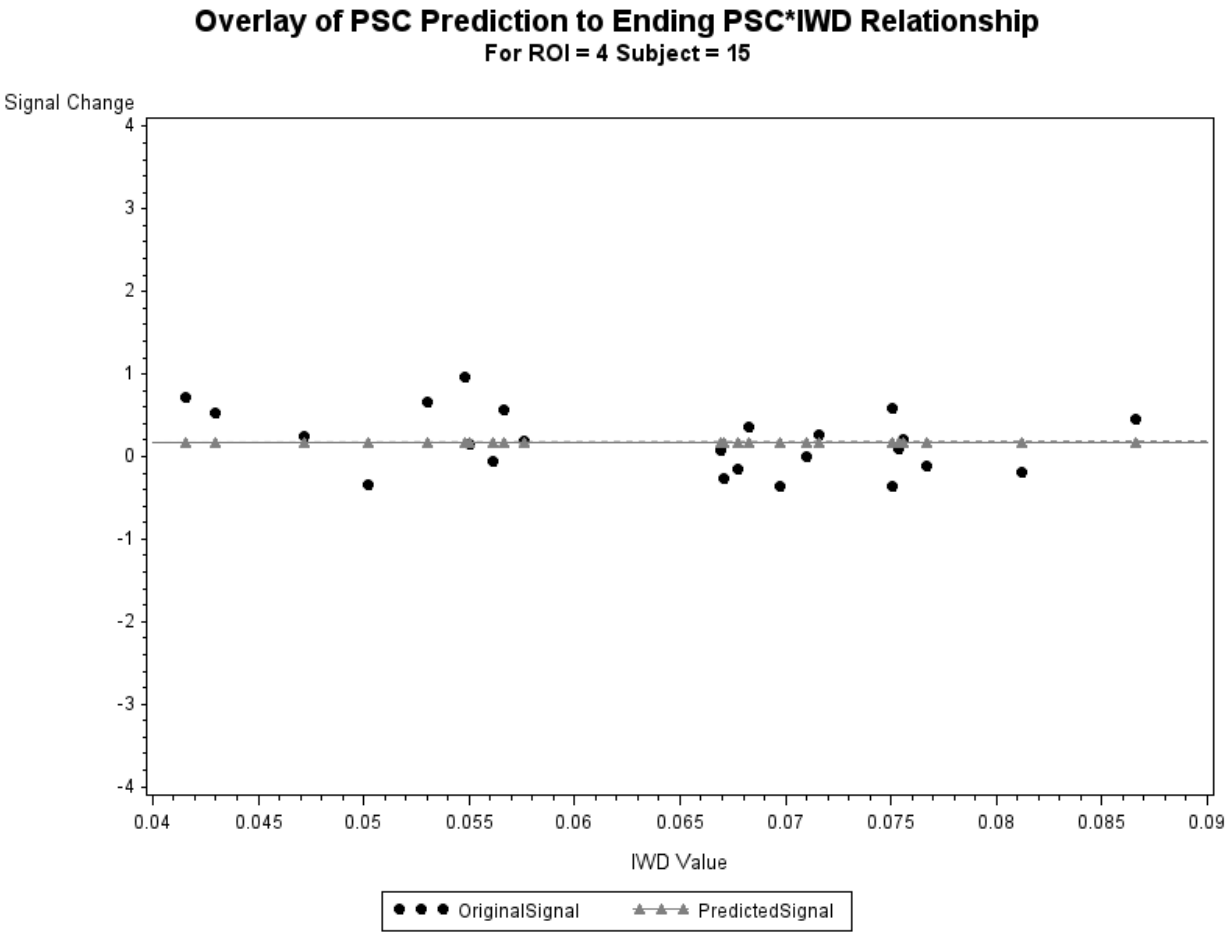
Overlay of PSC Prediction to Ending PSC*IWD Relationship
For ROI = 4 Subject = 15
Signal Change
4
3
2
1
0
-1
-2
-3
-4
0.04
0.045
0.05
0.055
0.06
0.065
0.07
0.075
0.08
0.085
0.09
IWD Value
OriginalSignal
PredictedSignal

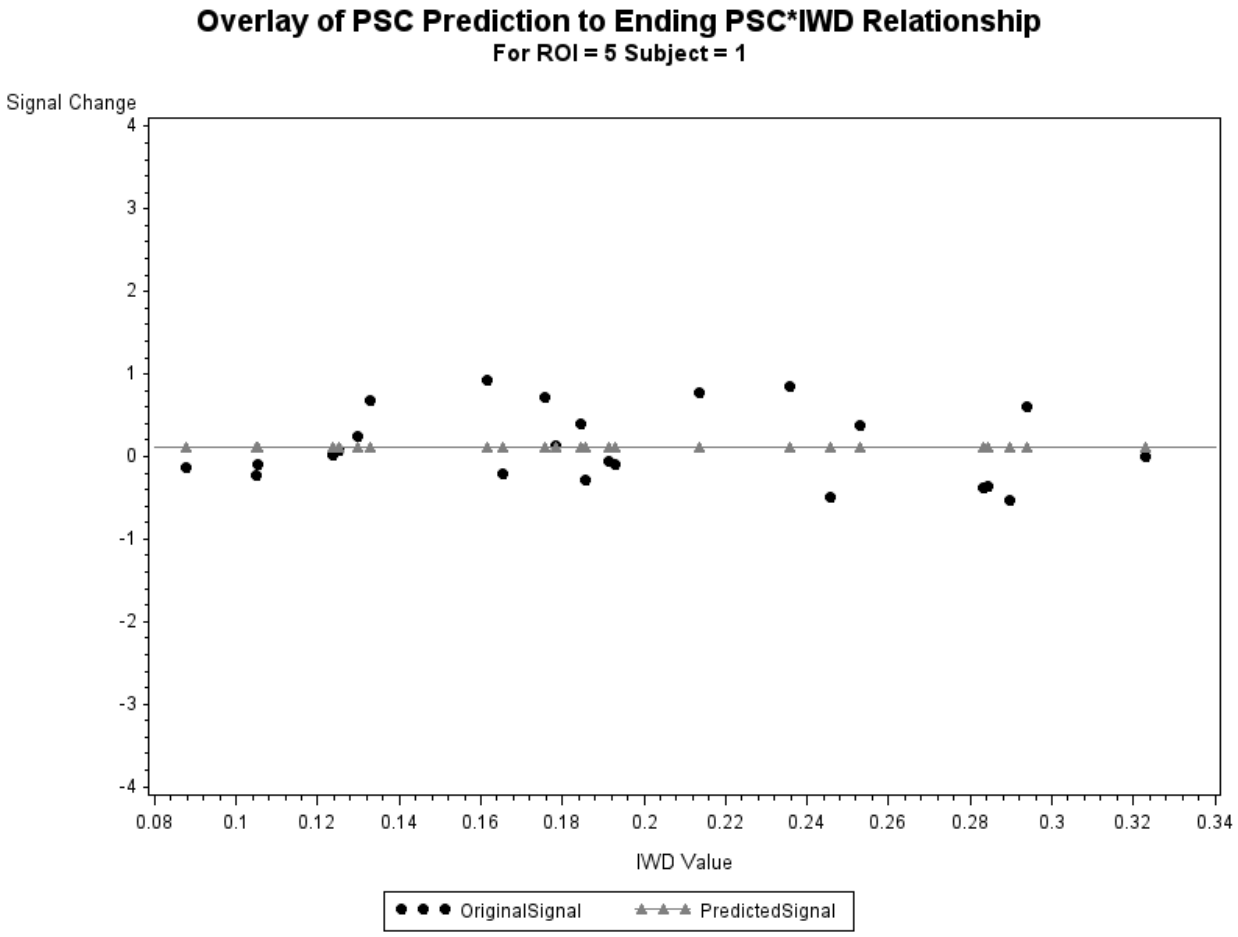
Overlay of PSC Prediction to Ending PSC*IWD Relationship
For ROI = 5 Subject = 1
Signal Change
4
3
2
1
0
-1
-2
-3
-4
0.08
0.1
0.12
0.14
0.16
0.18
0.2
0.22
0.24
0.26
0.28
0.3
0.32
0.34
IWD Value
OriginalSignal
PredictedSignal

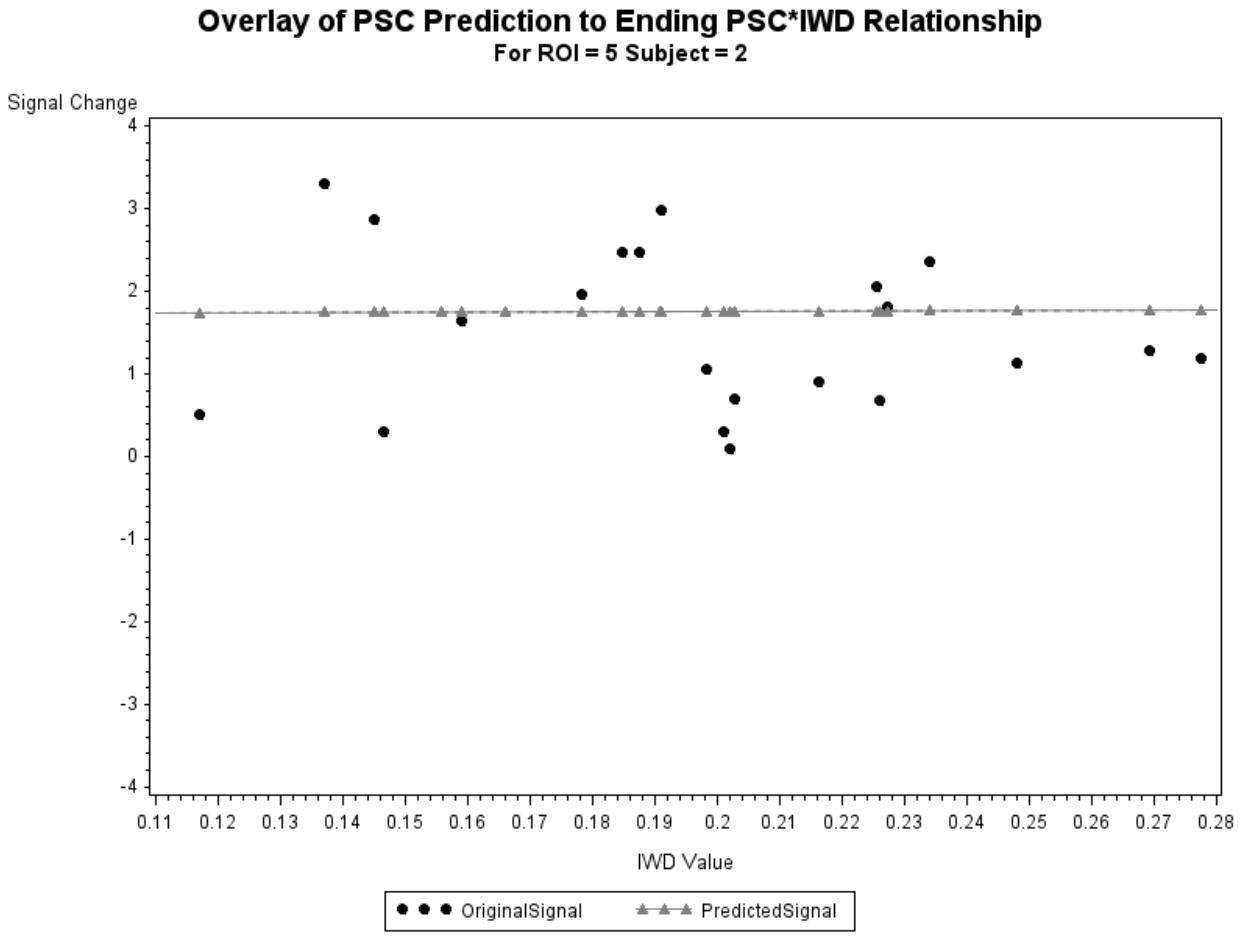
Overlay of PSC Prediction to Ending PSC*IWD Relationship
For ROI = 5 Subject = 2
Signal Change
4
3
2
1
0
-1
-2
-3
-4
0.11
0.12
0.13
0.14
0.15
0.16
0.17
0.18
0.19
0.2
0.21
0.22
0.23
0.24
0.25
0.26
0.27
0.28
IWD Value
OriginalSignal
PredictedSignal

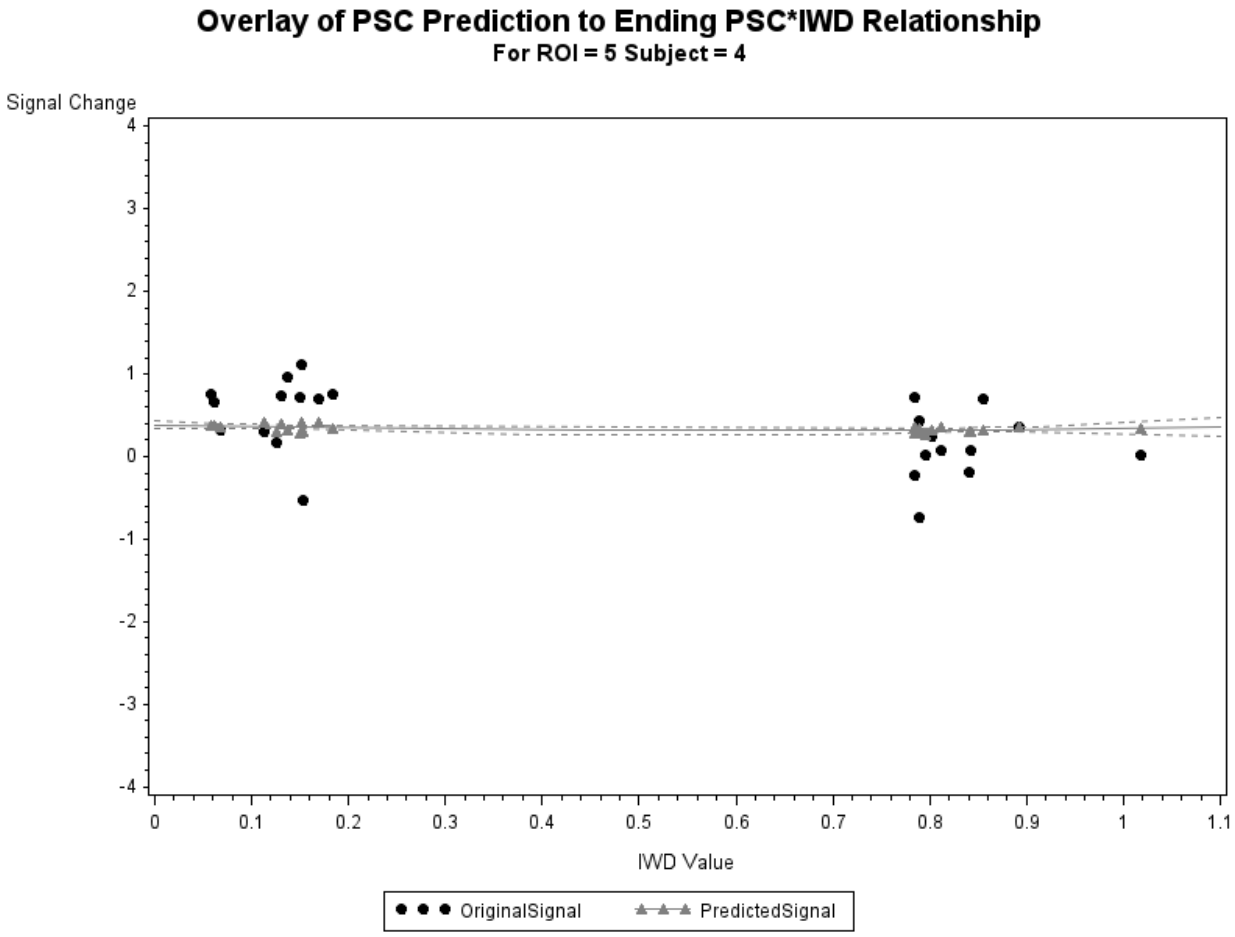
Overlay of PSC Prediction to Ending PSC*IWD Relationship
For ROI = 5 Subject = 4
Signal Change
4
3
2
1
0
-1
-2
-3
-4
0
0.1
0.2
0.3
0.4
0.5
0.6
0.7
0.8
0.9
1
1.1
IWD Value
OriginalSignal
PredictedSignal

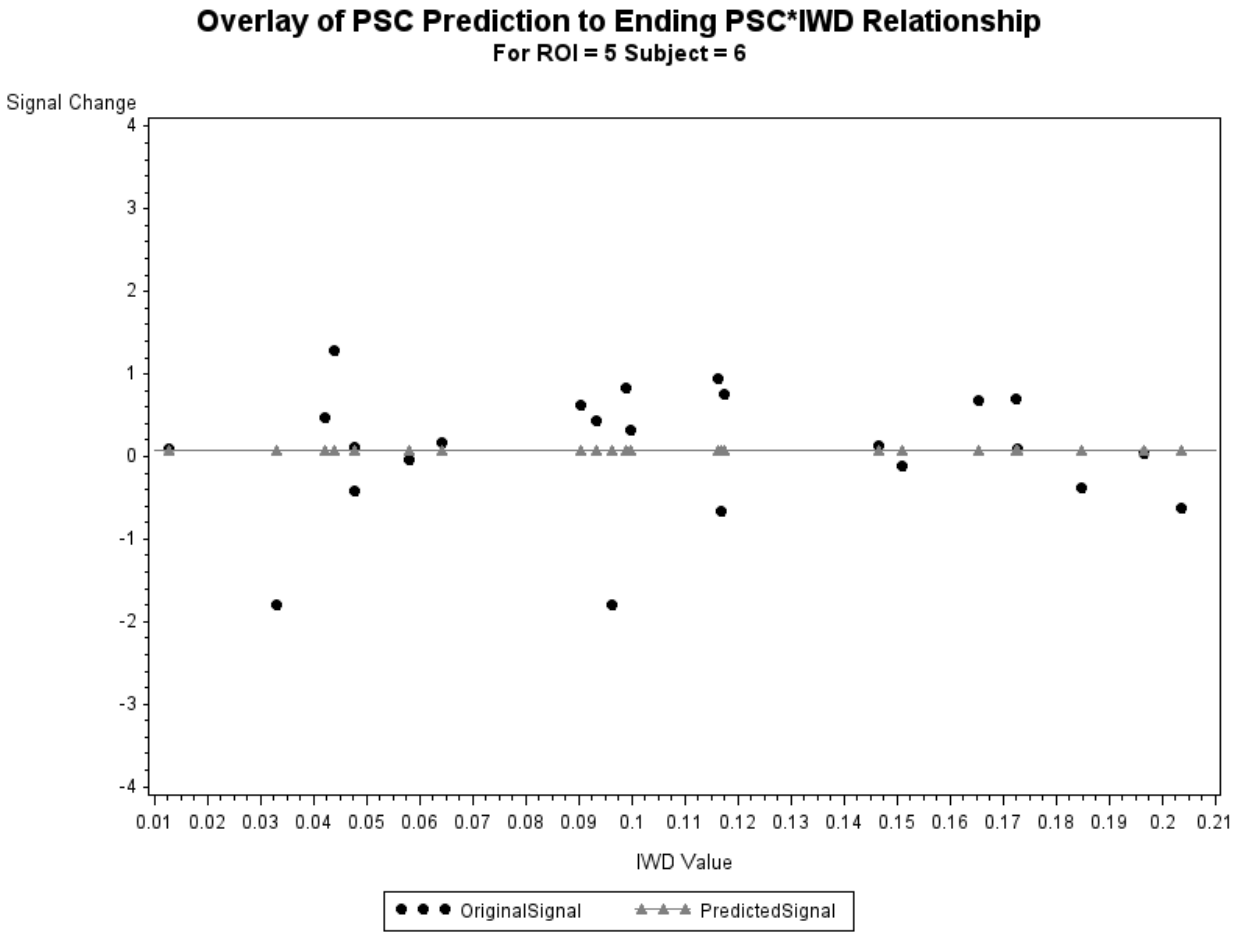
Overlay of PSC Prediction to Ending PSC*IWD Relationship
For ROI = 5 Subject = 6
Signal Change
4
3
2
1
0
-1
-2
-3
-4
0.01 0.02 0.03 0.04 0.05 0.06 0.07 0.08 0.09 0.1 0.11 0.12 0.13 0.14 0.15 0.16 0.17 0.18 0.19 0.2 0.21
IWD Value
OriginalSignal
PredictedSignal

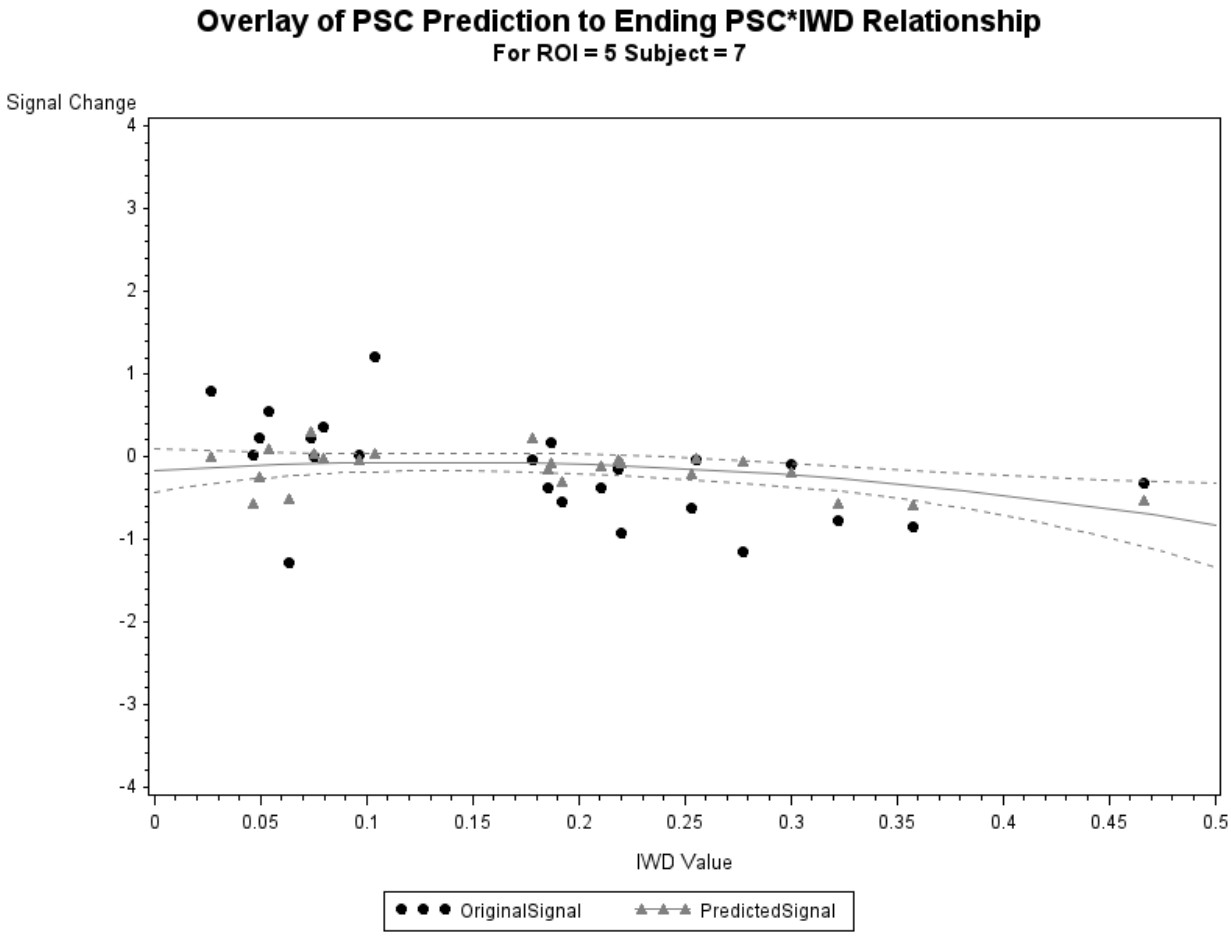
Overlay of PSC Prediction to Ending PSC*IWD Relationship
For ROI = 5 Subject = 7
Signal Change
4
3
2
1
0
-1
-2
-3
-4
0
0.05
0.1
0.15
0.2
0.25
0.3
0.35
0.4
0.45
0.5
IWD Value
OriginalSignal
PredictedSignal

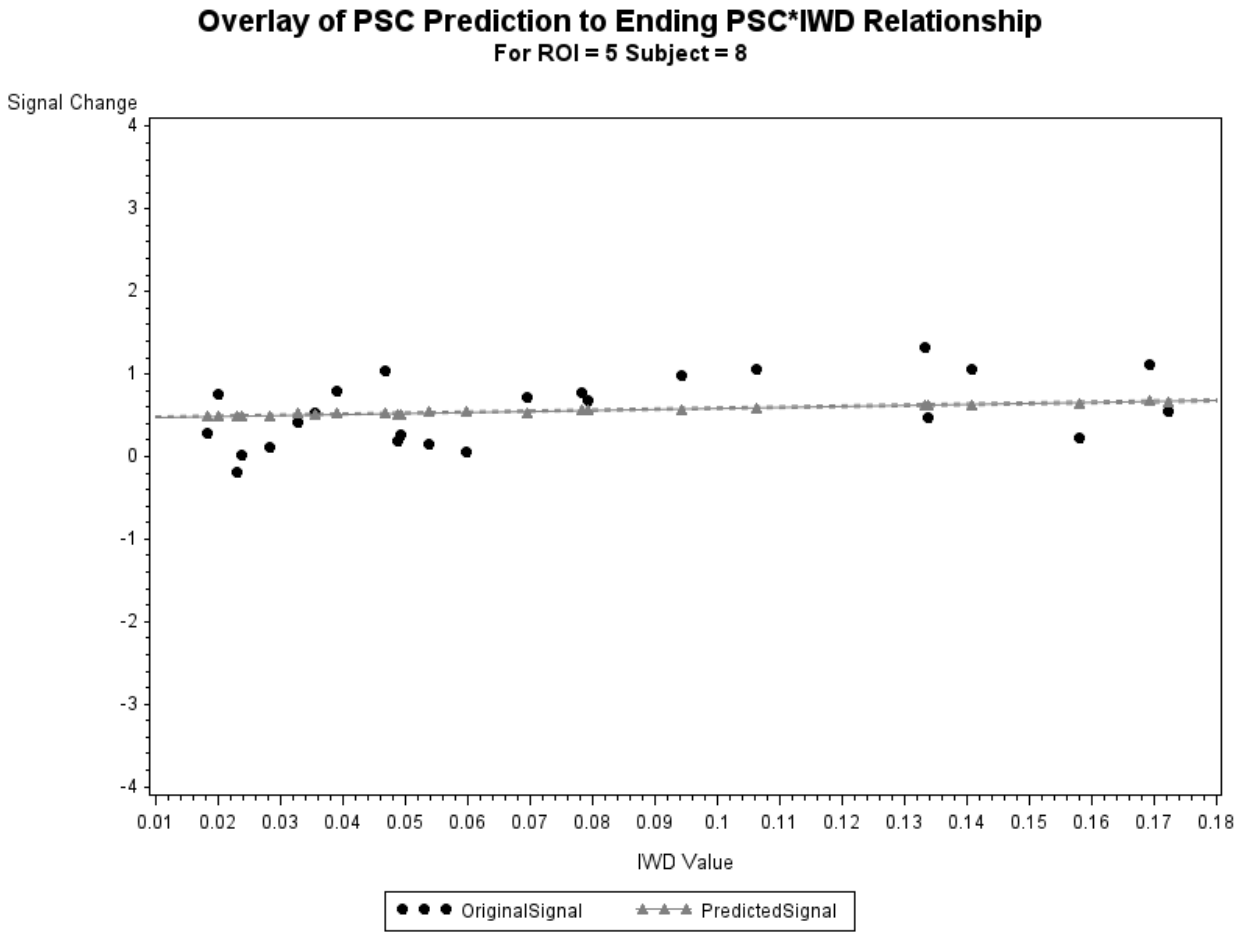
Overlay of PSC Prediction to Ending PSC*IWD Relationship
For ROI = 5 Subject = 8
Signal Change
4
3
2
1
0
-1
-2
-3
-4
0.01
0.02
0.03
0.04
0.05
0.06
0.07
0.08
0.09
0.1
0.11
0.12
0.13
0.14
0.15
0.16
0.17
0.18
IWD Value
OriginalSignal
PredictedSignal

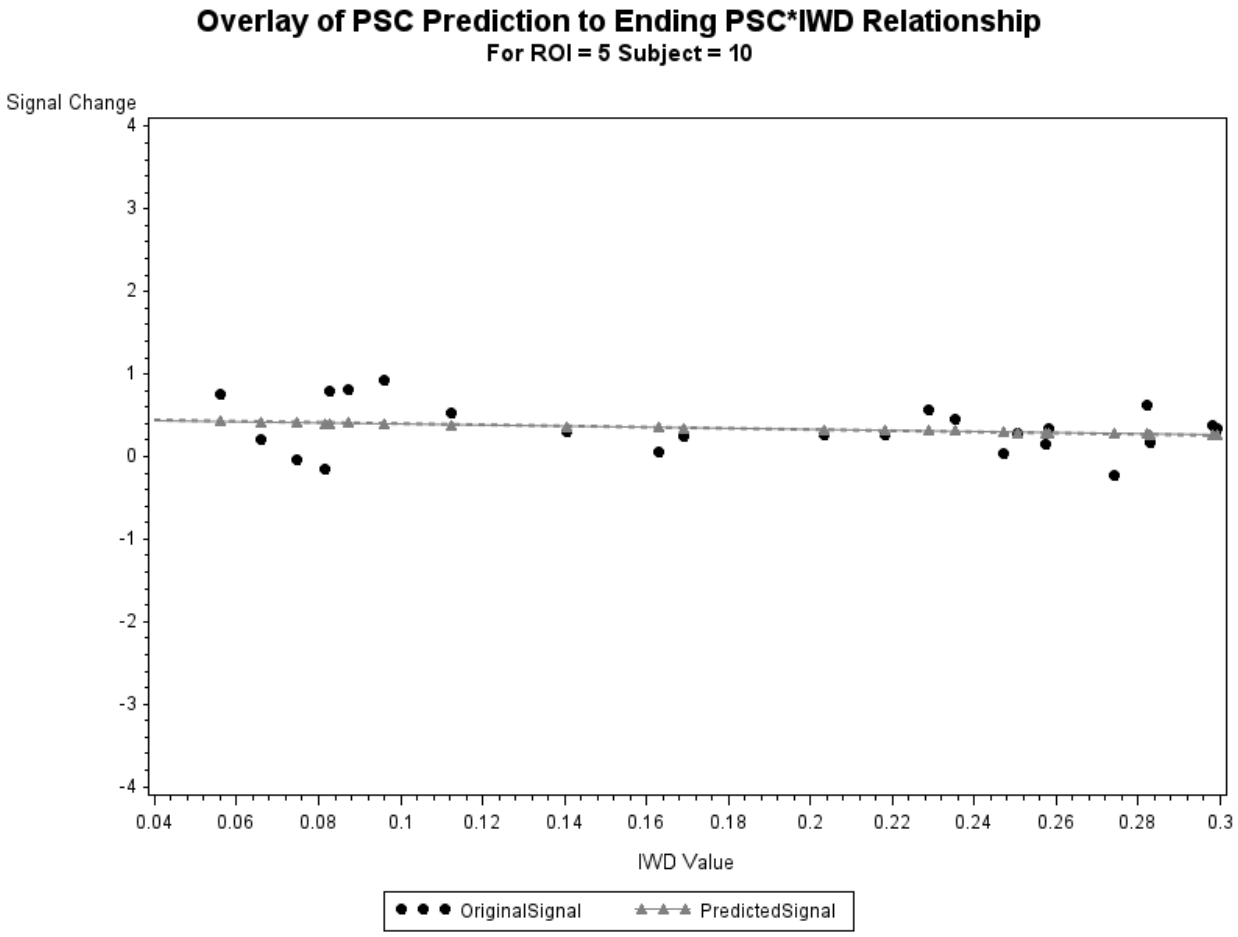
Overlay of PSC Prediction to Ending PSC*IWD Relationship
For ROI = 5 Subject = 10
Signal Change
4
3
2
1
0
-1
-2
-3
-4
0.04
0.06
0.08
0.1
0.12
0.14
0.16
0.18
0.2
0.22
0.24
0.26
0.28
0.3
IWD Value
OriginalSignal
PredictedSignal

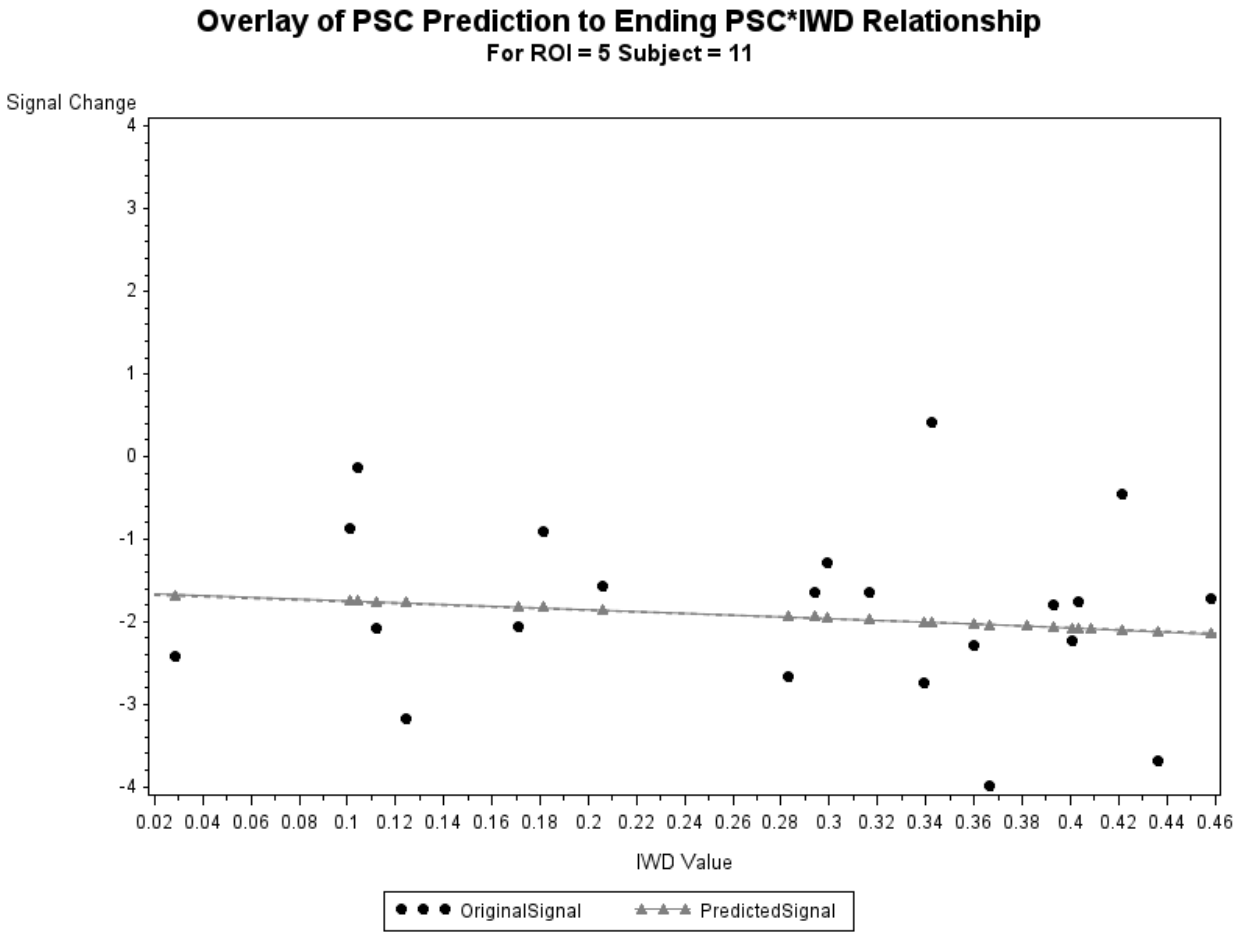
Overlay of PSC Prediction to Ending PSC*IWD Relationship
For ROI = 5 Subject = 11
Signal Change
4
3
2
1
0
-1
-2
-3
-4
0.02 0.04 0.06 0.08 0.1 0.12 0.14 0.16 0.18 0.2 0.22 0.24 0.26 0.28 0.3 0.32 0.34 0.36 0.38 0.4 0.42 0.44 0.46
IWD Value
OriginalSignal
PredictedSignal

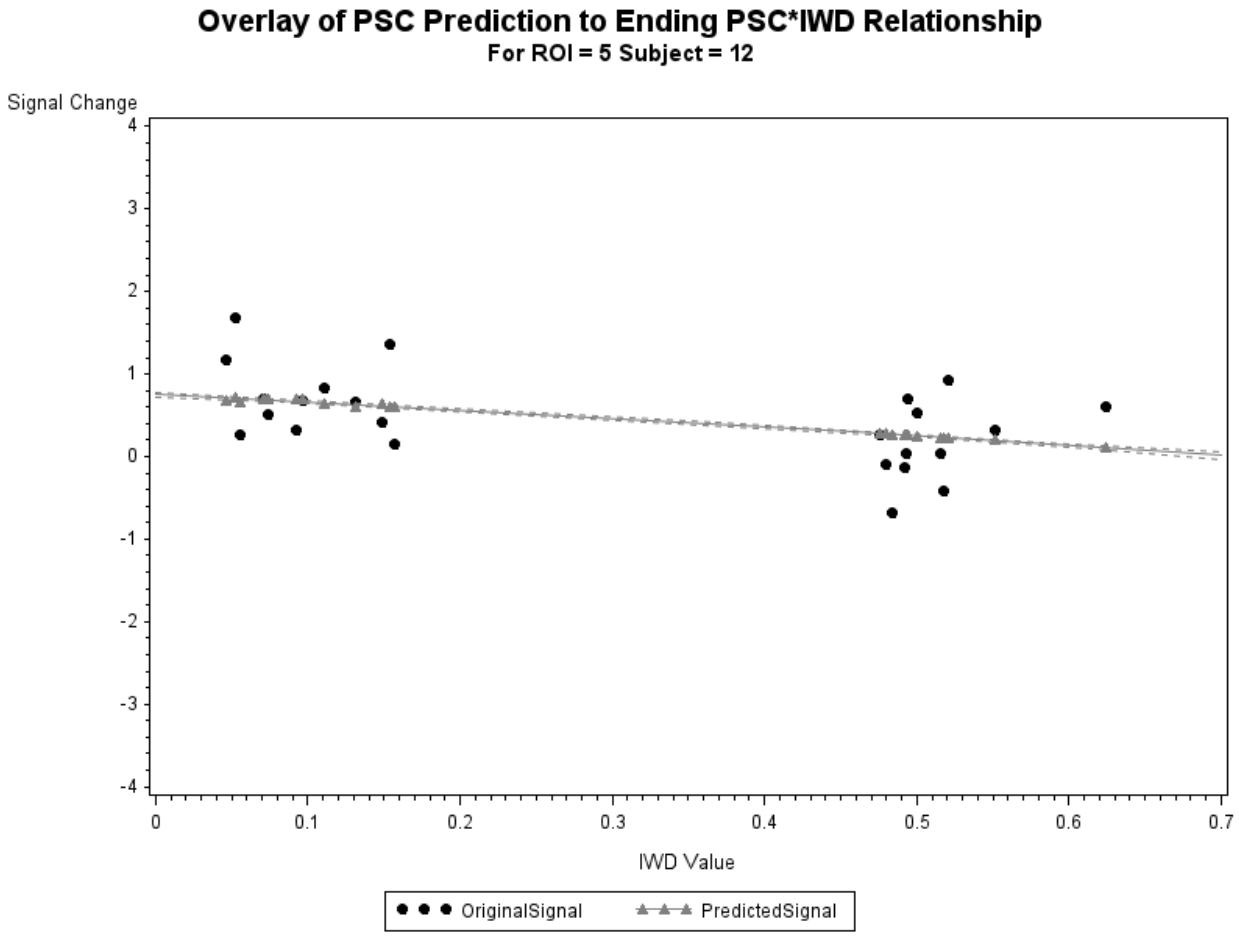
Overlay of PSC Prediction to Ending PSC*IWD Relationship
For ROI = 5 Subject = 12
Signal Change
4
3
2
1
0
-1
-2
-3
-4
0
0.1
0.2
0.3
0.4
0.5
0.6
0.7
IWD Value
OriginalSignal
PredictedSignal

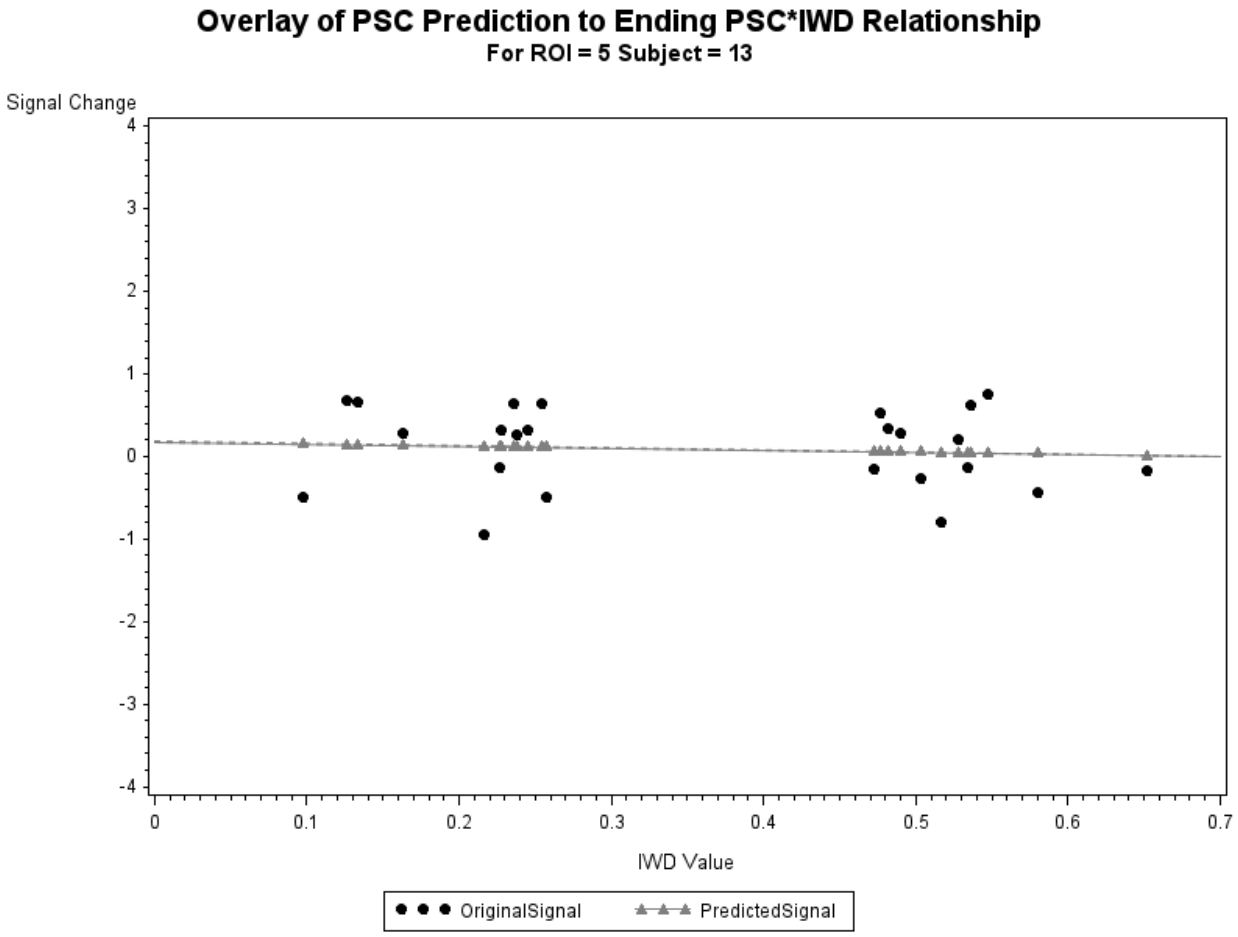
Overlay of PSC Prediction to Ending PSC*IWD Relationship
For ROI = 5 Subject = 13
Signal Change
4
3
2
1
0
-1
-2
-3
-4
0
0.1
0.2
0.3
0.4
0.5
0.6
0.7
IWD Value
OriginalSignal
PredictedSignal

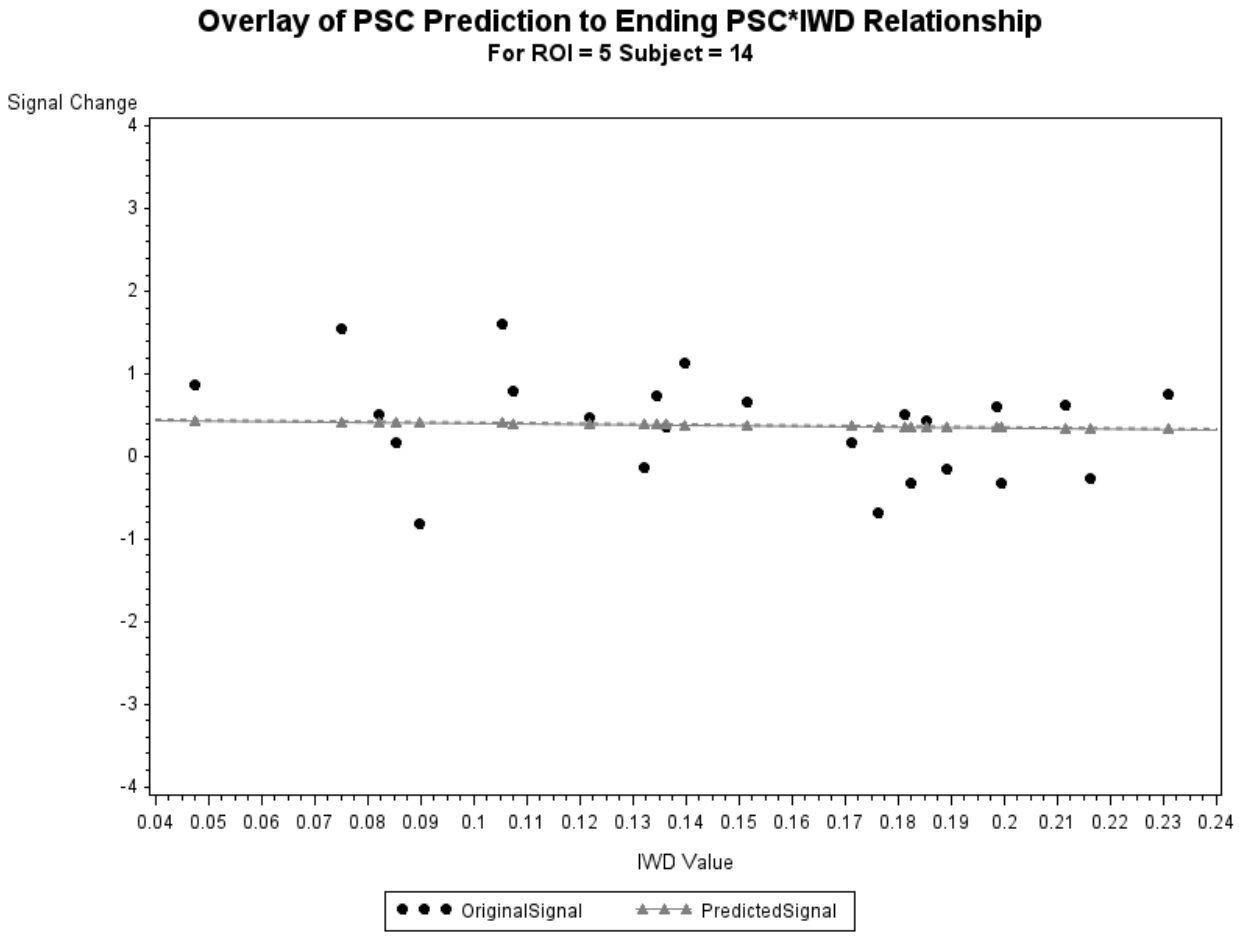
Overlay of PSC Prediction to Ending PSC*IWD Relationship
For ROI = 5 Subject = 14
Signal Change
4
3
2
1
0
-1
-2
-3
-4
0.04 0.05 0.06 0.07 0.08 0.09 0.1 0.11 0.12 0.13 0.14 0.15 0.16 0.17 0.18 0.19 0.2 0.21 0.22 0.23 0.24
IWD Value
OriginalSignal
PredictedSignal

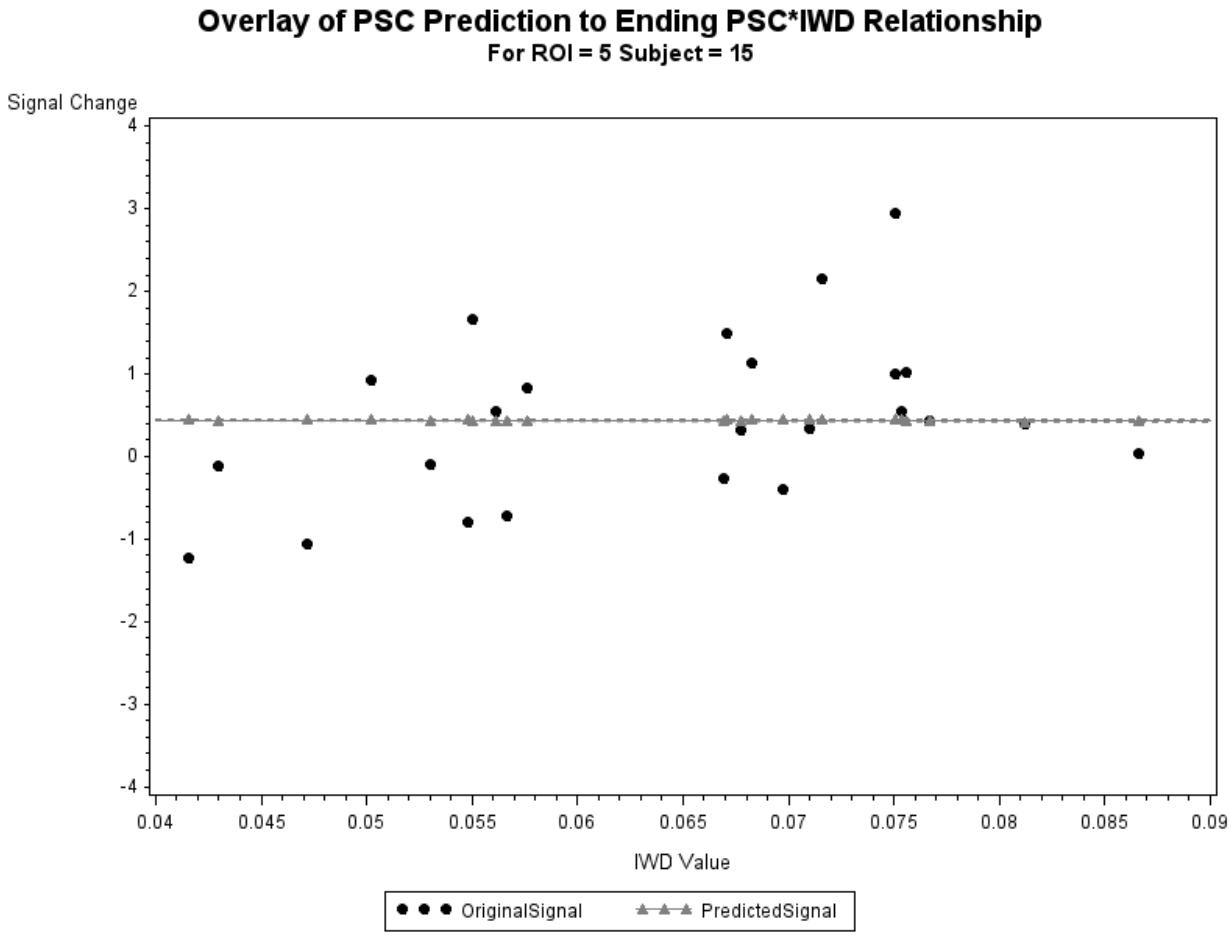
Overlay of PSC Prediction to Ending PSC*IWD Relationship
For ROI = 5 Subject = 15
Signal Change
4
3
2
1
0
-1
-2
-3
-4
0.04
0.045
0.05
0.055
0.06
0.065
0.07
0.075
0.08
0.085
0.09
IWD Value
OriginalSignal
PredictedSignal

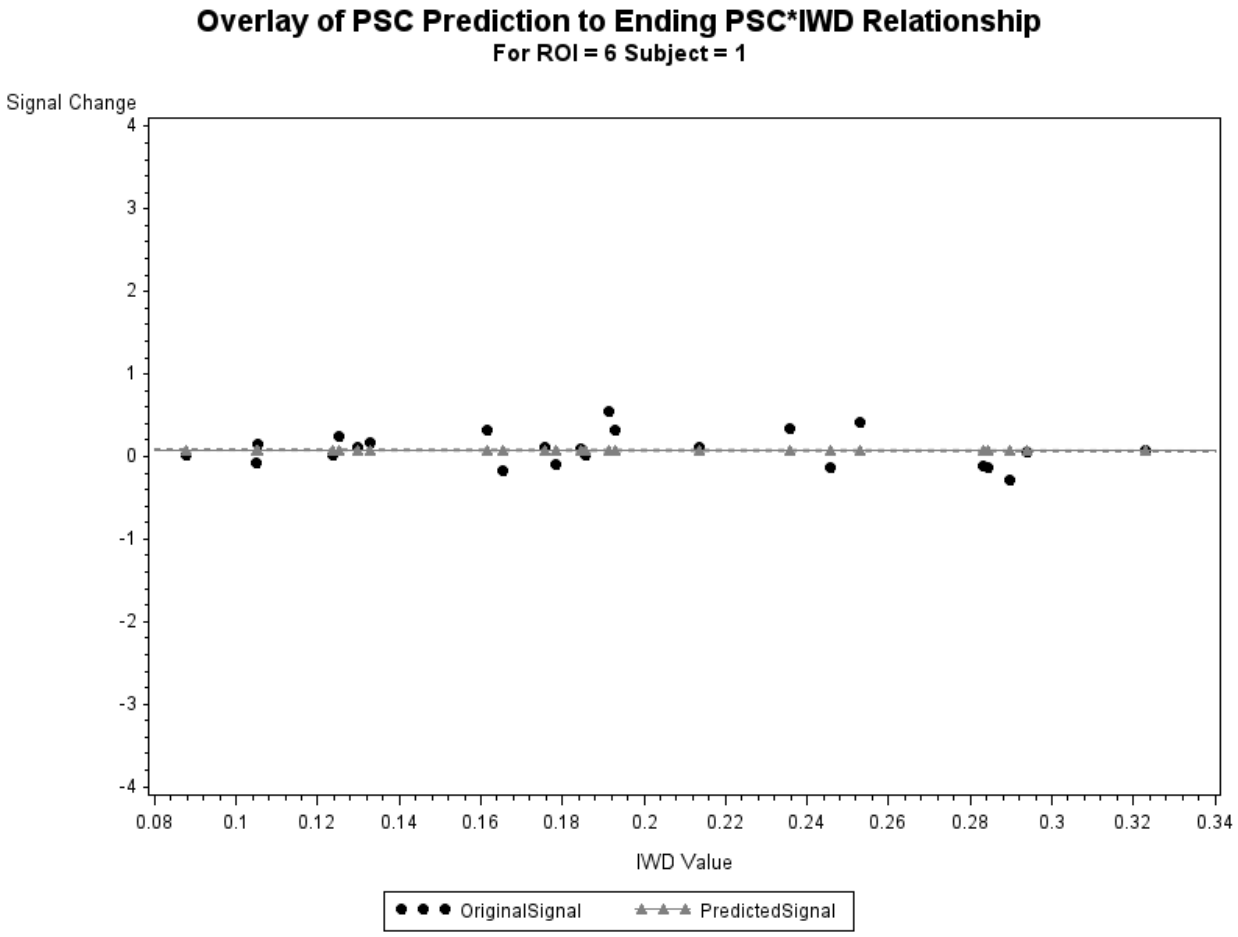
Overlay of PSC Prediction to Ending PSC*IWD Relationship
For ROI = 6 Subject = 1
Signal Change
4
3
2
1
0
-1
-2
-3
-4
0.08
0.1
0.12
0.14
0.16
0.18
0.2
0.22
0.24
0.26
0.28
0.3
0.32
0.34
IWD Value
OriginalSignal
PredictedSignal

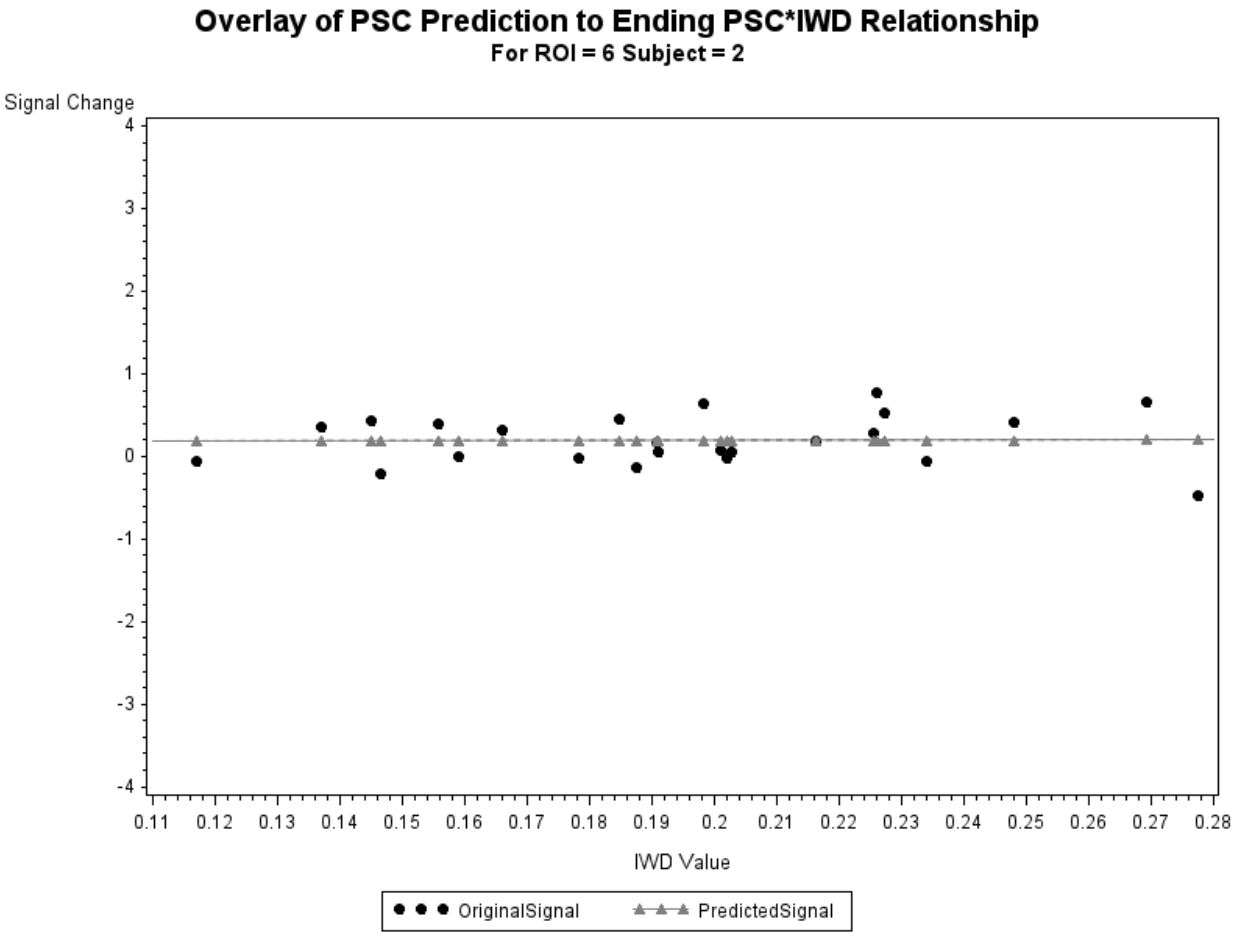
Overlay of PSC Prediction to Ending PSC*IWD Relationship
For ROI = 6 Subject = 2
Signal Change
4
3
2
1
0
-1
-2
-3
-4
0.11
0.12
0.13
0.14
0.15
0.16
0.17
0.18
0.19
0.2
0.21
0.22
0.23
0.24
0.25
0.26
0.27
0.28
IWD Value
OriginalSignal
PredictedSignal

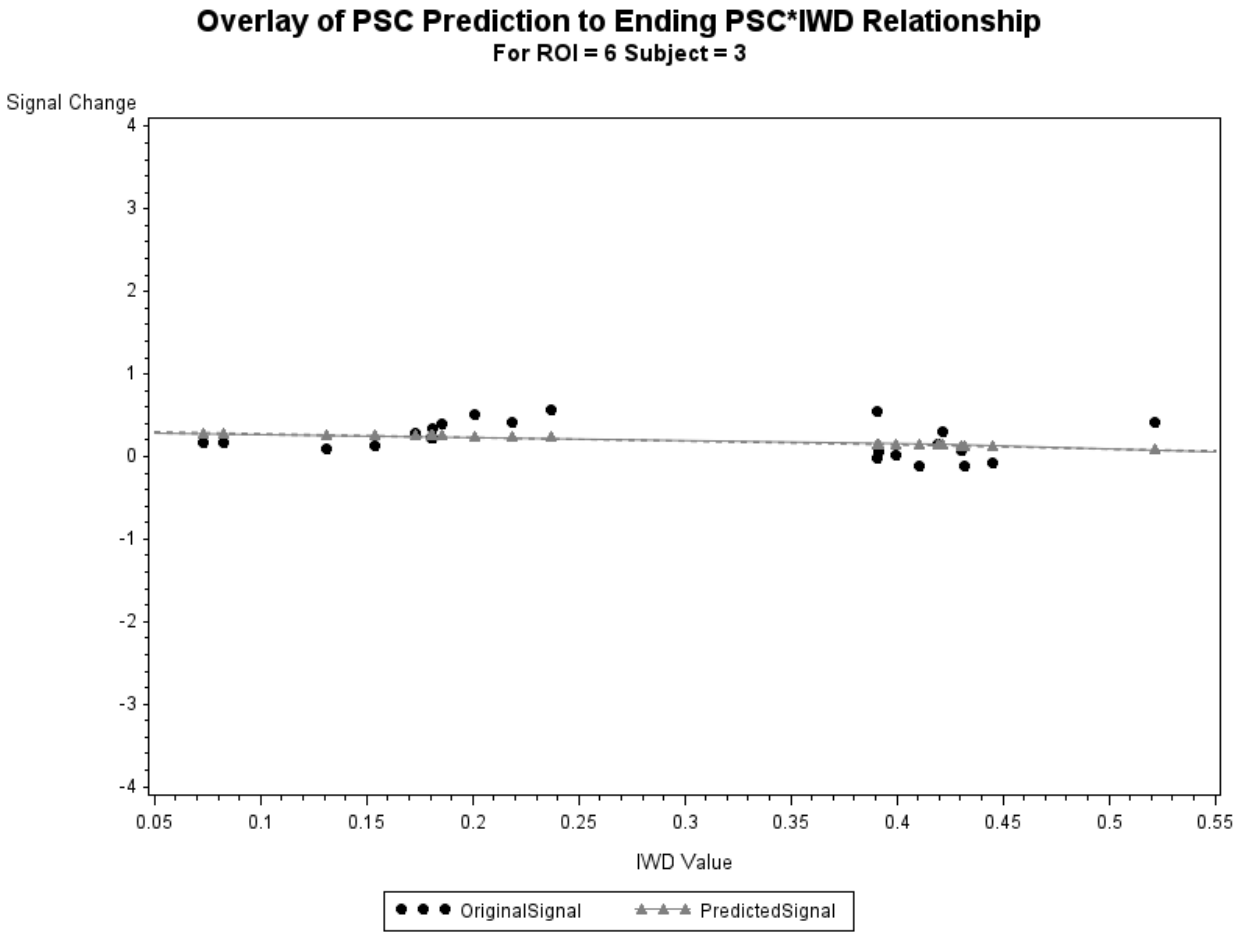
Overlay of PSC Prediction to Ending PSC*IWD Relationship
For ROI = 6 Subject = 3
Signal Change
4
3
2
1
0
-1
-2
-3
-4
0.05
0.1
0.15
0.2
0.25
0.3
0.35
0.4
0.45
0.5
0.55
IWD Value
OriginalSignal
PredictedSignal

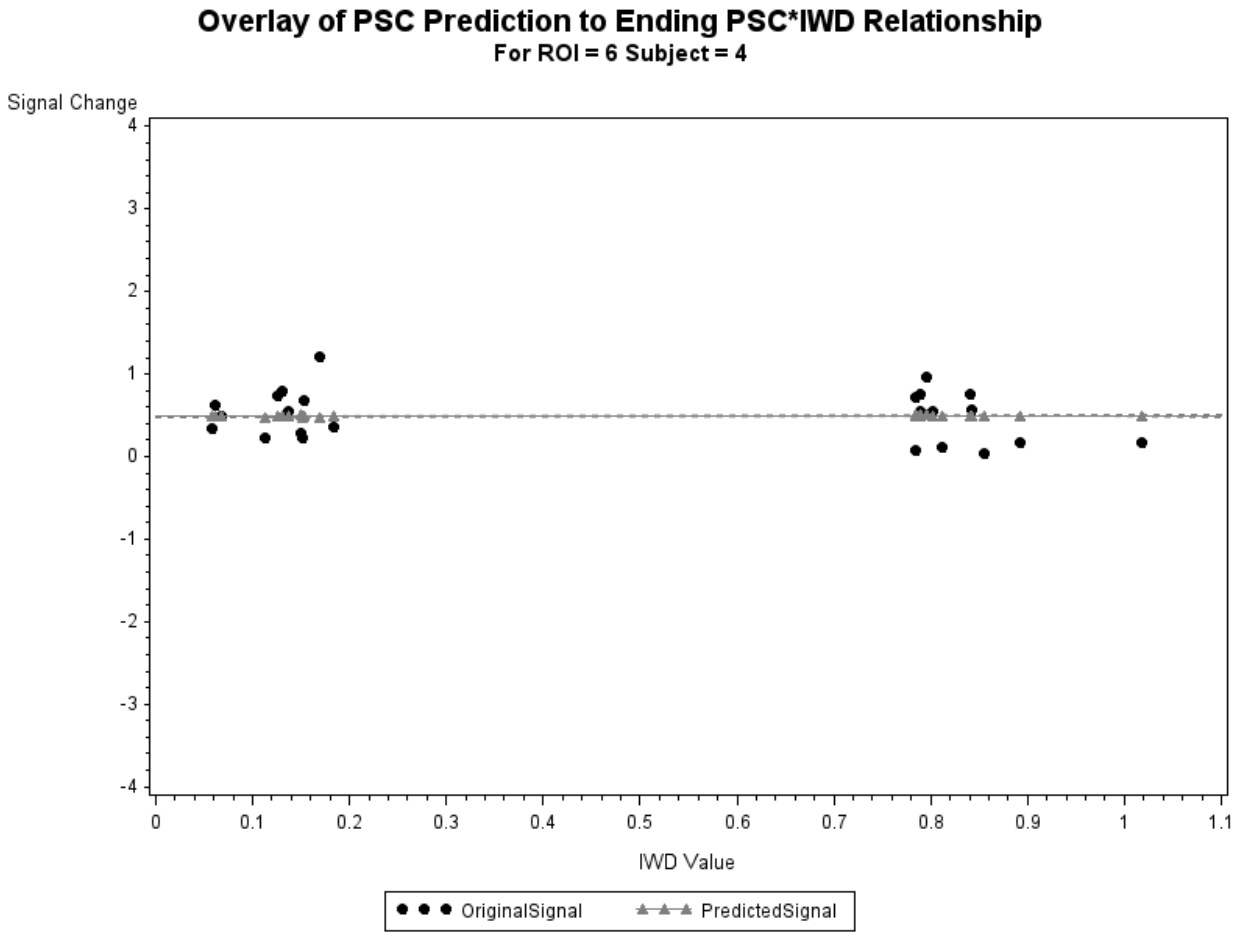
Overlay of PSC Prediction to Ending PSC*IWD Relationship
For ROI = 6 Subject = 4
Signal Change
4
3
2
1
0
-1
-2
-3
-4
0
0.1
0.2
0.3
0.4
0.5
0.6
0.7
0.8
0.9
1
1.1
IWD Value
OriginalSignal
PredictedSignal

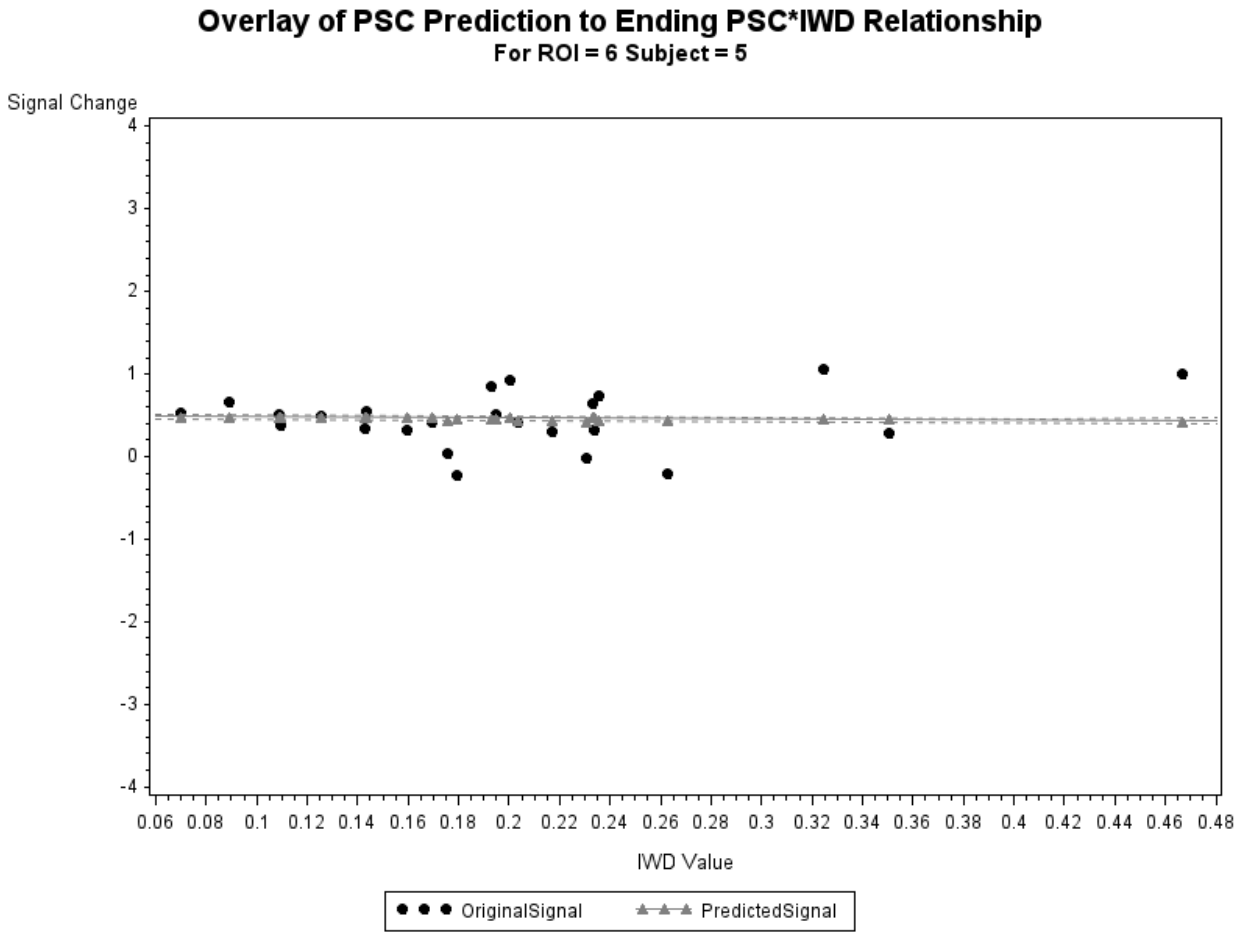
Overlay of PSC Prediction to Ending PSC*IWD Relationship
For ROI = 6 Subject = 5
Signal Change
4
3
2
1
0
-1
-2
-3
-4
0.06 0.08 0.1 0.12 0.14 0.16 0.18 0.2 0.22 0.24 0.26 0.28 0.3 0.32 0.34 0.36 0.38 0.4 0.42 0.44 0.46 0.48
IWD Value
OriginalSignal
PredictedSignal

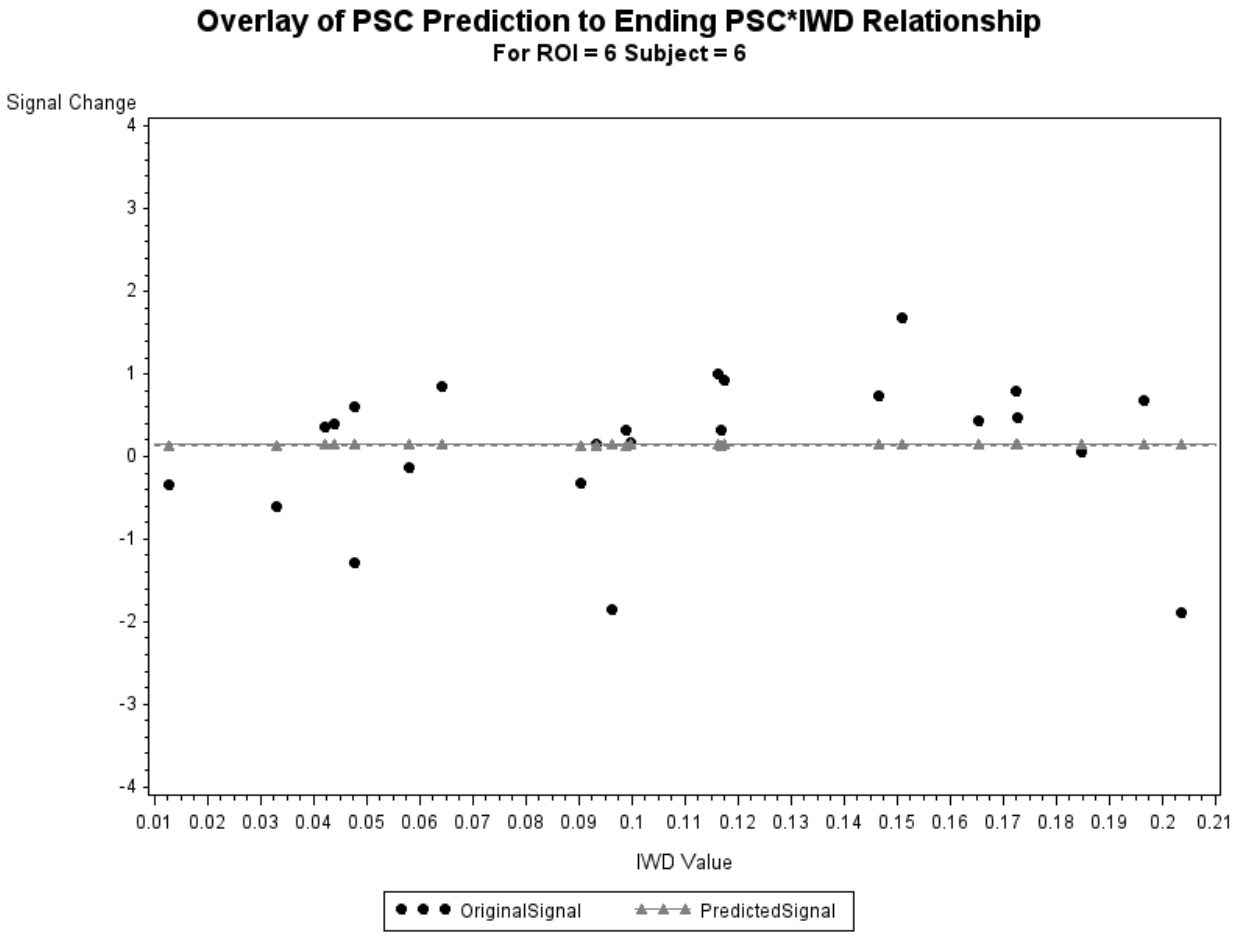
Overlay of PSC Prediction to Ending PSC*IWD Relationship
For ROI = 6 Subject = 6
Signal Change
4
3
2
1
0
-1
-2
-3
-4
0.01 0.02 0.03 0.04 0.05 0.06 0.07 0.08 0.09 0.1 0.11 0.12 0.13 0.14 0.15 0.16 0.17 0.18 0.19 0.2 0.21
IWD Value
OriginalSignal
PredictedSignal

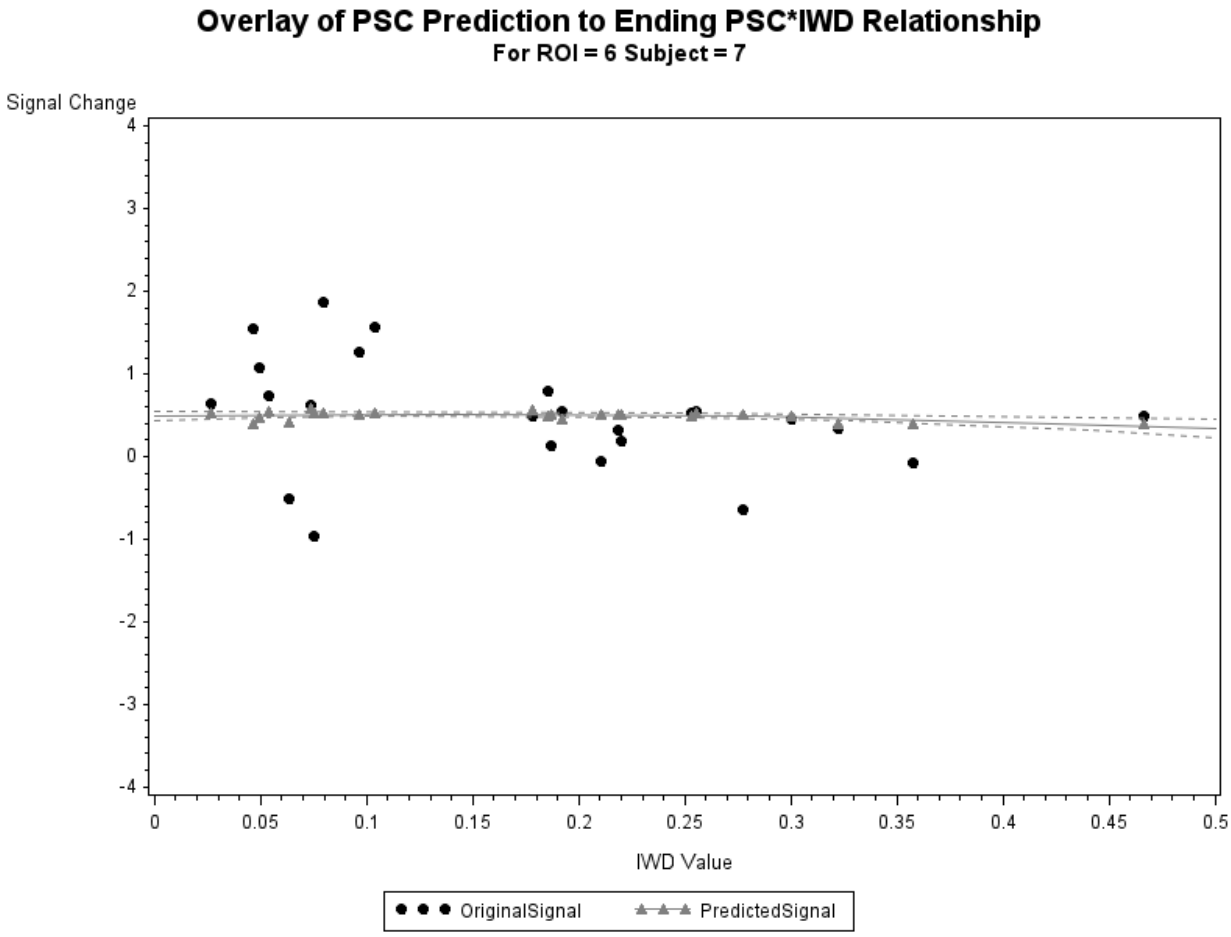
Overlay of PSC Prediction to Ending PSC*IWD Relationship
For ROI = 6 Subject = 7
Signal Change
4
3
2
1
0
-1
-2
-3
-4
0
0.05
0.1
0.15
0.2
0.25
0.3
0.35
0.4
0.45
0.5
IWD Value
OriginalSignal
PredictedSignal

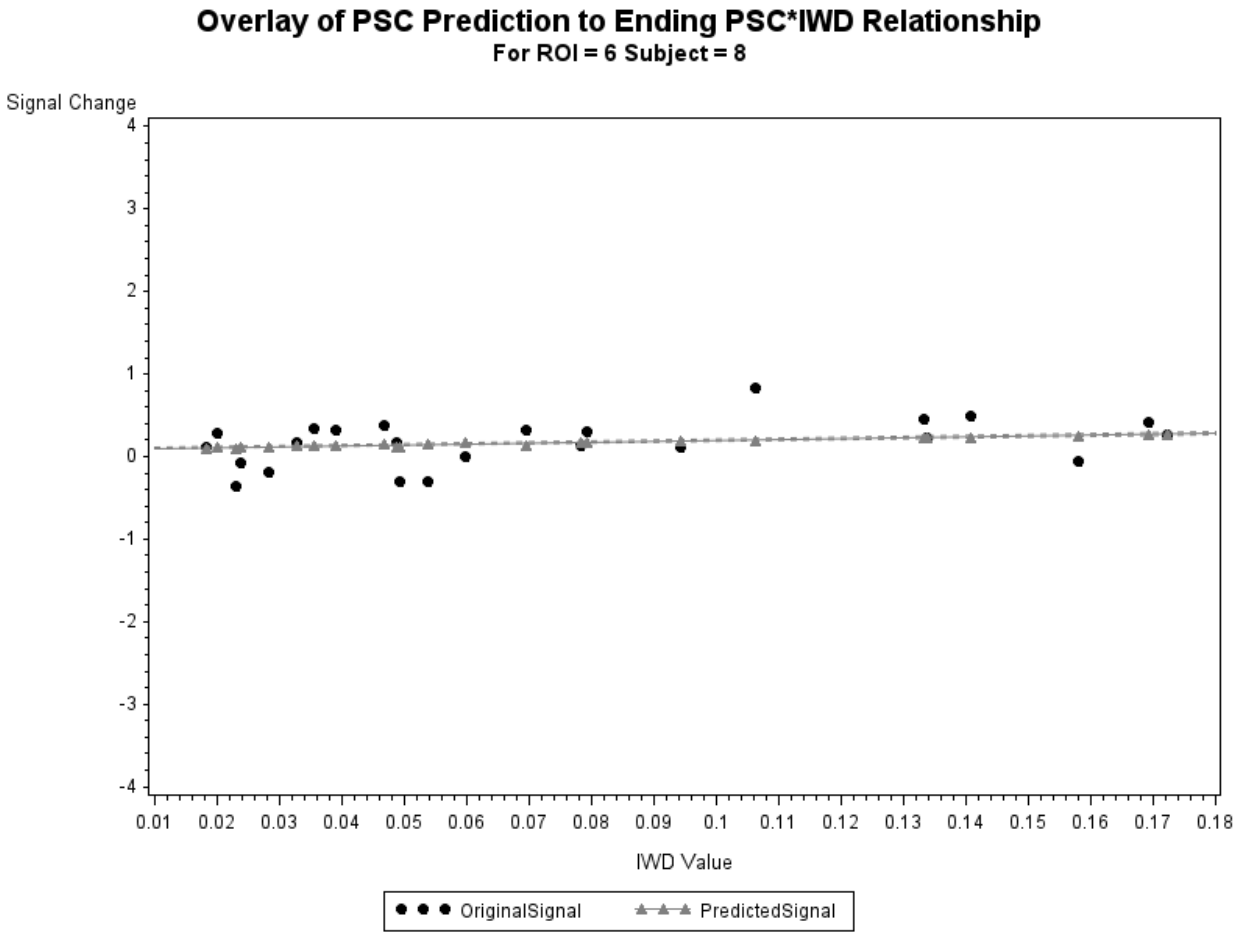
Overlay of PSC Prediction to Ending PSC*IWD Relationship
For ROI = 6 Subject = 8
Signal Change
4
3
2
1
0
-1
-2
-3
-4
0.01
0.02
0.03
0.04
0.05
0.06
0.07
0.08
0.09
0.1
0.11
0.12
0.13
0.14
0.15
0.16
0.17
0.18
IWD Value
OriginalSignal
PredictedSignal

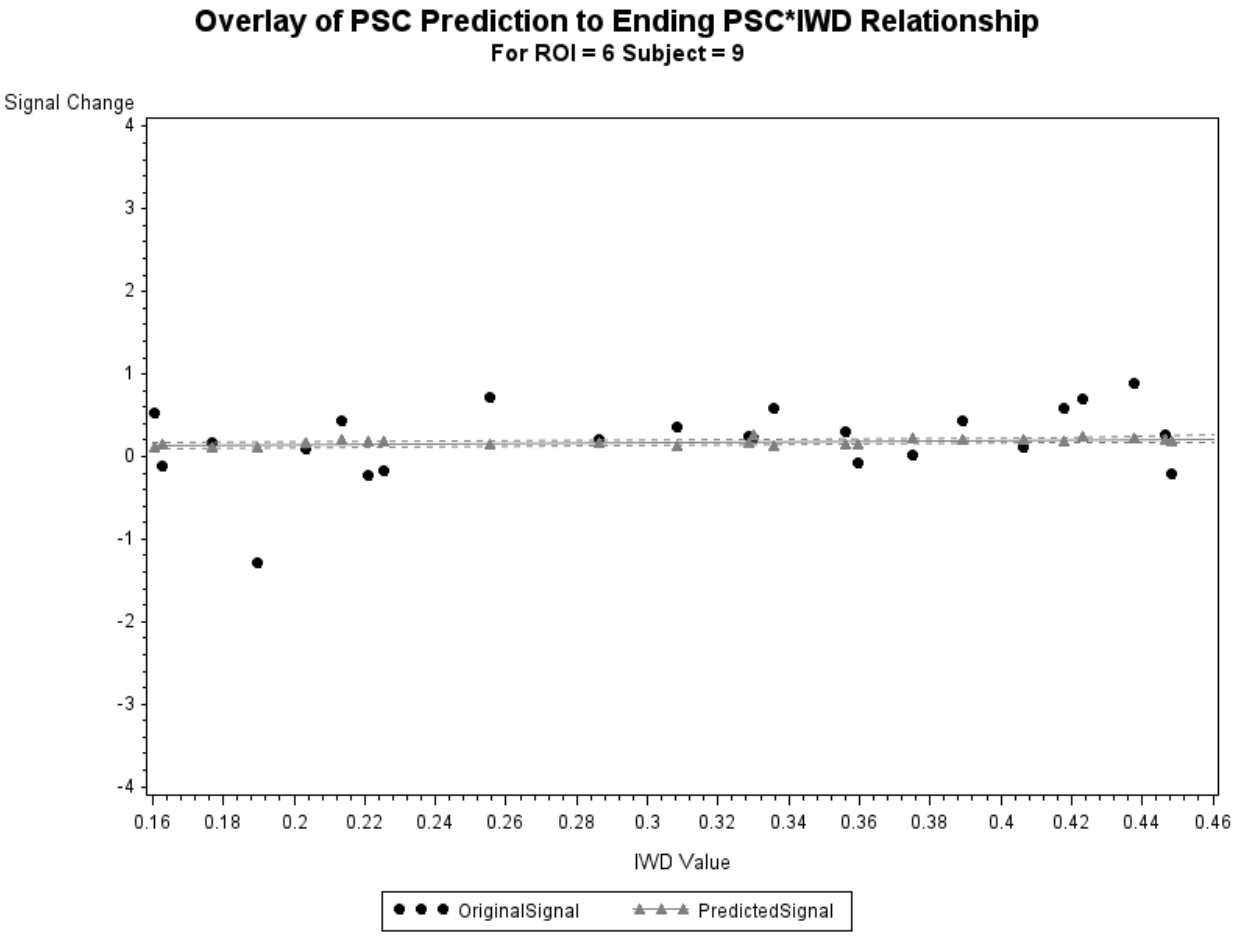
Overlay of PSC Prediction to Ending PSC*IWD Relationship
For ROI = 6 Subject = 9
Signal Change
4
3
2
1
0
-1
-2
-3
-4
0.16
0.18
0.2
0.22
0.24
0.26
0.28
0.3
0.32
0.34
0.36
0.38
0.4
0.42
0.44
0.46
IWD Value
OriginalSignal
PredictedSignal

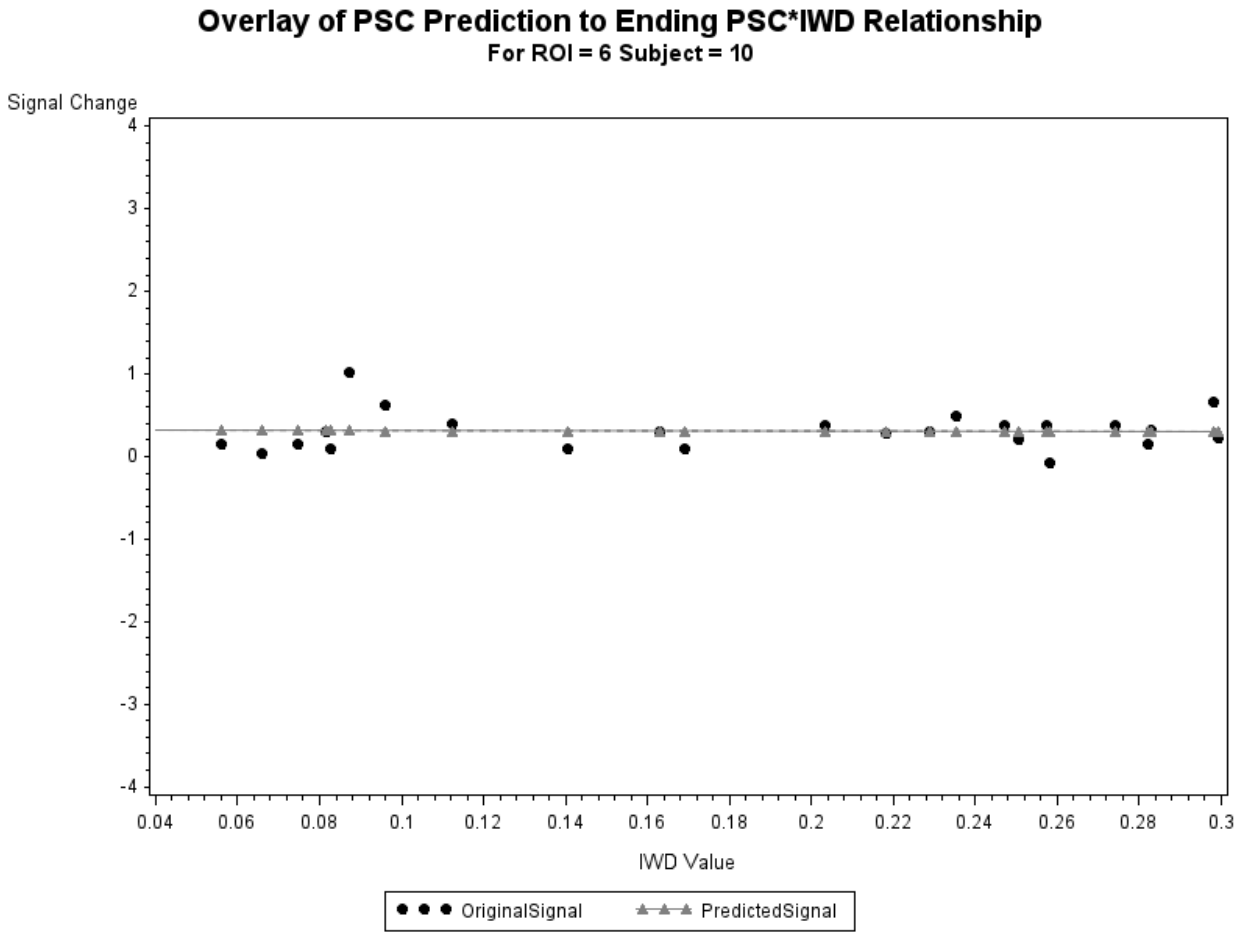
Overlay of PSC Prediction to Ending PSC*IWD Relationship
For ROI = 6 Subject = 10
Signal Change
4
3
2
1
0
-1
-2
-3
-4
0.04
0.06
0.08
0.1
0.12
0.14
0.16
0.18
0.2
0.22
0.24
0.26
0.28
0.3
IWD Value
OriginalSignal
PredictedSignal

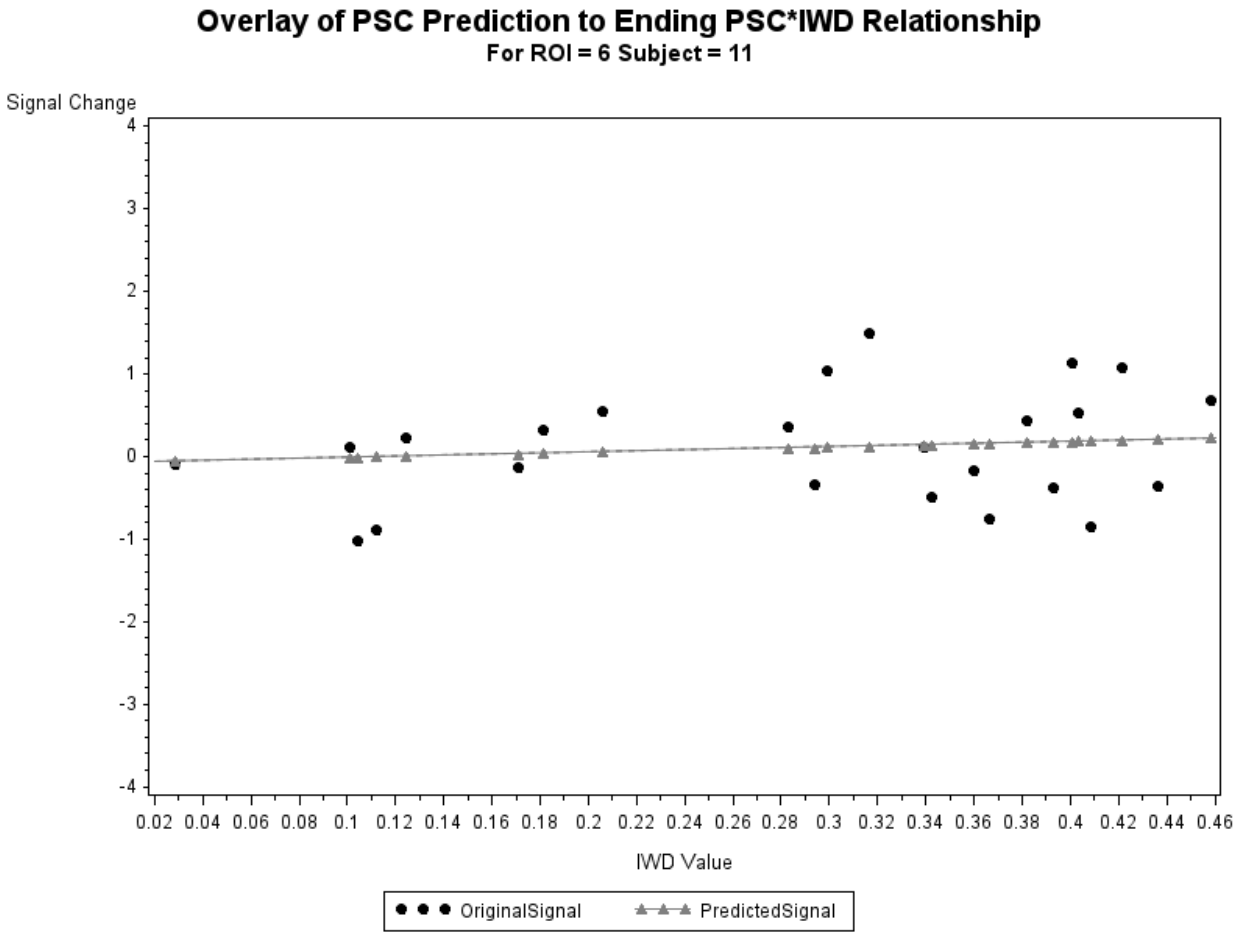
Overlay of PSC Prediction to Ending PSC*IWD Relationship
For ROI = 6 Subject = 11
Signal Change
4
3
2
1
0
-1
-2
-3
-4
0.02 0.04 0.06 0.08 0.1 0.12 0.14 0.16 0.18 0.2 0.22 0.24 0.26 0.28 0.3 0.32 0.34 0.36 0.38 0.4 0.42 0.44 0.46
IWD Value
OriginalSignal
PredictedSignal

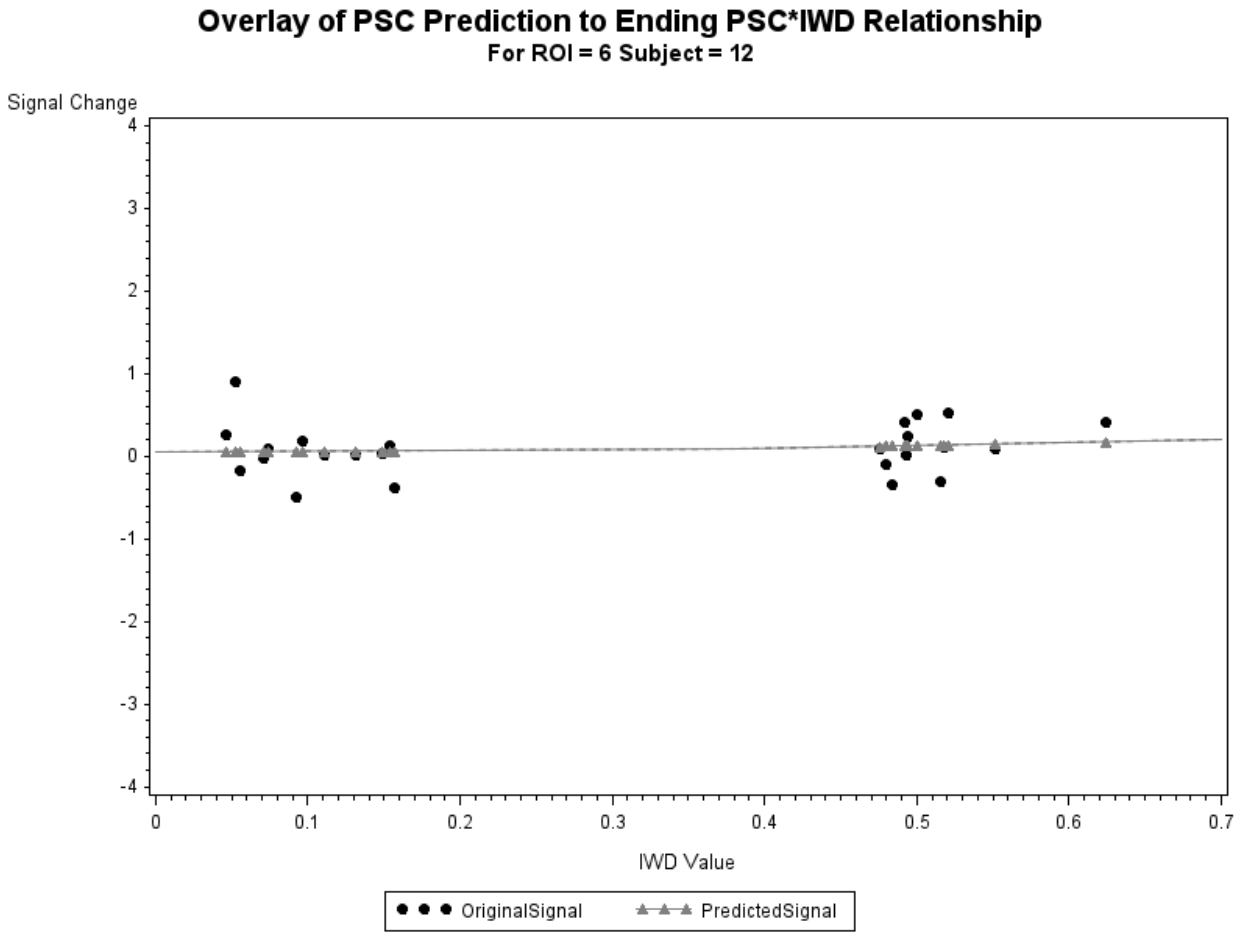
Overlay of PSC Prediction to Ending PSC*IWD Relationship
For ROI = 6 Subject = 12
Signal Change
4
3
2
1
0
-1
-2
-3
-4
0
0.1
0.2
0.3
0.4
0.5
0.6
0.7
IWD Value
OriginalSignal
PredictedSignal

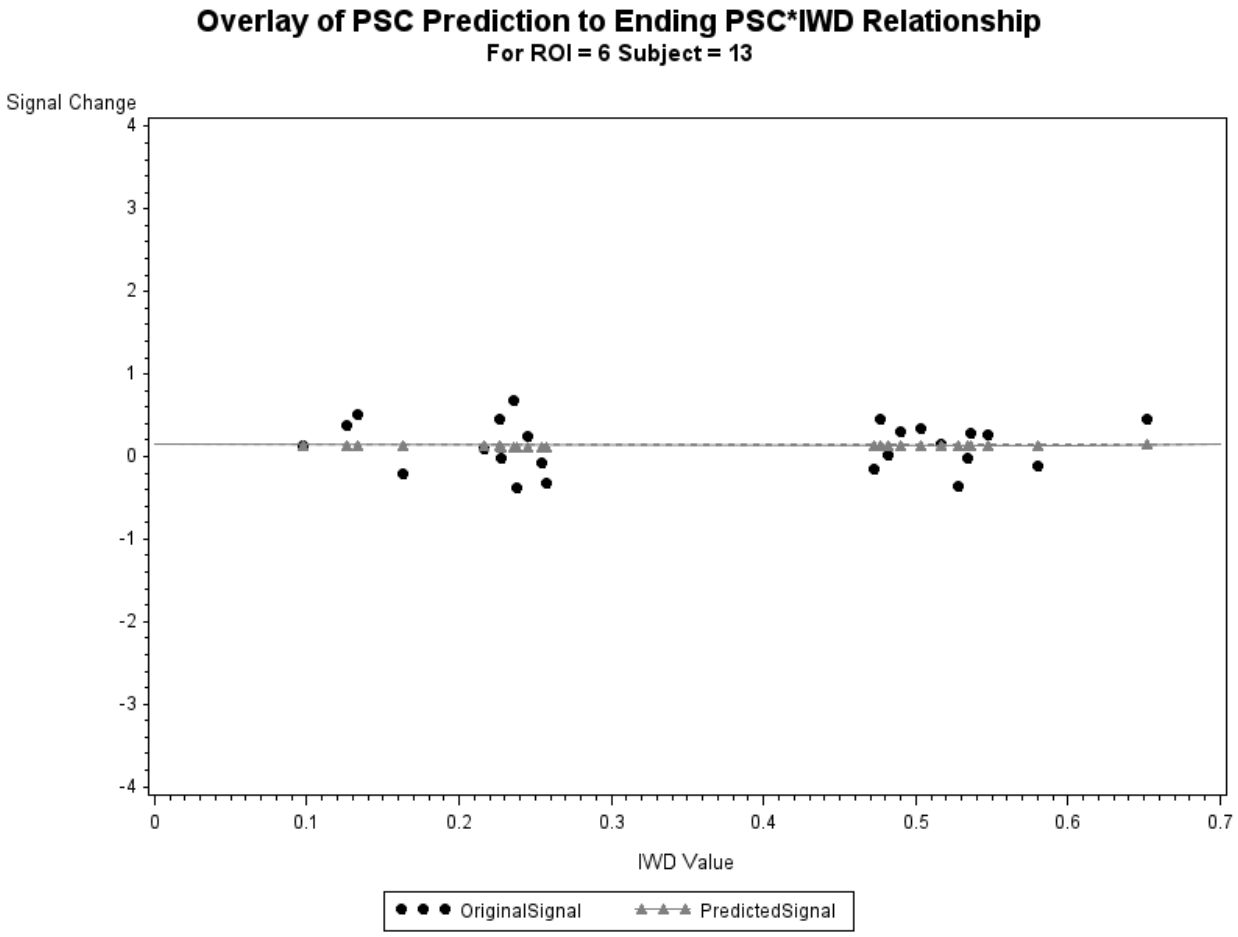
Overlay of PSC Prediction to Ending PSC*IWD Relationship
For ROI = 6 Subject = 13
Signal Change
4
3
2
1
0
-1
-2
-3
-4
0
0.1
0.2
0.3
0.4
0.5
0.6
0.7
IWD Value
OriginalSignal
PredictedSignal

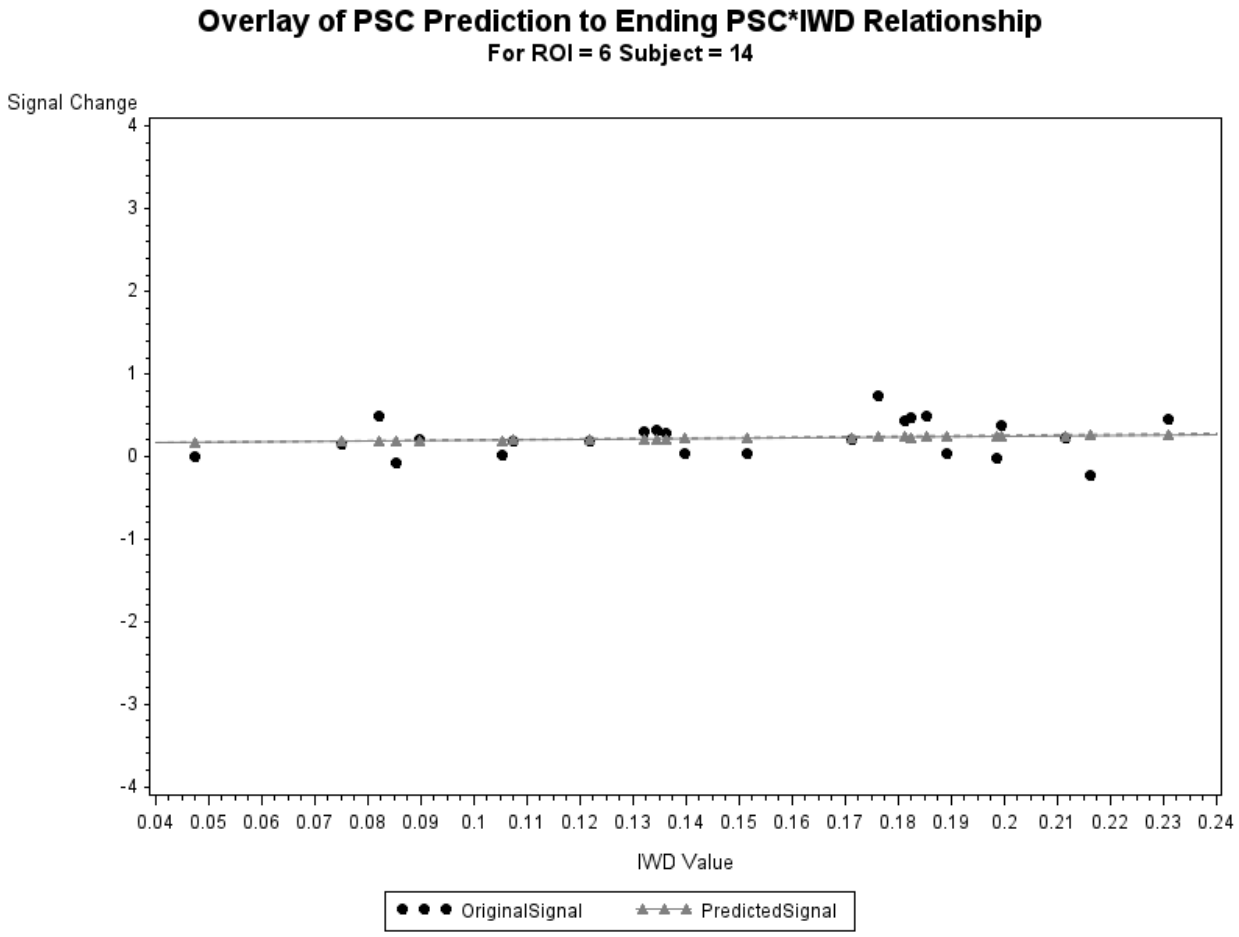
Overlay of PSC Prediction to Ending PSC*IWD Relationship
For ROI = 6 Subject = 14
Signal Change
4
3
2
1
0
-1
-2
-3
-4
0.04 0.05 0.06 0.07 0.08 0.09 0.1 0.11 0.12 0.13 0.14 0.15 0.16 0.17 0.18 0.19 0.2 0.21 0.22 0.23 0.24
IWD Value
OriginalSignal
PredictedSignal

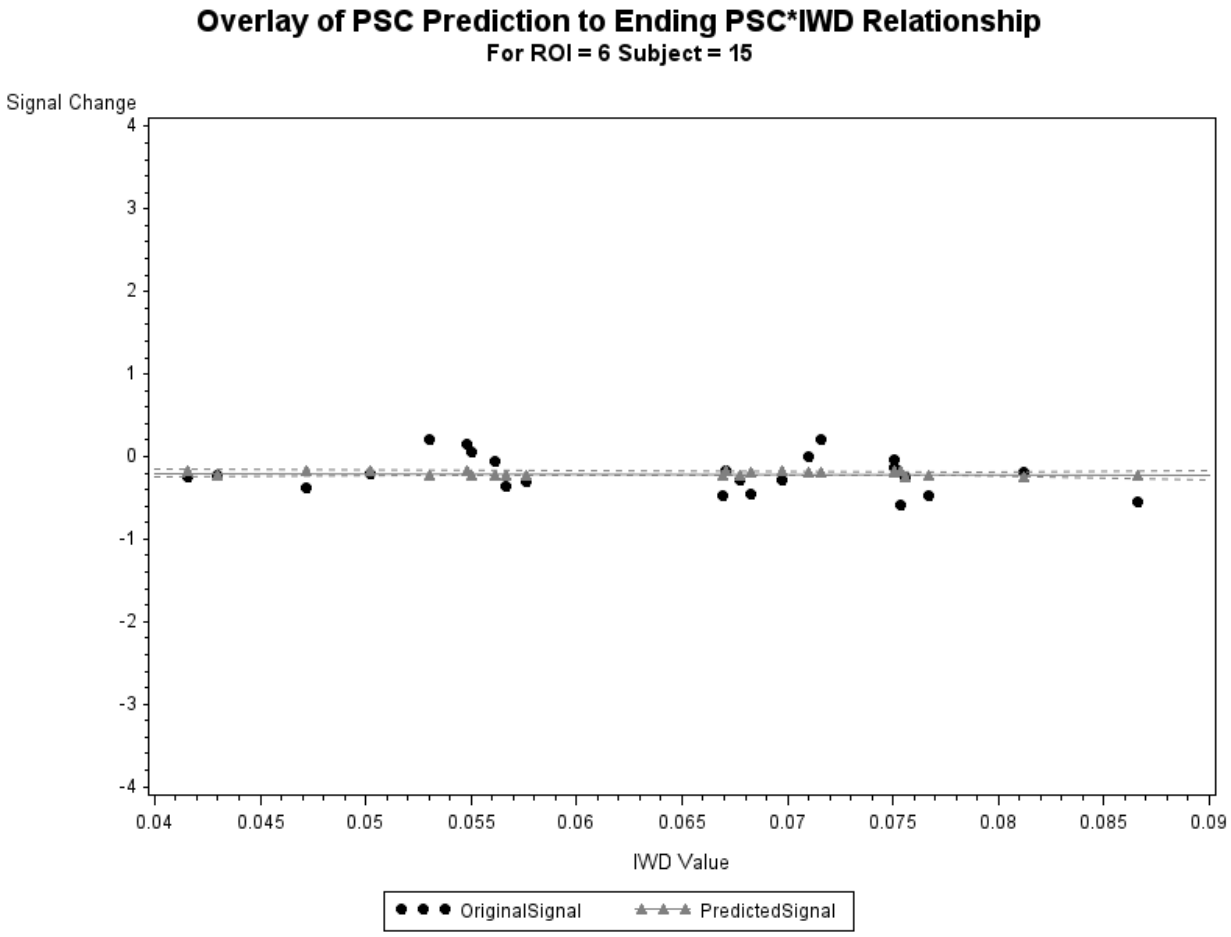
Overlay of PSC Prediction to Ending PSC*IWD Relationship
For ROI = 6 Subject = 15
Signal Change
4
3
2
1
0
-1
-2
-3
-4
0.04
0.045
0.05
0.055
0.06
0.065
0.07
0.075
0.08
0.085
0.09
IWD Value
OriginalSignal
PredictedSignal

APPENDIX: D – Theta Movement for i7 Region by Subject and Dimension

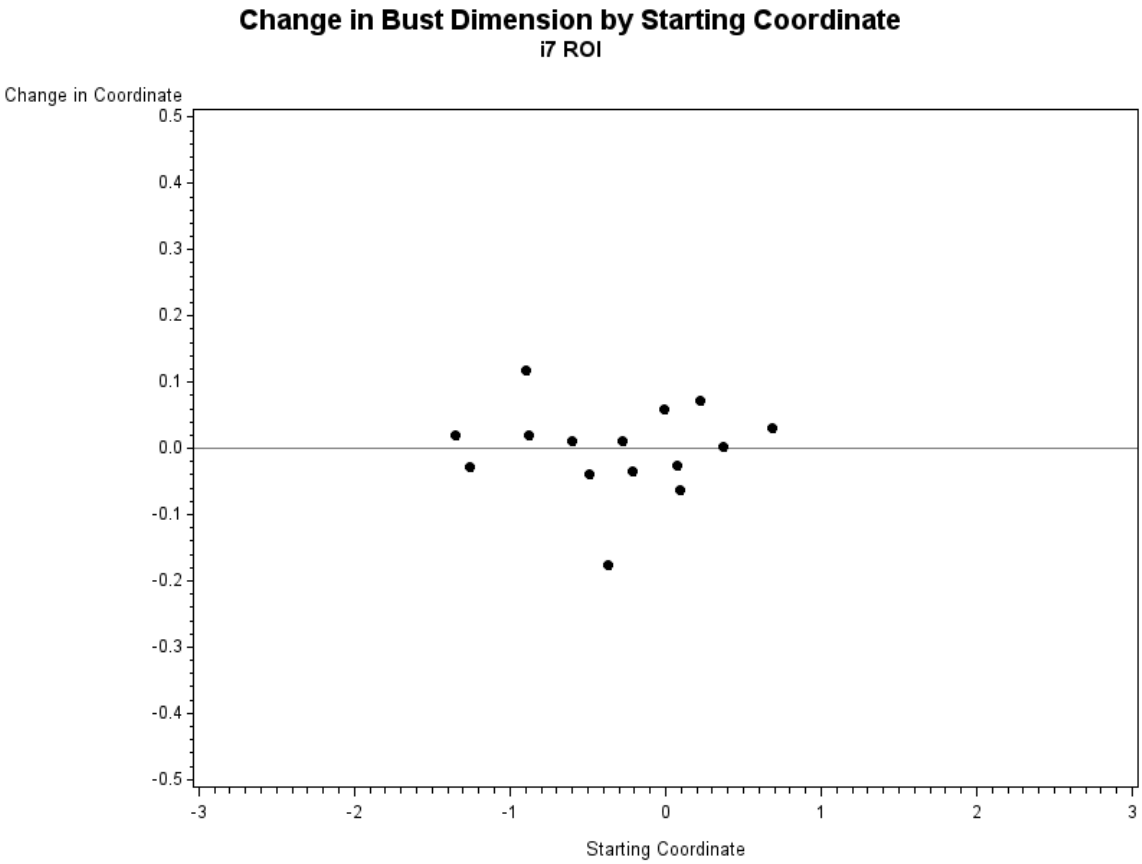

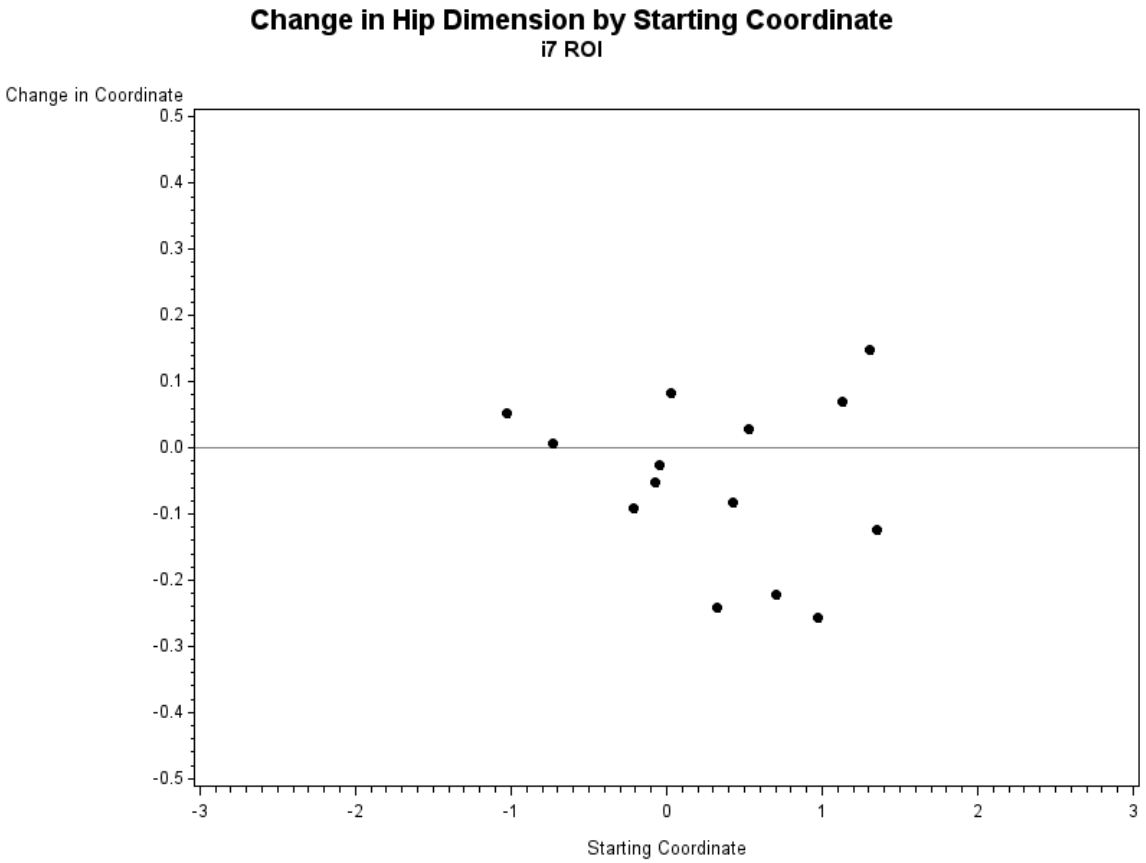
Change in Hip Dimension by Starting Coordinate
i7 ROI
Change in Coordinate
0.5
0.4
0.3
0.2
0.1
0.0
-0.1
-0.2
-0.3
-0.4
-0.5
-3
-2
-1
0
1
2
3
Starting Coordinate

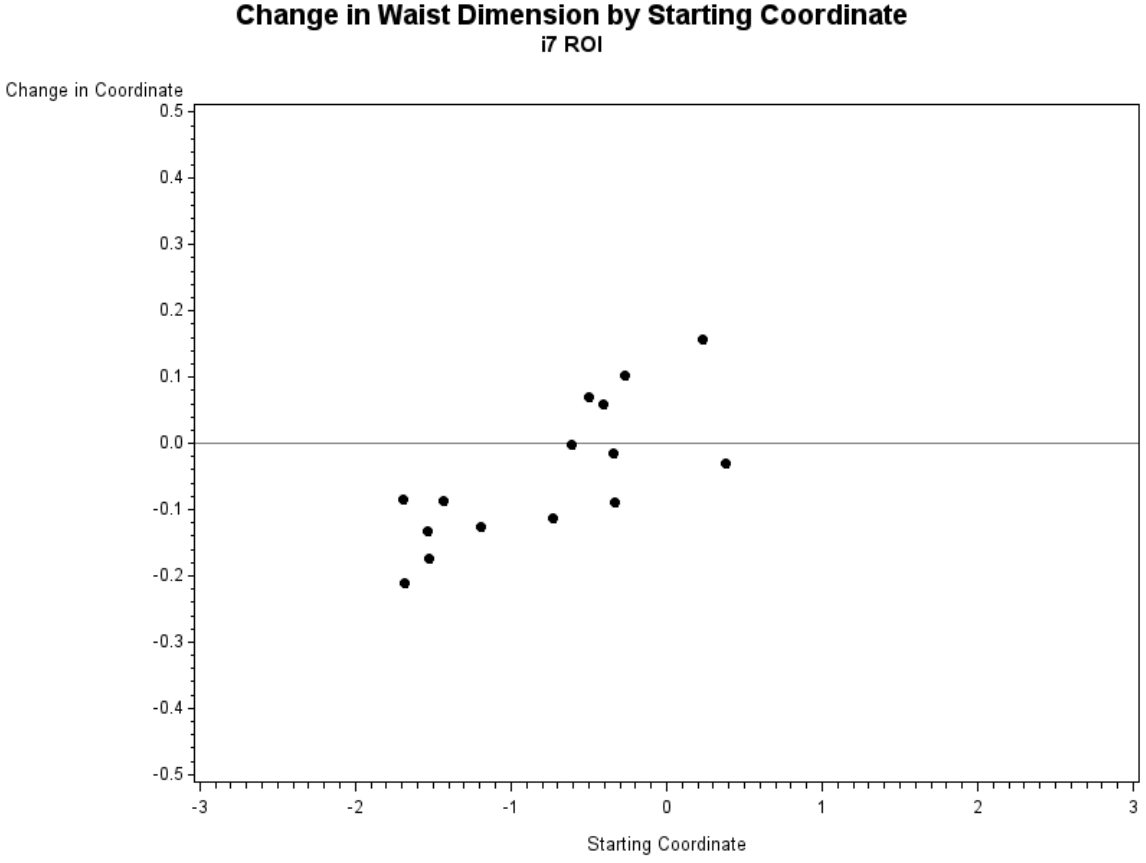
Change in Waist Dimension by Starting Coordinate
i7 ROI
Change in Coordinate
0.5
0.4
0.3
0.2
0.1
0.0
-0.1
-0.2
-0.3
-0.4
-0.5
-3
-2
-1
0
1
2
3
Starting Coordinate

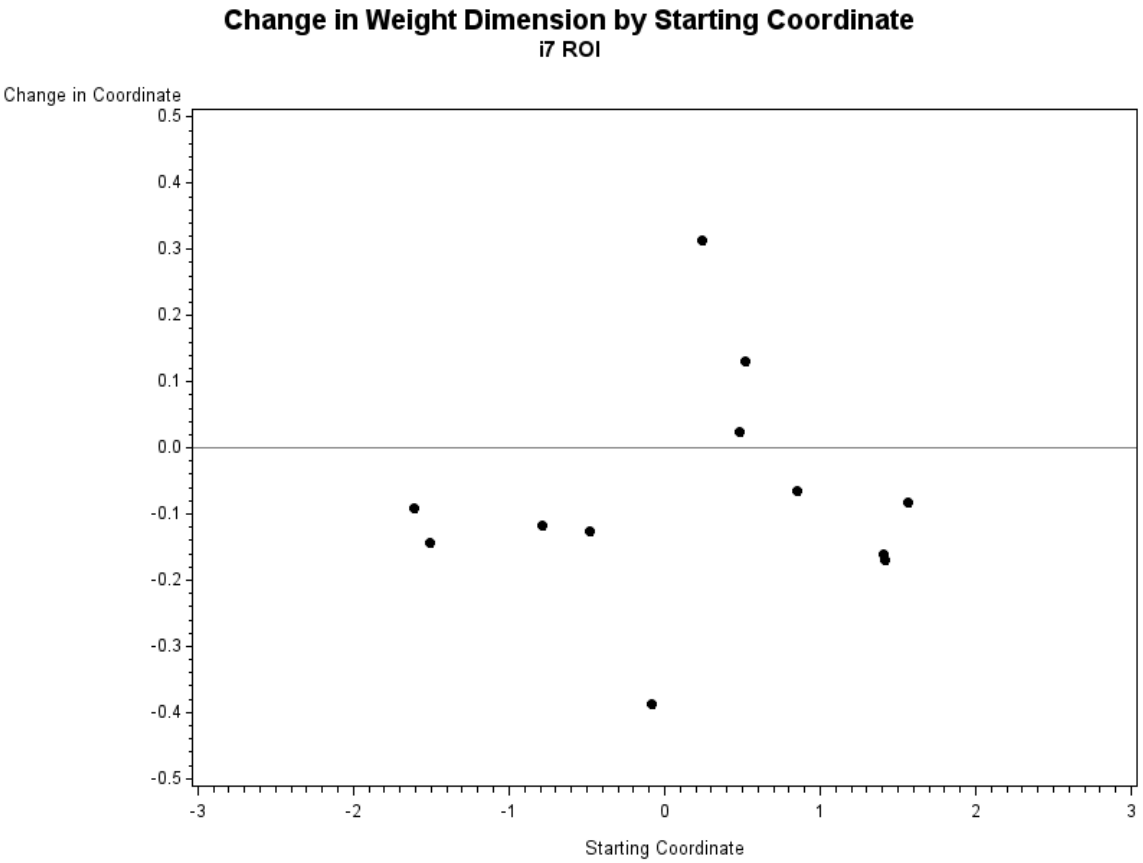
Change in Weight Dimension by Starting Coordinate
i7 ROI
Change in Coordinate
0.5
0.4
0.3
0.2
0.1
0.0
-0.1
-0.2
-0.3
-0.4
-0.5
-3
-2
-1
0
1
2
3
Starting Coordinate

Theta Movement for M1 ROI by Subject and Dimension

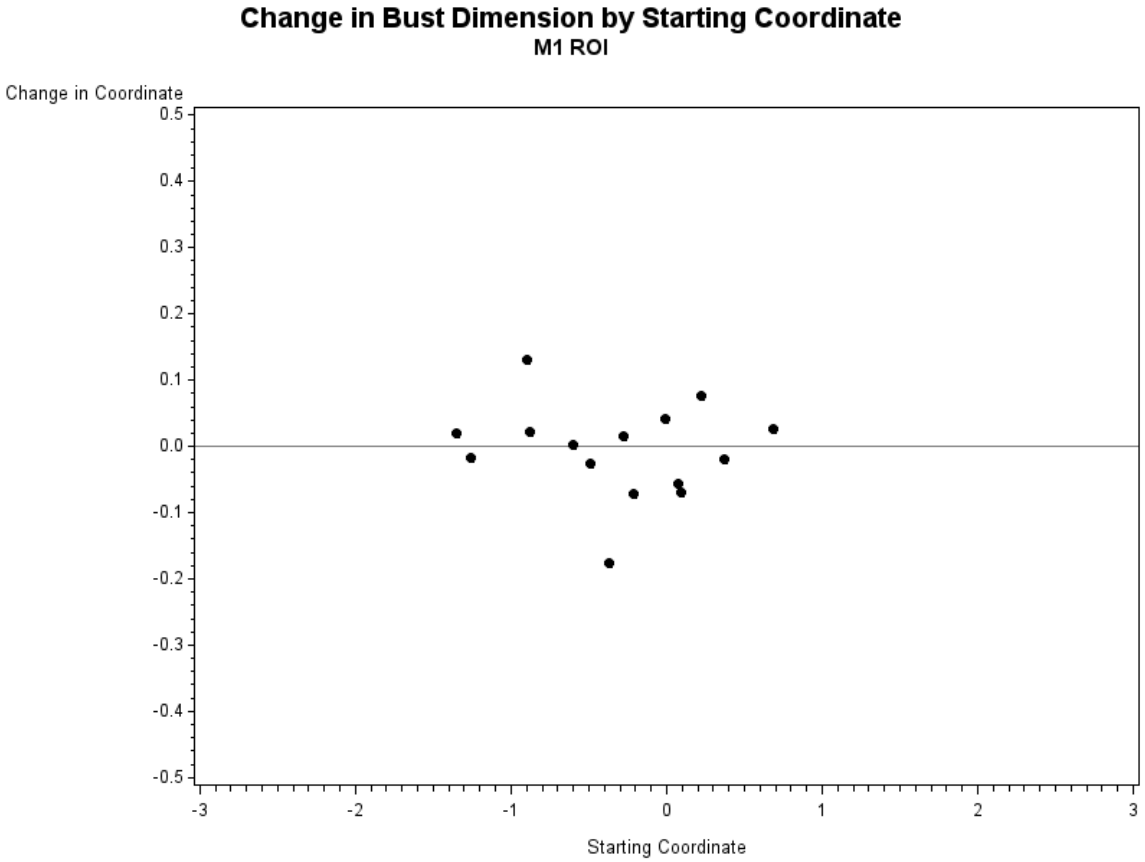

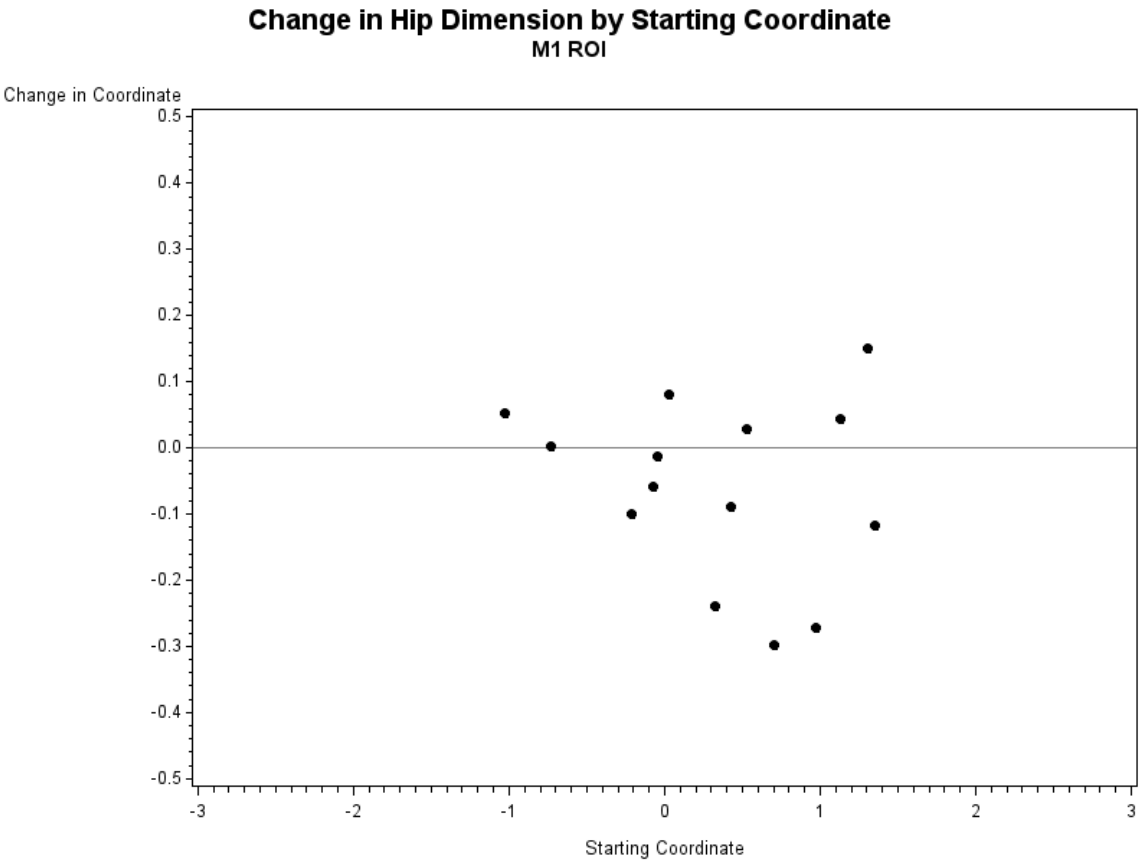
Change in Hip Dimension by Starting Coordinate
M1 ROI
Change in Coordinate
0.5
0.4
0.3
0.2
0.1
0.0
-0.1
-0.2
-0.3
-0.4
-0.5
-3
-2
-1
0
1
2
3
Starting Coordinate

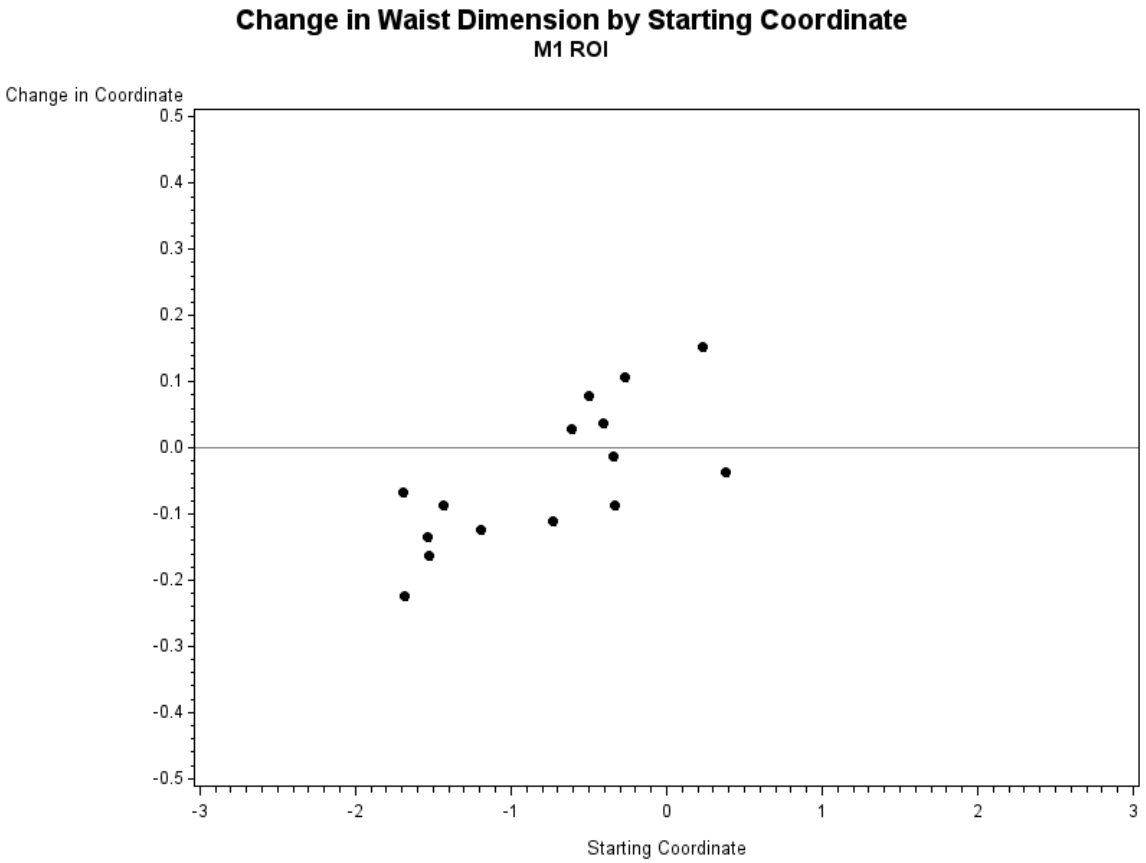
Change in Coordinate
Change in Waist Dimension by Starting Coordinate
M1 ROI
0.5
0.4
0.3
0.2
0.1
0.0
-0.1
-0.2
-0.3
-0.4
-0.5
-3
-2
-1
0
1
2
3
Starting Coordinate

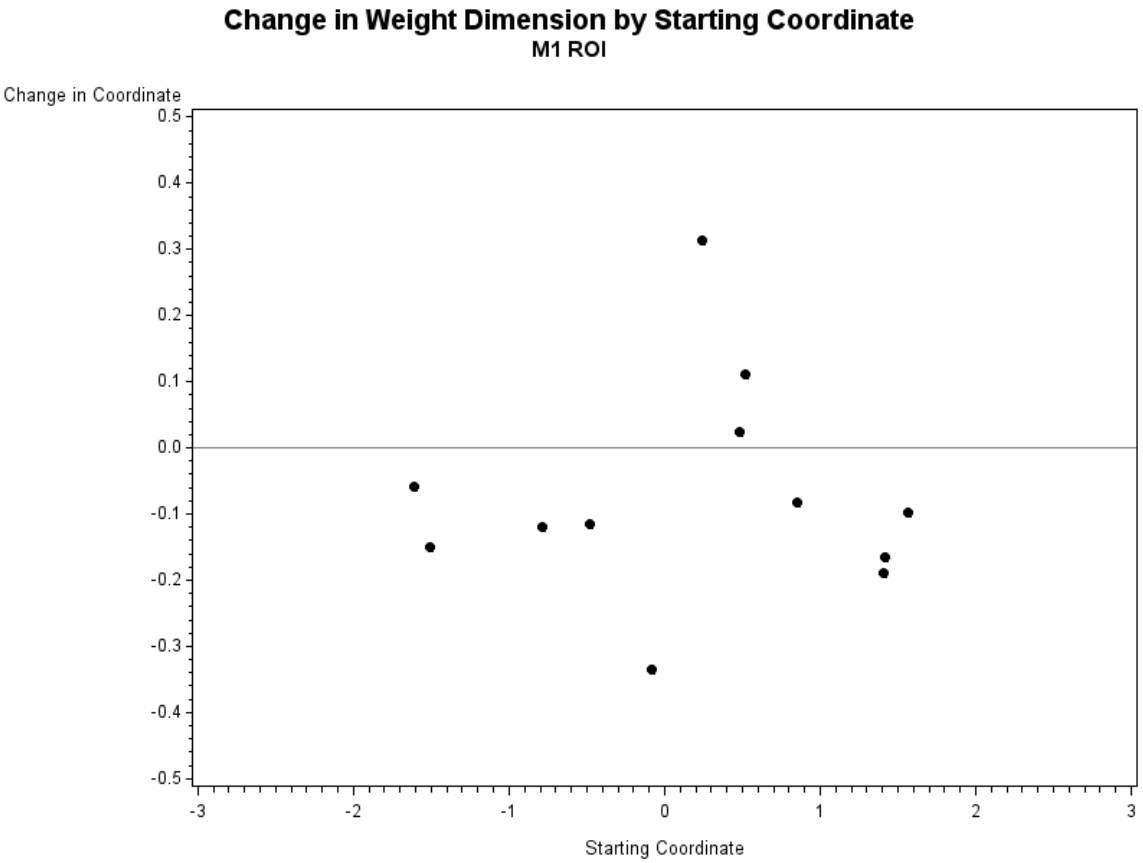
Change in Weight Dimension by Starting Coordinate
M1 ROI
Change in Coordinate
0.5
0.4
0.3
0.2
0.1
0.0
-0.1
-0.2
-0.3
-0.4
-0.5
-3
-2
-1
0
1
2
3
Starting Coordinate

Theta Movement for Subject-Level ROI by Subject and Dimension

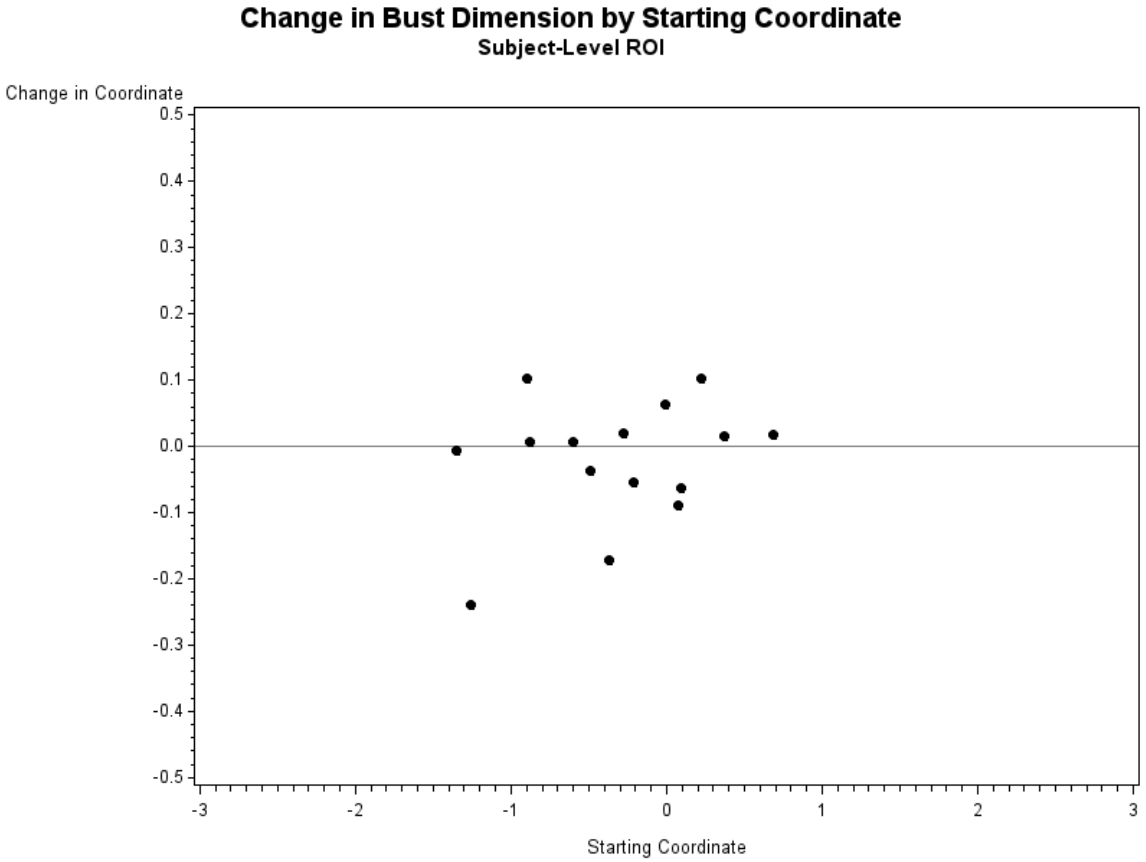

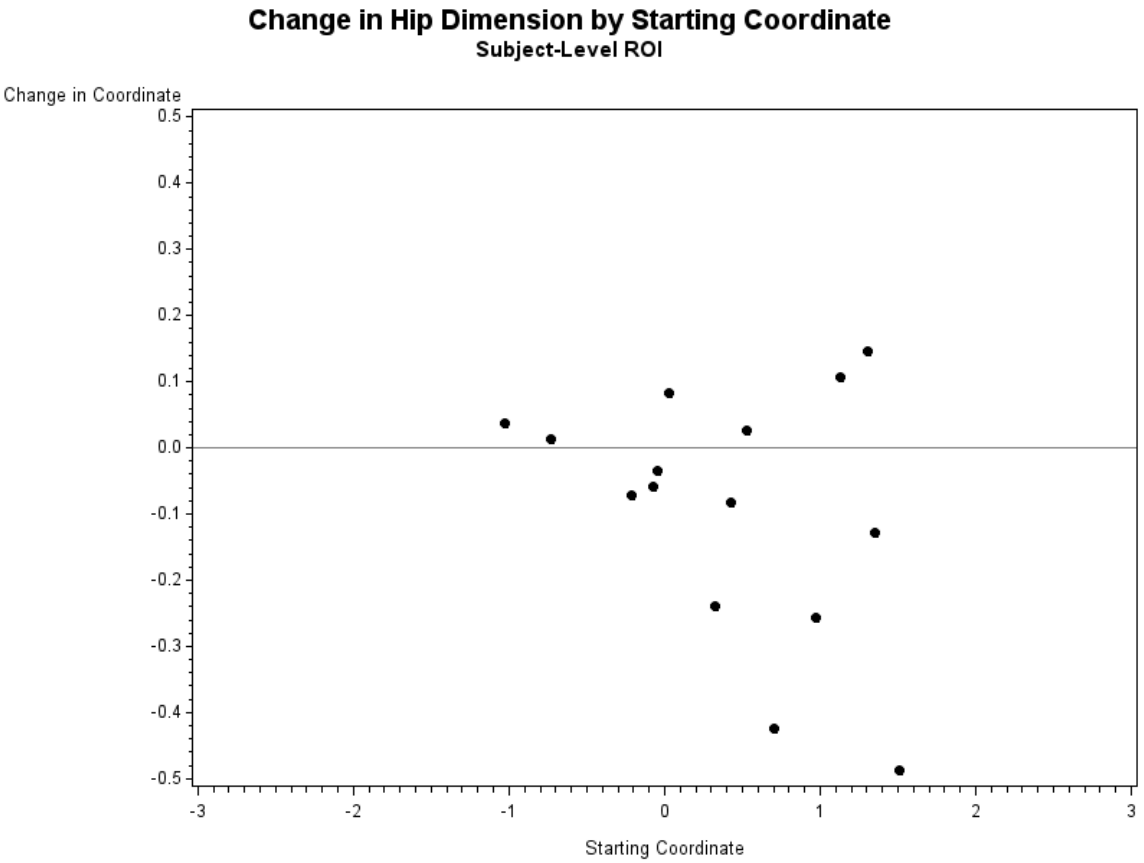
Change in Hip Dimension by Starting Coordinate
Subject-Level ROI
Change in Coordinate
0.5
0.4
0.3
0.2
0.1
0.0
-0.1
-0.2
-0.3
-0.4
-0.5
-3
-2
-1
0
1
2
3
Starting Coordinate

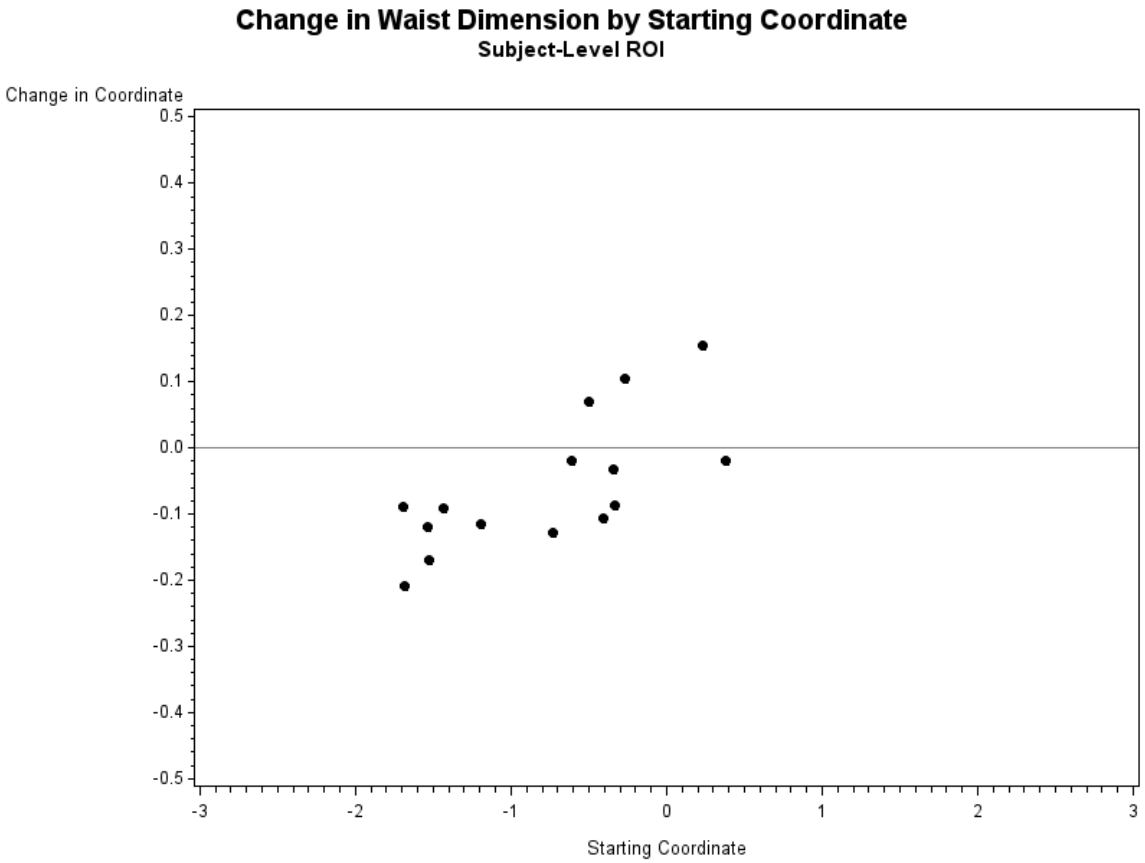
Change in Waist Dimension by Starting Coordinate
Subject-Level ROI
Change in Coordinate
0.5
0.4
0.3
0.2
0.1
0.0
-0.1
-0.2
-0.3
-0.4
-0.5
-3
-2
-1
0
1
2
3
Starting Coordinate

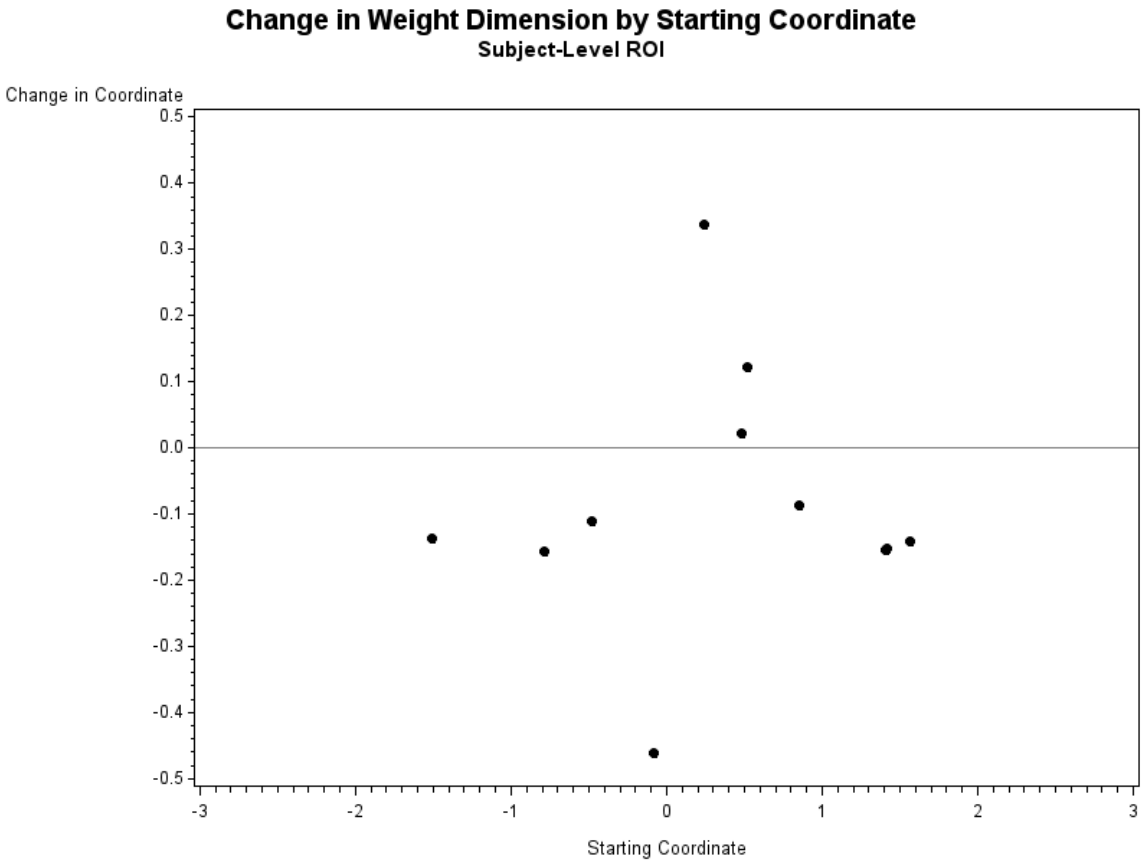
Change in Weight Dimension by Starting Coordinate
Subject-Level ROI
Change in Coordinate
0.5
0.4
0.3
0.2
0.1
0.0
-0.1
-0.2
-0.3
-0.4
-0.5
-3
-2
-1
0
1
2
3
Starting Coordinate

Theta Movement for Group-Level WHR ROI by Subject and Dimension

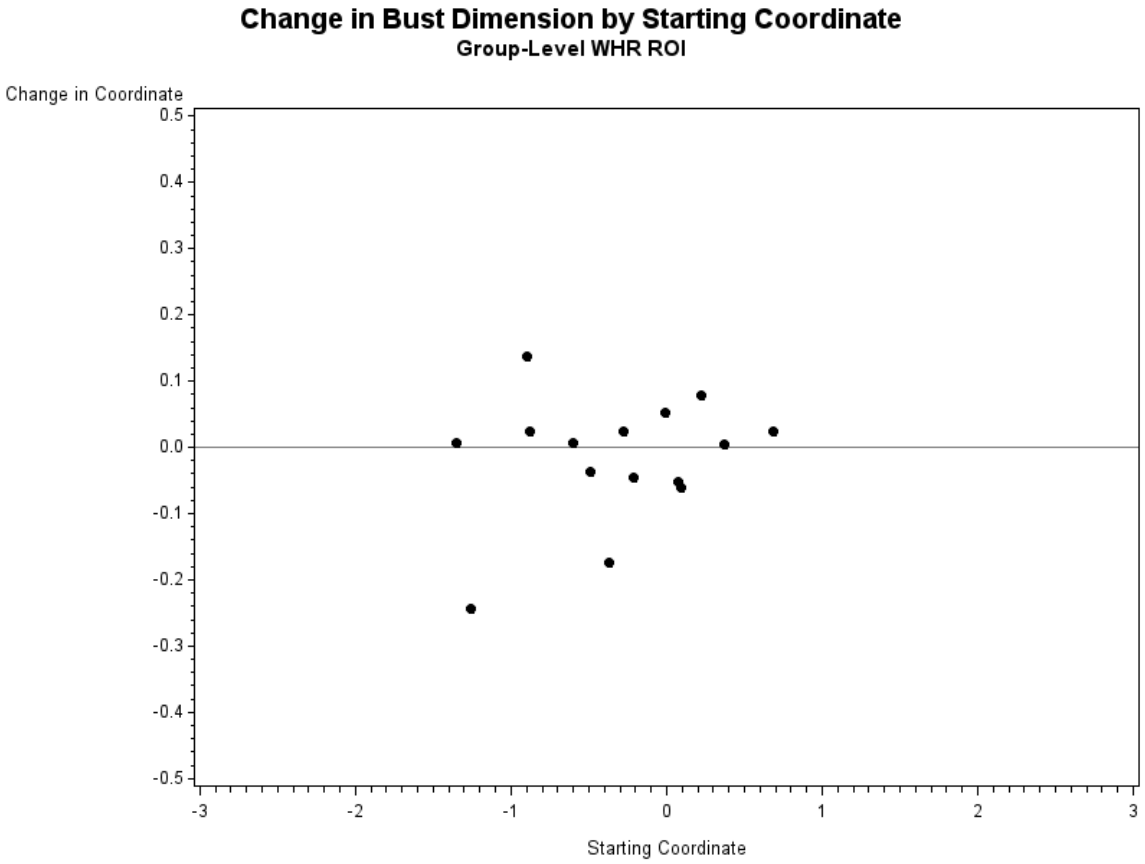

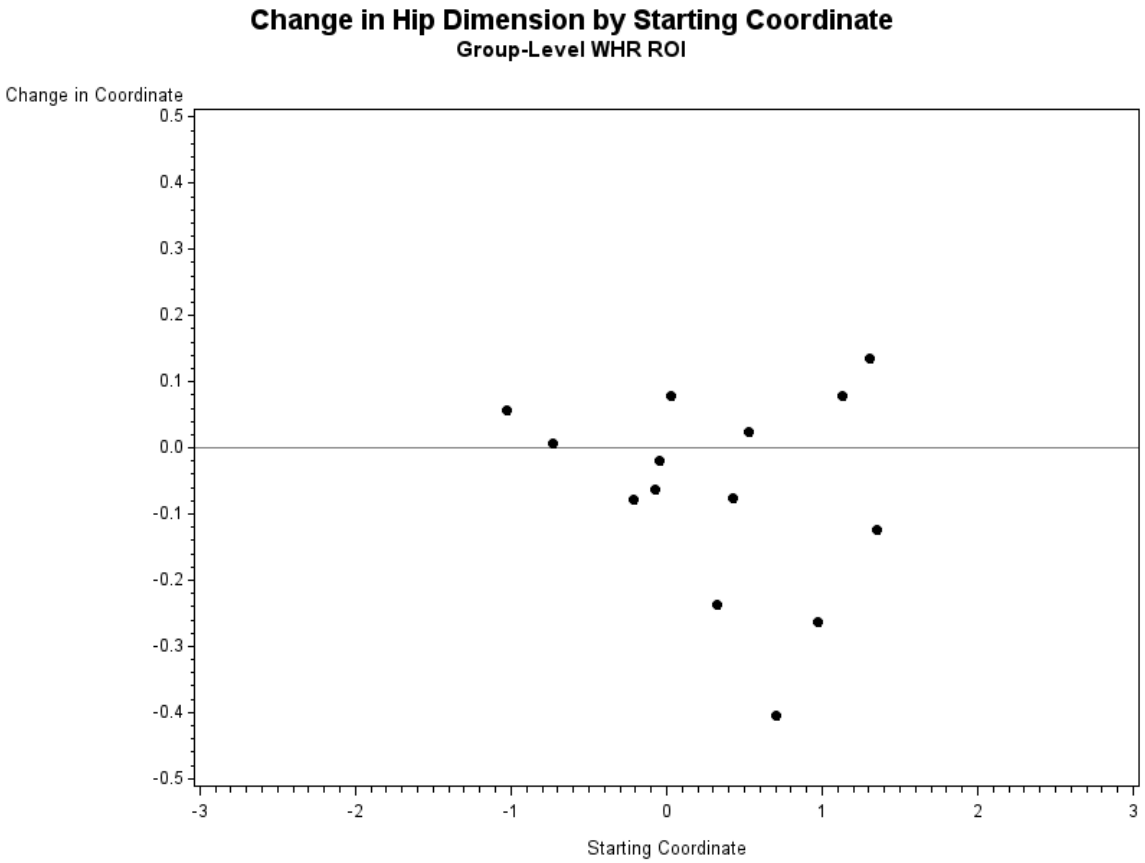
Change in Hip Dimension by Starting Coordinate
Group-Level WHR ROI
Change in Coordinate
0.5
0.4
0.3
0.2
0.1
0.0
-0.1
-0.2
-0.3
-0.4
-0.5
-3
-2
-1
0
1
2
3
Starting Coordinate

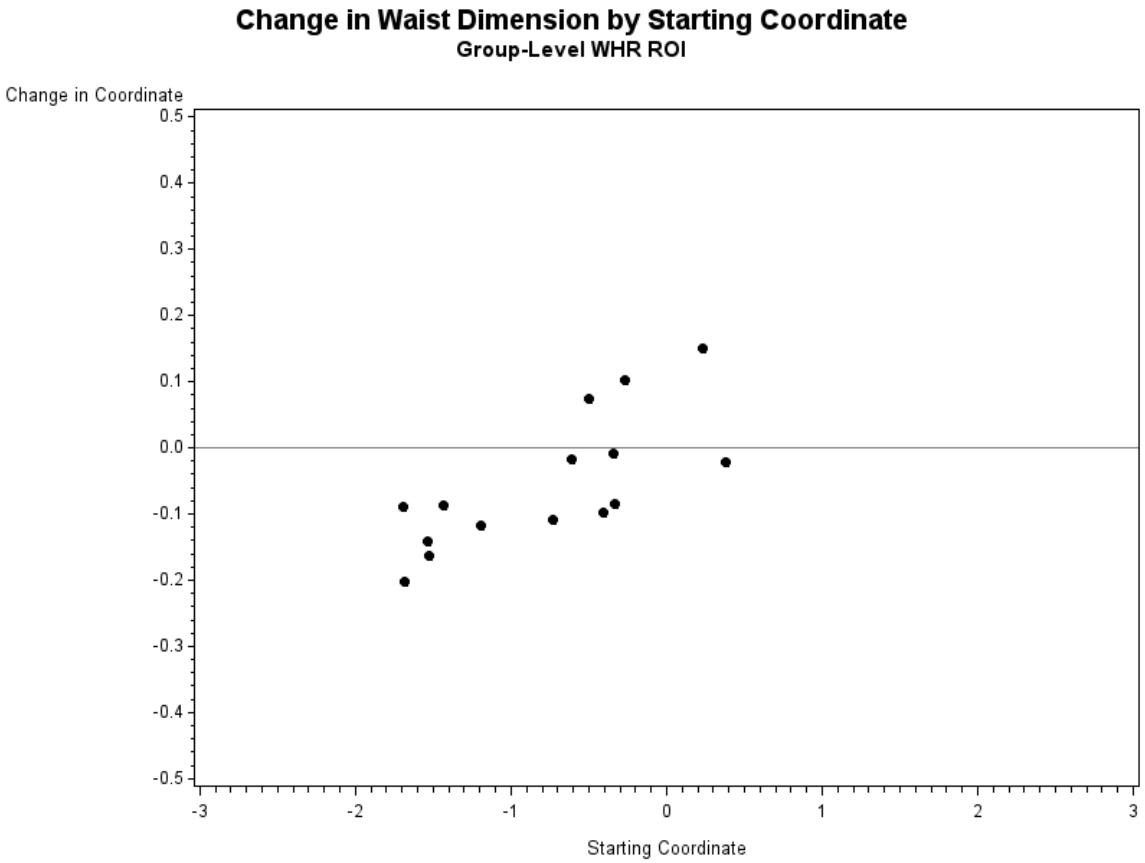
Change in Waist Dimension by Starting Coordinate
Group-Level WHR ROI
Change in Coordinate
0.5
0.4
0.3
0.2
0.1
0.0
-0.1
-0.2
-0.3
-0.4
-0.5
-3
-2
-1
0
1
2
3
Starting Coordinate

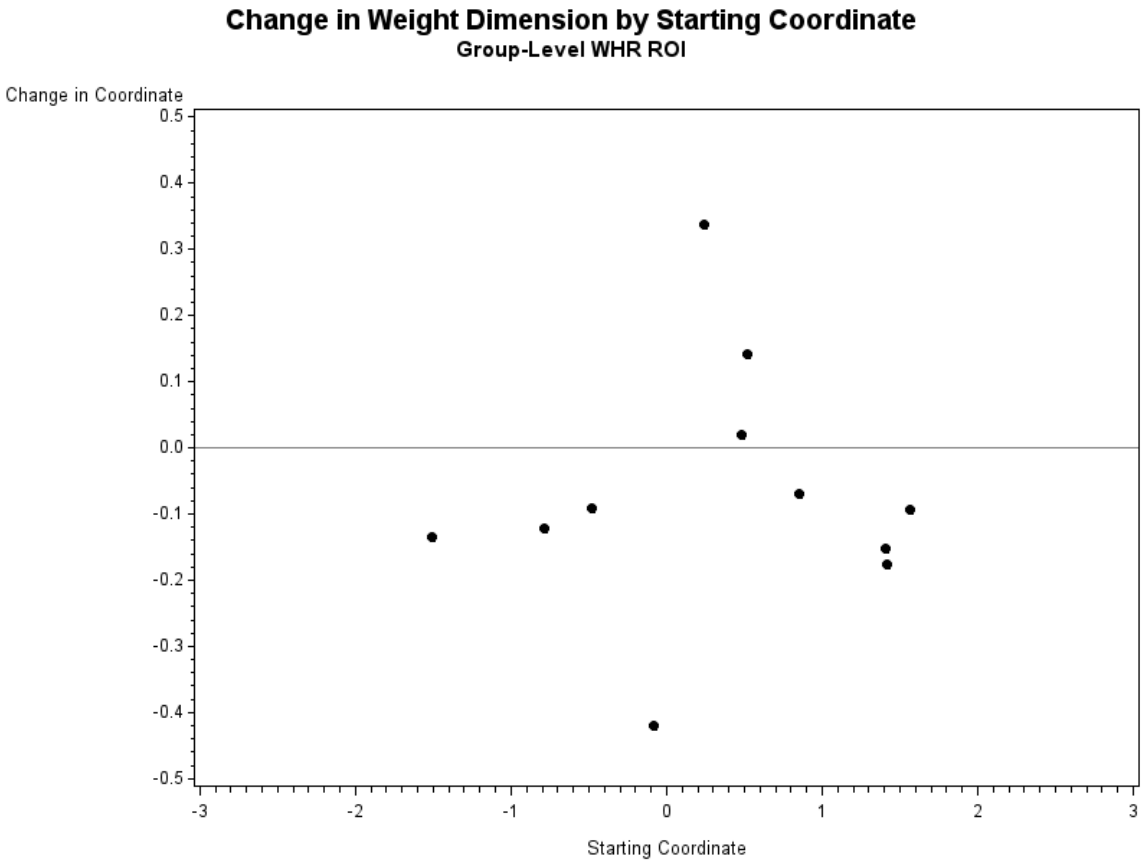
Change in Weight Dimension by Starting Coordinate
Group-Level WHR ROI
Change in Coordinate
0.5
0.4
0.3
0.2
0.1
0.0
-0.1
-0.2
-0.3
-0.4
-0.5
-3
-2
-1
0
1
2
3
Starting Coordinate

Theta Movement for Masked Subject-Level ROI by Subject and Dimension

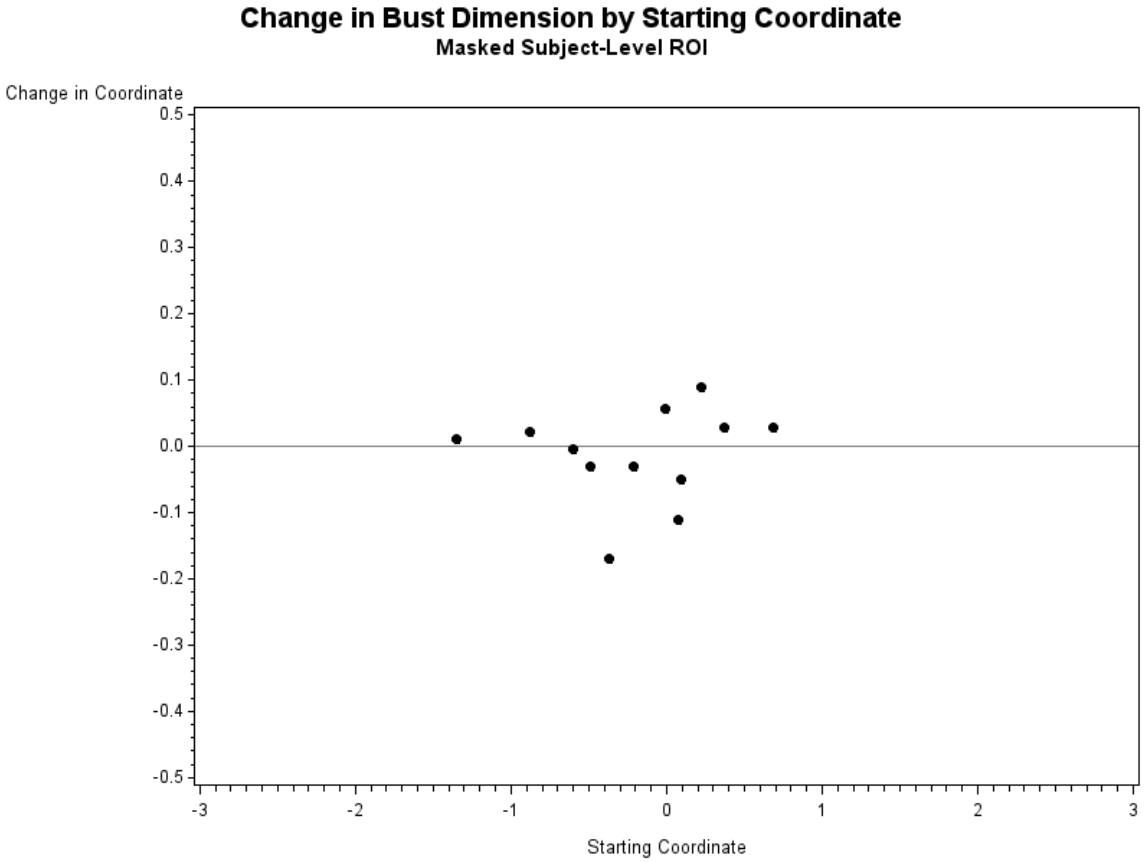

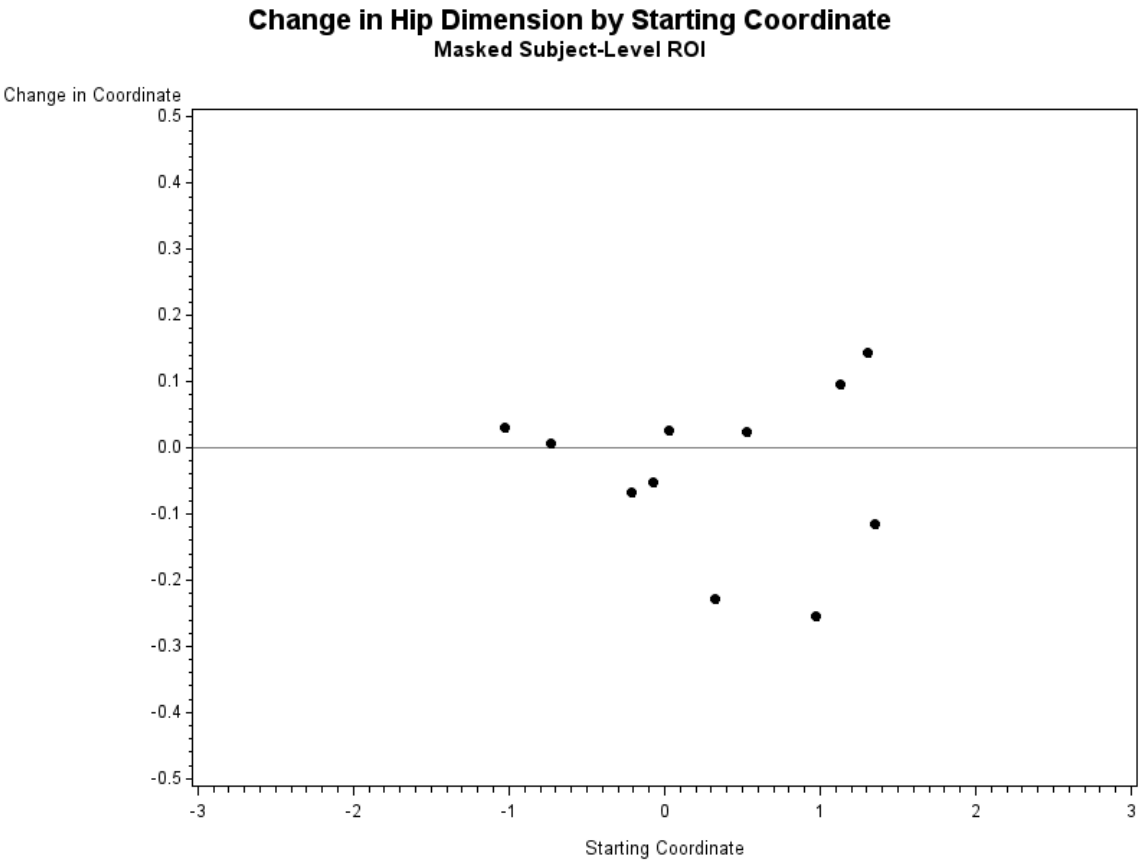
Change in Hip Dimension by Starting Coordinate
Masked Subject-Level ROI
Change in Coordinate
0.5
0.4
0.3
0.2
0.1
0.0
-0.1
-0.2
-0.3
-0.4
-0.5
-3
-2
-1
0
1
2
3
Starting Coordinate

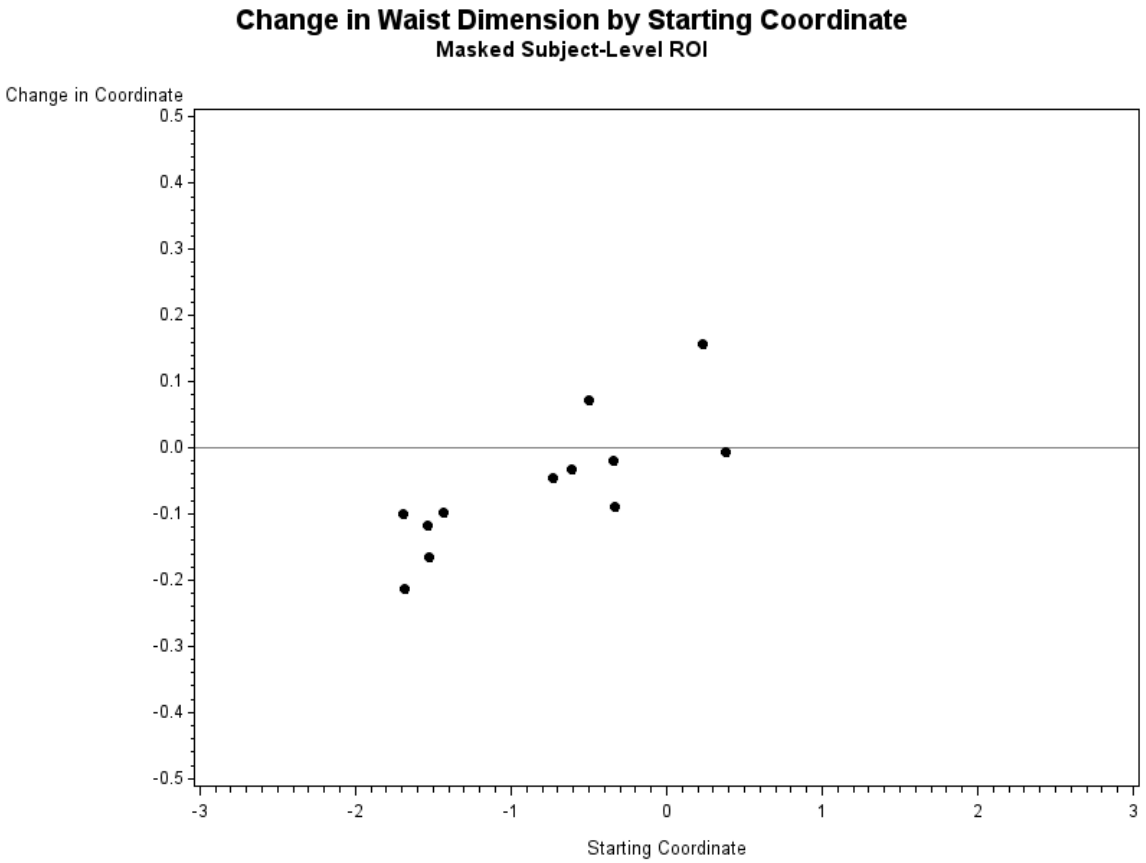
Change in Waist Dimension by Starting Coordinate
Masked Subject-Level ROI
Change in Coordinate
0.5
0.4
0.3
0.2
0.1
0.0
-0.1
-0.2
-0.3
-0.4
-0.5
-3
-2
-1
0
1
2
3
Starting Coordinate

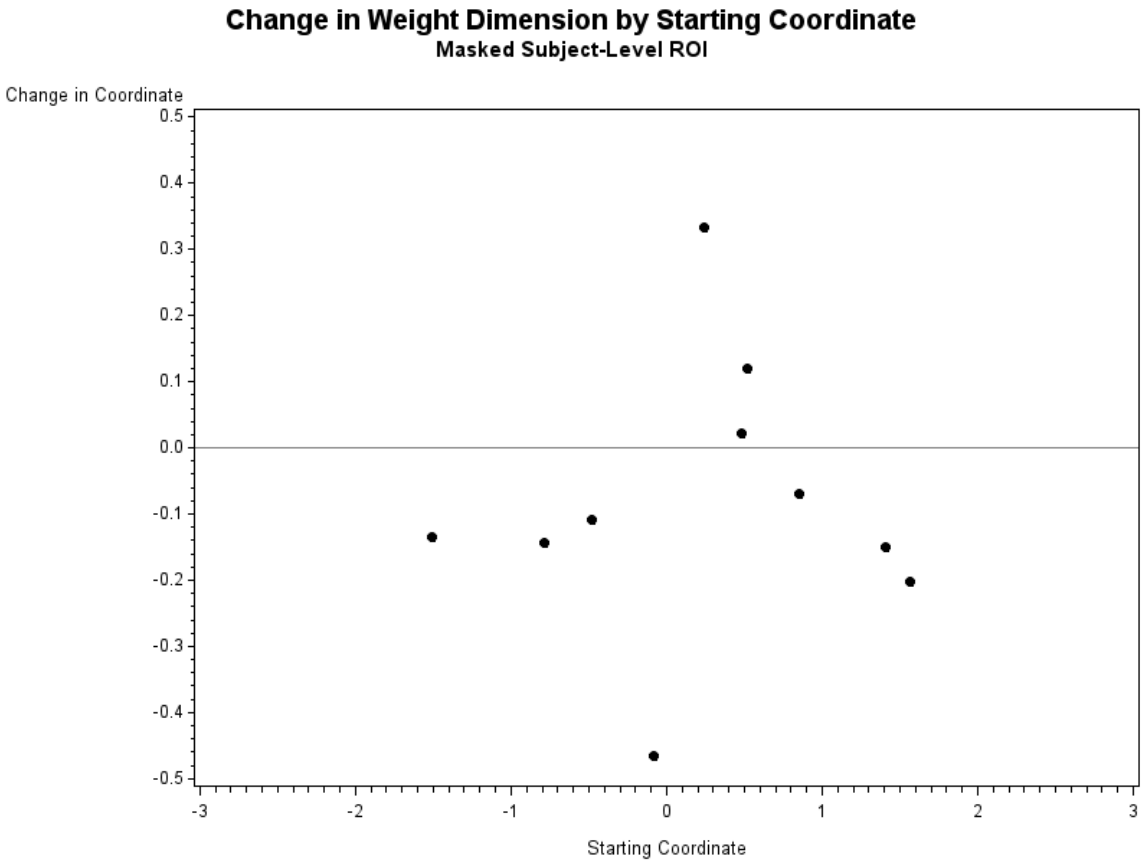
Change in Weight Dimension by Starting Coordinate
Masked Subject-Level ROI
Change in Coordinate
0.5
0.4
0.3
0.2
0.1
0.0
-0.1
-0.2
-0.3
-0.4
-0.5
-3
-2
-1
0
1
2
3
Starting Coordinate

APPENDIX: E – PSC Plotted by Attractiveness Rating

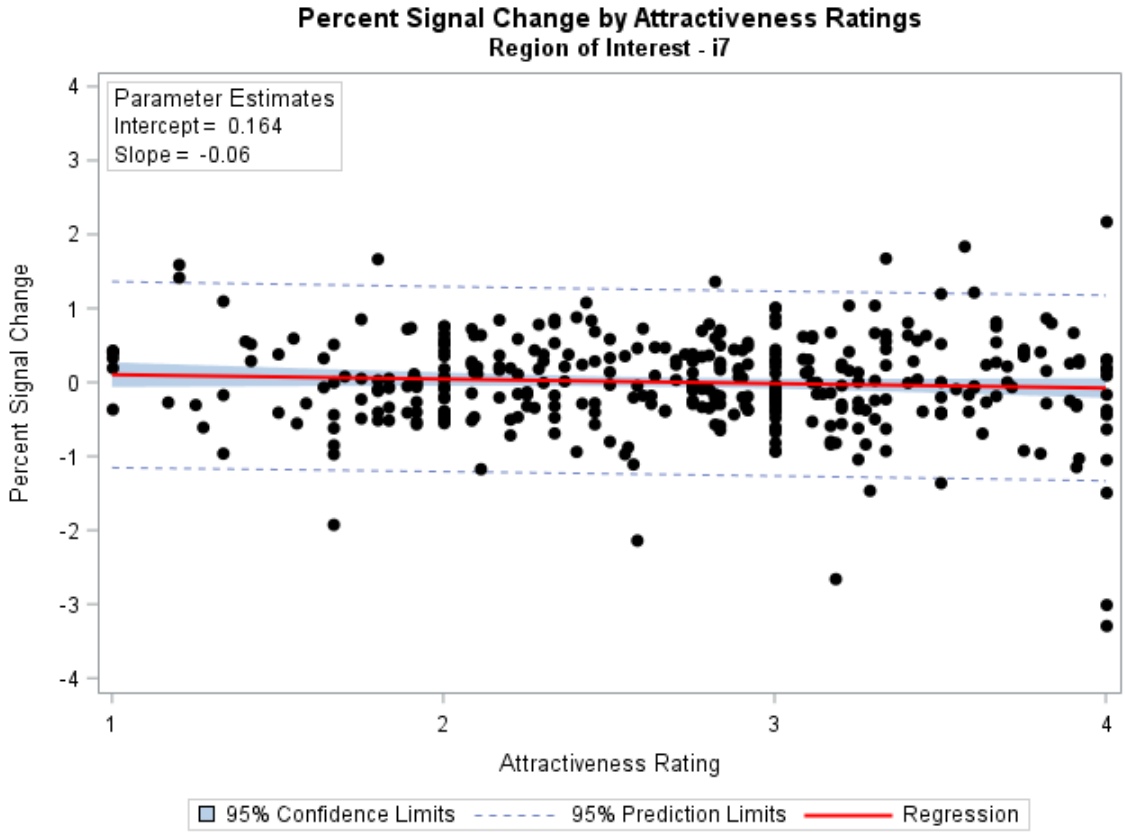

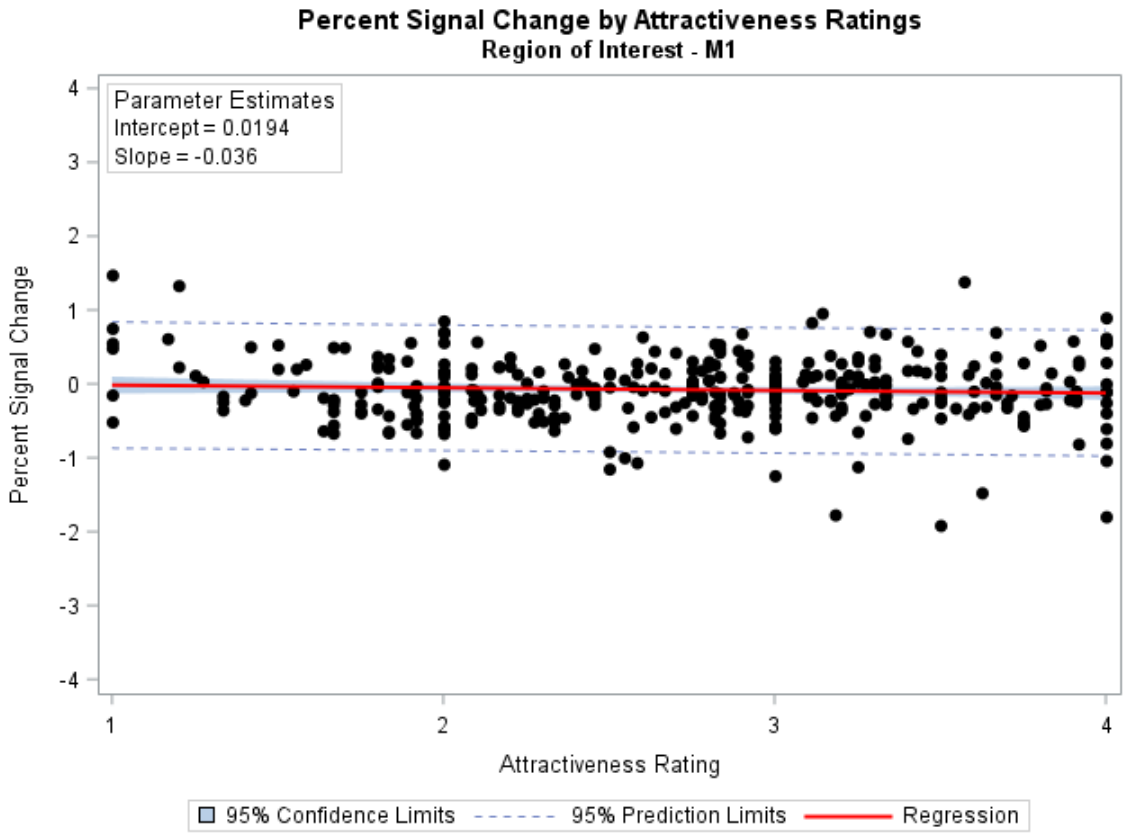
Percent Signal Change by Attractiveness Ratings
Region of Interest - M1
Parameter Estimates
Intercept = 0.0194
Slope = -0.036
Percent Signal Change
4
3
2
1
0
-1
-2
-3
-4
1
2
3
4
Attractiveness Rating
95% Confidence Limits
95% Prediction Limits
Regression

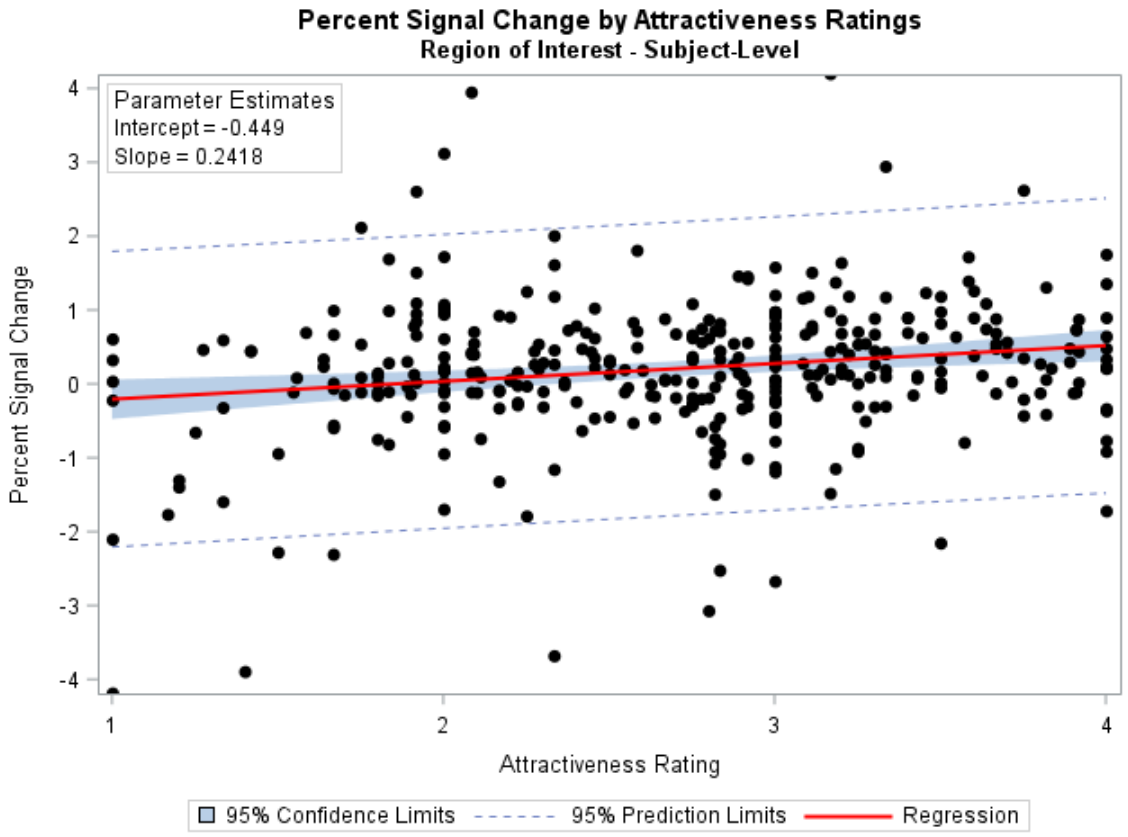
Percent Signal Change by Attractiveness Ratings
Region of Interest - Subject-Level
Parameter Estimates
Intercept = -0.449
Slope = 0.2418
Percent Signal Change
Attractiveness Rating
95% Confidence Limits
95% Prediction Limits
Regression

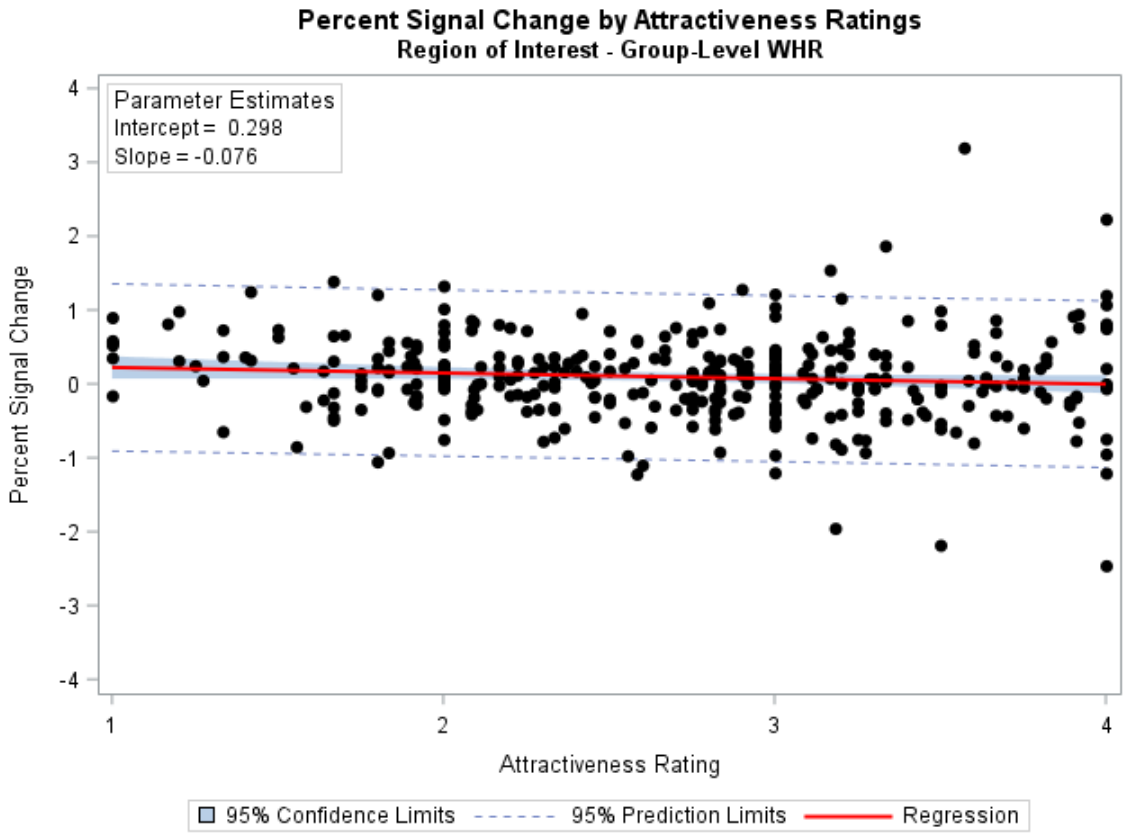
Percent Signal Change by Attractiveness Ratings
Region of Interest - Group-Level WHR
Parameter Estimates
Intercept = 0.298
Slope = -0.076
Percent Signal Change
Attractiveness Rating
95% Confidence Limits
95% Prediction Limits
Regression

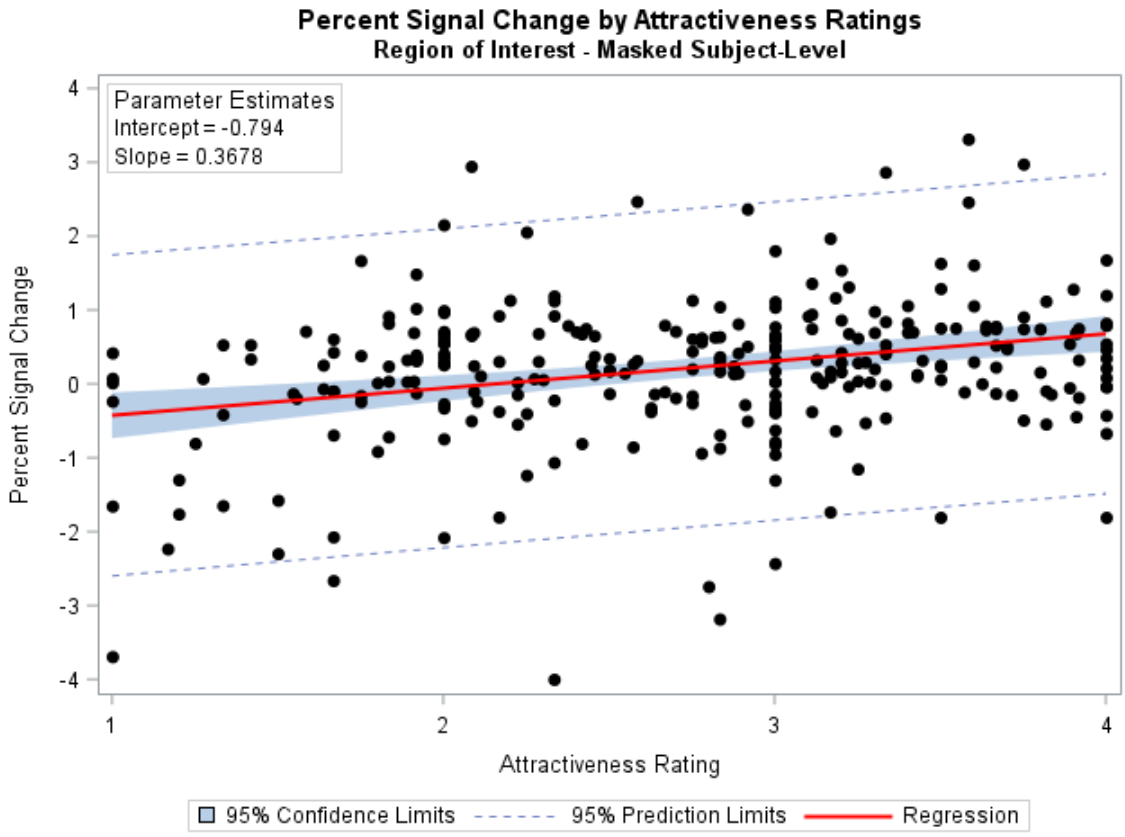
Percent Signal Change by Attractiveness Ratings
Region of Interest - Masked Subject-Level
Parameter Estimates
Intercept = -0.794
Slope = 0.3678
Percent Signal Change
Attractiveness Rating
95% Confidence Limits
95% Prediction Limits
Regression

APPENDIX: F – Plots of PSC by IWD

i7 ROI

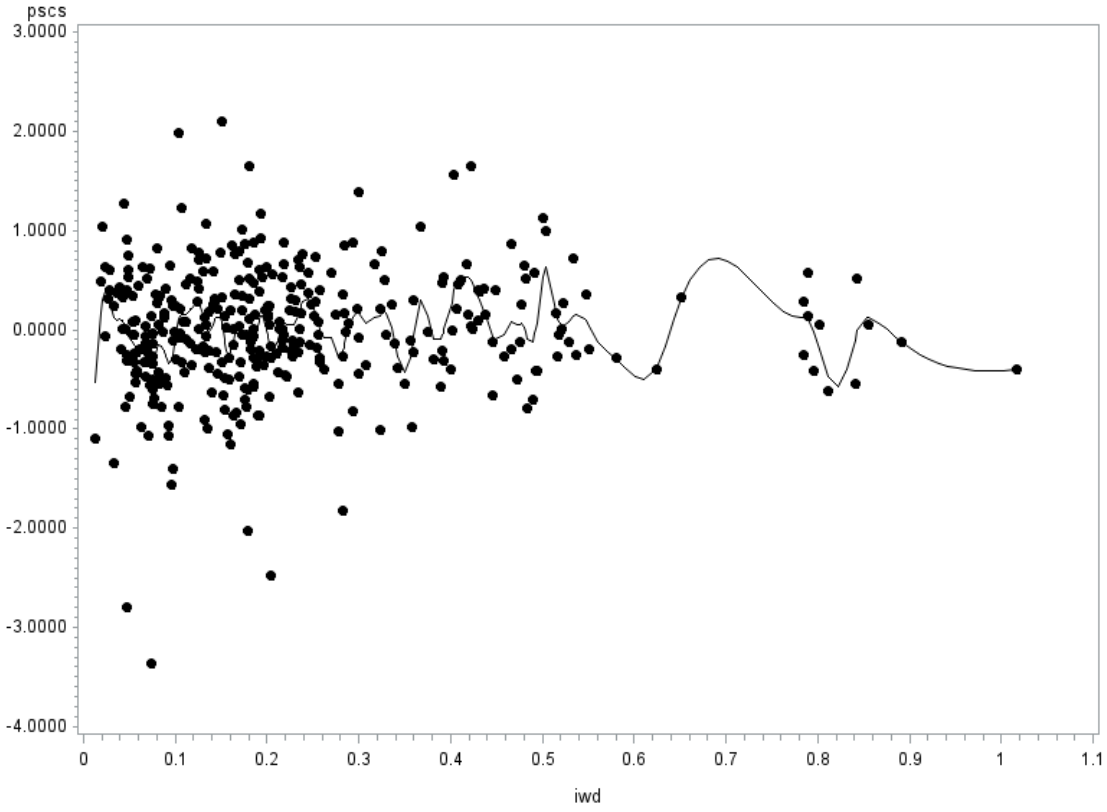

M1 ROI

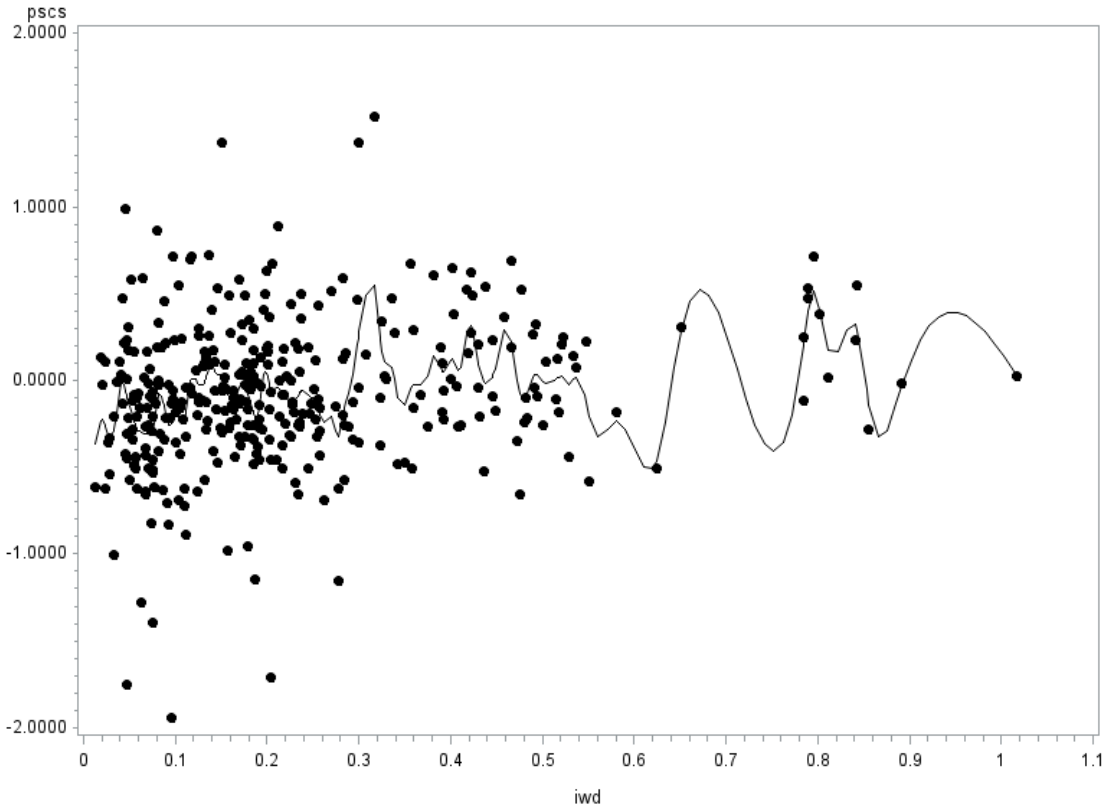
pscs
2.0000
1.0000
0.0000
-1.0000
-2.0000
0
0.1
0.2
0.3
0.4
0.5
0.6
0.7
0.8
0.9
1
1.1
iwd

Subject-level ROI

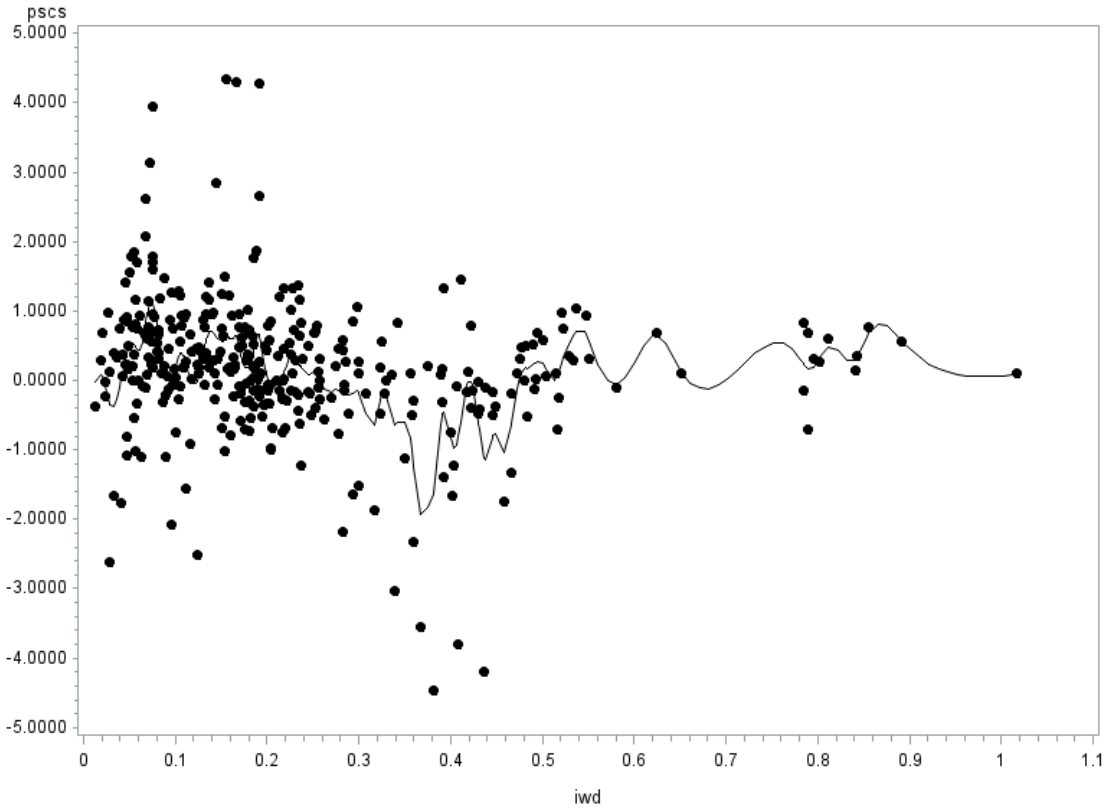

Group-level ROI

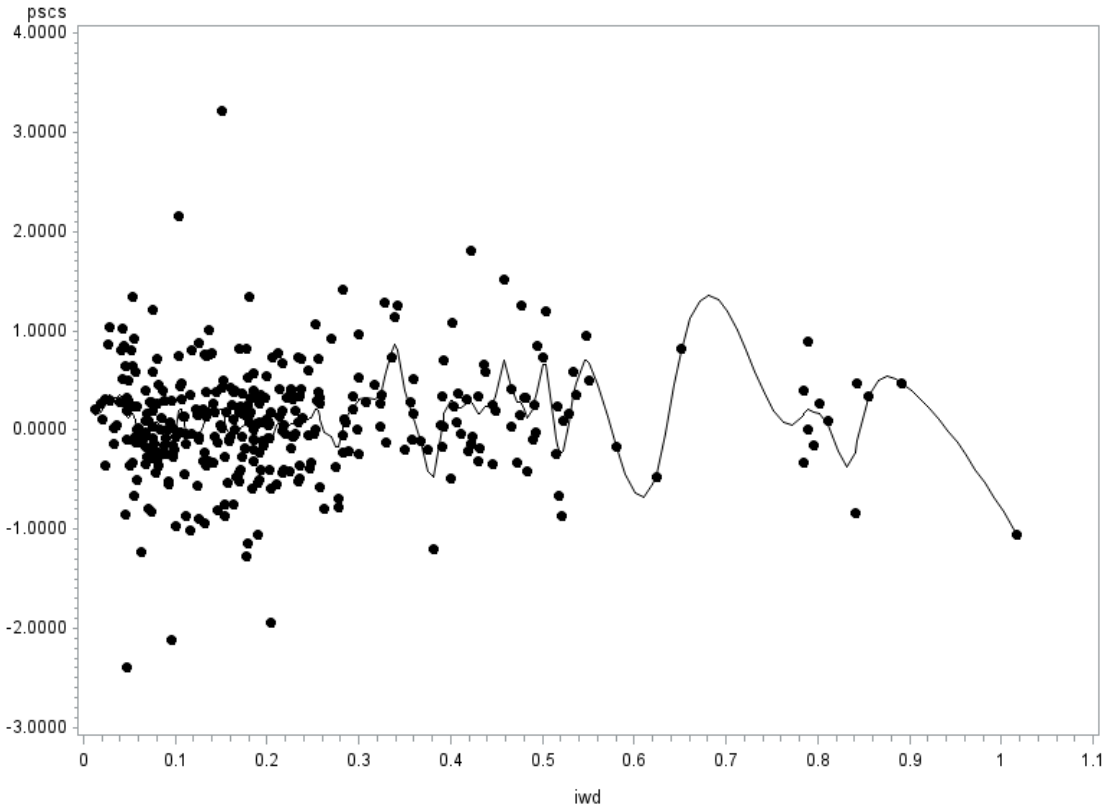

Masked subject-level ROI

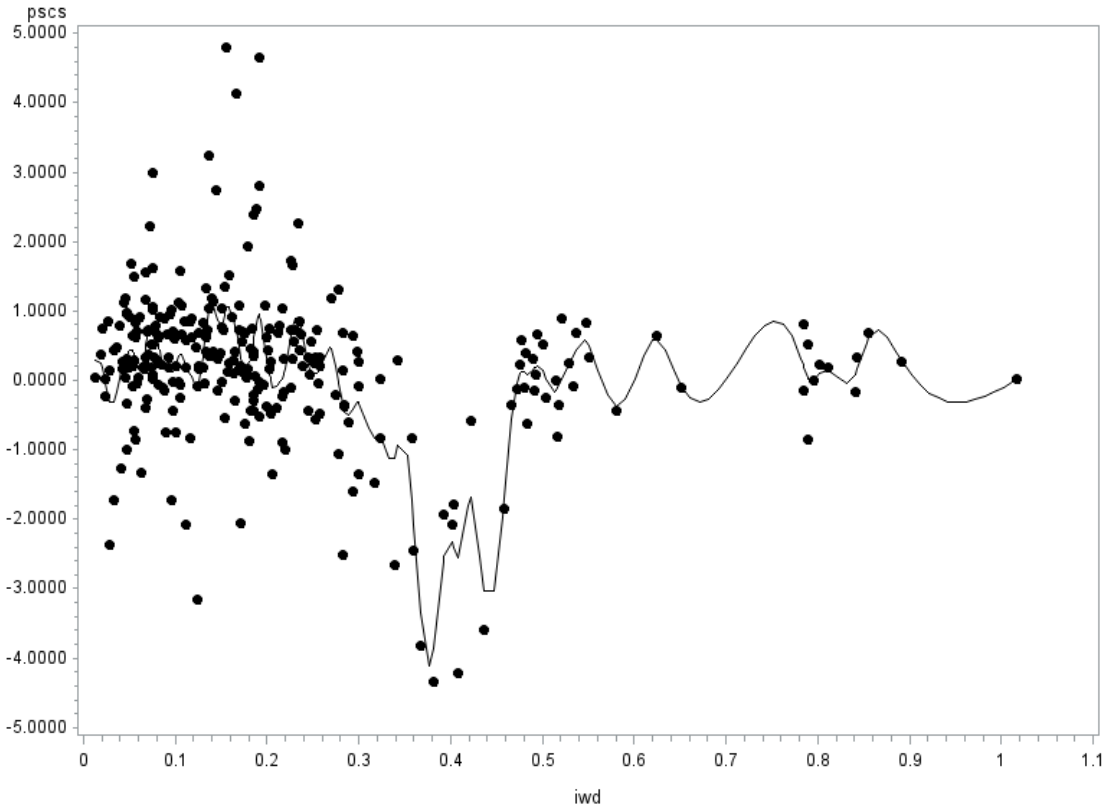

REFERENCES

Andrich, D. (1988). The application of an unfolding model of the PIRT type to the measurement of attitude. *Applied Psychological Measurement,* 12, 33-51

Andrich, D., & Luo, G. (1993). A hyperbolic cosine latent trait model for unfolding dichotomous single-stimulus responses. *Applied Psychological Measurement, 17*(3), 253-276.

Andrich, D. (1996). A general hyperbolic cosine latent trait model for unfolding polytomous responses: Reconciling Thurstone and Likert methodologies. *British Journal of Mathematical and Statistical Psychology, 49,* 347-365.

Ashby, F. G. (2011). *Statistical analysis of fMRI data*. Cambridge, Mass: MIT Press.

Barsalou, L. W. (1985). Ideals, central tendency, and frequency of instantiation as determinants of graded structure in categories. *Journal of Experimental Psychology: Learning, Memory, and Cognition, 11,* 629-654.

Bechara A, Damasio H, Damasio AR, Lee GP. Different contributions of the human amygdala and ventromedial prefrontal cortex to decision-making. *J Neurosci.* 1999 Jul 1; 19(13):5473-81

Bennett, J. F., & Hayes, W. L. (1960). Multidimensional unfolding: Determining the dimensionality of ranked preference data. *Psychometrika, 25,* 36-48.

Bennet, C. M., Baird, A. A., Miller, M. B., & Wolford. G. L. (2009). Neural correlates of interspecies perspective taking in the post-mortem Atlantic Salmon: An argument

for multiple comparisons correction. *Journal of Serendipitous and Unexpected Results, 1*(1) pp 1-5.

Bezdek, M. A., Gerrig, R. J., Wenzel, W. G., Shin, J., Revill, K. P., & Schumacher, E. H. (2015). Neural evidence that suspense narrows attentional focus. *Neuroscience, 303.* 338-345.

Birnbaum, A. (1968). Some latent trait models and their use in inferring an examinee's ability. In F. M. Lord & M. R. Novick (Eds.), *Statistical theories of mental test scores* (pp. 397-472). Reading, MA: Addison Wesley.

Bock, R. D., & Mislevy, R. J. (1982). Adaptive EAP estimation of ability in a microcomputer environment. *Applied Psychological Measurement, 6,* 431-444.

Boynton, G. M., Engel, S. A., Glover, G. H., & Heeger, D. J. (1996). Linear systems analysis of functional magnetic resonance imaging in human V1. *The Journal of Neuroscience, 16*(3). 4207-4221.

Brett, M., Anton, J., Valabregue, R., Poline, J. (2002). Region of interest analysis using an SPM toolbox. Abstract presented at the 8th International Conference on Functional Mapping of the Human Brain, June 2-6, Sendai, Japan. Available on CD-ROM in NeuroImage, Vol 16, No, 2.

Brett, M., Penny, W., & Kiebel, S. (2003). An introduction to random field theory in R Frackowiak et al. (Eds.) *Human Brain Function* (pp. 1-23) Elseview, London, England.

Carroll, J. D. (1972). Individual differences and multidimensional scaling. From Shepard, Romne & Nerlove (Eds). Multidimensional scaling: Theory and applications in behavioral sciences. Volume 1, Theory. NY: Academic Press.

Chaplin, W. F., John, O. P., & Goldberg, L. R. (1988). Conceptions of states and traits: Dimensional attributes with ideals as prototypes. *Journal of Personality and Social Psychology, 54,* 541-557.

Chen, J. E., & Glover, G. H. (2015). Functional magnetic resonance imaging methods. *Neuropsychology Review, 25,* 289-313.

Cho, S., & Bottge, B. (2015). Multilevel multidimensional item response model with a multilevel latent covariate. *British Journal of Mathematical and Statistical Psychology. 68,* 410-433.

Coombs, C.H. (1950). Psychological scaling without a unit of measurement. *Psychological Review, 57,* 145-158.

Corbetta, M., & Shulman, G.L. (2002). Control of goal-directed and stimulus-driven attention in the brain. *Nature Reviews, Neuroscience. 3*(3). 201-215.

Cook, R. D. (1977). Detection of influential observations in linear regression. *Technometrics. 19,* 15-18.

Cox, R. W. (1996). AFNI: Software for analysis and visualization of functional magnetic resonance neuroimages. *Computers and Biomedical Research, 29*(3). 162-173.

Cui, W. (2008). The multidimensional generalized graded unfolding model for assessing change in repeated measures (Doctoral dissertation).

Dale, A. M., (1999). Optimal experimental design for event-related fMRI. *Human Brain Mapping, 8.* 109-114.

Das, M. K., & Gogoi, B. (2015). Influential observations and cutoffs of different influence measures in multiple linear regression. *Int. J. Comp. Theo. Stat. 2*(2).

Davison, M.L. (1983). *Multidimensional scaling*. New York: Wiley.

Davison, M. L., Zieffler, A., Cabrera, J., Karl, S. R., & Cohen, H. S. (2012). Automated assembly of optimally spaced and balanced paired comparisons: Controlling order effects. *Behavior Research Methods, 44,* 753-764.

Dempster, A. P., Laird, N. M., & Rubin, D. B. (1977). Maximum likelihood from incomplete data via the EM algorithm. *Journal of the Royal Statistical Society, 39,* 1-38.

Desikan, R. S., Segonne, F., Fischl, B., Quinn, B. T., Dickerson, B. C., et al. (2006). An automated labeling system for subdividing the human cerebral cortex on mri scans into gyral based regions of interest. *NeuroImage, 31,* 968-980.

Evans, A. C., Collins, D. L., Milner B. (1992). An MRI-based stereotactic atlas from 250 young normal subjects. Journal Soc. Neurosci. Abstr. 18: 408.

Evans, A. C., Collins, D. L., Mills, S. R., Brown, E. D., Kelly, R. L., and Peters T. M. (1993). 3D statistical neuroanatomical models from 305 MRI volumes, Proc. IEEE-Nuclear Science Symposium and Medical Imaging Conference, 1813-1817.

Forrestell, C. A., Humphrey, T. M. & Stewart, S. H. (2004). Involvement of body weight and shape factors in ratings of attractiveness: A replication and extension of Tassinary and Hansen (1998). *Personality and Individual Differences, 36,* 295-305.

Fox, J., Entink, R. K., & van der Linden, W. (2007). Modeling of responses and response times with the package cirt. *Journal of Statistical Software, 20*(7). 1-14.

Friston, K. J., Jezzard, P., & Turner, R. (1994a). Analysis of functional MRI time-series. *Human Brain Mapping, 1,* 690-699.

Friston, K. J., Worsley, K. J., Frackowiak, R. S. J., Mazziotta, J. C., & Evans, A. C. (1994b). Assessing the significance of focal activations using their spatial extent. *Human Brain Mapping, 1,* 214-220.

Friston, K. J. (2003). Introduction: Experimental design and statistical parametric mapping. In Frackowiak et al. (Eds.) *Human Brain Function,* 2nd Edition.

Geissler, A., Gartus, A., Foki, T., Tahamtan, A. R., Beisteiner, R., Barth, M. (2007). Contrast-to-noise ratio (CNR) as a quality parameter in fMRI. *Journal of Magnetic Resonance Imaging, 25,* 1263-1270.

Gelman, A. (2006). Prior distributions for variance parameters in hierarchical models. *Bayesian Analysis, 3*(1). 515-533.

Gifford, J. A., & Swaminathan, H. (1990). Bias and the effect of priors in bayesian estimation of parameters of item response models. *Applied Psychological Measurement, 1*(14). 33-43.

Glover, G. H. (1999). Deconvolution of impulse response in event-related BOLD fMRI. *NeuroImage, 9,* 416-429.

Godwin, C. A., Hunter, M. A., Bezdek, M. A., Lieberman, G., Elkin-Frankston, S., Romero, V. L., Witkiewitz, K., Clark, V. P., & Schumacher, E. H. (In press). Functional connectivity within and between intrinsic networks correlates with trait mind wandering. *Neuropsychologica.*

Hayasaka, S., & Nichols, T. (2003). Controlling familywise error rate in functional neuroimaging: a comparative review. *Statistical Methods in Medical Research, 12,* 419-446.

Henss, R. (1995). Waist-to-hip ratio and attractiveness. Replication and extension. *Personality and Individual Differences, 19,* 479-488.

Henss, R. (2000). Waist-to-hip ratio and female attractiveness. Evidence from photographic stimuli and methodological considerations. *Personality and Individual Differences, 28,* 501-513.

Johnstone, T., Walsh, K. S. O., Greischar, L. L., Alexander, A. L., Fox, A. S., Davidson, R. J., & Oakes, T. R. (2006). Motion correction and the use of motion covariates in multiple-subject fMRI analysis. *Human Brain Mapping, 27,* 779-788.

Kim, J., & Bolt, D.M. (2007). Estimating item response theory models using Markov Chain Monte Carlo methods. *Educational Measurement: Issues and Practice, 26*(4), 38-51.

King, D. R. (2017). Stochastic approximation of the multidimensional generalized graded unfolding model. (Doctoral dissertation).

Li, T., Jiao, H., & Macready, G. B. (2016). Different approaches to covariate inclusion in the mixture rasch model. *Educational and Psychological Measurement. 76*(5). 848-872.

Likert, R. (1932). A technique for the measurement of attitudes. *Archives of Psychology, 140*, 44-53.

Liu, Y., Magnus, B. E., & Thissen, D. (2016). Modeling and testing differential item functioning in unidimensional binary item response models with a single continuous covariate: A functional data analysis approach. *Pyschometrika. 81*(2). 371-398.

Logothetis, N. K. (2003). The underpinnings of the BOLD functional magnetic resonance imaging signal. *J Neurosci, 23*(10). 3963-3971.

Lord, F.M. (1980). *Applications of item response theory to practical testing problems.* Mahwah, NJ: Lawrence Erlbaum Associates.

March, J. G., & Simon, G. A. (1958). *Organizations.* New York: Wiley.

Markey, C. N., Tinsley, B., Ozer, D. & Markey, P. (2002). Preadolescents' perceptions of females' body size and shape: Evolutionary and social learning perspectives. *Journal of Youth and Adolescence, 31*(2). 137-146.

Masters, G. (1982). A Rasch model for partial credit scoring. *Psychometrika, 47,* 149-174.

Mazziotta., J. C., Toga, A. W., Evans, A., Fox, P., and Lancaster, J. A (1995). Probablistic Atlas of the Human Brain: Theory and Rationale for Its Development, *NeuroImage* 2:89-101.

McKeown, M., & Sejnowski, T. (1998). Independent component analysis of fMRI data: Examining the assumptions. *Human Brain Mapping*, 6(5-6), 368-372

McKeown, M. J., Makeig, S., Brown, G. G., Jung, T., Kindermann, S. S., Bell, A. J., Sejnowski, T. J., (1998). Analysis of fMRI data by blind separation into independent spatial components. *Human Brain Mapping, 6,* 160-188.

Mckeown, M. J., Hansen, L. K., & Sejnowski, T. J. (2003). Independent component analysis of functional MRI: what is signal and what is noise? *Current Opinions in Neurobiology, 13*(5). 620-629.

Mendoza, J. L., Toothaker, L. E., & Nicewander, W. A. (1974). A Monte Carlo comparison of the univariate and multivariate methods for the groups by trials repeated measures design. *Multivariate Behavioral Research, 9*(2), 165–177. https://doi.org/10.1207/s15327906mbr0902_3

Menon, V., & Uddin, L. Q. (2010). Saliency, switching, attention and control: A network model of insula function. *Brain Structure Function, 214.* 655-667.

Morris, A., Ravishankar, M., Pivetta, L., Chowdury, A., Falco, D., Damoiseaux, J. S., Rosenberg, D. R., Bressler, S. L. & Diwadkar, V. A. (2018). Response hand and

motor set differentially modulate the connectivity of brain pathways during simple uni-manual motor behavior. *Brain Topogr*. *31*(6), 985-1000.

Muller, K. E., & Mok, M. C. (1997). The distribution of Cook's D statistic. *Commun Stat Theory Methods. 26*(3). doi: 10.1080/03610927708831932.

Muraki, E. (1992). A generalized partial credit model: Application of an EM algorithm. *Applied Psychological Measurement, 16*, 159-176.

Muraki, E., & Carlson, J. E. (1995). Full-information factor analysis for polytomous item responses. *Applied Psychological Measurement, 19,* 73-90.

Mayka, M.A., Corcos, D.M., Leurgans, S.E., Vaillancourt, D.E. 2006. Three-dimensional locations and boundaries of motor and premotor cortices as defined by functional brain imaging: a meta-analysis. Neuroimage. 31(4):1453-1474.

Nishimoto, S., Vu, A. T., Naselaris, T., Benjamini, Y., Yu, B., & Gallant, J. L. (2011). Reconstructing visual experiences from brain activity evoked by natural movies. *Current Biology, 21*. 1641-1646.Noel, Y. (1999). Recovering unimodal latent patterns of change by unfolding analysis: Application to smoking cessation. *Psychological Methods, 2*(2). 173-191.

O' Brien, M. G., & Kaiser, M. K. (1985). MANOVA method for analyzing repeated measures designs: An extensive primer, Psychological Bulletin, 97 (2), 316-333.

Ollinger, J. & Corbetta, M. (2001). Separating processes within a trial in event-related functional MRI. *Neuroimage, 13*(1). 218-229.

Pajula, J., Tohka, J. (2016). How many is enough? Effect of sample size in inter-subject correlation analysis of fMRI. *Computational Intelligence and Neuroscience. doi: 10.1155/2016/2094601*.

Patz, R. J., & Junker, B. W. (1999) A straightforward approach to Markov Chain Monte Carlo Methods for item response models. *Journal of Educational and Behavioral Statistics, 24,* 146-178. DOI: 10.3102/10769986024002146.

Platek, S. M., & Singh, D. (2010). Optimal waist-to-hip ratios in women activate neural reward centers in men. *PLoS ONE, 5*(2). 1-5.

Poldrack, R. A. & Mumford, J. A. (2009). Independence in ROI analysis: Where is the voodoo? *SCAN, 4*, 208-213.

Poldrack, R. A., & Farah., M. J. (2015). Progress and challenges in probing the human brain. *Nature, 526,* 371-379.

Rasch, G. (1960/1980). *Probabilistic models for some intelligence and attainment tests*. Chicago: The University of Chicago Press.

Reckase, M. D. (2009). *Multidimensional item response theory*. New York: Springer-Verlag. (pp. 79-112). (Chapter 4: Multidimensional item response theory models).

Roberts, J.S., & Laughlin, J.E. (1996). A unidimensional item response model for unfolding responses from a graded disagree-agree response scale. *Applied Psychological Measurement, 20*(3), 231-255.

Roberts, J.S., Donoghue, J.R., & Laughlin, J.E. (2000). A general item response theory model for unfolding unidimensional polytomous responses. *Applied Psychological Measurement, 24*(1), 3-32.

Roberts, J. S., Donoghue, J. R., & Laughlin, J. E. (2002). Characteristics of MML/EAP parameter estimations in the generalized graded unfolding model. *Applied Psychological Measurement, 26*(2). 192-207.

Roberts, J. S., Rost, J., & Macready, G. B. (2010). MIXUM: An unfolding mixture model to explore the latitude of acceptance concept in attitude measurement. In S. Embretson (Ed.), *Measuring psychological constructs: Advances in model-based approaches* (Chapter: 8 pp. 175-197). Washington, DC: American Psychological Association.

Roberts, J.S., & Shim, H. (July, 2010). *Multidimensional unfolding with item response theory: The multidimensional generalized graded unfolding model*. Paper presented at the 2010 Annual Meeting of the Psychometric Society, Athens, Georgia.

Roberts, J. S., & Sparks, J. L. (2015). Mapping the emotion space with the MGGUM. Paper presented at the National Council on Measurement in Education, Chicago, IL.

Roberts, J. S., Barrett, M. E., & King, D. R. (2016). Measuring physical attraction with the multidimensional generalized graded unfolding model. Paper presented at the International Meeting of the Psychometric Society, Asheville, N.C.

Ross, R. T. (1934). Optimum orders for the presentation of pairs in the method of paired comparisons. *Journal of Educational Psychology, 25*(5), 375-382. Doi:10.1037/h0070754

Samejima, F. (1969). Estimation of Latent Ability Using a Response Pattern of Graded Scores (Psychometric Monograph No. 17 – Chapters 1-6, & Chapter 11; pp 1-46, 93-94). Richmond, VA: Psychometric Society.

Schwartz, S., Vuilleumier, P., Hutton, C., Maravita, A., Dolan, R. J., Driver, J. (2005). Attentional load and sensory competition in human vision: modeulation of fMRI responses by load at fixation during task irrelevant stimulation in the peripheral visual field. *Cerebral Cortex 15,* 1153-1172.

Sherif, M., & Hovland, C. I. (1961). *Social judgment: Assimilation and contrast effects in communication and attitude change.* Yale Univer. Press.

Sherif C W, Sherif M & Nebergall R E. Attitude and attitude change. The social judgment-involvement approach. Philadelphia: W. B. Saunders, 1965. 264 p. [Inst. Group Relations and Dept. Speech, Univ. Oklahoma, OK]

Shinkareva, S. V., Malave, V. L., Mason, R. A.,Mitchell, T. M., & Just, M. A. (2008). Commonality of neural representation of words and pictures. *NeuroImage 54.* 2418-2425.

Singh, D. & Luis, S. (1995). Ethnic and gender consensus for the effect if waist-to-hip ratio on judgments of women's attractiveness. *Human Nature, 6,* 51-65.

Singh, D. (2002). Female mate value at a glance: Relationship of waist-to-hip ratio to health, fecundity, and attractiveness. *Human Ethology and Evolutionary Psychology, 23,* 81-91.

Singh, D. (2006). Universal allure of the hourglass figure: An evolutionary theory of female physical attractiveness. *Human Nature, 6,* 51-65.

Sparks, J. L. (2020). An unfolding IRT modeling framework for the simultaneous analysis of preference and response time data [Unpublished doctoral dissertation proposal]. Georgia Institute of Technology.

Spisak, T., Jakab, A., Kis, S. A., Opposits, G., Aranyi, C., Berenyi, E., & Emri, M. (2014). Voxel-wise motion artifacts in population-level whole-brain connectivity analysis of resting-state fMRI. *PLOSone, 9*(9). 1-19.

Stark, S., Chernyshenko, O. S., & Drasgow, F. (2005). An IRT approach to constructing and scoring pairwise preference items involving stimuli on different dimensions: An application to the problem of faking in personality assessment. *Applied Psychological Measurement, 29,* 184-201.

Stelzer J, Lohmann G, Mueller K, Buschmann T and Turner R (2014) Deficient approaches to human neuroimaging. *Frontiers in Human Neuroscience. **8***(462). doi: 10.3389/fnhum.2014.00462

Swami, V. & Furnham, A. (2008). The Psychology of Physical Attraction. NY: Routledge

Talairach, J. and Tournoux, P. (1998). Co-planar Stereotaxic Atlas of the Human Brain: 3-Dimensional Proportional System - an Approach to Cerebral Imaging. Thieme Medical Publishers, New York, NY.

Tassinary, L. G. & Hansen, K. A. (1998). A critical test of the waist-to-hip ratio hypothesis of female physical attractiveness. *Psychological Science, 9,* 150-155.

Tay, L., Huang, Q., & Vermunt, J. K. (2016). Item response theory with covariates (IRT-c): Assessing item recovery and differential item functioning for the three-

parameter logistic model. *Educational and Psychological Measurement. 76*(1). 22-42.

Thissen, D., Steinberg, L. A taxonomy of item response models. *Psychometrika* **51,** 567–577 (1986). https://doi.org/10.1007/BF02295596

Thompson, V. M. (2014). Marginal Bayesian parameter estimation in the multidimensional generalized graded unfolding model. (Doctoral dissertation).

Thurstone, L.L. (1928). Attitudes can be measured. *The American Journal of Sociology 33*(4), 529-553.Tzourio-Mazoyer N, Landeau B, Papathanassiou D, Crivello F, Etard O, Delcroix N, et al. (2002). Automated anatomical labeling of activations in SPM using a macroscopic anatomical parcellation of the MNI MRI single subject brain. *NeuroImage*; 15: 273-289.

Vul, E., Harris, C., Winkielman, P., & Pashlet, H. (2009). Puzzingly high correlations in fMRI studies of emotion, personality and social cognition. *Perspectives on Psychological Science. 4*(3). 274-290.

Wager, T. D., Vazquez, A., Hernandex, L., & Noll, D. C. (2005). Accounting for nonlinear BOLD effects in fMRI: Parameter estimates and a model for prediction in rapid event-related studies. *NeuroImage, 25*, 206-218.

Wang, T. & Hanson, B. A. (2005). Development and calibration of an item response model that incorporates response time. *Applied Psychological Measurement. 29*(5). 323-339.

Wang, W. & Liu, C. (2011). Computerized classification testing under the generalized graded unfolding model. *Educational and Psychological Measurement. 71*(1). 114-128.

Welvaert, M., & Rosseel, Y. (2013). On the definition of signal-to-noise ratio and contrast-to-noise ratio for fMRI data. *PLOSone, 8*(11). 1-10.

Widiatmo, H. & Wright, D. B. (2015). Comparing two item response models that incorporate response times. Paper presented at NCM. Chicago, IL.

Williams, E. (2016). Symposium presented at the 2016 International Meeting for The Psychometric Society. *Ashenville, NC.*

Woo, C., Krishnan, A., & Wager, T. D. (2014). Cluster-extent based thresholding in fMRI analyses: Pitfalls and recommendations. *NeuroImage, 91,* 412-419.

Woolrich, M. W., Ripley, B. D., Brady, M., & Smith, S. M. (2001). Temporal autocorrelation in univariate linear modeling of fMRI data. *NeuroImage, 14,* 1370-1386.

Wyer, R. S., Jr. (1976). An investigation of relations among probability estimates. *Organizational Behavior and Human Performance, 15,* 1-18.

Yen, W. M., & Fitzpatrick, A. R. (2006). Item response theory. In *Educational Measurement* (4th ed. Chapter: 4), Brennan, R. L. (Ed.). pp 111-154. American Council on Education and Praeger Publishers.

Zarahn, E., Aguirre, G., & D'Esposito, M. (1997). A trial-based experimental design for fMRI. *NeuroImage, 6,* 122-138